Using zebrafish for pre-clinical brain haemorrhage research

A thesis submitted to the University of Manchester for the degree of Doctor of Philosophy in the Faculty of Biology, Medicine and Health

2019

Siobhan C. Crilly

School of Biological Sciences, Division of Neuroscience and Experimental Psychology

List of Contents

Word count: 41,222

List of figures

List of tables

List of abbreviations

Abbreviation	Meaning	Page Number
AF	Alexa Fluor™	68
ANOVA	Analysis of variance	87
APOE	Apolipoprotein E	105
ARRIVE	Animal Research: reporting of *in vivo* experiments	78
ASPA	Animals (Scientific Procedures) Act	35
ATP	Adenosine triphosphate	26
ATV	atorvastatin	40
AVMs	Arteriovenous malformations	21
βpix	Encodes a Rho GTPase AFHGEF7, and is absent in *bbh* mutants	41
BBB	Blood-brain barrier	23
bbh	*Bubblehead* mutant	41
BMP	Bone morphogenetic protein	38
bp	basepair	63
BSA	Bovine serum albumin	46
CAA	Cerebral amyloid angiopathy	21
CADASIL	Cerebral Autosomal Dominant Arteriopathy with Subcortical Infarcts and Leukoencephalopathy	21
cAMP	Cyclic adenosine monophosphate	150
caspase	**c**ysteine-dependent **asp**artate-directed prote**ases**	40
cDNA	Complementary DNA	58
Ch25h	Cholesterol 25-hydroxylase	56
CNS	Central nervous system	24
CRISPR	Clustered regularly interspaced short palindromic repeats	36
CSF	Cerebrospinal fluid	21
CT	Computed tomography, a series of X-ray images used to diagnose brain haemorrhage	21
CVD	Cardiovascular disease	123
CXCL2	CXC motif chemokine ligand 2	26
CYP51	lanosterol 14α-Demethylase Cytochrome P450	71
DAB	3'-Diaminobenzidine	64
DAMPs	Damage-associated molecular pattern molecules	26

DAPI	4′,6-diamidino-2-phenylindole, a blue-fluorescent DNA stain	68
DFO	deferoxamine	52
DHCR24	24-dehydrocholesterol reductase	71
DMSO	Dimethyl sulfoxide	47
DNA	Deoxyribonucleic acid	23
DNase	deoxyribonuclease	61
dpf	days post fertilisation	36
dsRed	a red fluorescent protein	48
EBP	3β-hydroxysteroid-Δ8,Δ7-isomerase	71
EDTA	Ethylenediaminetetraacetic acid	45
ENU	N-ethyl-N-nitrosourea	41
FACS	Fluorescence-activated cell sorting	105
fli1	A blood vessel-specific restriction factor	48
g	gram	45
gata1	An erythroid-specific restriction factor	48
GEF	Guanine nucleotide exchange factor	76
GFP	Green fluorescent protein	48
H_2O_2	Hydrogen peroxide	45
HDL	High-density lipoprotein	51
HE	Haematoma expansion	22
HHT	hereditary haemorrhagic telangiectasia	21
Hi-DEF	high-dose deferoxamine in ICH clinical trial	120
HMG-CoA	3-hydroxy-3-methylglutaryl coenzyme A	42
HMGCR	3-hydroxy-3-methylglutaryl coenzyme A reductase	40
hmox1a	Heme oxygenase 1a zebrafish gene	193
HO-1	Heme oxygenase 1	151
hom	homozygous	113
hpf	hours post fertilisation	36
hpi	hours post injury/injection	49
hrIL-1β	Human recombinant Interleukin-1β	128
Iba1	ionized calcium binding adapter molecule 1, cytoplasmic marker of microglia and macrophages	69
ICH	Intracerebral haemorrhage	19
ICH-	Negative for ICH	49

ICH+	Positive for ICH	49
ICP	Intracranial pressure	23
i-DEF	Intracerebral haemorrhage deferoxamine clinical trial	120
IHC	Immunohistochemistry	64
IκB	inhibitor of nuclear factor B	119
IKK	inhibitor of nuclear factor B kinase	119
IL-1	Human interleukin 1, a pro-inflammatory cytokine	26
Il-1	Zebrafish interleukin 1 protein	119
il-1	Zebrafish interleukin 1 gene	47
IL-10	Interleukin 10, a regulatory cytokine	27
il1fma	*interleukin 1 family member A*	121
IL-1R	Interleukin 1 receptor	119
IL-1Ra	Interleukin 1 receptor antagonist	52
INFLAME-ICH	INFLammation After Minimally invasive Evacuation of IntraCerebral Haemorrhage	125
irf7	*interferon regulatory factor 7*	71
isg15	*interferon-stimulated gene 15*	71
IVH	Intraventricular haemorrhage	20
LDL	Low-density lipoprotein	22
LPS	Lipopolysaccharide	32
MAP kinase	Mitogen-activated protein kinase	118
MHRA	Medicines and Healthcare products Regulatory Agency for the UK	188
MISTIE III	Minimally Invasive Surgery Plus Alteplase for Intracerebral Haemorrhage Evacuation (MISTIE) III trial	125
ml	millilitre	45
mM	millimolar	46
MMP	Matrix metalloproteinase	27
mmp9	matrix metalloproteinase 9	71
MO	Morpholino	36
mpo	*myeloperoxidase*, a marker for neutrophils	48
mpeg1	*macrophage-expressed gene 1*	48
mRNA	Messenger ribonucleic acid	39
mRS	modified Rankin Scale	120
MS222	Tricaine methansulfonate	45

msmo1	Methylsterol Monooxygenase 1	71
µl	microlitre	45
µM	micromolar	49
NeuN	Neuronal nuclei	105
NLRP	Nucleotide-binding oligomerization domain, Leucine rich Repeat and Pyrin domain containing	154
NF-κB	Nuclear factor-κB	26
ng	nanogram	63
PAR-1	Proteinase activated receptor 1	118
PBS	Phosphate buffered saline	45
PCR	Polymerase chain reaction	58
Pcs2+	Cloning vector	57
Pcsk9	proprotein convertase subtilisin/kexin type 9	185
PFA	Paraformaldehyde	45
pH	Numerical scale to determine acidity or alkalinity of a solution	45
PPL	Home office project license	48
qPCR	Quantitative polymerase chain reaction	71
RBC	Red blood cells	22
relA	*REL associated protein, p65*	71
rig-I	*retinoic acid inducible gene-I*	71
ROS	Reactive oxygen species	27
RNA	ribonucleic acid	49
RNase	ribonuclease	61
RNASeq	RNA sequencing	143
rpm	rotations per minute	71
rsad2	Interferon-induced anti-viral gene	71
RT	room temperature	49
RQ	Relative quantification	121
SAH	Subarachnoid haemorrhage	20
sc5d	Sterol-C5-Desaturase	71
s.d	Standard deviation	89
SNPs	Single nucleotide polymorphisms	191
sqlea	Squalene epoxidase a	71
SREBP/F	Sterol response element binding proteins	71

stat1b	*signal transducer and activator of transcription 1β*	71
SVD	Small vessel disease	21
TAE	Tris-acetate-EDTA	45
TBI	Traumatic brain injury	125
TGF-β	Transforming growth factor beta	27
TLRs	Toll-like receptors	26
TNF-α	Tumour necrosis factor alpha	23
tPA	Tissue plasminogen activator	195
UK	United Kingdom	19
UNT	untreated	49
US	United States	142
UV	ultraviolet	50
WISH	Whole-mount *in-situ* hybridisation	57
WT	wildtype	53
25-HC	25-hydroxycholesterol	53
3R's	Replacement, reduction and refinement	35

Abstract

Intracerebral haemorrhage (ICH) is a devastating condition with limited treatment options, accounting for 49% of 6.5 million annual stroke deaths worldwide, and over half of all disability adjusted life years lost to stroke. Current understanding of pathophysiology is incomplete, partly due to limitations of the existing pre-clinical models of spontaneous disease. Here we show that zebrafish larvae can be used to model spontaneous ICH and exhibit comparable pathological outcomes to human condition, therefore offering an alternative model for pre-clinical study for ICH.

Zebrafish larvae are associated with several practical advantages including high fecundity, optical translucency and non-protected status prior to 5 days post fertilisation. Through live, non-invasive imaging of transgenic fluorescent reporter lines and behavioural assessment we can quantify pathological outcomes and neuroinflammation following ICH. Using these assessable outcomes we can quantify improvement after ICH with targeted drug treatment, to ameliorate primary injury and secondary neuroinflammatory responses. Due to the spontaneous nature of blood vessel rupture in this model we can investigate the relationship between clinically relevant risk factors and ICH in zebrafish.

In this study we show that the zebrafish larvae represent a novel model for pre-clinical ICH investigation that is appropriate for use in medium throughput drug screening. The zebrafish larval model has potential to reduce the number of protected animals used in pre-clinical ICH investigation and to support the advancement of the stroke field with practical translatable outcomes to directly benefit patients in the clinic.

Lay summary

Brain haemorrhages are the most severe type of stroke; however our understanding of how and why they occur is limited. In order to understand the disease better in a laboratory setting, it is currently modelled using rodents however these models differ vastly from human condition. Here, we model brain haemorrhage in a larval zebrafish, a small, transparent organism that can mimic aspects of human disease that rodents cannot. We have shown that brain haemorrhage in zebrafish larvae is similar to humans and that we can use this model to screen for therapeutic drugs, something that has never been done before for brain haemorrhage.

Declaration

I declare that no portion of the work referred to in the thesis has been submitted in support of an application for another degree or qualification of this or any other university or other institute of learning.

Copyright statement

Contributions to work

Chapter 3 - Crilly S, Njegic A, Laurie SE *et al.* Using zebrafish larval models to study brain injury, locomotor and neuroinflammatory outcomes following intracerebral haemorrhage [version 2; peer review: 2 approved]. *F1000Research*2018, 7:1617

(https://doi.org/10.12688/f1000research.16473.2)

Siobhan Crilly: Conceptualization, Data Curation, Formal Analysis, Investigation, Methodology, Project Administration, Software, Validation, Visualization, Writing – Original Draft Preparation, Writing – Review & Editing

Alexandra Njegic: Formal Analysis, Investigation, Methodology, Validation, Writing – Review & Editing, **Sarah E. Laurie**: Formal Analysis, Investigation, Validation, Writing – Review & Editing, **Elisavet Fotiou**: Formal Analysis, Investigation, Writing – Review & Editing, **Georgina Hudson**: Investigation, Methodology, Writing – Review & Editing, **Jack Barrington**: Formal Analysis, Writing – Review & Editing, **Kirsty Webb**: Investigation, Methodology, Writing – Review & Editing, **Helen L. Young**: Methodology, Validation, Writing – Review & Editing, **Andrew P. Badrock**: Methodology, Validation, Writing – Review & Editing, **Adam Hurlstone**: Resources, Writing – Review & Editing, **Jack Rivers-Auty**: Data Curation, Formal Analysis, Software, Writing – Review & Editing, **Adrian R. Parry-Jones**: Conceptualization, Funding Acquisition, Project Administration, Supervision, Writing – Review & Editing, **Stuart M. Allan**: Conceptualization, Funding Acquisition, Project Administration, Resources, Supervision, Writing – Review & Editing, **Paul R. Kasher**: Conceptualization, Formal Analysis, Funding Acquisition, Investigation, Methodology, Project Administration, Resources, Supervision, Validation, Visualization, Writing – Original Draft Preparation, Writing – Review & Editing

The time line qPCRs for *il-1β* and *ch25h* (figure 6.3.1) and WISH stains for *ch25h* (figure 6.2.2) were performed by Miss Annabel Chadwick

The video presented in appendix iv and stills for figure 3.3.8A was acquired by Miss Alex Njegic

The sequencing for *bbh* genotyping and cloning of *ch25h* mRNA was performed by the Genomic Technologies Core Facility at the University of Manchester

Fluorescence activated cell sorting was performed by Dr Gareth Howell and Mr Michael Jackson at the Genomic Technologies Core Facility at the University of Manchester

Human brain tissue acquired from the Edinburgh Brain Bank was sectioned by Miss Emily Williams in the Histology Core Facility at The University of Manchester

Dr Adrian Parry-Jones acquired data pertaining to INFLAME-ICH trial

Acknowledgements

A PhD is a wild ride and I have not made it to the end of this work alone. I'd like to share my utmost gratitude to my supervisors Stuart, Adrian and Paul for giving me this opportunity, for their brilliant support and guidance over the past three years and helping me realise this dream. A special thanks to Paul for being the most patient and understanding supervisor, believing in me when I didn't want to, and making this whole process a lot more entertaining.

Thank you to the NC3Rs for funding my PhD work and for their support through my doctoral training. I would like to thank all who have helped me from the University of Manchester by providing training, resources and consultation: the staff in the Bioimaging core facility and the Genomic Technologies core facility, all the staff in the Biological Service unit for the care of the fish, Dr Holly Shiels and Prof Richard Baines for use of their software and equipment, Prof Federico Roncaroli for his advice in neuropathological analysis, Emily Birleson and the Salford Stroke team for allowing me to visit and taking the time to teach me about the clinic, Dr Jack Rivers-Auty for statistical help and Dr Sarah Ryan for helping to review my work.

Thank you to all the members of the Kasher lab, past and present for being so helpful collaborating on experiments, supporting each other and being a dependable team. I would like to acknowledge all of the Brain Inflame Group for their endless care and support; we really are all in this together. And finally thank you to Peter for sharing this journey with me every second of the day and night, and reminding me that there is so much more to life than a PhD.

Dedication

I dedicate this work to my first supervisory team – Mum and Dad

Dubito, ergo cogito, ergo sum…

Chapter 1: Introduction

1.1 Stroke

In 2018 more than 100,000 people in the UK suffered from a stroke and disease prevalence is predicted to double in the next 20 years (The Stroke Association, 2018). A stroke is a serious neurovascular attack, characterised by a loss of oxygen supply to the brain, and is very often a life-threatening emergency with consequential disability adjusted life years. A stroke is usually a result of a multitude of cardiovascular co-morbidities and diseases, rising in prevalence in an ageing population (British Heart Foundation, 2017). Strokes are most common in women over the age of 55 (Seshadri and Wolf, 2007) though are now being reported more frequently in younger patients (Feigin et al., 2014). Globally, strokes are the third leading cause of mortality and disability, with higher incidence and fatalities in low-middle income countries (Johnson et al., 2016). Medications for cardiovascular disease, such as those that lower cholesterol and blood pressure to reduce stress on the cardiovascular system, are cost effective and widely prescribed. Despite this, global mortality from cardiovascular disease has increased over the last decade (Institute for Health Metrics and Evaluation, 2018). In the face of the enormous burden on global health and socio-economic pressures, there remains a limited approach to standardising post-stroke care guidelines, strategizing research for preventative measures and making treatments and rehabilitation accessible globally to benefit the most heavily affected countries.

A stroke is caused by a lack of oxygen to the brain tissue because of disrupted blood supply, resulting from a blockage in the cerebrovasculature (ischemia) or a vessel rupture (haemorrhage) and the subsequent leaking of blood into the brain tissue. A reduction in cerebral blood flow leads to rapid neuronal damage and loss of cerebral function that spreads as injury goes untreated (Saver, 2006). Presently, the only ways to treat an ischemic stroke are with a thrombolytic agent to break down the clot or to physically remove the clot by thrombectomy. In intracerebral haemorrhage (ICH) treatment options are limited to rapid reversal of anticoagulants in the 10-20% of patients taking them (Fuh et al., 2017), intensive blood pressure lowering which has been shown to modestly reduce disability (Butcher et al., 2013), and surgical evacuation of the haematoma in carefully selected cases (Dastur and Yu, 2017; Hanley et al., 2019). In the period between onset and surgery, as the blood clots and forms a

haematoma, re-bleeding is common as the damage in the brain causes the rupture of more vessels surrounding the haematoma. This disease progression and lack of specific targeted therapies mean that haemorrhagic stroke patients suffer the greatest severity and disability following the ictus. One million stroke survivors in the UK need specialised post-acute care, as studies have proven a correlation with decreased mortality (Parry-Jones et al., 2019), however across England, Wales and Northern Ireland there is a lack of specialist stroke consultants, senior nurses and stroke units that can provide professional care (The Royal College of Physicians, 2017). Stroke is the leading cause of adult disability, causing a loss of motor skills and memory, dysphagia, aspiration, speech and language problems and direct or indirect psychological disorders (Ayerbe et al., 2015; Bakheit et al., 2007; The Royal College of Physicians, 2017; The Stroke Association, 2016). Post-stroke immunosuppression results in an increase of infection rates and pneumonia cases in patients, contributing to worse outcomes (Westendorp et al., 2011). Despite this considerable public health burden, stroke research is less likely to be funded by the UK government and charity funding than cancer, coronary heart disease or dementia (Luengo-Fernandez et al., 2016). There is a desperate, immediate need for specific therapies and better understanding of the underlying disease etiology, in order to benefit the millions of global stroke patients and improve their clinical outcomes.

1.2 Intracerebral haemorrhage

An intracerebral haemorrhage (ICH) is caused by a bleed in the brain parenchyma, and to date is the most severe subtype of stroke, fatal in half of patients within one month after onset, and highest resulting disability in survivors (Caceres and Goldstein, 2012). A bleed directly into the brain tissue can result in immediate death, decreased consciousness, headache, seizures, vomiting and unilateral weakness (Morgenstern et al., 2010). Subarachnoid haemorrhage (SAH), bleeds in the space surrounding the brain, are more commonly resultant of a traumatic head injury (Abraham and Chang, 2016). Intraventricular haemorrhage (IVH), bleeds in the ventricular system, are often the result of an ICH that has extended into the ventricles noted in about 40% of ICH cases (Hanley, 2009). Spontaneous ICH accounts for 10-15% of all adult (Intercollegiate Stroke Working Party, 2012) and 50% of childhood (Lo, 2011) strokes in the UK with many potential causes. Globally the absolute number of haemorrhagic stroke cases is on the rise, and the most severely affected populations (80% stroke

cases) are in sub-Saharan Africa, Central and Southeast Asia (Krishnamurthi et al., 2014). A recent systematic review suggests that despite better surgical treatments in Western countries and widely available medical interventions for cardiovascular disease, there has been no significant change in ICH incidence rate, only a decline in mortality (Johnson et al., 2019). ICH can only be diagnosed at hospital using brain imaging, typically a computerised tomography (CT) scan, often combined with angiography to visualise circulation. Early diagnosis of stroke subtype in low-middle income countries is still not possible, preventing immediate treatment and thus resulting in the highest mortality rates (An et al., 2017).

The most common cause of ICH is hypertension as high blood pressure can go untreated for years until a symptomatic outcome like ICH is detectable (The Stroke Association, 2017). Increased resistance to blood flow raises outward pressure on vessel walls. Chronic hypertension causes the blood vessels in the brain to weaken and sometimes swell to form microaneurysms which are prone to rupture. Hypertensive haemorrhagic strokes are commonly located in the basal ganglia and the tissues of the posterior fossa (Zafar and Khan, 2008). Bleeds in this region and the cerebellum obstruct cerebrospinal fluid (CSF) drainage through the fourth ventricle causing hydrocephalus which can result in raised intracranial pressure and consequent loss of consciousness. Pontine haemorrhages carry the potential for the worst prognosis because of damage to vital brain stem structures. However, size of bleed and patient level of consciousness upon admission remain the most critical markers of patient outcome (Shaya et al., 2005).

Less common causes of ICH include traumatic head injury, small vessel diseases (SVD) such as cerebral amyloid angiopathy (CAA) and hypertensive arteriosclerosis, and macrovascular causes like arteriovenous malformations (AVMs), aneurysms, and cavernomas (Keep et al., 2012). There are genetic risk factors for ICH, for example those associated with conditions like hereditary haemorrhagic telangiectasia (HHT) and CADASIL which increase the risk of a brain haemorrhage in a younger population of patients.

Recent studies have shown that haemorrhage risk in aged patients is inversely related to total cholesterol levels (Y.-W. Chen et al., 2017; Phuah et al., 2016; Sun et al., 2019; X. Wang et al., 2013). Cholesterol is a major component of cell membranes,

modulating the fluidity by forming sphingolipid rafts for proteins to anchor into the bilipid layer (Massey, 2001). It is an essential precursor molecule for the synthesis of steroid hormones, sex hormones, bile acid and vitamin D. Biosynthesised cholesterol, and to some extent low-density lipoprotein (LDL) cholesterol in circulation from dietary sources, is essential for brain cell synthesis, chemical synapse formation and axonal myelination (Zhang and Liu, 2015). While too much cholesterol is a risk factor for cardiovascular disease and ischemic stroke, patients with low levels show increased haemorrhage incidence (Rist et al., 2019; Segal et al., 1999; Valappil et al., 2012).

Further investigation into risk and causation of ICH is necessary to guide clinical practice and prevent the severe disability in patients. Yet despite better management of blood pressure, there has not been any decline in ICH prevalence suggesting a new strategy is necessary. As yet, there is no specific medical treatment proven by phase III clinical trials to improve outcome in ICH patients, however clinical evidence suggests that there are three main targets for managing ICH outcomes: stopping the bleed, removing the haematoma and controlling perfusing blood pressure (Qureshi et al., 2009).

1.3 Injury pathology

Initial injury onset due to blood vessel rupture is caused by the toxic effects of extravasation of blood into the brain tissue. Primary injury causes loss of cell structure and an assault of toxic blood compounds such as iron, thrombin, and heme from red blood cell (RBC) lysis (Figure 1.3.1). Bleed location is associated with patient outcome and potential disabilities, and most common sites for bleeds are cerebral hemispheres, basal ganglia, thalamus, brainstem and cerebellum. Reduced perfusion of blood and oxygen causes cell death due to hypoxia in the core of the bleed, the hematoma. The hematoma is at high risk of expanding for 4-6 hours after initial onset and large haemorrhages are associated with very poor prognosis (Brouwers and Greenberg, 2013). Haematoma expansion (HE) in one third of patients (S. Chen et al., 2017) has been frequently clinically targeted by therapies to improve patient outcome by lowering blood pressure (Anderson et al., 2013; Qureshi et al., 2016) and medically initiating clotting (Mayer et al., 2008) however is difficult to predict progression in patients. In aged patients, normal tissue atrophy makes space to accommodate tissue

swelling and increased intracranial pressure (ICP) within the skull, however in younger patients, brain swelling may necessitate a craniotomy and haematoma evacuation in order to create space and decrease ICP. Oedema at the site of injury from the damaged blood-brain barrier (BBB) exacerbates raised ICP after bleeding has stopped, compressing surrounding tissue and further reducing blood flow (Xi et al., 2006). Surgical intervention trials targeting evacuation of the haematoma (Hanley et al., 2019; Mendelow et al., 2011; Morgan et al., 2008) have proven to be life-saving and are current best practice strategies, but success depends largely on the location of the bleed and patient admittance at a specialist stroke centre.

Thrombin, essential for blood clotting in the haematoma and preventing further HE, is released into the brain with the initial bleed. The role of thrombin beyond blood clotting remains controversial as *in vitro* studies have shown that at low concentrations thrombin protects against oxidative stress and ischemia, however other works show it is neurotoxic at high concentrations (Donovan et al., 1997; Striggow et al., 2000; Vaughan et al., 1995). *In vivo,* injecting thrombin into the brain following ICH reduces oedema in rats (Hua et al., 2003) but also increases tumour necrosis factor alpha (TNF-α) expression which in turn was seen to exacerbate oedema (Hua et al., 2006b). The overall effect of thrombin on the progression of pathology in humans may be dependent on haematoma size, location and HE. Complement activation causes haemolysis in the brain (Hua et al., 2000) releasing free heme which is degraded into iron and carbon monoxide producing free radicals, causing oxidative damage to lipids, proteins and DNA in neurons (Garton et al., 2016; Huang et al., 2002). Iron overload from haemoglobin release is also linked to an increase of oedema as high concentrations in the brain increase aquaporin 4, the water channel most highly expressed on astrocyte foot processes that is essential for regulating brain water content (Qing et al., 2009). Iron can also contribute to long term brain tissue atrophy (Hua et al., 2006a). There is evidence to suggest that iron accumulation is associated with other neurological disorders that may follow ICH such as Alzheimer's disease and dementia (LeVine et al., 2004; Quintana et al., 2006). Clinical trials thus far targeting oedema have proven non beneficial (Lyden et al., 2007; Mayer et al., 2008; Misra et al., 2007; Poungvarin et al., 1987; Yu et al., 1992) and iron chelation recently proved futile (Selim et al., 2019; Yeatts et al., 2013).

The hematoma gradually clears over weeks-months however will often leave a fluid-filled cavity in the brain tissue (G. Wang et al., 2018). Patient rehabilitation has proven that neuronal plasticity after haemorrhage can be refined through training, and pre-clinical studies support this showing increased cellular mechanisms mediating necessary neuronal plasticity (Saulle and Schambra, 2016). Scar formation in the central nervous system (CNS) is attributed to glial cells, which surround the damaged area and prevent axonal regrowth by forming a physical and chemical barrier (Stichel and Müller, 1998). In two thirds of survivors this damage leads to disability such as speech and language disorders, hemiparalysis, epilepsy, cognitive impairment, and secondary psychological conditions (The Stroke Association, 2018).

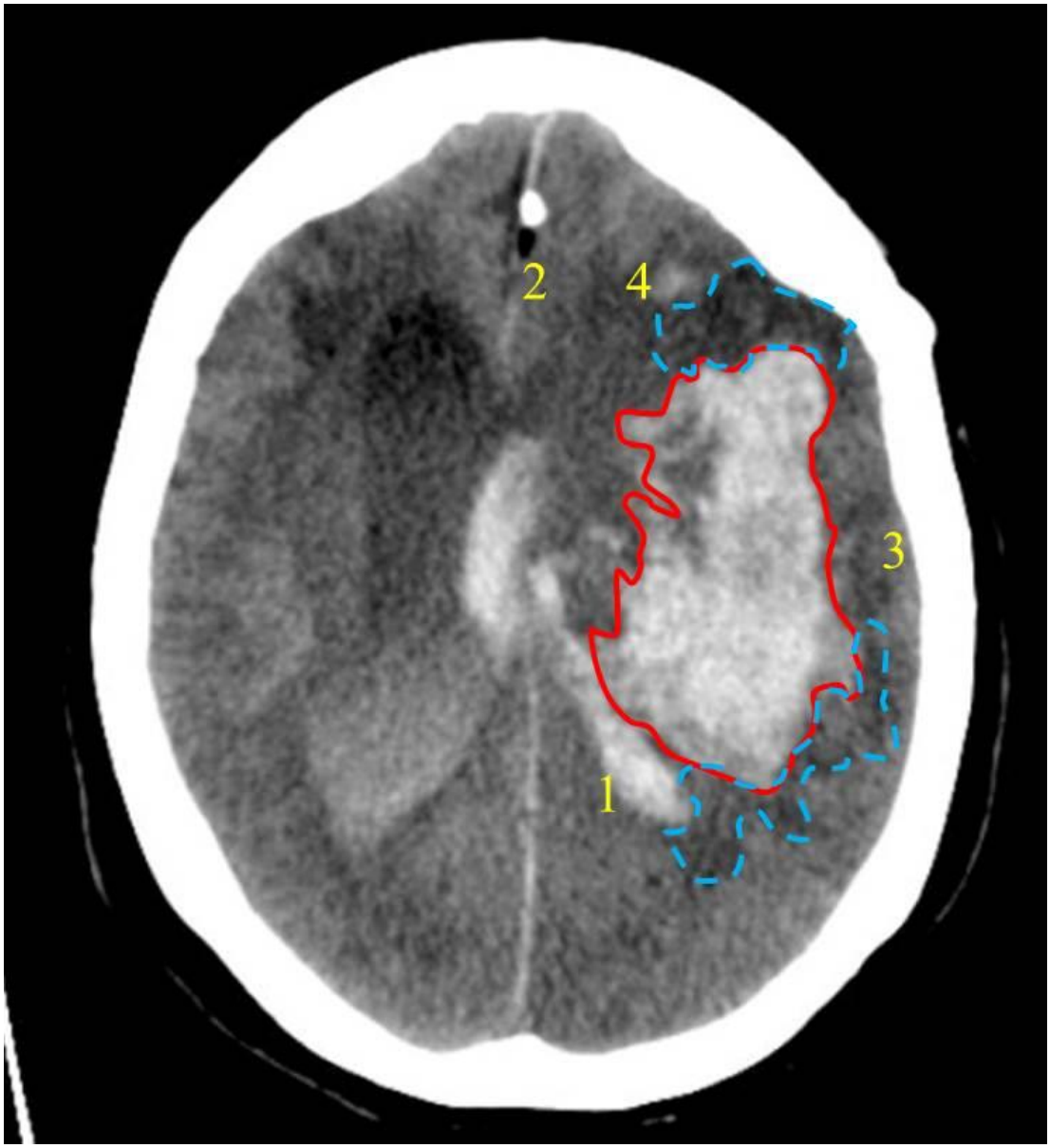

Figure 1.3.1 Non-contrast CT scan of an ICH shows extent of bleed damage and surrounding oedema (image from radiopaedia.org)

Primary injury of spontaneous blood vessel rupture seen on CT scan. ICH in the left cerebral hemisphere (red line) surrounded by a region of low density oedema (blue line). Blood has leaked into the lateral ventricle system (1 and 4) restricting normal CSF flow. Mass effect causes a midline shift (2) and loss of visible gyrated structure (3).

Secondary injury mechanisms (Figure 1.3.2), arising from an innate immune response to the blood compounds and necrotic tissue, are likely to be responsible for patient disability in cases that do not result in immediate death. Innate immune cells release pro-inflammatory cytokines promoting leukocyte migration from the periphery and contribute to overall oedema through extravasation into the brain. Microglia, the brain resident immune cells, respond to blood compounds and cellular debris within the injury site to initiate a signalling cascade of cellular recruitment. The innate inflammatory response has proven to be overall deleterious, for example by increasing oedema and the concentration of free radicals (Aronowski and Zhao, 2011). However, innate immunity is also vital for recovery and therefore modulating the immune response after ICH as a potential therapeutic strategy, needs to retain this fine balance (Mracsko and Veltkamp, 2014).

During an ICH endothelial cells, neurons, astrocytes and microglia are damaged by toxic blood factors and mechanical pressure within the swelling tissue, and release damage-associated molecular pattern molecules (DAMPs) (Veltkamp and Purrucker, 2017). DAMPs from apoptotic cells such as ATP, neurotransmitters and intracellular compounds (DNA, heat shock proteins, ribosomal proteins and cholesterol) bind pattern recognition receptors on cells and contribute to a sterile inflammatory reaction (Chen and Nuñez, 2010). Brain resident microglia are activated by these DAMPs in the first hour and exhibit a persistent response to the injury, releasing cytokines and chemokines to trigger further cell activation and migration to the site of injury (van Rossum and Hanisch, 2004). These molecules are carried in the circulation and activate more peripheral immune cells from the blood and spleen (Zhang et al., 2017). Microglia express Toll-like receptors (TLRs) that are stimulated by DAMP ligands and activate a phagocytic phenotype, removing dead cells and blood debris from the haematoma (Fang et al., 2013; Lin et al., 2012). Activation of TLR4 leads to the upregulation of downstream pro-inflammatory genes like nuclear factor-κB (NF-κB) which drives inflammation through cytokines interleukin (IL)-1α, IL-1β, TNF-α and IL-6. High expression of TLR4 on patient monocytes upon admission with an ICH has been associated with a poor outcome (Rodríguez-Yáñez et al., 2012) and therefore modulation of the TLR4 signalling in microglia may present a therapeutic target for secondary injury following ICH (Y.-C. Wang et al., 2013). Activated microglia and brain macrophages also release CXCL2 which acts as a chemoattractant for peripheral

leukocytes. Neutrophil extravasation through the BBB contributes to further oedema and an overall increase in ICP. Infiltrating leukocytes release more pro-inflammatory cytokines and matrix metalloproteinases (MMPs) to aid cell migration through tissue which catalyses the deleterious cascading immune response and peaks 3-4 days after injury (Xue and Del Bigio, 2000). Neutrophils have also been shown to release more reactive oxygen species (ROS) during brain injury and contribute to haemorrhage (Clark et al., 1996). An adaptive antigen-specific immune response is mounted 5-7 days later in which T-helper lymphocytes are seen in the peri-haematomal region. Evidence is lacking as to whether this delayed response is influential in regeneration and repair (Klebe et al., 2015). Later events involve the activation of astrocytes to clear the haemoglobin-derived product haemosiderin (Shivane and Chakrabarty, 2008).

The immune response to ICH can also be neuroprotective and therefore modulating cellular action must be finely balanced. Microglial phagocytosis of the haematoma is essential for clearing the mass and has been targeted therapeutically to protect from cellular damage in rodents (Zhao et al., 2007). Phagocytosis of blood debris and toxic compounds through scavenger receptor activation can stop the spread of damage and oxidative species (Taylor and Sansing, 2013). Microglia polarised to a neuroprotective phenotype by immune regulators IL-4 and IL-10, upregulate neurotrophic factors and scavenger receptor expression and decrease production of pro-inflammatory markers (Cherry et al., 2014). Microglia polarisation phenotypes are very plastic and can fluctuate with a change in cellular environments. Some studies reviewed by Cherry et al. have shown that in CNS injury or neurodegenerative disease immune modulators (IL-4, IL-10, galectin-3, TGF-β) that promote a neuroprotective microglial phenotype have been beneficial. In ICH alternative microglial activation as a therapy has only been investigated in animal models (Lively et al., 2016; Wu et al., 2016) but has proven favourable for outcomes and predicted to have beneficial action in patients (Klebe et al., 2015). Recovery from ICH is dependent on microglial activation and so inhibiting all responses may be detrimental and therefore must maintain equilibrium (Taylor and Sansing, 2013). Post stroke patients often exhibit inherent immunosuppression which leads to increased infection rates and worse outcomes in the long term (Shi et al., 2018). Immune responses represent a likely therapeutic target for improving stroke patient's outcomes, mitigating the deleterious inflammation and up regulating the neuroprotective and recovery mechanisms.

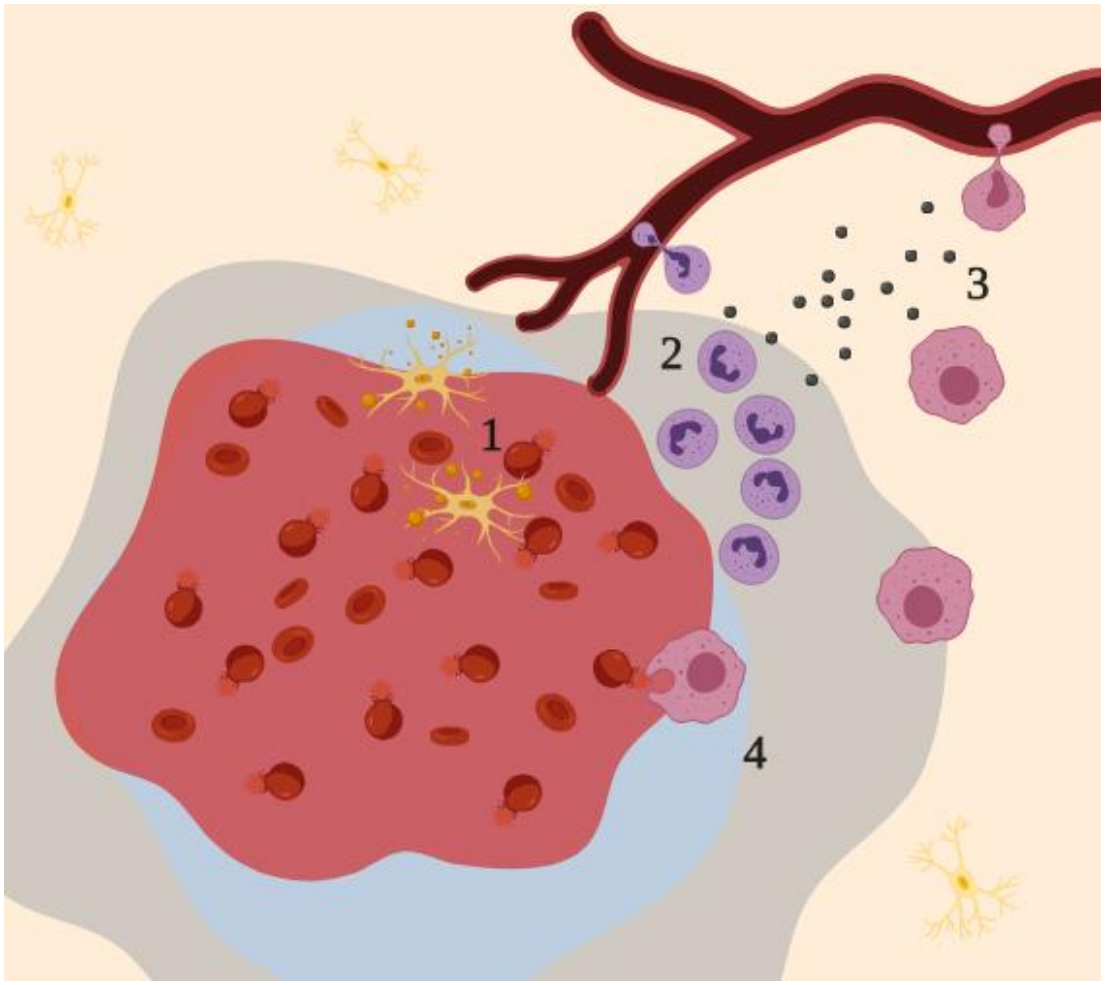

Figure 1.3.2 Diagrammatic representation of secondary injury pathology and immune response in ICH

The haematoma (red) in the brain parenchyma is surrounded by oedemic tissue (blue) and the spreading damage to healthy tissue (grey). Products of RBC lysis initiate an innate immune response to the bleed, microglia respond to DAMPs in the haematoma and release chemoattractant molecules (1). Peripheral neutrophils are recruited to the injury site contributing to BBB break down (2). Macrophages respond to IL-1β and migrate from the periphery into the parenchyma (3). Peripheral macrophages migrate into the tissue and phagocytose the debris in the haematoma (4).

1.4 Preclinical models of ICH

Over the past 30 years, animal models of ICH have advanced our understanding of clinical pathology and disease mechanisms. These models have mostly been developed in rodents as wide usage of these mammals for other biomedical research make easy accessibility of such a vast genetic and experimental toolbox (Ellenbroek and Youn, 2016). Practically, rodents are easy to handle, display injury behaviours like humans, have representative brain anatomy and can be genetically manipulated. Historically, rodent models have been well characterised in terms of aged co-morbidities and offer robust measures of neurological disease. The best, most accurate animal models resemble closely human disease in aetiology, biochemistry, symptomology and treatment (McKinney and Bunney, 1969). Mimicking all aspects of disease in one animal model is not feasible, thus leading to a multitude of rodent models of ischemic stroke being developed (Fluri et al., 2015). Each characterises different aspects of disease aetiology, to enable answering of specific research questions, but this development is lacking in the ICH field. Rodent models of comparable human neuroanatomy are limited in clinical relevance due to the low white matter content, fewer glial cells and a better capacity to accommodate a larger injury than humans (Treuting et al., 2017). Validating the use of rodent models is tricky in cerebrovascular disease because of the lack of translatability and therefore there is scope to develop new models to further understand ICH pathology.

The most commonly used rodent models for pre-clinical ICH study are direct injection into the striatum of autologous blood or bacterial collagenase to break down the basement membrane (Andaluz et al., 2002; Rosenberg et al., 1990), (MacLellan et al., 2010). A major limitation for these commonly used ICH models is that an invasive surgical procedure is required to initiate a cerebral bleed, rather than recapitulating the true spontaneous nature of vessel rupture seen in the human condition. Both autologous blood and collagenase models fail to exhibit key pathologies of human disease that would present likely targets for therapeutics. Autologous blood injection models mimic a mass of blood in the brain but do not involve vessel rupture and therefore lack HE. Collagenase breaks down basement membrane proteins that causes vessel rupture however lacks spontaneity and at high doses is directly neurotoxic, making it difficult to determine whether any neuroprotective strategies are due to the

presence of collagenase itself. Both models create consistent, hemispherical haematomas, which are good for evaluating differences in a laboratory setting. A rigorous battery of standardised behavioural tests can measure the effect of brain damage in rodents after a stroke (Schaar et al., 2010) but are not entirely comparable to the Glasgow Coma Scale used to determine severity in humans which uses verbal responses and eye opening as indicators of alertness (NICE, 2014). Rodents are far more accommodating of larger brain injuries than humans; with comparably less white matter volume, injuries can seem milder as there is a less significant loss of connectivity than in humans (Semple et al., 2013). Additionally, testing for deficits in humans is far more sensitive and therefore the smallest changes are apparent, as humans can communicate headache, dizziness, depression etc. that are difficult to detect in rodents. Also, surgically induced haemorrhages in rodents are not comparable to the size and position of a typical human haemorrhage (Manaenko et al., 2011) as they are created consistently in the same region and do not display the same morphological heterogeneity as human haematomas. Rodent models rarely exhibit other co-pathologies that contribute to disease in humans such as SVD, CAA or hypertension. In rodents, haematoma is seen to resolve by 21 days (Zhao et al., 2007) contrary to humans, in whom the timeline and bleed resolution contributes to much longer term pathological outcomes (Kitago and Ratan, 2017).

There have been some specific models of spontaneous ICH that do not require surgical intervention and are argued to reflect human pathology more closely, as summarised in Table 1.4.1. Unfortunately, although these models are more valid and represent the co-morbidities seen in humans, they present more practical problems such as increased variability in haemorrhage timing and location, higher cost, and higher mortality. Hypertensive models (Iida et al., 2005; Wakisaka et al., 2010) require long term changes to diet, drinking water and drug exposure, which increases the cost of model development and thus have lacked uptake in the pre-clinical community. Genetic models of Alzheimer's (Fisher et al., 2011) SVD (Van Agtmael et al., 2010; Weinl et al., 2015) CAA (Winkler et al., 2001), and metabolic disorders (Zinnanti et al., 2014) that exhibit spontaneous haemorrhage as secondary pathology, may present confounding influential factors over disease progression and are unlikely to make good ICH models as haemorrhage is inconsistently produced. Other models such as the neonatal rabbit (Lorenzo et al., 1982) and the aged squirrel monkey brains

(Elfenbein et al., 2007) are also unpredictable due to heterogeneous haemorrhage numbers and do not offer widely usable and informative models of ICH. Thus, the surgical intervention rodent models of ICH have become the most popular and ~100 articles (PubMed search 2019) are published every year investigating these models.

Table 1.4.1 adapted from Alharbi et al (2016) search terms. A summary of the spontaneous models of ICH, excluding any model that required a surgical intervention.

Author and year	Species	Age	ICH pathology	Disadvantages	Advantages	Induction method	Outcomes measured
(Elfenbein et al., 2007)	Squirrel monkeys	Aged (15-23years)	Co-morbidity related bleeds	Requires considerable aging and natural CAA development	Mimics an aged brain phenotype	Aged brains	CAA Aβ plaques, number of bleeds, vasculopathies
(Fisher et al., 2011)	Mouse	21mths	Microhaemorrhages, amyloid co-pathology	No HE, no loss of function tests	Mimics common co-morbidity	Tg2576 mutation	Number of microbleeds
(Iida et al., 2005)	Mouse	4-5mths	Location of bleed similar to human, bradykinesia, tremor	Requires high salt diet and Nω-nitro-L-arginine methyl ester treated drinking water	Models a common ICH co-morbidity/causation	Double transgenic hypertensive	Survival, blood pressure, histology
(Van Agtmael et al., 2010)	Mouse	Embryonic-9 month	Cerebral haemorrhage in pups, focal detachment of endothelium from basement membrane, reduced vessel homeostasis	20% viability at weaning	Mimics common co-morbidity	*Col4a1* missense mutants	Vessel histology, contractile strength, hypertension, blood volume, ER stress
(Kuramoto et al., 2010)	Rat (spontaneous dwarf)	18-36mths	Spontaneous death, more prevalent in females	Many co-morbidities, chronic neuropathy, posthumous analysis	Mimics an aged brain phenotype in a heterogenous population	Homozygous GH-deficiency	Gross pathology, number of cerebral bleeds
(Lorenzo et al., 1982)	Rabbit	Neonatal	Intraventricular bleeds	Only a 12.5% bleed rate	Mimics a paediatric ICH	Premature delivery	Survival, body weight, blood pressure, brain weight, histology
(Theriault et al., 2017)	Rat	Neonatal	Cerebral microbleeds and functional deficits associated with vaginal delivery	Ex vivo analysis, no hematoma, sex not recorded	Mimics a paedriatric ICH	Intrauterine ischemia at E19 and maternal LPS injection whilst in utero	Angiogenesis markers, collagen IV, number of microbleeds, neurofunctional analysis, myelination

(Wakisaka et al., 2010)	Mouse	8mths	Wide distribution of bleeds, size comparable to human condition, consistent, no use of genetic manipulation.	Ischemic lesions, no HE, short study duration, no neurological signs of damage	Models acute and chronic hypertension co-morbidities	Nω-nitro-L-arginine methyl ester treated drinking water and angiotensinII osmotic pump	Blood pressure, stroke incidence, ICH size, oxidative stress, MMPs expression
(Weinl et al., 2015)	Mouse	P5 pups and 4-6wk adults	Multiple cerebral-specific bleeds, found in cortex and deep brain in pups, larger volume haematoma in adults with neurodegeneration	Low survival rate with early deletion	Models SVD co-morbidity	Inducible endothelial cell deletion srf KO mice	Survival, functional behaviour, changes long term, BBB permeability
(Winkler et al., 2001)	Mouse	Adult and aged (20-28mths)	Co-morbidities, aneurysm, multiple recurrent bleeds,	Ex vivo analysis of bleed	Models CAA co-morbidity	CAA model of APP23 mutation	Size and number of bleeds, association with CAA
(Zinnanti et al., 2014)	Mice	4 weeks	Vessel dilation, increased venous blood pressure	Ischemia	Models GA1-related metabolic stroke independently from ischemia	Gcdh KO (GA1) mutation and protein-rich/lysine-rich diet	Neuromorphology, cerebrovascular abnormalities, number of bleeds.

It is therefore essential that new spontaneous models are explored, in different organisms, in order to support the understanding of ICH pathology and enable the identification of novel targets (Selim et al., 2018).

1.5 Replacement, reduction and refinement; the 3R's

In the UK the governmental framework for ethical animal research is defined by the 3R's; replacement, reduction and refinement. Any experimentation with protected species adheres to strict guidelines about how the animals are cared for, bred and applied in scientific investigation (ASPA, 1986 amendments 2012). As technology advances, where possible, it is essential to reduce the number of animals used for pre-clinical experimentation, whether by optimising the amount of data from one animal or using less animals for control and sham conditions with better planned experiments. Protected animal species can be replaced altogether by using appropriate *in vitro* and *in silico* techniques or by using non-protected species where possible and by generating directly translatable data from patient samples. In the cases where animal models are absolutely necessary, such as toxicology studies, then experimental technique and husbandry must be refined to minimise long term stress and suffering. Current pre-clinical ICH studies involve surgical procedures, potential suffering as a result of brain injury and increased likelihood of death. Genetic models require breeding colonies and result in unused offspring. Rodent studies are usually carried out in males only, to reduce the confounding factor of hormone differences in females and thus result in the termination of 50% unused animals. To continue pre-clinical study with a poor model of ICH, does not align with the 3R's framework and therefore development of alternative approaches is essential. This work investigates the validity of using zebrafish larval models, before protected status, to reduce the number of animals needed for pre-clinical ICH investigation.

1.6 Zebrafish as a model organism

Zebrafish (*Danio rerio*) are becoming an increasingly popular animal model for preclinical study of cerebrovascular disease (Walcott and Peterson, 2014). The cerebral vasculature is comparable in morphology and physiology to humans from early development. The zebrafish is a small vertebrate and offers many practical and scientific advantages over mammalian models which suggest this organism is suitable as an alternative species in which to model ICH. The current rodent models of ICH are costly, time intensive and are not amenable to large scale drug screening for identification of new drugs. An alternative approach may therefore elucidate new mechanisms and pathways to target for treating ICH pathology.

A single adult zebrafish pairing produces hundreds of offspring, providing a large sample size of genetically similar siblings suitable for high-throughput drug screening and assay techniques. Larvae are transparent and external embryogenesis makes genetic manipulation easy, allowing for the generation of numerous transgenic reporter lines. Prior to 5 days post fertilisation (dpf) larval zebrafish are not a protected species in the UK (ASPA, 1986 amendments 2012) so any genetic manipulation or experimentation is not procedural. Early development occurs rapidly and has been well characterised (Kimmel et al., 1995). By 24 hours post fertilisation (hpf) there is bilateral organisation of somites and notochord (figure 1.6.1). In wildtype fish, pigmentation begins at ~48 hpf at which point the heart, brain, somites and circulating erythrocytes are all visible by using non-invasive brightfield microscopy. Transparent adults that carry knock-out mutations to skin pigmentation genes enable non-invasive internal visualisation past the 48 hpf time point (White et al., 2008). Generating disease models using morpholino (MO) knockdowns and CRISPR technology to target orthologous disease specific genes has been exploited to establish a database of mutants for scientific investigation (Kettleborough et al., 2013). Furthermore, a vast range of transgenic reporter lines are available within the zebrafish research community that enable non-invasive *in vivo* imaging of internal cellular processes within the larvae. Zebrafish develop an innate immune system during initial haematopoietic stages to protect against infectious disease as adaptive immunity only matures 4-6 weeks after fertilisation (Willett et al., 1999). Zebrafish larvae are also suitable for behavioural studies, as they exhibit reflex reactions from hatching (48hpf) (Easter Jr and Nicola, 1996), thigmotaxis and hunting behaviours.

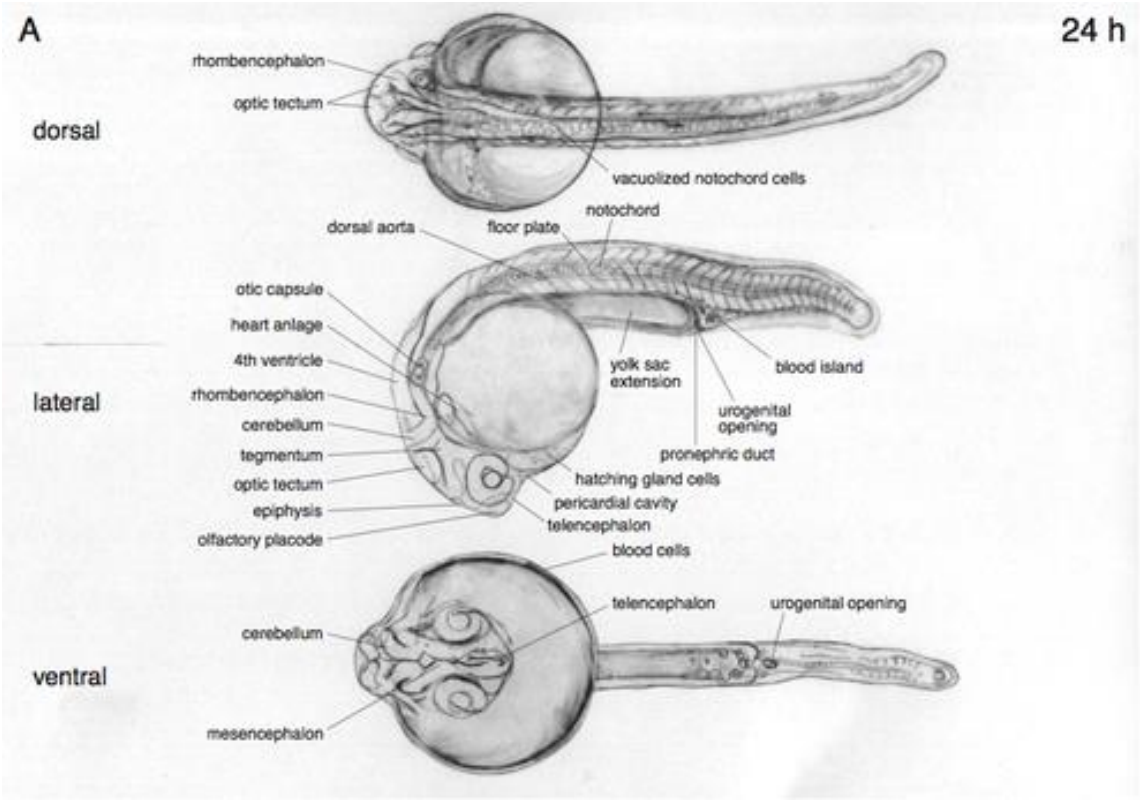

Figure 1.6.1 Visible embryogenesis in a 24 hpf zebrafish larvae
(Reproduced with permission from The Company of Biologists, Retrieved from http://www.biologists.com/development) Drawings of dorsal, lateral and ventral views of a 24 hpf developing zebrafish larvae. Structures that are visible with a compound microscope have been labelled (Haffter et al., 1996).

Zebrafish larvae are amenable to non-invasive chemical treatment by absorption of drugs introduced to the water, thus given their small size and abundance enables high-throughput drug screening (Wang et al., 2015). Non-invasive treatment and monitoring means pathological progression can be studied in real-time over all developmental stages. Zebrafish models have already been employed in research into cancer biology, infection, inflammation, cell biology and neurological disorders (Best and Alderton, 2008). Small molecule phenotype-based screens in zebrafish have contributed to drug discovery for a diverse range of diseases and have been utilised in repurposing existing drugs (MacRae and Peterson, 2015). For example dorsomorphin, a zebrafish-derived inhibitor of BMP signalling, has been shown in mammalian studies to treat hyperactive BMP signalling disorders (Paul et al., 2008a; Paul et al., 2008b). Currently in phase II trials, Prohema, a stabilised derivative of prostaglandin E2, was the first drug developed from zebrafish studies that passed phase I clinical trials and is used to enhance haematopoietic stem cell production in patients treated for leukaemia or lymphoma (Cutler et al., 2013; North et al., 2007) .

Thus far zebrafish studies have not been as successful in translational drug discovery for neurological disorders (Rennekamp and Peterson, 2015). However employing the advantages of a zebrafish model as a tool for experimentation can prove crucial to refining experimental technique for studying multi-systemic disease. Recently zebrafish have been used in a phenotype-based chemical screen to identify an anti-fungal drug miconazole as a potent brain haemorrhage suppressor (Yang et al., 2017). Researchers generated data from a large sample size of zebrafish embryos to show significant anti-haemorrhagic properties of their drug, verified by microscopy and whole-mount *in situ* hybridisation. As such, Yang et al (2017) have demonstrated the potential for zebrafish larvae to replace a rodent model in neurology research in order to reduce, replace and refine the use of animals in the laboratory.

1.7 Zebrafish preclinical models of human disease

With respect to human disease modelling, zebrafish possess genetic orthologues for 84% of human disease causing genes (Howe et al., 2013; The Wellcome Trust Sanger Institute, 2001). Zebrafish exhibit comparable biology and physiology with humans, similar early development and simple body systems (Mueller and Wullimann, 2015). Mechanisms and pathways are conserved not only across species but through

developmental stages also, making larvae convenient and valuable tools to model human diseases. Such models are not without limitations, as the speed of development, and the innate regenerative properties of zebrafish mean that recovery mechanisms differ vastly from human condition. The same limitations that separate rodents from clinical human condition also apply, the limited white matter content allow zebrafish to accommodate larger brain injuries than is possible in humans. Small organisms have practical husbandry advantages over mammals as they can be maintained in-house, and they are cost effective to house and feed. However, the small size of the zebrafish larvae means that they can absorb nutrients and water soluble molecules through their skin (Diekmann and Hill, 2013; Kanungo et al., 2014). The majority of the nutrients they need are absorbed from the endogenous yolk sac until 5 dpf which also contains maternal mRNA and is essential for early lipid processing (Fraher et al., 2016). These developmental features mean that individual microenvironments cannot always be tightly controlled. Zebrafish are relatively more outbred than lab mice strains, as there are more offspring from every pairing and have not been used as laboratory animals for as long. As a result, there is more genetic and experimental variation between individuals in a clutch. This individual variability more closely resembles the heterogeneity of the human population, and means much larger sample sizes are required than typically used in than rodent studies that are now widely recognised as underpowered (Button et al., 2013). A well powered experiment is essential for a high probability of detecting a difference from the null hypothesis.

Concerning the zebrafish immune system, there is a temporal separation between innate and adaptive response development and the fully mature immune system is not present until 4 weeks post fertilisation. Cells of the innate system are detectable at 1 dpf and larvae are excellent systems for investigating innate responses independent from adaptive responses to sterile and bacterial inflammation (Renshaw and Trede, 2012). Larval innate immune systems comprise mostly of neutrophils and macrophages that are capable of phagocytosing cellular particles and bacteria, and responding to wounds and infection sites (Novoa and Figueras, 2012). Primary immune responses involve TLRs and the expression of inflammatory cytokines; signalling pathways that are orthologous to human responses and that are well characterised (Renshaw and Trede, 2012; Trede et al., 2004; Zou and Secombes, 2016). Analysis of the teleost genome linage shows that a whole-genome duplication

occurred subsequent to mammalian divergence and retained duplicates of many immune genes offering functional innovation in zebrafish (Jaillon et al., 2004). Interleukin-1β, the master pro-inflammatory cytokine, has multiple copies in teleost fish; however other functional members of the IL-1 family in mammals (IL-1α, IL-33, etc.) are missing (Secombes et al., 2011). Mammalian IL-1β is made as a precursor molecule and cleaved for activation by caspase 1, shown to be the same mechanism in fish, though fish lack the conventional cleavage site for pro-IL-1β (Ogryzko et al., 2014b). It is unclear whether mature IL-1β in zebrafish is processed the same as in humans however evidence suggests that the diverse physiological functions stimulating inflammatory processes are conserved (Zou and Secombes, 2016). A simple and comparative immune system in early zebrafish larvae offers a useful and translatable model for pre-clinical ICH investigation of inflammatory consequences immediately subsequent to an ICH event.

1.8 Zebrafish stroke models

The aim for animal model development is to generate an imitation of the human pathophysiology via a non-invasive method that would cause the least amount of stress and suffering in as few animals as possible. Pharmacological agents can be used to induce a disease model, as they often have a wider range of targets in the organism to develop more complex phenotypes such as neurological disorders. Genetic mutations exhibited in human ICH pathologies can be replicated in the zebrafish using genome editing techniques so the model has an ICH phenotype similar to human disease. Both approaches to disease modelling can be employed in ICH research in zebrafish.

There have been zebrafish larval models published previously that exhibit defects in the developing cerebrovasculature that may have potential in ICH pre-clinical investigation. Zebrafish larvae exposed to atorvastatin (ATV) at 24 hpf display spontaneous brain-specific blood vessel rupture at the onset of circulation (~33 hpf) (Eisa-Beygi et al., 2013). Atorvastatin inhibits the 3-hydroxy-3-methyleglutaryl-CoA reductase (HMGCR) step in the cholesterol biosynthesis pathway, thus leading to a reduction in the cell membrane sphingolipid rafts essential for protein anchoring. A loss of cholesterol in these developing organisms results in a loss of tight junctions between the neuroendothelial cells and thus vessels are prone to leaking at the onset of outward haemostatic forces (figure 1.8.1). Specific pathway drug intervention

studies have employed the ATV model to reduce the risk of haemorrhage by stabilising the vasculature at early time points, inhibiting the internalisation of VE-cadherin and stabilising tight junctions (Huang et al., 2017; S. Li et al., 2017). Involved in a similar mechanism of action, a second, genetic based model of spontaneous cerebral blood vessel rupture identified by ENU mutagenesis is the *bubblehead* (*bbh*) model of vascular instability (Liu et al., 2007; Stainier et al., 1996). The *bbh* mutant exhibits a hypomorphic mutation in *arhgef7* (or *βpix*) that encodes a protein that regulates Rho GTPases, implicated in cytoskeletal remodelling (figure 1.8.1). Without adequate modelling of the actin cytoskeleton there is a loss of protein anchoring to the membrane, resulting in a loss of tight junction cadherin proteins from the cell surface. A second *bubblehead* mutant identified (bbh^{fn40a}) has been employed in similar intervention studies as the atorvastatin model, identifying miconazole by small molecule screen as a haemorrhagic suppressor (Yang et al., 2017). Similar to the *bubblehead* strain, the *redhead* zebrafish exhibits a hypomorphic mutation in *pak2a*, a kinase downstream of *βpix* involved in actin remodelling in angiogenesis (Buchner et al., 2007). Reduced expression of *pak2a* in rhd^{mi149} mutant zebrafish resulted in CNS haemorrhages at 2 dpf due to a loss of vascular integrity. Larval *notch3* mutant models of CADASIL syndrome have reduced expression of myelin basic protein and display stress-associated cerebral haemorrhage due to fewer oligodendrocyte precursor cells resulting in gaps in the vessel walls (Zaucker et al., 2013).

These models offer spontaneous, cerebral-specific bleed models that can be exploited in the reference of human ICH as a pre-clinical disease model. Currently there has been no study into the disease pathology in the zebrafish brain after an ICH, and all the current drug intervention studies aim to prevent haemorrhage from occurring and stabilise development rather than ameliorate pathology. Employing all the experimental advantages of zebrafish models may allow for non-invasive monitoring of the innate immune system, and large scale, rapid drug screening advancing our understanding of haemorrhage pathology.

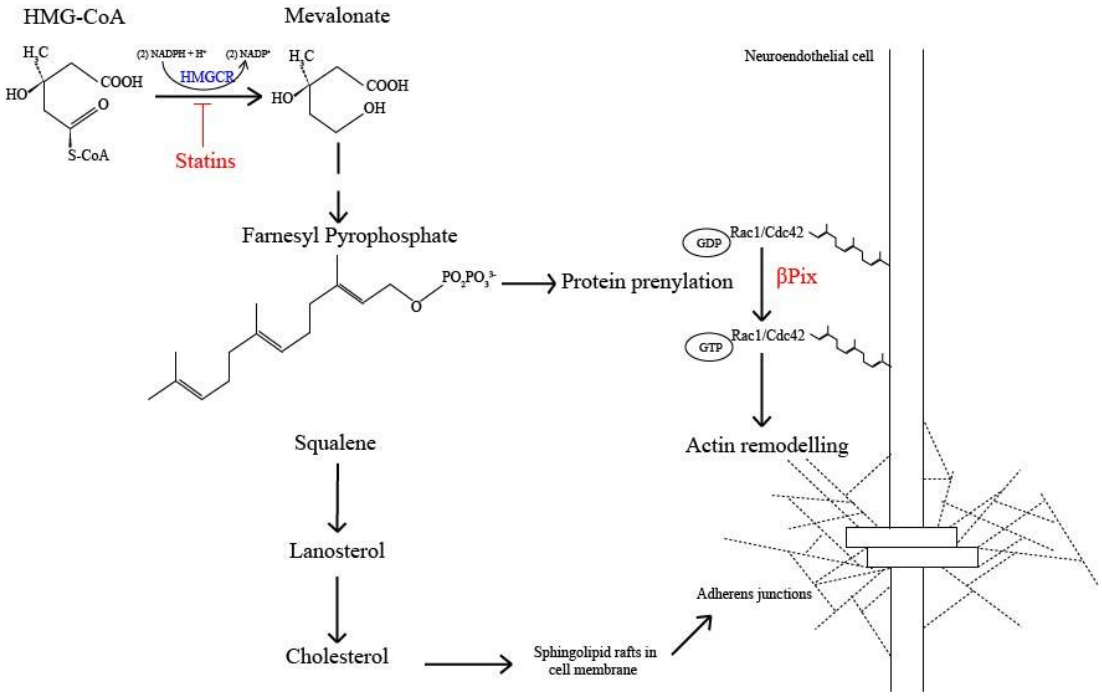

Figure 1.8.1 Mechanism of action of atorvastatin and the *bubblehead βpix* mutation

Statin-mediated HMG-CoA inhibition reduces overall cholesterol production, which effects tight junctions between endothelial cells by subsequently reducing protein binding rafts in the cellular membrane. *β-pix* mutation induces neurovascular weakness by preventing actin cytoskeleton remodelling and anchoring to the cell membrane. The weakness in formation of tight junctions results in 'leaky' endothelial junctions in the developing neurovasculature.

1.9 Summary

An ICH results in a devastating neurovascular attack and contributes substantially to global mortality and morbidity. Thus far, research carried out in rodent models has not contributed to an effective therapy for humans in the past 30 years, and experimental techniques used to create a brain bleed are invasive and classed as moderate interventions by the Animals (Scientific Procedures) Act (1986 amendments 2012). Priorities for pre-clinical ICH research outline the need for new spontaneous bleed models, consistent with human condition (Selim et al., 2018). Zebrafish larval models of cerebrovascular instability exhibit cerebral haemorrhages spontaneously and therefore may represent an alternative for a stable and clinically relevant model of ICH. Such a model will enable exploration of the immediate innate immune response in the context of ICH secondary injury *in vivo* as haemorrhage can be rapidly detected in the see-through animal. Practically, a zebrafish larval model would allow investigation into potential treatment approaches through non-invasive techniques. A reliable and reproducible model of spontaneous ICH is essential to understanding the causes of blood vessel rupture in human condition.

1.10 Aims

The zebrafish larva is a powerful experimental tool for neurological research, displaying genetic and physiological conservation with human and rodents. Currently in pre-clinical ICH research many questions remain, such as what other models could be developed to investigate aetiology? Do we understand the immediate innate immune pathology of ICH? Are there any therapies that target secondary injury mechanisms that result in better patient outcomes? Presently the available pre-clinical models cannot offer answers to these questions and therefore a priority for ICH research is to develop models of spontaneous ICH consistent with human characteristics (Selim et al., 2018).

The primary aim of this study is to characterise two of the existing zebrafish models of impaired vascular development in the context of human ICH, investigating disease pathophysiology after a bleed event. We hypothesise that by identifying specific pathologies comparable with human condition we can assay severity. Additionally, this study may identify pathways and mechanisms involved in causation or recovery from ICH.

Specifically, the aims of this work are to:

1. Validate the atorvastatin and *bbh* zebrafish larvae models of cerebrovascular weakness as spontaneous ICH models
2. Characterise the pathology associated with disease
3. Employ the model and assayable outcomes in a drug screen, to investigate whether interventions after a bleed has occurred have beneficial effects on injury
4. Investigate the factors in both models that contribute to the spontaneous nature of blood vessel rupture

The long-term aim is to establish the use of zebrafish larvae as a new model of brain haemorrhage in the stroke research community, providing an ethically more acceptable and rapid throughput system for future pre-clinical drug development.

Chapter 2: Materials and methods

2.1 List of reagents

Name	Protocol	Recipe
E3 Embryo media	Zebrafish husbandry and embryo collection	4% Instant ocean, 500µl methylene blue in 1L Milli-Q H_2O
4% MS222	Larvae termination, light sheet microscopy	2g Tricaine, 10.5ml Tris (pH 8.0) in 500ml Milli-Q H_2O
0.02% Phosphate buffered saline (PBS)-Tween		1 tablet PBS per 200ml Milli-Q H_2O, and 200µl Tween-20
4% paraformaldehyde (PFA)	Fixing embryonic tissue	10ml 16% PFA (Alfa Aesar) in 30ml PBS
SZL Buffer	DNA extraction	25ml 1M KCL, 1.25ml 1M $MgCl_2$, 5ml 1M Tris (pH 8.3), 2.25ml NP40, 2.25ml Tween-20, 50ml Gelatine 0.1% in 500ml Milli-Q H_2O.
Orange G Loading Dye	Gel electrophoresis	4ml 100% glycerol, 1ml Orange G loading dye in 10ml Milli-Q H_2O
50X TAE Buffer	Gel electrophoresis	121g Tris base, 50ml 0.5M EDTA (pH 8.0), 28.5ml acetic acid in 500ml Milli-Q H_2O
Pigment Bleach	Whole-mount *in situ* hybridisation, immunofluorescence and staining protocols	500µl formamide, 3.3ml of 30% H_2O_2, 250µl of 20X SSC into 5.6ml Milli-Q H_2O

O-dianisidine stain	Haemoglobin stain	6mg o-dianisidine, 4ml of 100% ethanol, 100µl 1M sodium acetate (pH 4.5), 210µl 30% H_2O_2 into 5.69ml Milli-Q H_2O
Hybridisation + buffer	Whole-mount *in situ* hybridisation	25ml Formamide, 12.5ml 20X SSC, 460µl 1M citric acid, 250µl Tween 20, 0.5ml 50mg/ml tRNA, 25µl heparin and 11.25ml Milli-Q H_2O
Hybridisation – buffer	Whole-mount *in situ* hybridisation	25ml formamide, 12.5ml 20X SSC, 460µl 1M citric acid, 250µl Tween 20, and 11.8ml Milli-Q H_2O
BCL buffer	Whole-mount *in situ* hybridisation	2.5ml 1M Tris (pH9.5), 500µl 5M NaCl, 1.25ml 1M $MgCl_2$, 125µl Tween 20 in 25ml of Milli-Q H_2O
MAB-Tween	Whole-mount *in situ* hybridisation	5ml 1M maleic acid, 1.5ml 5M NaCl, 50µl Tween 20 in 50ml Milli-Q H_2O (pH 7.5)
Tris-EDTA	Immunohistochemistry	1.21g Tris, 0.37g EDTA in 1L Milli-Q H_2O (pH8.6 and pH9.0)
Sodium Citrate	Immunohistochemistry	2.94g trisodium citrate in 1L Milli-Q H_2O (pH6.0)
TNT	Immunohistochemistry	50ml 100mM Tris (pH7.5), 15ml 5M NaCl, 250µl Tween 20 in 500ml Milli-Q H_2O

Primary antibody buffer	Immunohistochemistry	1.5ml Triton-X, 5g BSA, 25µl sodium azide into 500ml PBS
PBDT	Whole-mount Immunohistochemistry	1% DMSO, 1% BSA, 1% Triton X, 5% goat serum in 1X PBS
IL-1Ra vehicle	IL-1Ra injection	1.29g sodium citrate, 5.48g sodium chloride, 0.12g disodium EDTA, 0.7g Polysorbate 80 into 1L Milli-Q H_2O at pH 6.5

2.2 List of primers

Name	Sequence
il-1β	F: TGGAGATGTGGACTTCGCAG R: AGCTTCTGGTTCATGCAGAC
ch25h (WISH)	F: GCATGGATCCATGTTTGGACTACAGCACATCT R: GGCCGAATTCTCATTCAAAGTGCAGTGTCC
bbh ^{m292}	F: GGGACAAGCAGACAGCTCAT R: CAGATCACCTGGATCCGCTC
il-1β (WISH)	F: ATGGCATGCGGGCAATATGA R: CTAGATGCGCACTTTATCCT
nephrin (WISH)	F: TCCGCCCAAACCAAATTCAG R:GGATCCAATTAACCCTCACTAAAGGGCTCGCAGGTGATTTCGTCTG

2.3 Zebrafish

2.3.1 Zebrafish husbandry

Zebrafish were raised and maintained at The University of Manchester Biological Services Unit under standard conditions as previously described (Westerfield, 2000). Adult zebrafish are housed in tanks with a recirculating water supply at 28°C under a 14/10 hour light/dark cycle. All adult husbandry was approved by the University of Manchester Animal Welfare and Ethical Review Board. All experiments were performed in accordance with U.K. Home Office regulations (PPL:70/9091 and PPL: P132EB6D7).

2.3.2 Zebrafish strains

Transgenic lines used in this study include macrophage-specific lineage Tg(*mpeg1:*GAL4-Vp16/UAS:nfsB-mCherry) (constructed in-house as previously described (Ellett et al., 2011)), neutrophil-specific Tg(BAC*mpo:*GFP)^{i113} (Renshaw et al., 2006), erythroid-specific Tg(*gata1:*dsRed) (Traver et al., 2003), endothelial cell specific Tg(*fli1*:EGFP)^{y1} (Lawson and Weinstein, 2002) and Tg(*ubiq:*secAnnexinV-mVenus), a reporter for apoptosis (re-derived in house (Morsch et al., 2015)) on wild-type, nacre (*mitfa*$^{w2/w2}$*)* and mutant (*bbh*^{m292}) backgrounds.

2.3.3 Embryo collection

Fertilized embryos were collected from natural spawning and incubated at 28°C in standard E3 embryo medium and staged according to standard guidelines (Kimmel et al., 1995). At experiment end zebrafish larvae were terminated prior to protected status using a lethal dose of MS222 anaesthesia and freezing. Larvae older than 5 dpf were schedule 1 terminated with a lethal dose of MS222 and death confirmed by maceration.

2.3.4 Embryo dechorionating

From 24 hpf embryos were dechorionated for drug treatment or injection. Using two pairs of ultra-sharp dissection forceps (Agar Scientific AG502) the chorion was cut open and removed from the dish. The embryos were then transferred to drug treatment plates, or control plates.

2.3.5 ICH models – Atorvastatin

For the ATV model, nacre or transgenic embryos were dechorionated at 24 hpf and transferred to clean petri dishes in E3 embryo medium. ATV (Merck PZ0001) was solubilised in distilled water to a stock concentration of 0.5mM. Embryos (n=60-100) were treated with a final concentration of 1μM ATV through water bath incubation at 28°C for 24 hours and equivalent numbers were left as untreated controls. A proportion of ATV-treated embryos did not develop ICH and therefore these animals were used as controls for the treatment (ICH-) alongside untreated (UNT) siblings. Embryos with evident brain haemorrhages (ICH+) were separated from non-haemorrhaged (ICH-) siblings at ~52 hpf for downstream analyses.

2.3.6 ICH models – *Bubblehead*

For the *Bubblehead* (*bbh*) line (Liu et al., 2007), embryos were obtained from adult in-crosses from heterozygous *bbh*^{m292} mutant animals (maintained on wild type and transgenic reporter backgrounds). Embryos with evident haemorrhages (ICH+) were separated from non-haemorrhaged (ICH-) siblings at ~52 hpf for downstream analyses.

2.3.7 Experimental powering

Experimental power for the sample sizes were determined assuming 5% significance and 80% power and 2-sided differences. For cell death investigation the standardised effect size was found to be 0.8 based on a sample size of n=6-8 for 3 replicates. For motility assay the standardised effect size was found to be 0.5 based on a sample size of n=24 for 3 replicates.

2.3.8 Head injury

Larvae at 2dpf were anaesthetised using 0.02% MS222 until cessation of movement. With a bevelled glass capillary needle a single stab injury was induced into the midbrain (adapted from (Schmidt et al., 2014). Control larvae groups were anaesthetised for equivalent time however no injury was induced. Larvae were washed into fresh E3 embryo media and allowed to recover. At 1, 2 and 5 hours post injury (hpi) whole larvae were harvested and tissue fixed in 4% paraformaldehyde for 4 hours at RT or RNA extracted using Trizol protocol (2.9.1).

2.3.9 Locomotion assay

Locomotion was measured at 120 hpf to determine if ICH resulted in a physical phenotype. To remove locomotor function bias (ie. always selecting the slowest moving individuals) larvae were briefly anesthetised at 72 hpf using 0.02% MS222 in embryo water and selected at random for plating. Following recovery, n=24 larvae were individually transferred to each well of a 24 well plate in 1 ml of fresh methylene-blue free E3 medium. Cumulative time spent mobile was measured using the DanioVision camera chamber and Ethovision XT software (Noldus version XT 11) at room temperature. Analyses were performed on larvae at 72, 96 and 120 hpf. Swimming movement of each individual larva was tracked in the x and y plane for 10 minutes using a white light stimulus to initiate a startle response every 60 seconds. Cumulative time spent swimming was measured from 3 independent replicates.

2.3.10 Light sheet microscopy

Transgenic ICH+ and ICH- larvae were imaged using light sheet microscopy to analyse apoptotic cell death (*ubiq:*secAnnexinV-mVenus), neutrophils (*mpo:*GFP) and macrophages (*mpeg1:*mCherry). At ~72 hpf, randomly selected larvae were anaesthetised using 0.02% MS222 and mounted in 1.5% low-melt agarose (Promega), maintained at room temperature. Images were acquired using a W Plan-Apochromat 20X/1.0 UV-VIS objective for light-sheet microscope (Carl Zeiss Lightsheet Z.1) and processed with ZEN imaging software (version 2.3). Maximum intensity projection (MIP) composites were generated from z-stack images and brain regions (excluding the eyes) were analysed for average intensity fluorescence of cells with image background removal using an ImageJ (version 1.52a) macro (appendix i). Numbers of fluorescent cells in the brain were also verified by blind manual counts from MIPs. Data were collected from n=6-12 randomly selected larvae per group from 3 independent replicates for ATV studies and verified in 2 replicates for *bbh*. For time-lapse recording, MIP composites were stitched from a series of successive z-stack images over a period of 18 hours.

2.3.11 Analysis of blood flow

Embryos between 24 and 72 hpf were analysed for blood flow rate following IL-1Ra treatment. Larvae were anaesthetised in MS-222 and mounted in the light sheet microscope in 1.5% low melt agarose. Brightfield was used to focus on the blood flow in the head and a 30s recording was made using OBS Studio screen capture software

(version 23.0.2). Regions of interest were selected using the DanioScope (Noldus version 1.1) software over the head circulation (mesencephalic vein) and analysed for flow percentage and heart rate.

2.3.12 Total cholesterol analysis

Bubblehead embryos were injected with 1nl water and with cholesterol at 1mg/ml at 2 dpf and then taken for total cholesterol analysis using Abcam HDL and LDL/VDL Colourimetric Cholesterol Assay Kit (Ab65390) according to manufacturer's instructions for tissue lysates. 100 embryos were homogenised using Kontes Dounce tissue grinders (885300-0002) 10 times in 100µl of cholesterol assay buffer and tissue debris pelleted. 30µl of supernatant for each sample was made to 50µl with assay buffer and then mixed 1:1 with the assay reaction mix. Samples were plated in duplicate in a clear bottom 96 well plate (Corning Costar), incubated for 1 hour at 37^{o}C in the dark and absorbance read at 570nm on a FLUOstar Omega plate reader (BMG labtech).

2.3.13 Statistical analysis

All data was analysed using Graphpad Prism (v7.0) or R (R Core Team, 2018) for non-parametric data and analysis of batch variation. Data presented as mean +/- s.d. unless stated otherwise.

2.4 Drug treatments

2.4.1 Preparation of injection plates

A 4% agarose gel was made in 50ml of E3 embryo media and poured into a 90mm petri dish (Thermo Scientific). Plastic groove moulds (Adaptive Science Tools) were placed on the surface of the agarose and left to set at room temperature. For manipulation of larvae beyond the 1 cell stage, no groves were made in the agarose and plates were left to dry flat. Once set, E3 embryo media was added to the dish to prevent the agarose drying out and plates stored at 4°C.

2.4.2 Embryo injection – IL-1Ra

At 72 hpf larvae were injected into the hindbrain with 100mg/ml of IL-1Ra (Anakinra, Kineret®, SOBI). Larvae were separated into ICH- and ICH+ groups from ~52 hpf. Larvae were anesthetised using 0.02% MS222 and plated onto a flat agarose mould at room temperature. Using a glass microneedle, 1nl of IL-1Ra or a water control was injected into the hindbrain ventricle. Following injection the larvae were moved into fresh E3 medium to recover from anaesthesia.

2.4.3 Embryo injection – Cholesterol

Fertilised embryos were collected from breeding pairs and mounted on a grooved injection plate. Using a glass microneedle 0.5-5nl of water soluble cholesterol (C4951 Merck) or a water control was injected into the yolk sac before the 2-cell stage. Embryos were moved into fresh E3 embryo water.

Larvae from 1 dpf were dechorionated for injection. Larvae were anesthetised using 0.02% MS222 and plated onto a flat agarose mould at room temperature. Excess liquid was removed to allow water tension to hold the larvae. Using a glass microneedle 0.5-5nl of water soluble cholesterol (C4951 Merck) or water control was injected into the yolk sac. Following injection the larvae were moved into fresh E3 medium to recover from anaesthesia.

2.4.4 Deferoxamine treatment

Deferoxamine (DFO) (Merck) was solubilised in distilled water to make a stock concentration of 50mg/ml. Larvae were separated for ICH- and ICH+ groups from ~52 hpf and plated in a 6 well plate in 10mls of E3 embryo media. A volume of 13µl of DFO was added to the media in each well for a final dilution of 100µM.

2.4.5 Miconazole treatment

Bubblehead heterozygous and homozygous mutants and wildtype (WT) siblings were treated with miconazole (Fluorochem) at 10 and 12.5µmol in 1% DMSO from 6 hpf until 24 hpf. Larvae were transferred into fresh embryo water. WT larvae were treated with 1.5µM ATV to induce ICH. RNA was extracted at 2 and 3 dpf for qPCR analysis (2.9.3). Remaining larvae (n=9 per group) were stained for haemoglobin. The experiment was repeated with *bbh ubiq:*secAnnexinV-mVenus in order to analyse brain cell death and locomotion.

2.4.6 25-hydoxycholesterol treatment

Bubblehead heterozygous and homozygous mutants and wildtype (WT) larvae were treated with 25-hydoxycholesterol (25-HC) (Sigma) at 50µg/ml in 1% ethanol pre and post haemorrhage. Larvae were transferred into fresh embryo water. WT larvae were treated with 1.5µM ATV to induce ICH. RNA was extracted at 2 and 3 dpf for qPCR analysis (2.9.3). Remaining larvae (n=9 per group) were stained for haemoglobin (2.7.5) or for dying cells using acridine orange (2.7.6). The experiment was repeated with *bbh ubiq:*secAnnexinV-mVenus in order to analyse brain cell death using light sheet.

2.4.7 DMSO dose response

Wildtype AB larvae were treated with increasing doses of DMSO at 24 hpf. Larvae were plated n=30 per well into a 6 well plate with 10 ml of E3 embryo media. DMSO was added at 0.001%, 0.01%, 0.1% and 1% and one well left untreated. At 72 hpf larvae were collected for RNA extraction and qPCR analysis (2.9.3).

2.4.8 Drug screening

Bubblehead homozygous *ubiq:*secAnnexinV-mVenus positive larvae were confirmed for ICH+ at 2 dpf and dechorionated using ultra fine forceps. The Spectrum Library (MicroSource Drug Systems Inc.) consisting of 25x 96 well plates with 2.5µl of 2.5mM drugs in DMSO was acquired from the University of Sheffield. Drug plates were defrosted to room temperature and 1µl removed into clean 96 well plates. 99µl of embryo water without methylene blue was added to each well and thoroughly mixed. In columns 1 and 12 1µl of DMSO was added as a control to each well. Larvae were plated n=3 to wells A2 – H12 and ICH- *ubiq:*secAnnexinV-mVenus nacre controls plated in A1 - A12 (figure 2.4.1). At 3 dpf larvae were screened for cell death

clusters in the brain, cranial oedema and overall health. Drugs with a positive outcome were repeated using n=5 larvae in 150µl with the remaining volume of DMSO.

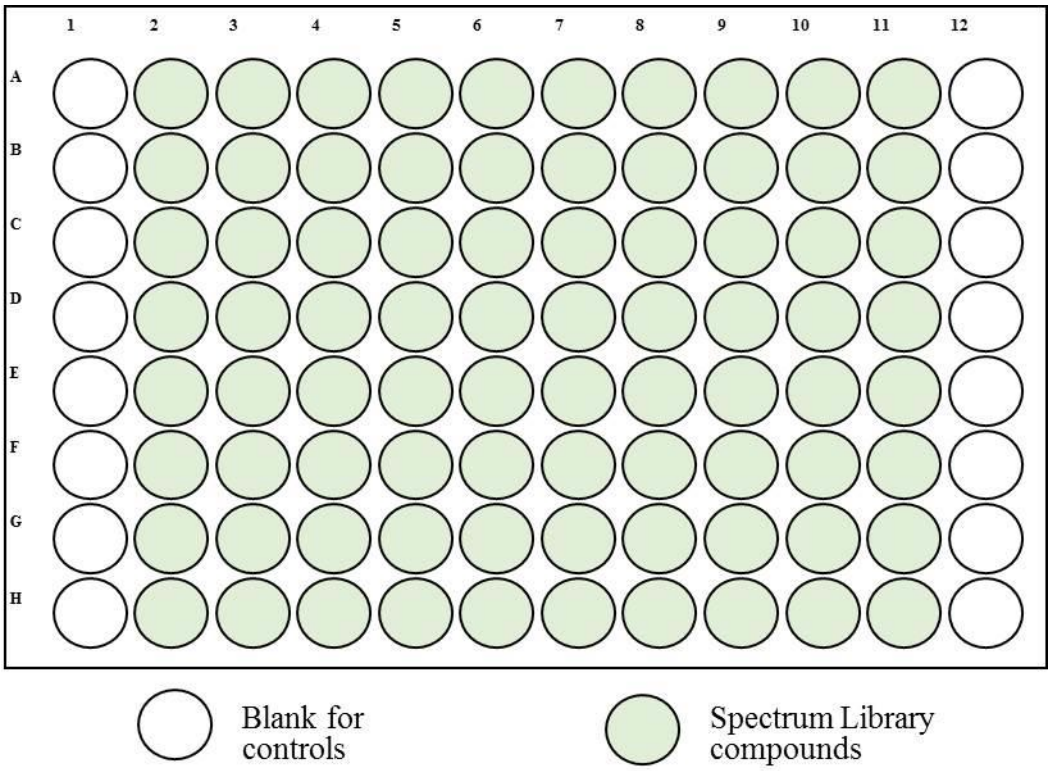

Figure 2.4.1 Example plate layout for the Spectrum Library drug plates

2.5 Designing an antisense RNA probe for *ch25h*

2.5.1 Primer design

Zebrafish *ch25h* gene sequence (Ensembl ENSDARG00000045190) was analysed for forward and reverse primer design for the single exon (appendix ii), using Primer3 (primer3.ut.ee version 4.1.0) and blast ncbi as illustrated in figure 2.5.1.

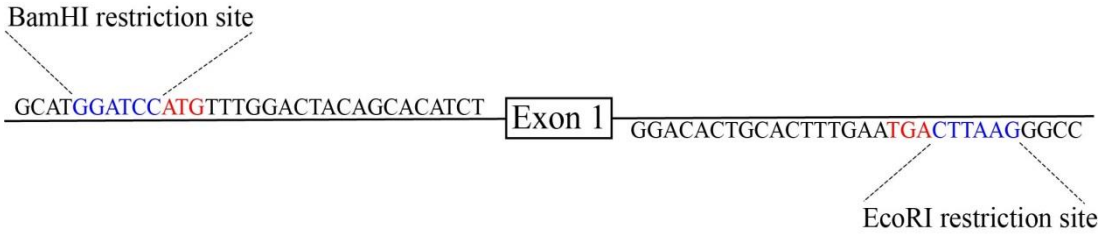

Figure 2.5.1. Primer design for *ch25h* WISH probe.
Forward and reverse primers were designed to flank exon 1, the only coding exon in *ch25h*. Restriction sites for BamHI and EcoRI were added to the 5' ends of the forward and reverse primers respectively in order to isolate the fragment with sticky ends for ligation into the pcs2+ plasmid.

2.5.2 Cloning plasmid

A pcDNA3.1+ plasmid containing the full length *ch25h* cDNA (GenScript) was purchased containing ampicillin resistance gene site.

2.5.3 Transformation

A pcDNA3.1 plasmid containing the *ch25h* gene (GenScript), and the PCS2+ DNA vector were amplified using a transformation of *E.coli* cells. One Shot Top10 chemically competent *E.coli* (Thermo Fisher #C4040-03) were heat shocked for 45 seconds at 42^{o}C and 1µl of plasmid DNA was added. *E.coli* were plated on 100µg/ml ampicillin plates overnight at 37^{o}C according to manufacturer's protocol. Single colonies were selected and were cultured in LB broth containing 100µg/ml ampicillin overnight in a shaking incubator to amplify.

2.5.4 Isolation of DNA (miniprep)

Plasmid DNA was extracted using the GenElute plasmid miniprep kit (Sigma PLN350) following manufacturer's instructions, eluted into 30µl dH_2O and quantified using the nanodrop (Thermo Scientific).

2.5.5 PCR amplification and extraction of plasmid DNA

Isolated pcDNA3.1+ *ch25h* plasmid was used to amplify gene of interest region using the primers containing BamHI and EcoR1 sites as previously outlined (2.5.1) (Eurofins). PCR amplification was performed using a 68-58^{o}C Touchdown program with high fidelity Phusion Taq polymerase (Thermo Fisher) on a thermocycler (G-Storm) to reduce off target primer binding. PCR product was run on a 1.5% gel using 150µl wells to pool and purify the insert and isolated from the gel using QIAquick gel extraction and PCR clean up kit (Qiagen)

	Step	Temperature (^{o}C)	Time (s)
1	denature	98	40
2	touchdown anneal	68-58	40
Repeat 10 cycles			
3	denature	98	40
4	anneal	63	30
5	elongate	72	120
Repeat 35 cycles			

6	elongate	72	600
7	hold	10	-

2.5.6 Digest

PCS2+ plasmid and *ch25h* DNA from PCR product was incubated at 37ºC for 1 hour with restriction enzymes EcoR1 and BamHI (New England Biolabs) to linearise. Alkaline phosphatase (New England Biolabs) was added for 30 minutes to prevent re-ligation of sticky ends. Cut plasmid product was run on a 1.5% gel to check for full linearisation. Digested products were isolated from cut fragments using the QIAquick gel extraction and PCR clean up kit (Qiagen).

2.5.7 Ligation reaction

PCS2+ plasmid DNA and *ch25h* complementary DNA (cDNA) insert were incubated for 1 hour at RT with T4 DNA ligase (Promega, pGEM-T easy vector systems) at ratios 1:2 to 1:5 to join the cut plasmid to the *ch25h* fragment. Different restriction sites ensured correct insertion orientation. Complete plasmid was amplified using a transformation step and miniprep isolation and sequence verified using Sanger sequencing with an SP6 primer (Genomic Technologies core facility, The University of Manchester) (figure 2.5.2).

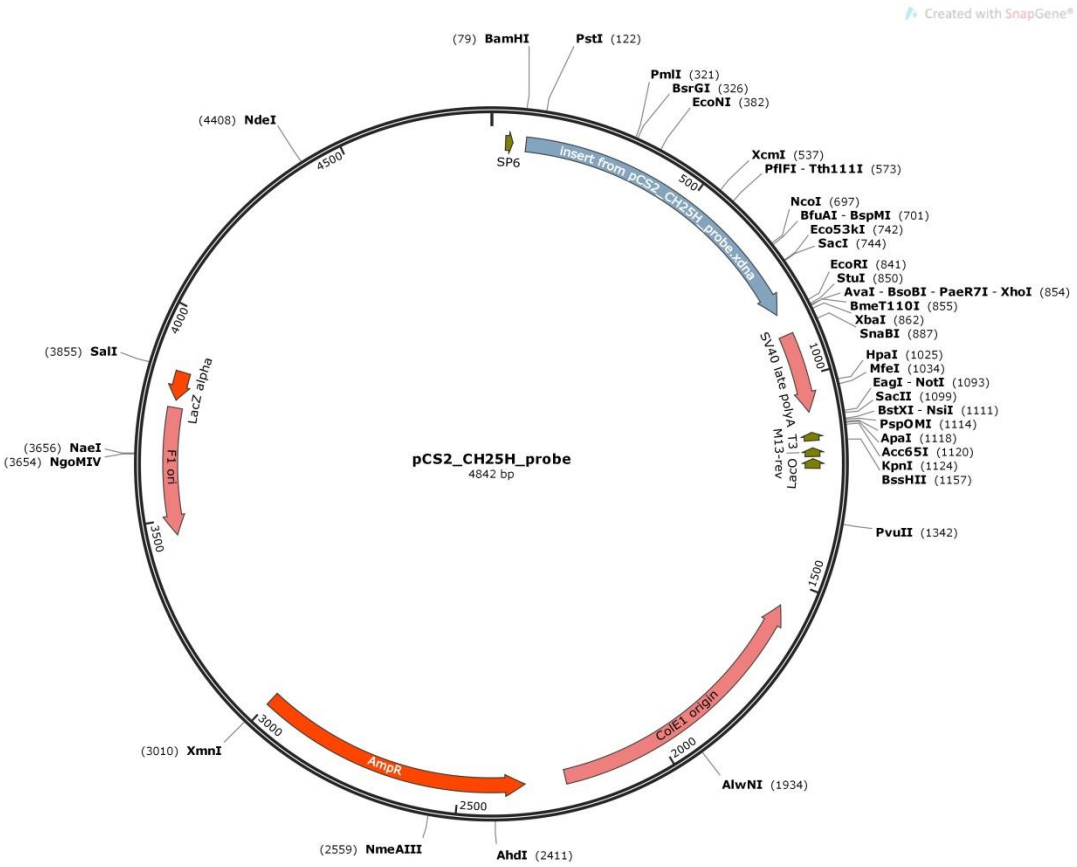

Figure 2.5.2 PCS2+ vector with *ch25h* gene insert

2.5.8 Synthesis of DIG-labelled RNA probe for WISH stain

10µg of *ch25h* pcs2+ plasmid was linearised using BamHI restriction enzyme and DNA was transcribed to mRNA using a T7 polymerase and labelled with DIG using manufacturer's instructions (Sigma) in a 20µl reaction for 2 hours at 37ºC (figure 2.5.3). RNase inhibitor was added to prevent immediate degradation of product and residual DNA was degraded using DNaseI for 15 minutes. Reaction was stopped with 2µl of 0.5M EDTA and diluted into 50µl with RNase-free H_2O. RNA was purified using QIAquick gel extraction and PCR clean up kit (Qiagen) according to manufacturer's instructions. The final probe was run on a 3% gel and quantified using the nanodrop (Thermo Scientific).

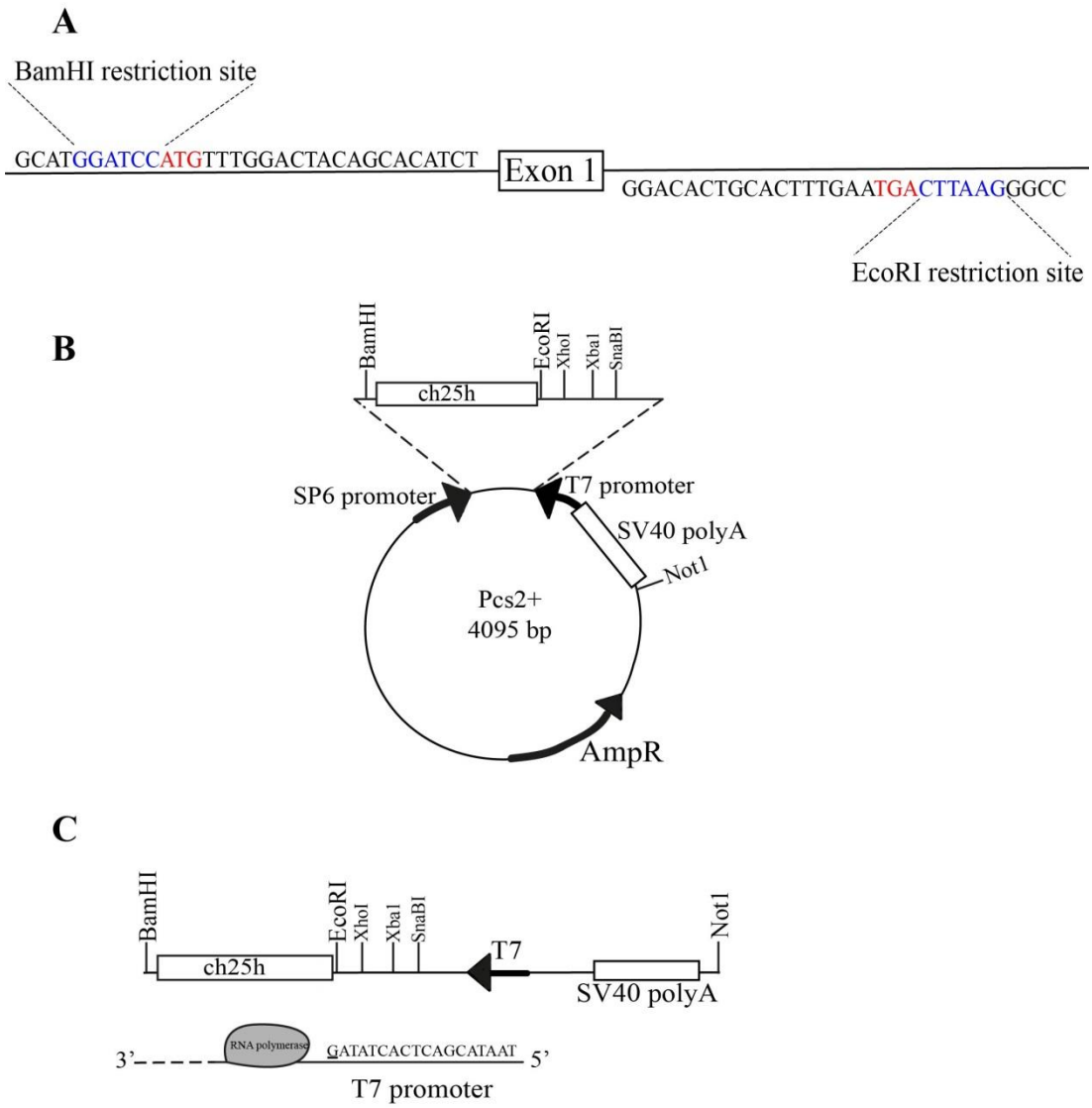

Figure 2.5.3. The process of generating an antisense RNA probe from plasmid DNA.

(A) PCR amplification isolated the coding region of *ch25h* with primers designed to have restriction sites. A digestion reaction resulted in the formation of sticky ends at the specific cut sites. (B) Sticky ends allow for the fragment to be ligated into the pcs2+ plasmid, digested with the same enzymes, in the correct orientation. (C) Plasmid DNA was digested with BamH1 to linearise the DNA and using a T7 specific promoter, RNA polymerase transcribes an antisense RNA sequence for *ch25h.*

2.6 Genotyping

2.6.1 Fin clipping

Adult fish were anaesthetised using 0.02% MS222 and the tip of the caudal fin was removed using a scalpel. Fish were returned to recover in fresh system water and monitored for recovery signs. Adult fish were then kept in single housing genotyping trays for 3-5 days for genotyping results and were subsequently housed accordingly

2.6.2 DNA extraction and amplification

Adult fin clip or single embryos, were collected and DNA extracted using SZL buffer and Proteinase K at 100ng/ml. DNA was amplified with ready-made Master Mix (Thermo Fisher) and forward and reverse primers at 10µg/ml (Table 2.2) using a 68-58^{o}C Touchdown program for 35 cycles in a thermocycler (G-Storm) (2.5.5)

2.6.3 Gel electrophoresis

PCR product was separated on an agarose gel. For products >200bp 1.5% agarose into 100ml of 1X TAE buffer gel was made. SafeView (NBS Biologicals Ltd) dye was added to enable DNA visibility. Gel moulds were set and samples loaded into wells using 2X orange G loading dye. Samples were separated for ~30 minutes at 120V and imaged under a UV transilluminator (Alpha Innotech).

2.6.4 Sequencing

Bubblehead mutants were genotyped by sequencing reaction. PCR product was purified using ExoSap (Exonuclease I ThermoScientific, Shrimp Alkaline phosphatase Amersham Biosciences) 1:5 and incubated for 15 minutes at 37^{o}C. Big Dye terminator reaction (Thermo Fisher) was used to sequence PCR product according to manufacturer instructions and using forward primers only. The reaction was run for 26 cycles of 96^{o}C, 50^{o}C, 60^{o}C. The reaction was cleaned using 125mM EDTA and 100% ethanol before adding HI-DI formamide (Thermo Fisher) for the sequencing reaction using a ABI 3730 Genetic analyser sanger platform at the Genomic Technologies core facility at the University of Manchester. Sequences were analysed for heterozygous and homozygous mutations using a reference cDNA sequence acquired from ensembl.org and GeneScreen software (University of Leeds).

2.7 Whole-mount stains

2.7.1 Fixing embryos

Staged embryos and larvae were collected with groups of sibling controls and washed in 1X PBS. To fix the tissue samples were fixed in 4% PFA (Alfa Aesar) for 3 hours at RT or overnight at 4^{o}C. PFA was removed and samples washed in 1X PBS-Tween before use. To store samples longer term, embryos were dehydrated into methanol and stored at -20^{o}C until use.

2.7.2 Bleaching pigment

Pigment was bleached from WT background larvae melanocytes after initial fixation with 4% PFA for staining, whole-mount *in situ* hybridisation (WISH) or whole-mount immunohistochemistry (IHC) protocols. Larvae were washed using PBS-Tween, and bleaching solution (Table 2.1) was added for 10-12 minutes and monitored carefully. Solution was removed and larvae washed 3X in PBS-Tween.

2.7.3 Filipin stain

Protocol adapted from Louwette et al. (2012). Larvae were fixed using 4% PFA and washed into PBS-Tween. Filipin (Merck) was made to 125µg/ml solution in 1% goat serum in PBS. Larvae were incubated in filipin solution in the dark for 2 hours and then washed 3X in PBS-Tween. Larvae were mounted into the light-sheet microscope (Carl Zeiss Lightsheet Z.1) and images were acquired using a W Plan-Apochromat 20X/1.0 UV-VIS objective and processed with ZEN imaging software (version 2.3). Maximum intensity projection (MIP) composites were generated from z-stack images and brain regions (excluding the eyes) were analysed for average intensity fluorescence of cells with image background removal using an ImageJ (version 1.52a) macro (appendix iii) as a measurement for unesterified cholesterol concentration.

2.7.4 Iron stain

Protocol adapted from Lumsden et al. (2007). Fixed embryos were immersed in 2.5% potassium ferrocyanide (Merck) solution in 0.25M HCl for 30 minutes at RT and rinsed 3X in PBS-Tween. Potassium ferrocyanide reacts with ferric iron in the embryo producing ferric ferrocyanide (Prussian blue). Endogenous peroxide activity was quenched using 0.3% H_2O_2 in methanol for 20 minutes at RT followed by 2X rinse in PBS-Tween. DAB (Thermo Scientific) was dissolved in 50mM Tris (pH 7.2) to 1mg/ml concentration and equal volume of 0.02% H_2O_2 was added. Embryos were

incubated for 7-15 minutes in DAB substrate. Ferric ferrocyanide catalyses the H_2O_2-mediated oxidation of DAB and produces a reddish brown stain. Embryos were washed 3X in PBS-Tween and mounted in 80% glycerol for microscopy on a Leica M165FC light stereo microscope with DFC7000T camera and processed using LAS-X software (version 3.3.3.16958).

2.7.5 Haemoglobin stain

Live, dechorionated embryos were moved into glass vials and E3 media was removed. 500µl of O-dianisidine (Sigma) stain was added and larvae were incubated in the dark for 30 minutes. Once stain was completed larvae were washed 3X in deionised H_2O and fixed in 4% PFA for at least 2 hours at RT or 4^{o}C overnight. If larvae were pigmented, bleaching was carried out after fixation (2.7.2). Larvae were mounted in 80% glycerol for imaging on a Leica M165FC light stereo microscope with DFC7000T camera and processed using LAS-X software (version 3.3.3.16958).

2.7.6 Staining for dying cells

Live, dechorionated embryos were incubated in the dark for 30 minutes at 28^{o}C in methylene blue-free E3 media containing 2µg/ml of acridine orange (Merck). Embryos were washed 5X following staining in methylene blue-free E3 media and imaged using 540nm wavelength absorbance using a Leica M165FC light stereo microscope with DFC7000T camera and processed using LAS-X software (version 3.3.3.16958).

2.7.7 Whole-mount in situ hybridisation (WISH) protocol

Fixed, bleached embryos were permeabilised using 10µg/ml proteinase K and WISH stained according to published protocol (Thisse and Thisse, 2008). Embryos were stained with NBT and BCIP at 50µg/ml in BCL buffer for up to ~6 hours. Stained embryos were then fixed in 4% PFA and stored in 100% glycerol before imaging using a Leica M165FC light stereo microscope with DFC7000T camera. Images were processed using LAS-X software (version 3.3.3.16958).

Age (hpf)	Proteinase K incubation time (minutes)
24	5-10
48	25
72	45

96	60
120	60-90

2.7.8 WISH probes

Probes used for WISH stain include *mpeg1* (Zakrzewska et al., 2010), *mpx* and *il-1β* (Ogryzko et al., 2014a) which were obtained as gifts from Prof Stephen Renshaw's lab from the University of Sheffield. *Ch25h* probe was made in house as described in 2.6.7. Nephrin (*nphs1* ENSDARG00000060758) probe was used as a positive control, made using the primers (Table 2.2) and was gifted from Prof Adam Hurlstone at the University of Manchester.

2.8 Immunohistochemistry

2.8.1 Zebrafish adult brain tissue

Adult *bubblehead* homozygous and WT sibling fish were terminated using lethal MS222 overdose at 4% at 1 year of age. Following respiratory arrest at stage 4 anaesthesia, fish were washed in 1X PBS for 10 minutes. The heads were then removed and fixed in 4% PFA for 2 days at 4^{o}C. Heads were washed 3X in PBS for 5 minutes before being transferred into 0.5M EDTA for 5 days to decalcify the bones. Brains were dissected from the head using surgical scalpel and forceps and tissue dehydrated in series of 70%, 90% and 100% ethanol for 30 minutes each.

2.8.2 Human brain tissue

Paraffin embedded human patient brain tissue samples were obtained through the University of Edinburgh Brain and Tissue bank (MTA TR75.17). Tissue was donated from 3 patients who suffered lethal ICH at acute (45, 51 and 60 hours post ICH) and subacute time points (10, 43 and 60 days post ICH). Age and region matched control tissue was donated from 3 sudden death brain healthy volunteers. Patients were between the ages 63 and 91 at time of death and single haemorrhages were located in basal or thalamic regions. Human tissue was sectioned using a rotary microtome (Leica) to 5µm thick, mounted on Superfrost glass microscopy slides (Thermo Fisher) and baked at 60^{o}C to ensure tissue adhesion.

2.8.3 Mouse brain tissue

By-product brain tissue was obtained for histological examination from 5 C57BL/6 mice (Charles River) that underwent bacterial collagenase ICH surgery for experimental gut analysis . Two stroke, two sham and 1 naïve brains were fixed in 4% PFA overnight at 4^{o}C and dehydrated into a series of 70%, 90%, 100% ethanol. Before paraffin embedding, tissue was sliced into three parts using a 1mm cutting matrix. Tissue sections were cut at 5µm thick using a rotary microtome (Leica) and mounted on Superfrost glass microscopy slides (Thermo Fisher).

2.8.4 Larval tissue

Both *bubblehead* ICH+ homozygotes and ICH- control WT larvae at 3 dpf were fixed in 4% PFA overnight at 4^{o}C. Tissue was dehydrated in series of 70%, 90% and 100% ethanol solutions for 30 minutes each.

2.8.5 Zebrafish tissue embedding and sectioning

Zebrafish larvae were embedded randomly in paraffin at 58ºC in the histology core facility at the University of Manchester. Tissue sections cut at 5µm thick using a rotary microtome (Leica) and mounted on Superfrost glass microscopy slides (Thermo Fisher).

2.8.6 Haematoxylin and eosin stain

Paraffin embedded slides were deparaffinised using xylene and rehydrated into water in a sequence of ethanol solutions. Haematoxylin solution (Gill No.1, Merck) was vacuum filtered before use and slides submerged for 10 seconds. Lithium carbonate was used as a bluing agent for 10 seconds. If haematoxylin was too dark then stain was removed using acid alcohol. Eosin counter stain (Merck) was used for 45 seconds before tissue was dehydrated in an increasing series of ethanol solutions and xylene. Slides were mounted using DPX (Merck) and images taken using the 3D Histech Pannoramic-250 Flash Slide Scanner (Bioimaging core facility, The University of Manchester).

2.8.7 Interleukin-1β immunohistochemistry in zebrafish

Paraffin embedded slides were deparaffinised using xylene and rehydrated into water in a sequence of ethanol solutions. Slides were incubated at 95ºC in Tris-EDTA pH8.6 to break crosslinks and retrieve antigen binding sites. Primary antibody rabbit anti-zebrafish *il-1β* (Vojtech et al., 2012) was diluted 1:100 in primary antibody buffer and added to slides overnight at 4ºC. Slides were mounted into the Sequenza coverplates (Thermo Scientific) under water and washed 3X in TNT. Secondary anti-rabbit biotinylated antibody (BA-1000, Vector Labs) was made 1:500 in 1% BSA TNT and incubated for 2 hours. Slides were stained with DAPI 1µg/ml (Merck) for 10 minutes and mounted using ProLong Diamond Antifade Mountant (P36961 Invitrogen). Slides were imaged using a Zeiss Axioimager.D2 upright microscope using a 20x / 0.5 EC Plan-neofluar *o*bjective and captured using a Coolsnap HQ2 camera (Photometrics) through Micromanager software v1.4.23. Specific band pass filter sets for DAPI and AF488 were used to prevent bleed through from one channel to the next. Images were then processed and analysed using ImageJ (http://imagej.net/Fiji/Downloads).

2.8.8 CH25H immunohistochemistry in human tissue

Paraffin embedded slides were deparaffinised using xylene and rehydrated in to water in a sequence of ethanol solutions. Slides were incubated at 95ºC in Tris-EDTA pH9.0 to break crosslinks and retrieve antigen binding sites. Primary antibody rabbit anti-human CH25H (#OABF01697 Aviva Systems Biology) was diluted 1:100 in primary antibody buffer and added to slides overnight at 4ºC. Slides were mounted into the Sequenza coverplates (Thermo Scientific) under water and washed 3X in TNT. Secondary anti-rabbit biotinylated antibody (Vectorlabs) was made 1:500 in 1% BSA TNT and incubated for 30 minutes. ABC HRP Vectastain reagent (Vectorlabs) was made 30 minutes in advance and added to slides for 30 minutes. HRP substrate (AK-5000 Vector Labs) was added for 30 minute incubation in the dark. Slides were removed from the sequenza, counterstained in haematoxylin and dehydrated through ascending ethanols into xylene (2.8.6). Slides were mounted using DPX (Merck) and images taken using the 3D Histech Pannoramic-250 Flash Slide Scanner (Bioimaging core facility, The University of Manchester).

2.8.9 CH25H and LY6G/IBA1 co-stain immunofluorescence in mouse tissue

Mouse brain slices were deparaffinised using xylene and rehydrated into water using a sequence of ethanol solutions. Slides were incubated at 95ºC in Tris-EDTA pH8.6 to break crosslinks and retrieve antigen binding sites. Primary antibody rabbit anti-human CH25H (#OABF01697 Aviva Systems Biology) was diluted 1:100 in primary antibody buffer and added to slides overnight at 4ºC. Using the AF555 tyramide superboost streptavidin kit (Invitrogen) endogenous peroxidases were quenched using H_2O_2 and secondary biotin-conjugated anti-rabbit antibody (Vectorlabs) was added 1:200 in 1% BSA TNT for 30 minutes. Slides were rinsed and HRP-conjugated streptavidin added for 45 minutes. Slides were incubated with a working solution of 1:200 tyramide AF555 for 8 minutes and reaction was stopped using stop solution. Slides were rinsed from the sequenza into dH_2O and staining checked using an upright microscope (Zeiss Axio Imager.D2). For the co-stain, antigen retrieval was performed again and primary rat anti-mouse LY6G antibody (Biolegend #127602) or rabbit anti-mouse IBA1 (Abcam ab178846) was added 1:500 overnight at 4ºC. Secondary donkey anti-rabbit AF647 (Invitrogen A31573) and goat anti-rat AF647 (Invitrogen A21247) was added 1:500 for 2 hours at RT before staining with DAPI 1µg/ml (Merck) for 10 minutes and mounting using ProLong Diamond Antifade Mountant (P36961

Invitrogen). Images taken using the 3D Histech Pannoramic-250 Flash Slide Scanner (Bioimaging core facility, The University of Manchester).

2.9 Gene expression analysis

2.9.1 RNA extraction

Into a 1.5ml Eppendorf, 20-30 embryos were collected at the desired developmental stages (Kimmel et al., 1995) and washed in PBS. To lyse samples, 250µl Trizol (Thermo Fisher) was added to each tube and samples were manually homogenised using a microfuge tube pestle (Astral Scientific). A volume of 75µl of chloroform was added and agitated vigorously before centrifugation at 10,000rpm for 15 minutes to separate the homogenate into a clear upper aqueous layer that contains RNA, an interphase of debris and a lower organic layer containing DNA and proteins. The upper RNA layer was transferred to new tubes and precipitated using 0.8 volumes of isopropanol incubated at -20^{o}C for 30 minutes. Precipitate was pelleted and washed using 250µl of 75% RNase-free filter sterilised ethanol before drying and resuspended in 30µl RNase-free H_2O. RNA was purified with a DNase I (Invitrogen) incubation before being quantified.

2.9.2 cDNA synthesis

To generate complementary DNA sequence from isolated RNA, 800ng of RNA was incubated with 1µl of reverse transcriptase from the High-Capacity RNA-to-cDNA kit (Applied Biosystems) for 37^{o}C for 1 hour before reaction was terminated at 95^{o}C for 5 minutes.

2.9.3 Quantitative reverse transcription PCR

Gene expression analysis was performed using RT-qPCR using sample cDNA and Taqman Universal PCR Master Mix (Applied Biosystems). Taqman FAM probes (Thermo Fisher) were used targeting the following genes: *irf7* (dr03081134_g1), *mmp9* (dr03139883_g1), *stat1b* (dr03151121_m1) *il-1β* (dr03114368_m1), *rsad2* (dr03096955_g1), *rig-I* (ZF_DHX58), *isg-15* (Kasher et al., 2015), *ch25h* (dr03147520_s1), *hmgcra* (dr03428701_m1), *sqlea* (dr03131214_m1), *cyp51* (dr03114750_m1), *dhcr24* (dr03423142_m1), *ebp* (dr03076172_m1), *msmo1* (dr03133463_m1), *sc5d* (dr03115434_m1), *srebf1* (dr03093012_m1), *relA* (dr03114752_m1) *mpx/mpo* (dr03075669_m1), *mpeg1* (dr03439207_g1), *il-10* (dr03103209_m1). Relative quantities were normalised to the expression of housekeeper genes, *hprt1* (dr03095131_g1) and *eef1a1b* (dr03423920_m1). Data

was acquired using the Applied Biosystems StepOne Software (version 2.1) Relative Quantification evaluated from $2^{\Delta\Delta C_T}$ (Livak and Schmittgen, 2001).

Chapter 3: Using zebrafish larval models to study brain injury, locomotor and neuroinflammatory outcomes following intracerebral haemorrhage

DOI: 10.12688/f1000research.16473.2

Siobhan Crilly, BSc[1] 0000-0003-1046-9884, Alexandra Njegic, MRes[2], Sarah E. Laurie[1], Elisavet Fotiou, MRes[2], Georgina Hudson, MSc[1], Jack Barrington, BSc[1], Kirsty Webb, MRes[2], Helen L. Young, PhD[3], Andrew P. Badrock, PhD[4], Adam Hurlstone, PhD[3], Jack Rivers-Auty, PhD[1], Adrian R. Parry-Jones, PhD[2], Stuart M. Allan, PhD[1*], Paul R. Kasher, PhD[1*] 0000-0002-9213-502X

[1]Division of Neuroscience and Experimental Psychology, School of Biological Sciences, [2]Division of Cardiovascular Sciences, School of Medical Sciences, [3]Division of Cancer Sciences, School of Medical Sciences, [4]Division of Evolution and Genomic Sciences, School of Biological Sciences, Faculty of Biology, Medicine and Health, Manchester Academic Health Science Centre, University of Manchester, Michael Smith Building, Oxford Road, Manchester, M13 9PT, UK.

* These authors contributed equally to this article.

Correspondence: Dr Paul Kasher, E-mail: paul.kasher@manchester.ac.uk

Telephone: +44 161 306 8059

Abstract

Intracerebral haemorrhage (ICH) is a devastating condition with limited treatment options, and current understanding of pathophysiology is incomplete. Spontaneous cerebral bleeding is a characteristic of the human condition that has proven difficult to recapitulate in existing pre-clinical rodent models. Zebrafish larvae are frequently used as vertebrate disease models and are associated with several advantages, including high fecundity, optical translucency and non-protected status prior to 5 days post fertilisation. Furthermore, other groups have shown that zebrafish larvae can exhibit spontaneous ICH. The aim of this study was to investigate whether such models can be utilised to study the pathological consequences of bleeding in the brain, in the context of pre-clinical ICH research.

Here, we compared existing genetic (*bubblehead*) and chemically inducible (atorvastatin) zebrafish larval models of spontaneous ICH and studied the subsequent disease processes. Through live, non-invasive imaging of transgenic fluorescent reporter lines and behavioural assessment we quantified brain injury, locomotor function and neuroinflammation following ICH. We show that ICH in both zebrafish larval models is comparable in timing, frequency and location. ICH results in increased brain cell death and a persistent locomotor deficit. Additionally, in haemorrhaged larvae we observed a significant increase in macrophage recruitment to the site of injury. Live *in vivo* imaging allowed us to track active macrophage-based phagocytosis of dying brain cells 24 hours after haemorrhage. Morphological analyses and quantification indicated that an increase in overall macrophage activation occurs in the haemorrhaged brain.

Our study shows that in zebrafish larvae, bleeding in the brain induces quantifiable phenotypic outcomes that mimic key features of human ICH. We hope that this methodology will enable the pre-clinical ICH community to adopt the zebrafish larval model as an alternative to rodents, supporting future high throughput drug screening and as a complementary approach to elucidating crucial mechanisms associated with ICH pathophysiology.

Key words: Intracerebral haemorrhage, zebrafish, neuroinflammation, animal models, pre-clinical

3.1 Introduction

Intracerebral haemorrhage (ICH) accounts for 10-15% of strokes and has the worst stroke outcomes, with a 1-month case fatality of 40% and disability in most survivors (An et al., 2017). The effects of ICH in the brain are biphasic. Primary injury following an ICH event arises due to an influx of blood into the brain and haematoma expansion which increases intracranial pressure on cerebral structures causing neuronal death and cell necrosis (Mracsko and Veltkamp, 2014; Xi et al., 2006). A secondary wave of injury is induced by the breakdown of blood compounds which activates the immune system, further exacerbating cellular damage and death in the brain parenchyma and induces a breakdown in blood-brain barrier integrity (Lok et al., 2011). This inflammatory component is considered a viable therapeutic target in ICH and other forms of stroke (Veltkamp and Gill, 2016) and targeting the toxic insult of blood components after bleed onset is being investigated clinically (Yeatts et al., 2013). However at present, apart from acute and chronic blood pressure lowering, we have no specific treatments to prevent ICH or improve patient outcomes once bleeding has occurred.

Despite representing a significant public health burden (WHO, 2017), an understanding of the fundamental pathogenesis of ICH is still lacking. Pre-clinical studies to-date have depended heavily on rodent models of ICH, which have improved our knowledge of the basic mechanisms associated with the disease (Casals et al., 2011). However, current rodent models of ICH involve severe surgical intervention, poorly recapitulating the spontaneous and immediate nature of the human disease and presenting welfare implications associated with severe experimental procedures in mammals (ASPA, 1986 amendments 2012). Autologous blood injection and collagenase injection models (Andaluz et al., 2002) are used worldwide, and typical experimental groups include 6-8 rats, sacrificed at various time points for *ex vivo* histological analysis, which can result in ~150 animals used per publication (J. Wang et al., 2018) highlighting scope for a change of strategy from a 3Rs perspective. Unfortunately, this research has not yet resulted in the translation of any specific drugs to the clinic (Kellner and Connolly, 2010; Kirkman et al., 2011). Potential reasons for this include difficulties in observing cellular responses in ‘real-time’ within whole brains of intact live animals, and the invasive and artificial procedures required to induce cerebral haematomas (MacLellan et al., 2010; Selim et al., 2018). Mammalian

models of spontaneous ICH models do exist, such as cerebral amyloid angiopathy co-morbidity studies and use of hypertensive mice, but their usefulness is limited due to variability in haematoma size, timing and location (Alharbi et al., 2016). Alternative and complementary approaches are therefore needed to bridge the 'translational gap' for novel drug target discovery in ICH.

Zebrafish (*Danio rerio*) are becoming an increasingly popular tool for studying cerebrovascular disease (Walcott and Peterson, 2014). Due to the production of hundreds of offspring from a single adult pairing, zebrafish larvae can be utilised for high-throughput drug screening, thus offering an attractive model for pre-clinical research. Larval transparency and the availability of numerous transgenic reporter lines amount to an extremely powerful system for studying and visualising cellular responses and disease processes *in-vivo* in real time. Prior to 5 days post fertilisation (dpf), larval zebrafish are not a protected species (in the UK) and could therefore replace a significant number of protected mammals used for pre-clinical study. Furthermore, spontaneous brain-specific bleeding can be observed in zebrafish larvae using non-invasive techniques (Eisa-Beygi et al., 2013; Liu et al., 2007), thereby eliminating specific constraints associated with mammalian models. As such, the use of larval zebrafish models of ICH could offer critical insight into the immediate cellular responses after a bleed to support the rodent community and provide a potential platform for future drug discovery addressing pre-clinical ICH priorities (Selim et al., 2018).

As previously described, zebrafish larvae exposed to atorvastatin (ATV) at 24 hours post fertilisation (hpf) exhibit spontaneous cerebral-specific blood vessel rupture at the onset of circulation (~33 hpf) (Eisa-Beygi et al., 2013; Huang et al., 2017; S. Li et al., 2017; Shen et al., 2013). Comparably, the '*bubblehead*' (*bbh*) mutant line, which expresses a hypomorphic mutation in the *arhgef7* gene, encoding the Rac GEF βpix, also exhibit spontaneous ICH and hydrocephalus within a similar time frame to the ATV model (Liu et al., 2007; ten Klooster et al., 2006). ICH is induced through comparable mechanistic defects in both ATV and *bbh* models (Eisa-Beygi and Rezaei, 2016) (figure 1.8.1). Although several groups have utilised these models to study the development and integrity of the cerebrovasculature (Buchner et al., 2007; Huang et al., 2017; S. Li et al., 2017; Liu et al., 2007; Yang et al., 2017), they have not yet been

used to study the pathological and neuroinflammatory consequences of bleeding in the zebrafish larval brain in the context of human ICH. Furthermore, drug intervention studies have focussed on preventing cerebrovascular rupture in zebrafish rather than targeting the disease outcomes, which represent a more realistic therapeutic avenue. In this study, we show that spontaneous ICH in non-protected zebrafish larvae induces quantifiable pathological and inflammatory phenotypes that relate to the human condition. As such, these data support the use of this model species as a valuable complementary system for pre-clinical ICH research.

3.2 Methods

Zebrafish *(Danio rerio)* strains

Zebrafish were raised and maintained at The University of Manchester Biological Services Unit under standard conditions as previously described (Westerfield, 2000). Adult zebrafish husbandry was approved by the University of Manchester Animal Welfare and Ethical Review Board. All experiments were performed in accordance with U.K. Home Office regulations (PPL:70/9091) and reported according to ARRIVE guidelines. Transgenic lines used in this study include macrophage-specific lineage *mpeg1:*mCherry (constructed in-house as previously described (Ellett et al., 2011)), neutrophil-specific *mpo:*GFP (Renshaw et al., 2006), erythroid-specific *gata1:*dsRed (Traver et al., 2003) and *ubiq:*secAnnexinV-mVenus, a reporter for apoptosis (re-derived in house (Morsch et al., 2015)) on wild-type, nacre (*mitfa*$^{w2/w2}$*)* and mutant (*bbh*^{m292}) backgrounds. Fertilized embryos were collected from natural spawning and incubated at 28°C in standard E3 embryo medium and staged according to standard guidelines (Kimmel et al., 1995). At experiment end, zebrafish larvae were terminated prior to protected status using a lethal overdose of MS222 anaesthesia and freezing at -20^{o}C.

ICH models

ICH was modelled using genetic (*bbh*) and chemical (ATV) approaches. For the *bbh* line (Liu et al., 2007), embryos were obtained from adult in-crosses from heterozygous *bbh*^{m292} mutant animals (maintained on wild-type and transgenic reporter backgrounds). For the ATV model, nacre or transgenic embryos were dechorionated at 24 hpf and transferred to clean petri dishes in E3 embryo medium. ATV (Sigma-Aldrich, PZ0001) was solubilised in distilled water to a stock concentration of 0.5 mM. Embryos (n=100) were treated with a final concentration of 1 μM ATV through water bath incubation at 28°C for 24 hours and equivalent numbers were left as untreated controls. A proportion of ATV-treated embryos did not develop ICH and therefore these animals were used as controls for the treatment (ICH-) alongside untreated (UNT) siblings. For both *bbh* and ATV models, embryos with evident haemorrhages (ICH+) were separated from non-haemorrhaged (ICH-) siblings at ~52 hpf for downstream analyses.

Locomotion assay

Locomotion was measured at 120 hpf to determine if ICH resulted in a physical phenotype. To remove locomotor function bias, larvae were briefly anesthetised at 72 hpf using 0.02% MS222 in embryo water and selected at random for plating. Following recovery, n=24 larvae were individually transferred to each well of a 24-well plate in 1 ml of fresh methylene-blue-free E3 medium. Cumulative time spent mobile was measured using the DanioVision camera chamber and Ethovision XT software (Noldus version 11) at room temperature. Analyses were performed on larvae at 72, 96 and 120 hpf. Swimming movement of each individual larva was tracked in the x and y plane for 10 minutes using a white light stimulus to initiate a startle response every 60 seconds. Cumulative time spent swimming was measured from three independent replicates.

Light sheet microscopy

Transgenic ICH+ and ICH- larvae were imaged using light sheet microscopy to analyse apoptotic cell death (*ubiq*:secAnnexinV-mVenus), neutrophils (*mpo:*GFP) and macrophages (*mpeg1:*mCherry). At ~72 hpf, randomly selected larvae were anaesthetised using 0.02% MS222 and mounted in 1.5% low-melt agarose (Promega), maintained at room temperature. Images were acquired using a W Plan-Apochromat 20X magnification/1.0 UV-VIS objective for light-sheet microscope (Carl Zeiss Lightsheet Z.1) and processed with ZEN imaging software (version 2.3). Maximum intensity projection (MIP) composites were made from z-stack images and brain regions (excluding the eyes) were analysed for average intensity fluorescence of cells with image background removal using an ImageJ (version 1.52a) macro (appendix i). Numbers of fluorescent cells in the brain were also verified by blind manual counts from MIPs. Data were collected from n=6-12 randomly selected larvae per group from 3 independent replicates for ATV studies and verified in 2 replicates for *bbh*. For time-lapse recording, MIP composites were stitched from a series of successive z-stack images over a period of 18 hours.

Statistical analysis

Experimental sample sizes were determined by using power calculations from preliminary data using α=0.05 and β=0.80. All statistical analysis was first performed using GraphPad Prism 7.0 and then verified using R (R Core Team, 2018) for non-

parametric data and subsequent significance values plotted. Linear mixed modelling (LMM) was used to evaluate the effects of independent factors on the continuous dependent variables (Bates et al., 2015). All factors and interactions were modelled as fixed effects. As there is a lack of independence in fish from the same clutch, "Clutch" was treated as a random effect, modelled with random intercepts for all models. The significance of inclusion of an independent variable or interaction terms were evaluated using log-likelihood ratio. Holm-Sidak post-hocs were then performed for pair-wise comparisons using the least square means (Lenth, 2016). Homoscedasticity and normality of the Pearson residuals were evaluated graphically using predicted vs residual and Q-Q plots, respectively, and transformations were applied when necessary.

For discrete data and data with non-normal distributions, generalized linear mixed modelling was used (GLMM) (Bates et al., 2015; Fournier et al., 2012; Skaug et al., 2013). Again "Clutch" was treated as a random effect modelled with random intercepts for all models. Appropriate families were selected based on the data distribution. Numerous families and link functions were evaluated where necessary and the optimal parameters were selected based on the Akaike information criterion (AIC). For mobile or non-mobile (yes/no) data, a logistic regression with cloglog link was selected; for count data (number of dead cells) a negative binomial family was selected. The significance of inclusion of an independent variable or interaction terms were evaluated using log-likelihood ratio. Holm-Sidak post-hocs were then performed for pair-wise comparisons using the least square means (Lenth, 2016). Pearson residuals were evaluated graphically using predicted vs level plots. All analyses were performed using R (R Core Team, 2018) (available as supplementary information (Crilly et al., 2018)).

3.3 Results

ATV and* bbh *mutant models show comparable cerebral bleeding phenotypes

It has been shown that both the ATV and *bbh* models share similar underlying mechanisms that are responsible for neuroendothelial weakness in the developing larvae and spontaneous cranial vessel rupture (Eisa-Beygi et al., 2013; Liu et al., 2012). In this study we compared these models in the context of ICH and characterised the pathological outcomes of haemorrhage to develop a new platform for pre-clinical interrogation of post-bleed consequences. Using the translucent nature of the zebrafish embryo we observed brain-specific bleeding non-invasively, using light and fluorescent microscopy (Figure 3.3.1A). Bleeds were observed in fore, mid and hindbrain regions at comparable frequencies, as described by others (Eisa-Beygi et al., 2013; Liu et al., 2007). ATV absorption induced haemorrhages in a dose-dependent manner when embryos were treated at 24 hpf (Figure 3.3.1B). Homozygous mutant *bbh* embryos and ATV-treated embryos both exhibited ICH between 38 and 48 hpf (Figure 3.3.1C, D). In homozygous mutant *bbh* embryos, ICH was frequently accompanied with severe cranial oedema (Liu et al., 2007) (Figure 3.3.2). Wild-type and heterozygous *bbh* siblings had no haemorrhages and were utilised as ICH-controls.

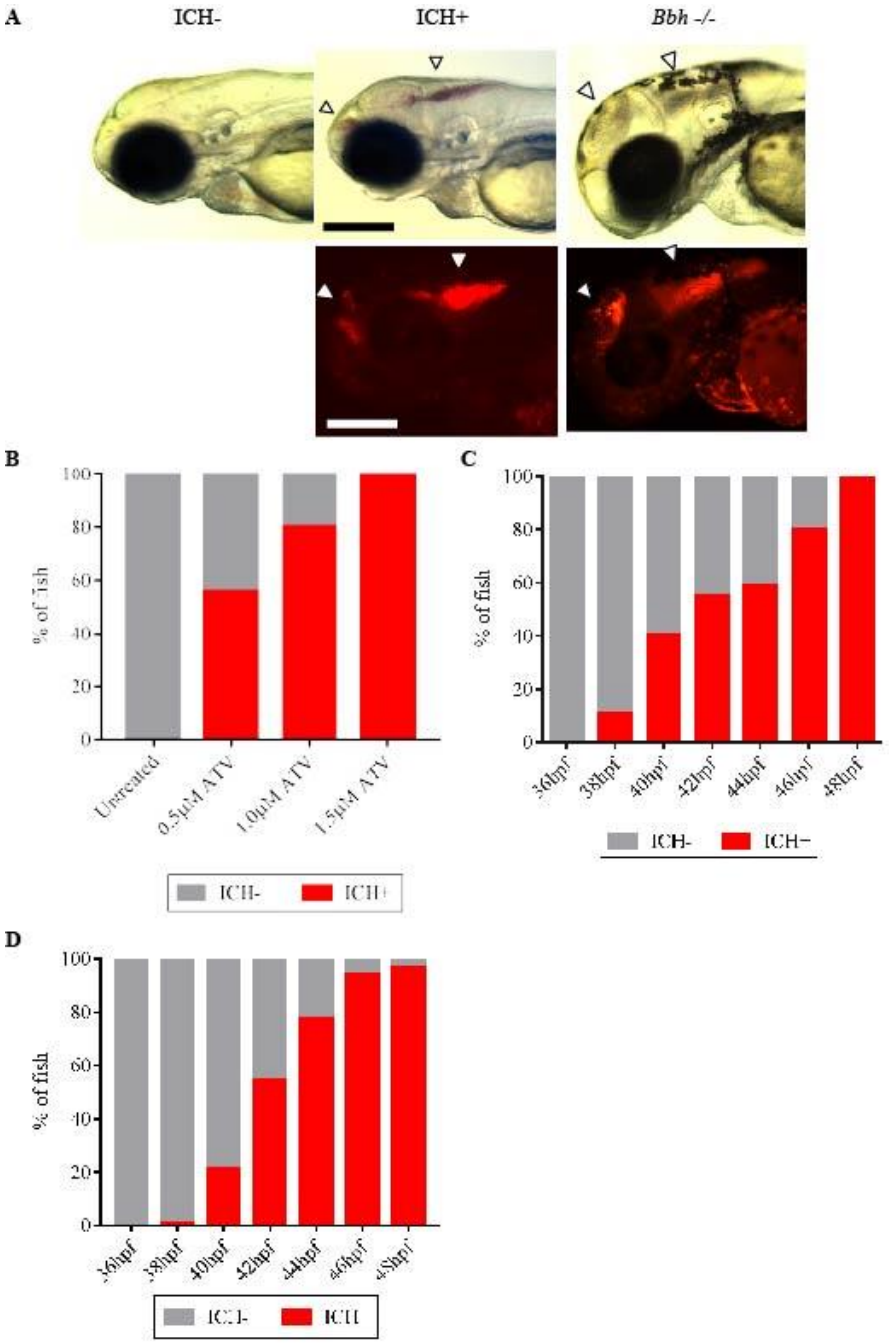

Figure 3.3.1 Atorvastatin (ATV)-induced and *bubblehead* (*bbh*) mutant intracerebral haemorrhage (ICH) show comparable models of brain-specific bleeding.

(A) Brain-specific bleeds were observed at 3 dpf in both ATV and bbh models maintained on the transgenic RBC *gata1*:DsRed reporter background using both brightfield (top panels) and fluorescence (bottom panels) microscopy. Bleeds formed in both forebrain and mid-hindbrain regions, as described by others (Eisa-Beygi et al., 2013) (arrows denotes haemorrhages). Bleeds in *bbh* mutants are frequently associated with severe cranial oedema making blood pooling more disperse. Images representative of n=16 per group (B) ATV treatment causes ICH to occur in a dose-dependent manner. (C) Timeline of ICH development in ATV-treated and untreated embryos and (D) *bbh* homozygotes. Scale bar represents 250μm.

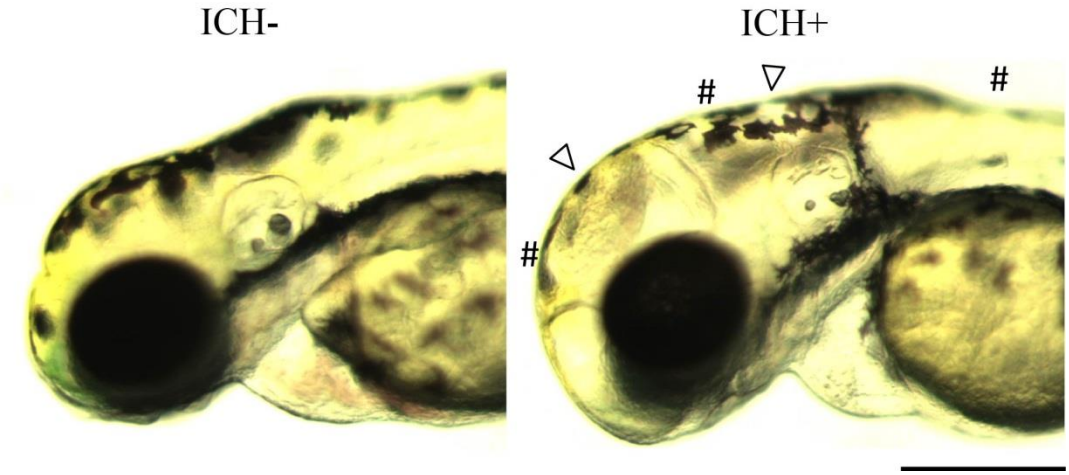

Figure 3.3.2 ICH in *bubblehead* larvae is frequently accompanied by cranial oedema.

Severe cranial oedema (affected regions denoted by hashtags) associated with cerebral bleeds at 3 dpf in '*bubblehead*' homozygous mutants (right panel) and subsequently exhibit more dispersed bleeds (arrows) compared to heterozygous and wild-type intracerebral haemorrhage (ICH-) (left panel). Images representative of n=16. Scale bar represents 250µm

ICH in zebrafish larvae results in a quantifiable brain injury

To determine the pathological consequences of ICH in zebrafish larvae, we next assessed brain injury using a transgenic *ubiq:*secAnnexinV-mVenus cell death reporter line (Morsch et al., 2015). AnnexinV binding was assessed between 48 and 120 hpf, to characterise the timeline of cell death following an ICH event (Figure 3.3.3). We observed peri-haematomal brain-damaged lesions as 'clusters' of dying cells formed by 72 hpf, which had receded before 96 hpf (Figure 3.3.3). We quantified brain lesions from images taken at 72 hpf (Figure 3.3.4A). In both ATV and *bbh* models, bleeding was associated with a significant, two-fold increase in intensity of fluorescent signal in the brain compared to ICH- controls (Figure 3.3.4B, C). These data were verified using blinded, manual counts of annexinV-positive cells from MIP images (Figure 3.3.5) and analysed using a Mann-Whitney U test for non-parametric data. Large variation between individual data points may be due to number/location of haemorrhages, ICH size and severity, or whether oedema is present/absent. These specific details have not yet been investigated. Taken together, these data provide convincing evidence that ICH in zebrafish larvae induces a reproducible cell death phenotype that can act as a quantifiable readout of brain injury.

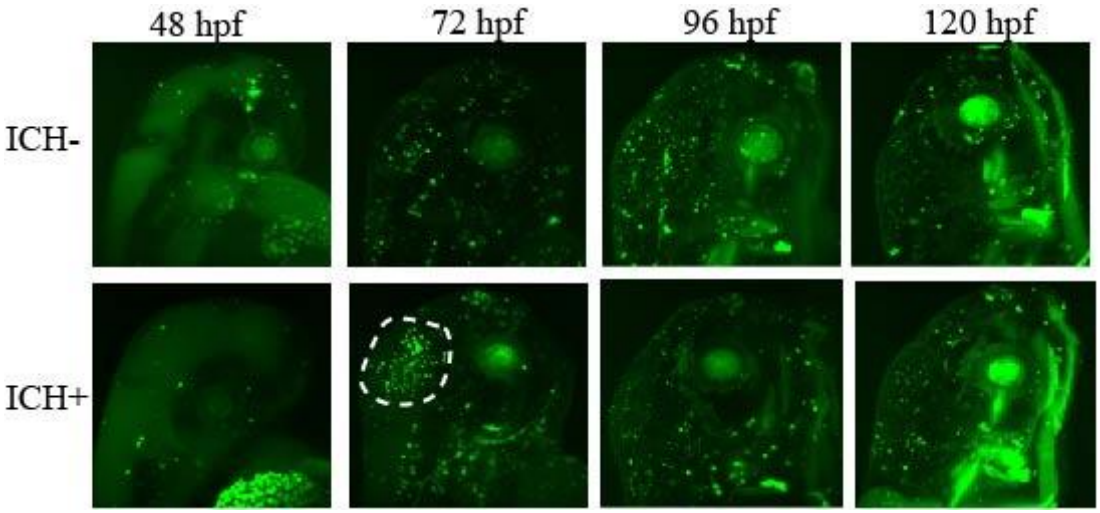

Figure 3.3.3 AnnexinV binding after ICH between 48 and 120 hpf.
Representative images of the brain injury phenotype in ICH+ larvae (bottom panels), in comparison to ICH- age-matched siblings (top panels), at 48-120 hpf. Fluorescent microscopy was performed to visualise cell death in the *ubiq*:secAnnexinV-mVenus reporter line to determine the timeline of cell injury following an ICH event. White line denotes cell death 'clusters' at 3 dpf that were quantified.

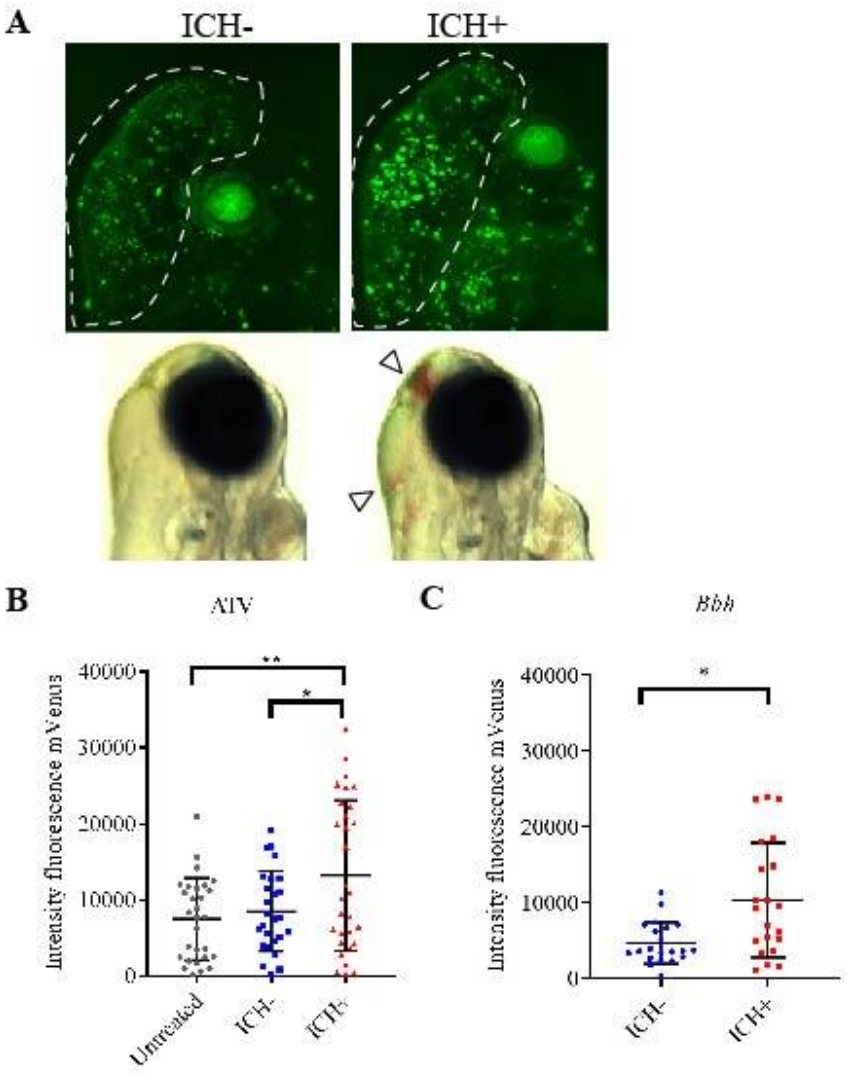

Figure 3.3.4 Intracerebral haemorrhage (ICH) in zebrafish larvae results in a quantifiable brain injury.

(A) Representative images of the brain injury phenotype in ICH+ larvae (right panels), in comparison to ICH- siblings (left panels), at 72 hpf. Brightfield images (bottom panels, scale bar = 250µm) demonstrate the presence of brain bleeds (arrows) in ICH+ larvae. Fluorescent microscopy was performed to visualise cell death in the *ubiq:*secAnnexinV-mVenus reporter line (top panels, scale bar = 100 µm). Clusters of dying cells were observed in peri-haematomal regions. Images were cropped to brain only regions and analysed for total green fluorescence intensity in round particles bigger than 30 pixels in diameter (white line). (B) Quantification of fluorescent signal in the brains of untreated, ICH- and ICH+ larvae obtained through the ATV model (n=12 per group; 3 independent replicates) at 72 hpf. Significant differences were observed when comparing ICH+ with untreated (**p=0.004) and with ICH- (*p=0.03) siblings. (C) Quantification of fluorescent signal as a read out for annexinV binding in the brains of ICH- and ICH+ larvae obtained through the *bubblehead* (*bbh*) model (n=12 per group; 2 independent replicates) at 72 hpf. A significant difference in mVenus fluorescence was observed between ICH+ and ICH- age-matched siblings when data analysed using a Mann-Whitney U test (**p=0.0182).

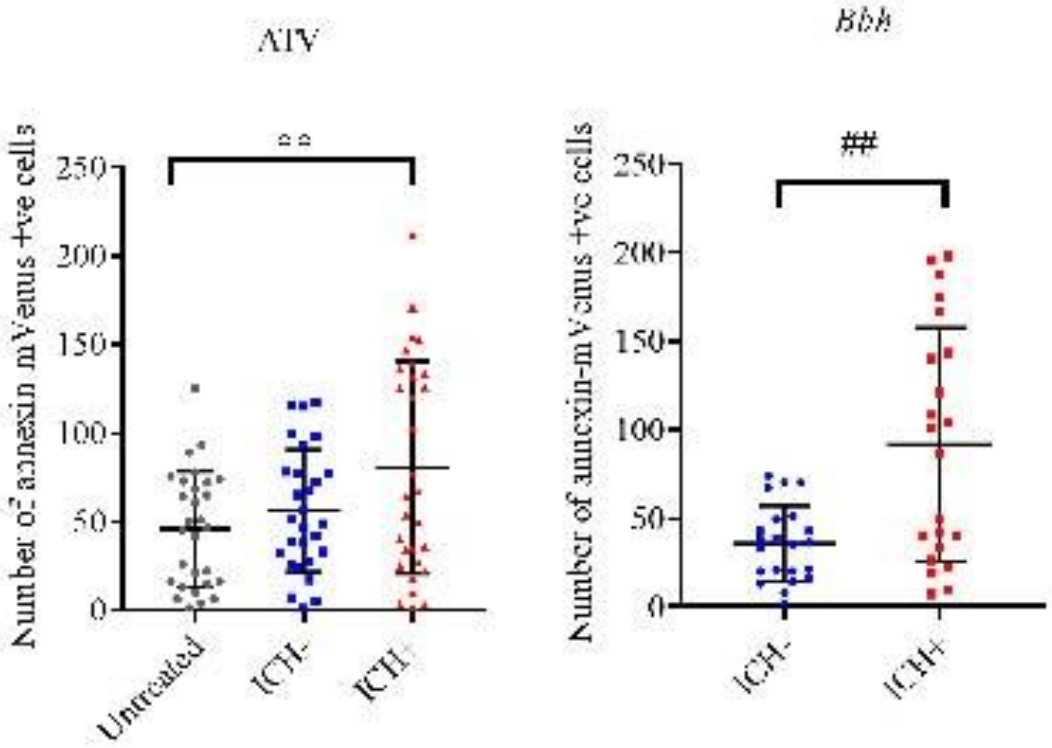

Figure 3.3.5 Counts of dying cells in the brain.
Manual counts of fluorescent cells from blinded analysis of the *ubiq*:secAnnexinV-mVenus reporter line in atorvastatin (ATV) and *bubblehead* (*bbh*) models show a significant increase in intracerebral haemorrhage (ICH)+. Data analysed using a one-way ANOVA (ATV) and Mann-Whitney U (*bbh*) (**p=0.0097, ##p=0.0057).

ICH-induced brain injury results in a quantifiable locomotor deficit in zebrafish larvae

To investigate whether ICH-induced brain injury was associated with a locomotor deficit, as frequently seen in stroke patients (Kloter et al., 2011; Saulle and Schambra, 2016), we tracked swimming behaviour between 72 and 120 hpf. Larvae were analysed across 3 days to account for the improvement in baseline swimming performance associated with increasing age. Representative tracks are shown in figure 3.3.6A. ICH+ larvae spent significantly less time swimming in the cumulative time spent mobile during the 10 minute recording period at both 72 and 96 hpf compared to ICH- siblings, implying a persistent physical deficit (Figure 3.3.6B). Although a reduction was observed in ICH+ larvae at 120 hpf, this was not significantly different to ICH- siblings ($p=0.08$). However ATV-treated larvae assayed at 120 hpf did show a significant reduction in swimming in ICH+ larvae and not in controls. Comparable motility phenotypes in both models imply that the swimming deficit is due to cerebral bleed and not statin treatment. Reproducing these results in both models suggests that the impairment in locomotion is not caused by any one mechanistic factor but due to ICH itself.

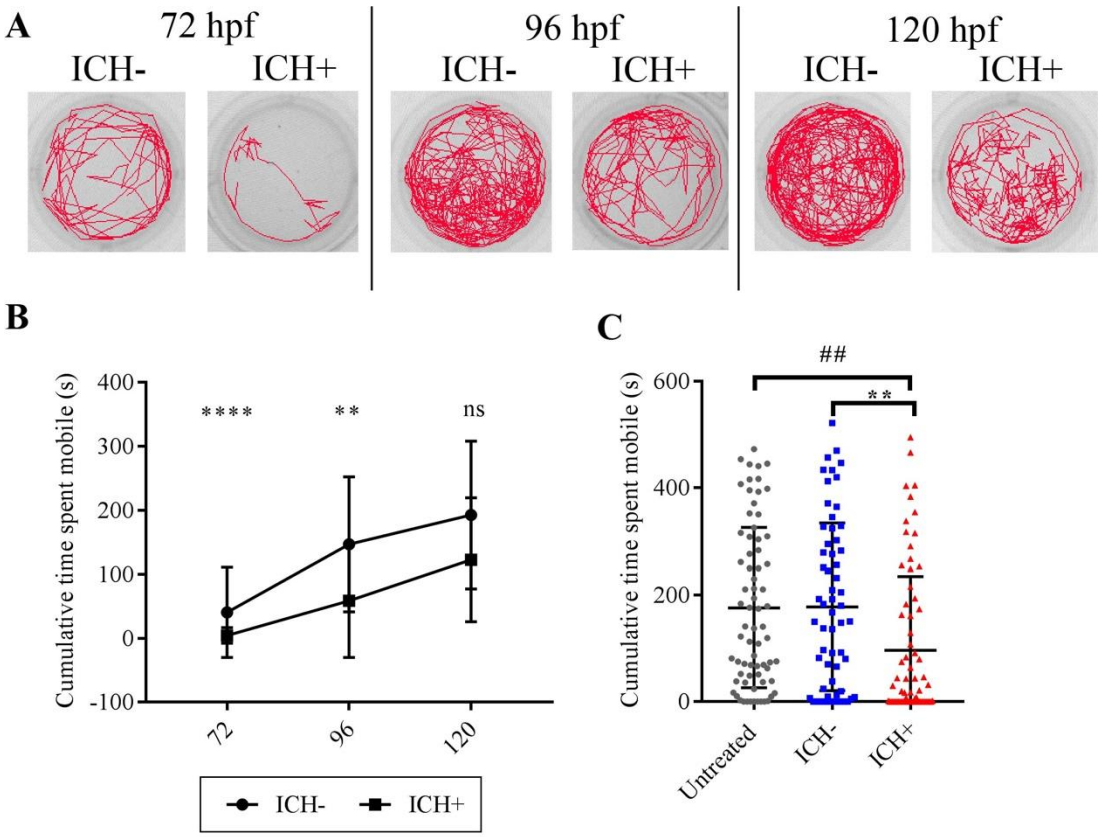

Figure 3.3.6 ICH-induced brain injury results in a quantifiable locomotor deficit in *bubblehead* (*bbh*) zebrafish larvae.

(A) Representative examples of the swimming tracks in ICH- and ICH+ larvae at 72, 96 and 120 hpf. (B) ICH+ larvae exhibited a significant decrease in the cumulative time spent mobile during the 10 minute recording period at both 72 and 96 hpf. Significance was lost at the 120 hpf time point potentially alluding to recovery from brain injury (n=24 larvae per group; 3 independent replicates; ****p=0.00006; **p=0.003 ns p=0.08) (C) Quantification of cumulative time spent moving in untreated and ATV-treated ICH- and ICH+ larvae at 120 hpf. ICH+ larvae exhibited a significant decrease in the cumulative time spent mobile during the 10 minute recording period. Data analysed using a one-way ANOVA, three technical replicates (n=24 larvae per group) were used to calculate s.d from the mean (***p=0.00004, **p=0.0003).

ICH-induced brain injury in zebrafish larvae initiates an innate immune response

In order to determine whether ICH in zebrafish larvae initiated inflammation at the cellular level, neutrophils and macrophages in the brain were quantified using the *mpo*:GFP and *mpeg1*:mCherry reporter lines. At 72 hpf, the number of macrophages increased significantly, doubling in the brains of ICH+ larvae compared to ICH- siblings (Figure 3.3.7). At the same time point, neutrophil numbers were greater in ICH+ larvae than ICH- larvae; however, the difference did not reach significance.

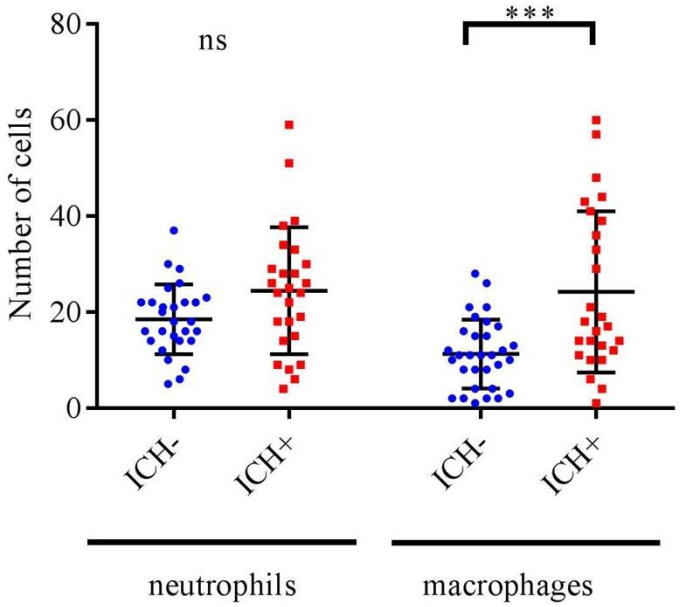

Figure 3.3.7 Intracerebral haemorrhage (ICH) initiates an innate cellular immune response in the zebrafish larval brain.
Numbers of leukocytes quantified within the brains of *mpo:*GFP;*mpeg1:*dsRed double transgenic larvae (n=8 per group; 2 independent replicates) at 72 hpf reveals a significant increase in macrophages (*p=0.01), but not neutrophils (p=0.5), in response to ICH.

Activated macrophage cells show a phagocytic response to the brain lesion

We investigated the phagocytic response of activated macrophages to the brain lesion sites in *ubiq:*secAnnexinV-mVenus;*mpeg1*:mCherry ICH+ larvae using real time microscopy. The formation of a new brain lesion site was recorded between 55 and 65 hpf (appendix iv) and macrophages were seen migrating to sites of injury and actively phagocytosing annexinV positive dying cells (Figure 3.3.8A). We next analysed total macrophage activity within the brain, using morphology as an indication of phagocytic activation. Amoeboid, rounded cells were considered phagocytic and ramified cells considered inactive, as previously defined (Morsch et al., 2015). We found a substantial increase in the proportion of activated, amoeboid macrophages in the ICH+ brain compared to ICH- siblings (Figure 3.3.8B, C). These results indicate that the innate immune response to ICH can be examined at the cellular level in zebrafish ICH models using real-time microscopy.

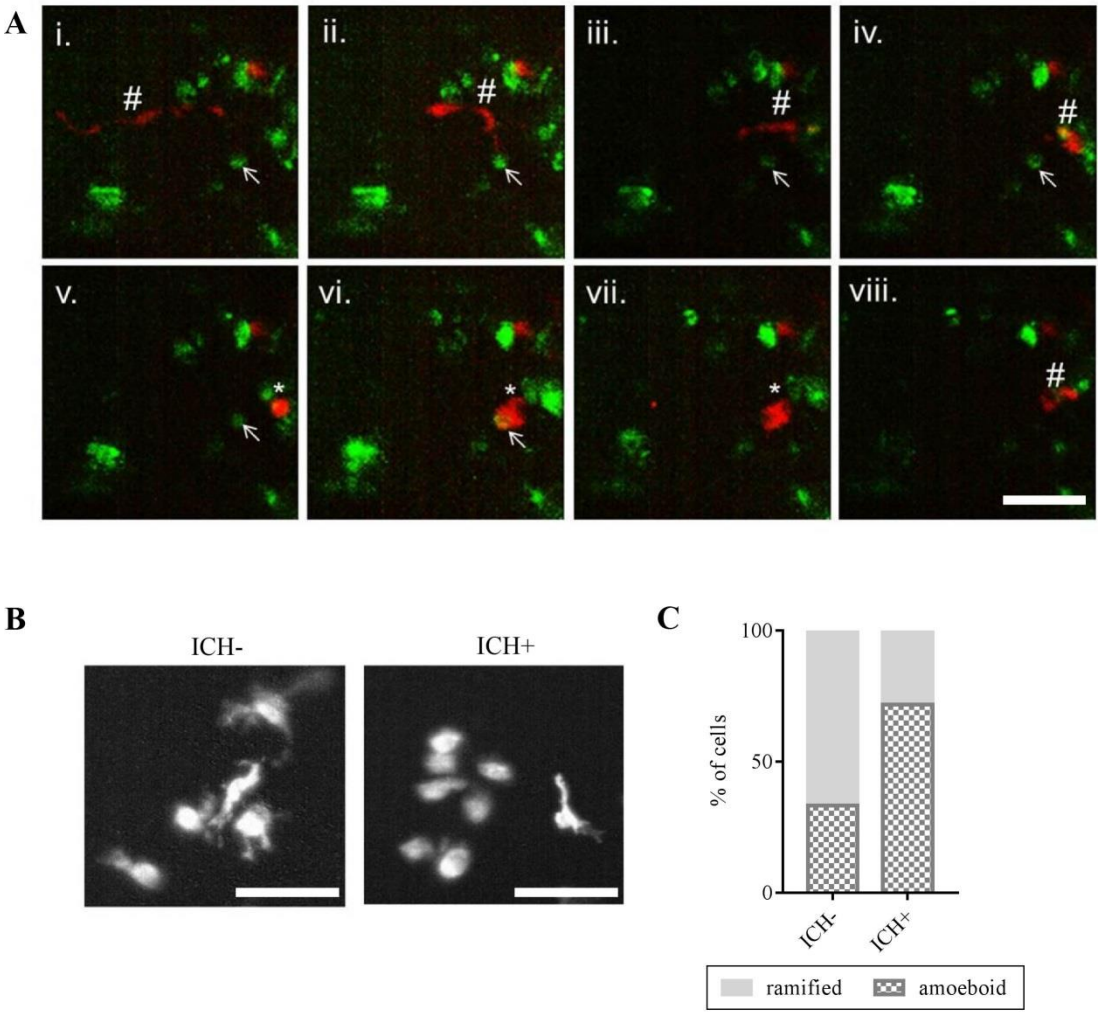

Figure 3.3.8 Activated macrophage cells show a phagocytic response to the brain lesion.

(A) Representative time-lapse stills (from appendix iv) showing a ramified patrolling macrophage migrating towards an annexinV positive cell (i - vi). Stills are obtained from a series of images taken of the whole brain using a 20X objective. Scale bar represents 50 µm. The macrophage acquires an amoeboid morphology (v) before phagocytosing the annexinV-positive cell (vi, vii). After phagocytosis the macrophage resumes a ramified morphology and migrates away and the annexinV-positive cell can no longer be seen (viii). Ramified macrophage (#), annexinV positive cell (arrow), amoeboid macrophage (*). (B) Representative images of *mpeg1*-positive cells in the intracerebral haemorrhage ICH- and ICH+ larval brain exhibiting amoeboid and ramified morphologies from n=9. Scale bars represent 50µm. (C) An increased proportion of amoeboid (phagocytic) and decreased proportion of ramified (inactive) macrophages was observed in ICH+ brains in comparison to ICH- siblings.

3.4 Discussion

Here, we reveal that ICH in zebrafish larvae induces quantifiable pathological and inflammatory consequences that mimic aspects of human pathophysiology. Several groups have previously described the mechanisms underlying neurovascular instability in zebrafish larval models of ICH (Buchner et al., 2007; Eisa-Beygi et al., 2013; Liu et al., 2007), and drug intervention studies have attempted to identify compounds that can inhibit cerebral bleeding (S. Li et al., 2017; Yang et al., 2017). However, the relevance and translational impact of intervention before onset of haemorrhage is unclear. As such, we focussed our attention on characterising the pathological and immunological consequences of blood in the brain in zebrafish models, which we consider to be a more realistic therapeutic target.

In general, ICH can be predominantly considered as a disorder associated with older age. Consequently, it is remarkable that the phenotypes observed in developing zebrafish recapitulate those associated with the aged human brain, indicating the innate injury response to blood in the brain is both evolutionarily conserved between species and analogous during development and adulthood. Zebrafish models have been employed in other neurological and neuropsychiatric disease investigation, including epilepsy, schizophrenia, Alzheimer's and Parkinson's disease, because of these conserved fundamental mechanisms and behaviours (Fontana et al., 2017; Vaz et al., 2018). Although these models present their own limitations, the use of non-invasive *in vivo* imaging, ease of genetic manipulation and availability of large sample sizes offers new insights and overcomes some of the common restrictions associated with rodent models. Given that ICH occurs spontaneously using non-invasive techniques in zebrafish, it can be argued this system more accurately models some aspects of the human condition than the most commonly used rodent models (Andaluz et al., 2002; Rosenberg et al., 1990). The use of rodents has not been successful in terms of identifying translatable therapeutic targets for ICH. As such, we propose that the post-ICH pathologies presented in this study (Figure 3.4.1) represent an alternative, complementary platform for pre-clinical ICH research and future drug discovery.

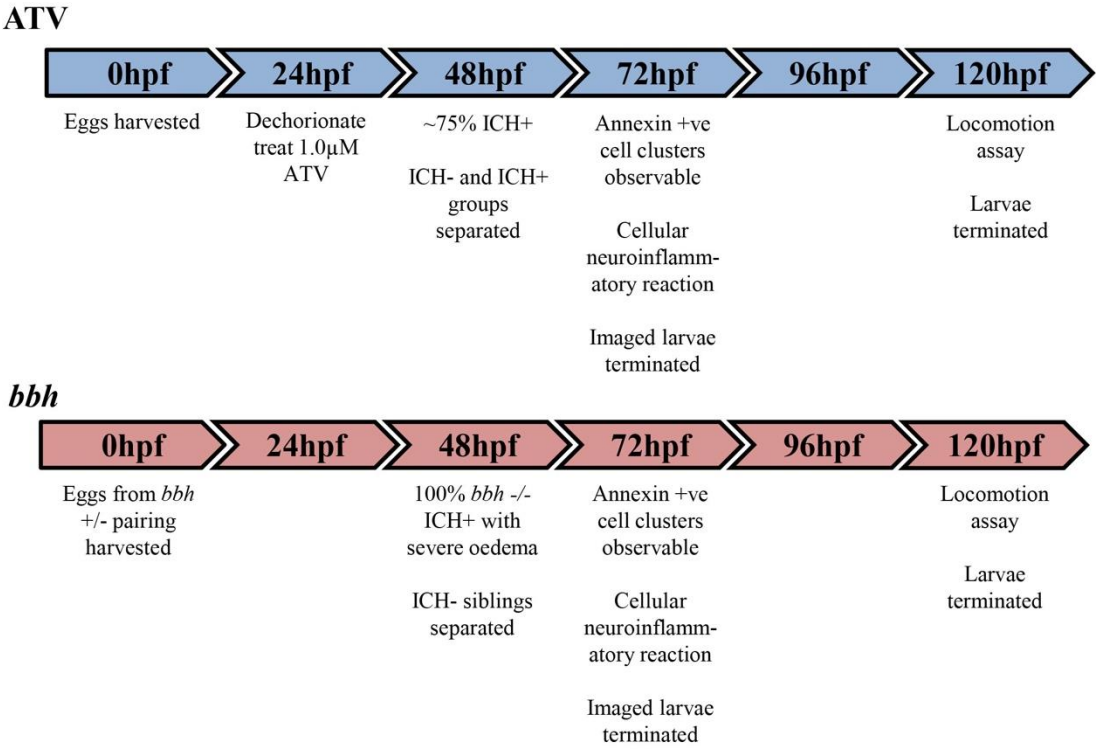

Figure 3.4.1 Graphic of experimental timeline to characterise brain injury, locomotor and neuroinflammatory outcomes.
ICH, intracerebral haemorrhage; *bbh*, *bubblehead*.

The transferability of employing these zebrafish larval models would address the 3Rs welfare issue of prolonged severe surgical procedures in mammals by replacing some of these animals with zebrafish larvae of unprotected status. We have used equipment and procedures that are commonplace and would be relatively simple to adopt in other labs. We would like to see these models used to determine the translatability of drugs that prevent cerebral bleeding in zebrafish (Huang et al., 2017; Yang et al., 2017), to investigate the clinical relevance of post-ICH treatment. We also propose these endpoint assays can be used to develop medium/high-throughput drug screening to identify new compounds for pre-clinical investigation.

In humans, an influx of blood into the brain causes primary brain injury through neuronal death and cell necrosis, inducing a secondary phase of injury triggered by the production of inflammatory mediators and innate immune cell migration towards the site of injury (Mracsko and Veltkamp, 2014). We show that cerebral bleeding in zebrafish larvae causes an increase in cell death in the brain not shown before in zebrafish haemorrhage models. This lesion was associated with a physical impairment, as observed by a reduction in swimming ability, which we propose is either due to a defect in stimulus perception or through a motor deficiency. This impairment is seen to begin to recover at 3 days post injury, suggesting the zebrafish larval model system as a useful tool for further investigation to reveal recovery processes responding to brain cell death. Importantly, these observations mimic outcomes that are exhibited in rodent models (MacLellan et al., 2008) and ICH patients (Saulle and Schambra, 2016). In clinical presentation of ICH the initial haematoma mass effect and increase in intracranial pressure exacerbates brain damage, compressing surrounding structures (Xi et al., 2006) and increases risk of death following ICH (Yang et al., 2015). In zebrafish larvae, cerebral oedema is regularly associated with ICH (Kasher et al., 2015; Liu et al., 2007). However without a fully developed cranium, oedema is unlikely to result in the same injury severity seen in humans, which may be one limitation of this particular model system.

An increase in recruitment and activation of macrophages in the brain was also observed in zebrafish following haemorrhage corresponding to time of cell death. A trend towards increased recruitment of neutrophils was also observed, but this result did not reach statistical significance. It is possible that a rapid temporal neutrophil response was not fully captured during our analytical time frame. However, it has been

shown that neutrophils are not involved in the clearance of cellular debris in a zebrafish larval model of brain injury (van Ham et al., 2014), suggesting neutrophils are less vital to early injury responses in the brain than macrophages. It remains unclear whether activation of macrophages post ICH is overall beneficial or deleterious in the short term after injury. Pro-inflammatory cells contribute to the breakdown of the blood-brain barrier (Abbott, 2000); however, phagocytic cells promote clearance of red blood cells and tissue debris, which occurs from 7 days post haemorrhage in rodent models of ICH (Mracsko and Veltkamp, 2014; S.-S. Yang et al., 2016). Early responses to laser-induced cerebral bleeding in zebrafish have shown that macrophages are essential for vessel repair (Liu et al., 2016) and in zebrafish stab wound brain injury models, inflammation is necessary for regeneration and recovery (Kyritsis et al., 2012). Studies show that polarisation of macrophages to M1-like and M2-like states change over time in rodent models of ICH in response to brain damage molecules (Wan et al., 2016; J. Yang et al., 2016) and some drugs in clinical trials target microglial polarisation in an attempt to prevent the pro-inflammatory phenotype (Lan et al., 2017). *In vivo* imaging of ICH-induced inflammatory processes has barely been explored (Mracsko and Veltkamp, 2014), and so the translucent nature of zebrafish larvae and availability of transgenic lines offer an accessible model for further interrogation. Observations of cellular interactions within whole, intact rodent brains at ongoing time points are currently not possible, therefore utilising the zebrafish system will allow us to learn more about leukocyte behaviour after spontaneous ICH. Furthermore, immune responses observed in real time in this system will have been elicited by spontaneous vessel rupture and not as an artefact of ICH surgery or *ex vivo* analysis (Kirkman et al., 2011; Xue and Del Bigio, 2003). For better translation of therapies from pre-clinical to patients, understanding of early innate immune responses to spontaneous bleeding needs to be improved, thus zebrafish offer a powerful resource to facilitate this.

In conclusion, given the advantages associated with zebrafish larvae and the potential for a 3Rs approach to pre-clinical stroke research, we propose that this model organism can provide critical insight into ICH pathophysiology during the early phases of injury and offers a future platform for drug discovery.

Research Highlights

Scientific benefits	• No surgery is required so the models more accurately recapitulate spontaneous ICH • Ease of genetic manipulation associated with zebrafish allows for the use of transgenic and mutant lines • Transparency of zebrafish larvae allows for non-invasive monitoring of cellular processes over time (live imaging)
3Rs benefits	• Unprotected zebrafish larvae (before 5 dpf) can be used as an alternative to rodent models in pre-clinical ICH research
Practical benefits	• High fecundity of zebrafish pairings means that a large sample size of genetically comparable siblings can be produced easily • Zebrafish are a lower cost organism to host than rodents • Experimental timeline is less time consuming than typical rodent studies which look at long term outcomes of stroke commonly up to 3 months
Current applications	• Elucidating immediate pathological outcomes of spontaneous ICH in the brain of intact animals
Potential applications	• High throughput drug screens for ICH therapies • Replacing the current rodent models for analysis of immediate ICH pathology

Grant information

This study was supported by the NC3Rs (NC/N002598/1), Stroke Association (TSA LECT 2017/02), ERA-NET NEURON (MR/M501803/1) and The British Heart Foundation (FS/14/64/31291, FS/15/67/32038). We are also particularly thankful to The Natalie Kate Moss Trust for their continued financial support.

Acknowledgements

We would like to thank Prof Yanick Crow and Dr Gillian Rice for use of equipment and reagents, Dr David Spiller and the University of Manchester Systems Microscopy Core Facility for use of the light sheet microscope, and Prof Richard Baines for the use of DanioVision. The *bbh* line was kindly shared by Nicole Munsie from Dr Sarah Child's lab at the University of Calgary. We also thank Prof. Stephen Renshaw for sharing the *mpo*:GFP line.

Chapter 4: Characterising the zebrafish larval models of ICH

4.1 Introduction

Zebrafish larvae as non-protected organisms, offer a replacement strategy for rodent usage in the pre-clinical stroke field. The use of adult fish for breeding is considered a mildly stressful procedure in comparison to the moderate severity of surgery and potential for lasting harm of stroke in rodents. From a 3Rs perspective, reducing the number of animals by employing the zebrafish larval model has an ethical benefit in addition to the scientific advantages highlighted previously that a new model can offer. If the zebrafish model can be adopted by the wider stroke community, complementary to the rodents, there is potential for a global reduction of animal usage. The zebrafish larval model utilises the speed of development and larval transparency to allow for investigation of brain cell atrophy, functional deficit and neuroinflammation non-invasively over time after an ICH (Crilly et al., 2018; Crilly et al., 2019). In this study we continue to characterise different aspects of disease pathology, to draw parallels with ICH outcomes observed in both rodents and human patients and offer additional translational comparisons.

In order to generate an ICH model comparable to the widely used *in vivo* collagenase model in rodents, we considered the multitude of measureable outcomes of disease severity in rodents and aimed to develop some equivalents in zebrafish. Fully characterising the ICH pathology in the zebrafish will provide many parameters by which to measure severity and improvement. We have observed previously that the location of haemorrhages, another predictor of clinical severity, is consistent between ATV and *bbh* models appearing in the forebrain and hindbrain (figure 3.3.1). We sought to determine the severity of the injury in zebrafish compared to the human condition by estimating the haematoma volume. We have monitored the progression of brain injury after ICH using transgenic larvae to observe cell death in real time (figure 3.3.3) however the question remains as to which cells are contained in this apoptotic population and whether they are directly linked to the loss of motility function. ICH patients and rodent models also exhibit a decrease in cerebral blood flow following injury which is associated with the prevention of haematoma expansion and further increase of intracerebral pressure (Gould et al., 2013). Some clinically relevant measurements are however impossible in zebrafish larvae, such as

cognitive testing for neuroscore, ICP and brain water content because of their size and developmental nature.

Zebrafish exhibit regenerative properties in tissues such as the heart (Poss et al., 2002), fin, skin and nervous tissues (Becker et al., 1997) at larval stages. This improves the chances of full recovery after injury, which may be explored in terms of ICH in this model. If the zebrafish larvae recover fully from a haemorrhage, with no long lasting pathology, then through further investigation it may be possible to exploit these recovery mechanisms in the adult human tissue to promote faster and fuller recovery after stroke.

4.2 Identification of pathological characteristics of zebrafish larval ICH

Following on from the publication of the motility and cell death assays (Crilly et al., 2018; Crilly et al., 2019), we aimed here to further investigate whether other pathologies were conserved between zebrafish and humans, and to further define the pathological outcomes in the zebrafish ICH model.

Estimating the volume of haematoma and the region of cell death

In human ICH location of bleed and haematoma volume are two vital predictors of disease severity (Shaya et al., 2005). We have observed consistent and comparable haemorrhage locations in our larval models, in both forebrain and hindbrain, presenting a heterogeneous population. In order to estimate the volume of the haematoma in zebrafish larvae we used 3D rendering of images (n=7) acquired from light sheet microscopy (Broderick et al., 1993; Jordan et al., 2009). Using IMARIS software (version *9.3*) to generate a 3D image from z stacks of *fli1:*GFP;*gata1*:dsRed ICH+ larvae at 3 dpf (figure 4.2.1, appendix v) we determined the average haemorrhage volume to be 9.6x10^5 μm^3 (figure 4.2.1B). As an estimate of total brain volume of the larva we used the x,y and z measurements from the acquired whole brain images of 3 dpf larvae in Ahrens et al. (2013) to equal 3.1x10^7 μm^3. Haematoma volume therefore was found to be 3.1% of the total brain volume. In comparison to humans, a haematoma volume greater than or equal to 2% (~30cm^3) of the total brain is associated with moderate neurological deficit (Kleinman et al., 2011), with volumes greater than this increasing the risk of death and vegetative state. In the mouse collagenase model, average haematoma sizes differ depending on the concentration of collagenase injected. In one study, characterising the collagenase double injection model in mice, average lesion volume was measured at 2.0±0.2mm^3 (mean±SEM), equating a haematoma of 0.39% of the total brain volume (508.91±23.42mm^3) (Badea et al., 2007; Belayev et al., 2003). This implies that in comparison to the human condition, the representative zebrafish larval haematoma volume we observe most likely equates to a moderate neurological deficit.

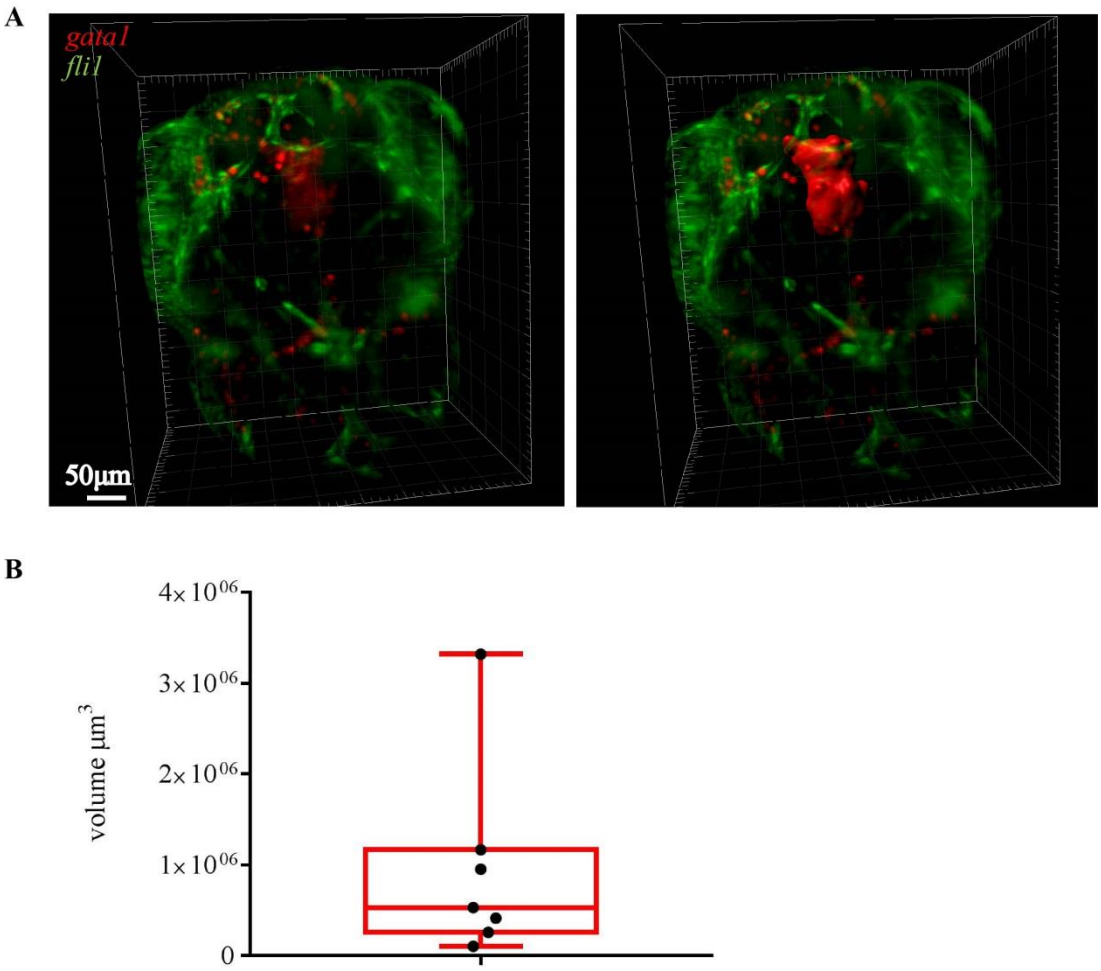

Figure 4.2.1 3D rendering of the haematoma volume
(A) Images acquired of *fli1:*GFP;*gata1*:dsRed ICH+ larvae were opened in IMARIS software and using the surpass tool were rendered to 3D images. A region of interest was drawn around the dsRed expressing RBCs in the haematoma (right panel) and the volume selected as the chosen output. Representative image of n=7. (B) Haemorrhage volume measurements. Boxplot shows maximum/minimum values and interquartile range.

To determine the volume of the region of cell death, z stack images (n=8) of *ubiq:*secAnnexinV-mVenus ICH+ larvae were made into 3D images (IMARIS 9.3) (appendix vi). The region of interest was determined to include the most intense regions of mVenus expression. A 3D image shows that the most concentrated clusters of dying cells are in the forebrain and in the midbrain right and left optic tectum, present in all larvae imaged (figure 4.2.2). The average total volume of the annexinV positive region was 1.2x10^5 μm^3 which equates to 0.39% of total brain volume.

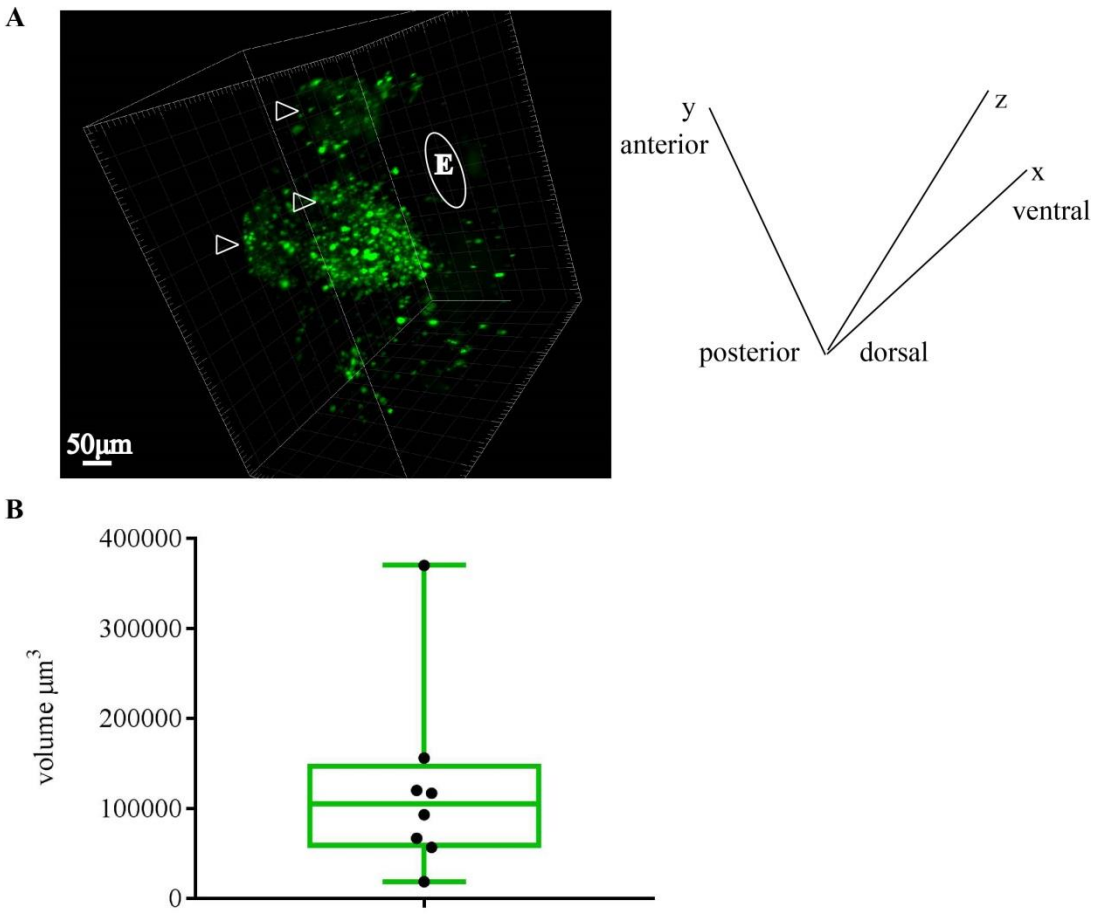

Figure 4.2.2 3D rendering of the annexinV positive region of cell death
(A) 3D rendering of the mVenus positive cells in an *ubiq:*secAnnexinV-mVenus ICH+ larvae shows there are 3 regions of interest, the forebrain and two bilateral clusters in the midbrain denoted by arrows. E-eye. (B) AnnexinV region volume measurements. Boxplot shows maximum/minimum values and interquartile range.

Dying cells in the brain after ICH have not been identified

In order to characterise the populations of cells that were expressing annexinV in our cell death assay, we isolated fluorescent cells from *bbh ubiq:*secAnnexinV-mVenus ICH+ larvae using FACS to probe for cell type markers by western blot and whole-mount staining. We expected a mixed population of cells and therefore probed the blots using antibodies targeting neuronal nuclear antigen (NeuN), apolipoprotein E (Apoe) indicative of macrophages and myeloperoxidase (Mpo) for neutrophils. Baseline annexinV expression was too low in ICH- larvae to extract a large enough cell population for protein analysis in a control. Western blot analysis (not shown) was inconclusive, perhaps due to polyclonal antibodies and lack of specificity. Additionally, extracting protein from a small population of dying cells from whole embryos did not result in adequate concentrations for blotting analysis. Whole-mount staining for Mpo showed that cells do not localise where we see the annexinV positive cells in the brain, implying that Mpo positive cells are not part of the cluster population (figure 4.2.3). No other antibodies were suitable for whole-mount staining and so results are inconclusive. Future assessment of dying cells could make use of the transgenic lines for specific cell types and whole mount stains for dying cells like acridine orange or TUNEL.

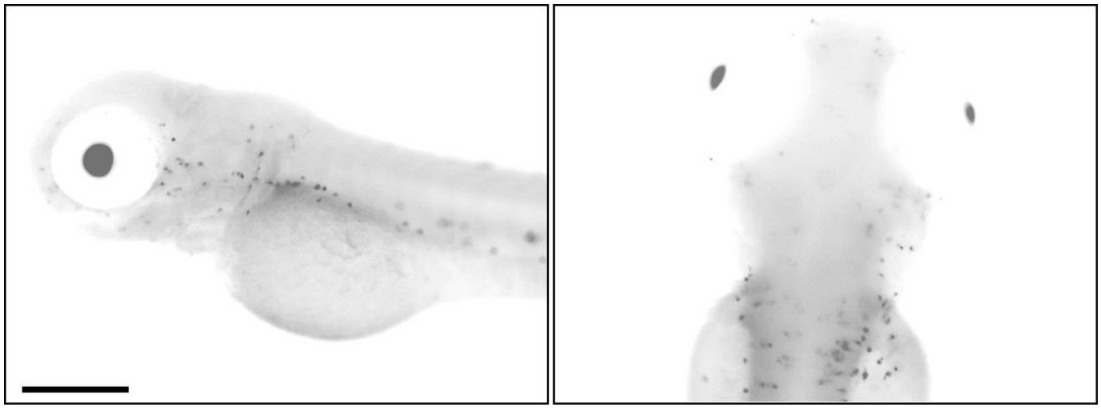

Figure 4.2.3 Immunohistochemical analysis of mpo positive cells after ICH
Whole-mount stains for 3 dpf ICH+ larvae with an antibody detecting Mpo expression indicates neutrophils do not cluster within the cerebral hemispheres. Images are representative of n=15. Images processed and inverted on ImageJ. Scale bar represents 250µm.

Brain haemorrhage decreases local blood flow activity

We next investigated the blood flow rate in larvae with and without brain haemorrhage. Clinically, a brain haemorrhage reduces local cerebral blood flow (Lee et al., 1997; Yang et al., 1994), therefore we utilised the transparency of larvae to measure the local blood flow in live, intact animals. ICH- and both ATV and *bbh* ICH+ larvae were analysed for blood flow rate in the head through the mesencephalic vein (figure 4.2.4), and heart rate using the DanioScope (Noldus version 1.1). Compared to ICH- sibling controls, local blood flow following haemorrhage in both models was significantly reduced by ~85% at 2 dpf and 3 dpf (figure 4.2.5). Heart rate in all the groups was unchanged at both time points (figure 4.2.5). At 3 dpf we have observed an increase in the level of *il-1β* expression (figure 5.2.1) which we hypothesise is contributing to the innate immune response and progressing brain damage as is observed in rodent models and humans (Sobowale et al., 2016). Locally IL-1β can also act as a vasodilator, to enable the extravasation of immune cells and we anticipated that the blood flow in the head of the zebrafish larvae would increase at this time point (Osuka et al., 1997; Plata-Salaman et al., 1995). Our data suggests that one or two individual larvae may be exhibiting vasodilation and restored blood flow at 3 dpf (figure 4.2.5 A and B). This sustained reduction in blood flow in the majority of animals may suggest why peak levels of brain cell death are seen at 3 dpf (~24 hpi). It may also suggest why regions of annexinV expression do not overlap with the hematoma location in the head as loss of circulation is damaging secondary to the mass of the haematoma due to loss of nutrients, sugars, ions etc (figure 4.2.6). Cells within the haematoma are known to undergo different forms of death such as ferroptosis, necrosis and necroptosis (Zille et al., 2017) and therefore not observed to be annexinV expressing. We can utilise the high throughput measurement of blood flow as another translatable indicator of disease severity.

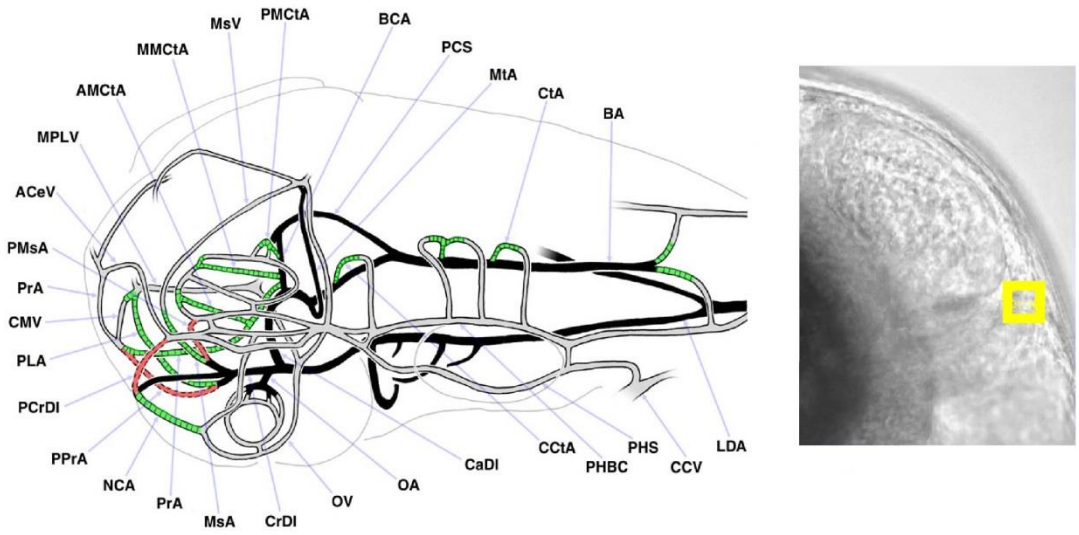

Figure 4.2.4 Blood flow was measured through the mesencephalic vein at 3 dpf
Larvae at 2 and 3 dpf were immobilised and filmed for 30 seconds to record blood flow. The videos were analysed using DanioScope over the mesencephalic vein (MsV, left panel (Inagawa et al., 2003)) and flow activity over the S01 region calculated (yellow highlight).

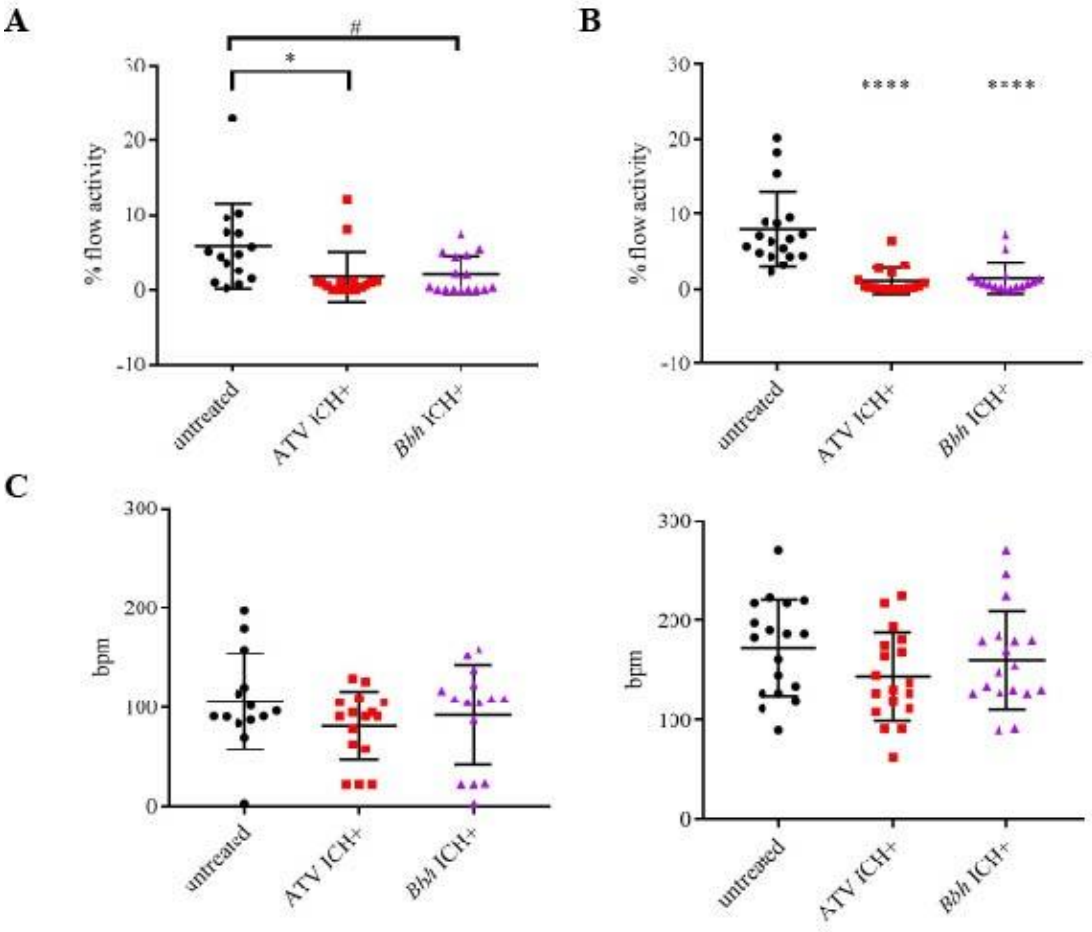

Figure 4.2.5 Effect of brain haemorrhage on local blood flow following ICH
(A) Blood flow videos were recorded for ICH- and ATV and *bbh* ICH+ larvae at 2 dpf and analysed for blood flow activity % using DanioScope software. Data were analysed using a one-way ANOVA to show significant reduction in ICH+ larvae (*p=0.01, #p=0.03, n=7-8 per group, 2 independent replicates). (B) ICH+ larvae show decreased blood flow activity % in the brain local to the hematoma at 3 dpf (n=7-8 per group, 2 independent replicates). Data were analysed using a one-way ANOVA to show significant reduction in ICH+ larvae (****p<0.0001). (C) Heart rate measured using the DanioScope was analysed as a control for global blood flow and there was no difference between the ICH- and ICH+ groups at either 2 dpf (left) or 3 dpf (right) (n=7-8 per group, 2 independent replicates).

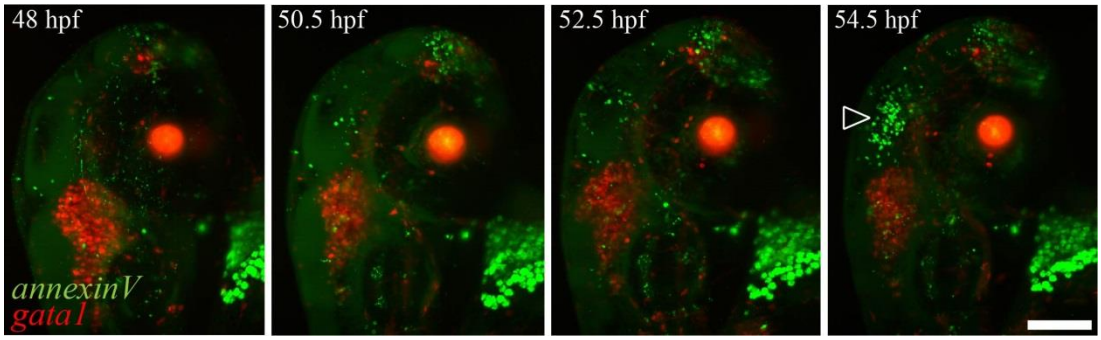

Figure 4.2.6 Analysis of brain cell death region with respect to haematoma location

ICH+ double transgenic *gata1*dsRed:*ubiq:*secAnnexinV-mVenus larvae were mounted in the light sheet microscope and time lapse images were taken between 48 hpf and 72 hpf. Green shows annexinV binding and red is *gata1* positive RBCs. Still images show the development of a region of annexinV positive cells dying in relation to the *gata1*:dsRed positive red blood cells in the head over 6.5 hours (arrow). Scale bar represents 100µm.

4.3 Investigating long term outcomes of larval ICH

Following the characterisation of immediate pathology in this model we sought to determine whether there were longer term outcomes of brain haemorrhage that occurred during larval stages. Zebrafish demonstrate neuroregenerative properties into adulthood (Becker et al., 1997; Ghosh and Hui, 2018; Kishimoto et al., 2012) and further understanding these pathways in this ICH model may provide insight into the endogenous mechanisms that could potentially be exploited therapeutically. As such we next investigated whether there was any evidence of lasting pathology in juvenile and adult zebrafish after an ICH.

Locomotor function recovers after 5 dpf

To determine whether the loss of significance at 5 dpf in the motility assay was indicative of a rapid recovery process (figure 3.3.6), we tested motility in larvae up to 21 dpf to see if swimming function was recovered following ICH. Untreated ICH-ATV treated ICH+ and *bubblehead* ICH+ larvae were assayed for locomotion at 5-21 dpf at daily then weekly intervals. ATV treated larvae at 5 dpf showed a significant reduction in swimming time compared to untreated and *bbh* larvae. Data from *bbh* larvae suggests that swimming recovers to baseline as juveniles however there is a trend to show that ATV ICH+ larvae do not fully recover although the differences are not significant (figure 4.3.1). ATV ICH+ larvae did not live until 21 dpf so this data point is missing and further investigation could reveal if survival is dependent on haemorrhage. A Kaplan-Meyer survival curve for both haemorrhage models could show if ATV ICH+ larvae results in significant loss of larvae.

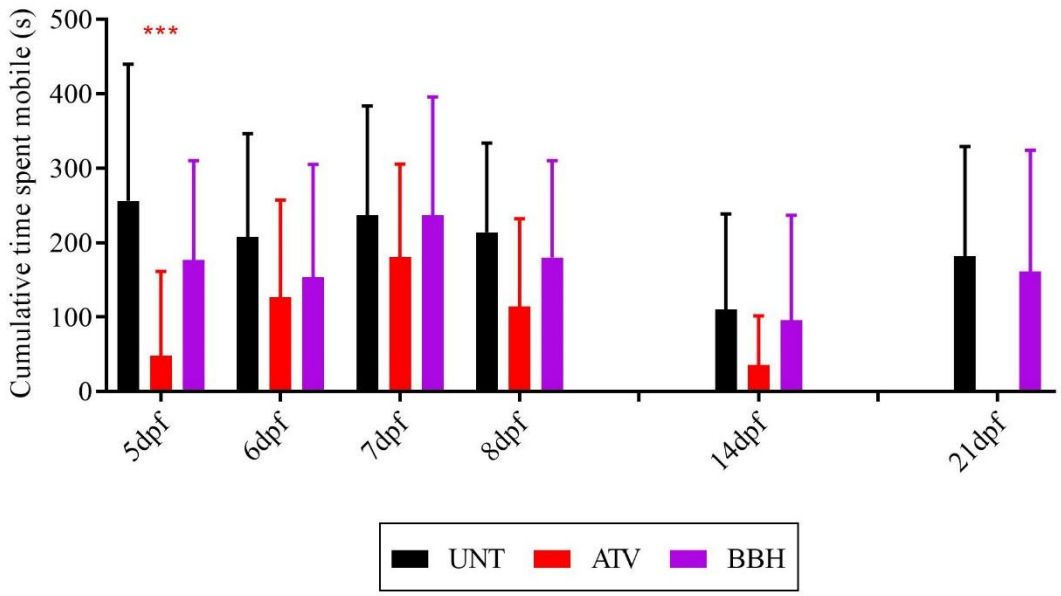

Figure 4.3.1. Long term analysis of locomotor function in ICH+ larvae
Untreated ICH-, ATV treated ICH+ and *bubblehead* ICH+ were assayed for locomotion at 5-21 dpf (n=24 larvae per group, 1-3 independent replicates). ATV treated larvae were dead at 21 dpf and therefore data point is missing. Data analysed using one-way ANOVA with non repeating measures (***p=2e^{-7}ATV vs UNT, *bbh*).

Adult zebrafish brains exhibit no pathological morphology following larval ICH

To assess whether ICH during larval stages could cause long term neuropathological changes, adult brains from *bbh* homozygotes and wildtype siblings were harvested at ~1 year old. Brains were paraffin embedded, sectioned and stained with haematoxylin and eosin to identify white matter changes, presence of hemosiderin, evidence of hypoxia, neuronal stretching or gliosis (Finnie, 2016; Perry and Brat, 2010). Both the ICH+ and ICH- control brains look comparable at 1 year after injury and there was no evidence of previous haemorrhage and brain damage suggesting that the larvae fully recover by adulthood (figure 4.3.2). Representative images of sections were chosen to be as comparable as possible between WTs and homs however challenges with tissue orientation when sectioning means these are not exact. Additional images are available in appendix vii. Some evidence of astrocyte stretching and microvacuolisation was present in the hindbrain of the ICH+ homozygote brains however this could be attributed to natural ageing as it was identified infrequently and was highly dispersed throughout the tissue.

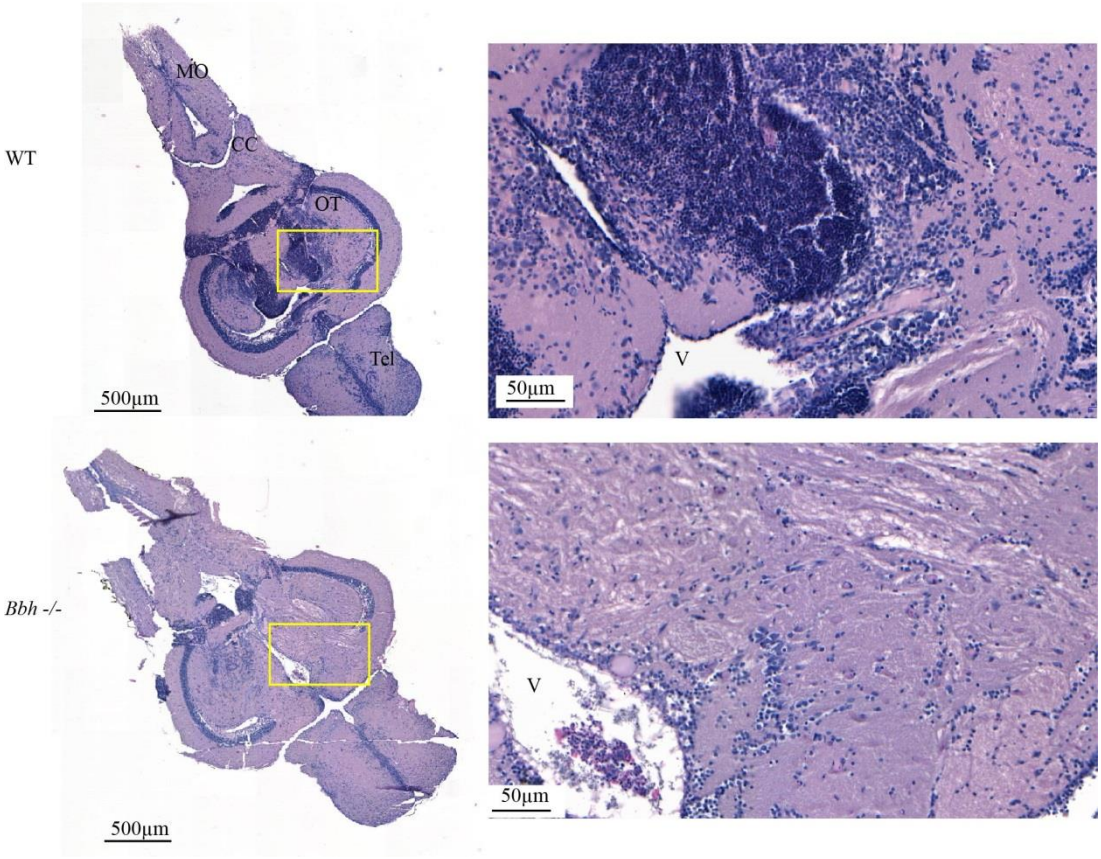

Figure 4.3.2. H and E stains of adult zebrafish brains from WT and *bbh* ICH+ homozygotes

Homozygous *bubblehead* adult brains (bottom panels) show no neuropathological differences associated with larval haemorrhage from wildtype brains (top panels). Images are representative of n=3. MO – medulla oblongata, CC – cerebellar crest, OT – optic tectum, Tel – telencephalon, V – ventricle.

4.4 Discussion

In this study we have further shown characteristics of the zebrafish larval ICH model that aids analysis of disease processes and may help to elucidate novel therapeutic strategies. Although zebrafish are more evolutionarily distant from humans, the compromise made for a faster model in a smaller vertebrate that is amenable to drug screens enables investigation that is impossible in rodents. Thus far the use of rodent models has not resulted in successful translatability of drugs to clinic. We hypothesise that by investigating more broadly in a simpler organism, and by taking advantage of the spontaneous nature of ICH, we might develop new strategies for therapy and medication. The zebrafish model has shown that important disease mechanisms are conserved across species and developmental stages.

There are limitations associated with this model, for first instance, the aquatic environment zebrafish larvae develop in is very different to that of the adult human brain. Secondly, due to the lack of calcified bone and a fully developed cranium at this developmental stage, intracranial pressure is not increased due to the larval head's capacity to swell (*bubblehead*). Additionally, the zebrafish can withstand considerable injury without exhibiting the equivalent symptoms we would expect in a human patient due to their regenerative properties. Also, zebrafish larvae are not amenable to cognitive studies comparable to neuroscore measurements in rodents. Here we show that the zebrafish models a moderate haemorrhage compared to humans, and they manage well with this size of haematoma. There have been no cases of haemorrhage related sudden death recorded in our study, which occurs in 10% of human patients (Intercollegiate Stroke Working Party, 2012). However, the ability to fully recover after a haemorrhage offers a unique platform to investigate the biomechanics of swift recovery from an ICH. Determining the difference between developmental processes and recovery mechanisms that may be activated in an adult is a contentious subject in zebrafish biology. Further studies should focus on understanding the developmental processes that allow for such rapid recovery in the zebrafish model and investigate whether these pathways, normally dormant in the mature human brain, could be activated to aid recovery from ICH-induced injury.

AnnexinV binding is not a true accurate measure of total brain cell death following haemorrhage, as annexinV binds to phosphatidylserine only in apoptotic cells and it

has been shown that many other cell death processes are active during ICH such as necrosis, pyroptosis and necroptosis (Zille et al., 2017). However by measuring programmed cell death, there is a chance that these cells can be rescued, and apoptosis can be stopped, whereas other mechanisms of cell death are less controlled. Determining the cell types in this slowly dying population would reveal if the brain tissue was salvageable if the phagocytic macrophage response could be inhibited. Future work could elucidate the cell type population by using mass spectrometry on protein isolated from the annexinV positive cells, or immunofluorescent staining of the cell extract smeared onto a slide.

Interestingly, annexinV clusters of dying cells always occur in the same bilateral regions in the mid and fore brain, that do not overlap with the bleed site. This is potentially because of the sustained reduction in cerebral blood flow which affects the entire brain, observed in the recordings. Specific brain areas that require high blood flow for development and function at this time point may suffer due to ischemia caused by ICH and therefore the regions of cell death are consistently located. Reduced autoregulation of cerebral blood flow following ICH also occurs in humans (Butcher et al., 2013) and experimental models (Liu et al., 2011) and leads to the spread of ischemia and death of hypoxic tissues (Garg et al., 2012). By reducing cerebral blood flow, expansion of the haematoma is prevented and some suggest this is mechanistically due to an increase in ICP (Lowell and Bloor, 1971) or perhaps due to increased interleukin-1β expression (Bray et al., 2016). The global reduction in blood flow in response to ICH offers a new translatable high throughput assay to quantify severity of the injury and recovery projection. Effective ICH therapies that improve pathological outcomes may be acute blood pressure lowering, or by latent restoration of blood flow to the peri-haematomal area and this assay offers a platform for measuring that response in zebrafish.

The model is also amenable to further study of the *mpeg1* and *mpo* positive cells that respond to the bleed. Previously we showed that ICH results in increased activated macrophage numbers in the brain. By extracting these populations through FACS and extracting RNA we can investigate the regulation of genes associated with the immune recruitment between ICH- and ICH+ in macrophages and neutrophils. This information could be used to control the ‘switching’ between neuroinflammatory and neuroprotective mechanisms. It would also be useful to determine when cell

populations are recruited from the periphery by resident immune microglia, as the transgene *mpeg1* is expressed in both cell types. This could be performed in the fish using a Hoechst stain injection, as this fluorescent nuclear dye will be phagocytosed by peripheral macrophages only, as it is unable to cross the BBB (Davis and Ramakrishnan, 2009). The caveat with the experiment is that the BBB is damaged following ICH and therefore new transgenic animals, specific for microglia/macrophage markers are needed.

Additional characterisation shows that the zebrafish larvae fully recover from the ICH event and do not display any long term pathology in brain morphology. This is vastly different from the human condition, as even with surgical removal of the haematoma, the haemorrhage and brain oedema can still be seen 14 days after surgery and chronically, surrounding tissue undergoes organisation leaving a gliotic cavity that can be identified post mortem (Love, 2011; Takasugi et al., 1985). The full functional recovery of swimming ability after 6 dpf in zebrafish larvae implies that the damage is reversed in the developing organism. These recovery processes require further investigation, but there may be potential to exploit the regenerative properties of zebrafish to speed up recovery in humans and restore brain function. The prolonged presence of RBC lysis debris and hemosiderin after the haematoma clears forms a glial scar, preventing full repair (Li et al., 2018). Here we have shown that this extensive damage is not replicated in zebrafish models and 1 year after ICH there is no neuropathological evidence. Obtaining brains from 3 – 6 month old zebrafish may show a residual immune response or physical damage from the embryonic bleed however this is yet to be determined.

Here we have demonstrated how the zebrafish larval models of pre-clinical ICH exhibit translational pathologies that provide additional high throughout, assayable outcomes to determine disease severity.

Chapter 5: Using a zebrafish larval model of ICH for target drug discovery

5.1 Introduction

Treatment options for ICH patients are limited to anticoagulant reversal, blood pressure lowering and surgical haematoma evacuation upon admission to hospital. This requires access to trained, experienced clinicians, neurosurgeons and specialist stroke care staff. A surgical intervention can only occur once ICH has been diagnosed from a scan and HE has stopped. Surgery is not always a possibility, especially for patients from low-middle income countries where ICH prevalence is highest. There is a requirement for a targeted medical therapy that can be administered to patients as early as possible to prevent the severe pathological outcomes of ICH.

A widely reported therapeutic research approach in mammalian models of ICH is to modulate the immediate immune response to blood in the brain. Secondary injury contributes to considerable decline in patient prognosis as extravasation of active immune cells results in HE and oedema, meaning it is an ideal target for ICH therapies (Abid et al., 2018). In rodent studies, drug treatments that reduce the neuroinflammatory responses have enhanced functional outcomes and recovery following ICH (Kathirvelu and Carmichael, 2015). Microglia, the resident brain immune cells, are activated by thrombin in the haematoma to release pro-inflammatory cytokines following ICH (Wu et al., 2008). Thrombin has also been shown to drive the neuroprotective phenotype in microglia (Rohatgi et al., 2004). Thrombin activates the proteinase activated receptor 1 (PAR-1) and downstream MAP kinase signalling to increase the production of tumour necrosis factor alpha (TNF-α), a deleterious cytokine contributing to neuronal death (Mracsko and Veltkamp, 2014). In preclinical studies, targeting TNF-α with an antibody to reduce receptor binding and downstream signalling improved the performance of ICH+ mice in a rotarod task by reducing oedema and BBB breakdown (Lei et al., 2013). Haemoglobin mediated pro-inflammatory signalling on microglia through TLR4 also contributes to neuronal death. Blocking the activation of TLR4 reduced oedema in mouse studies (Fang et al., 2013; Y.-C. Wang et al., 2013) downregulating NFκB and downstream pro-inflammatory cascades. Neither of these treatments has yet been taken to clinical trial with human patients.

Interleukin-1β is an early activator of inflammation and also presents a likely target in ICH therapy. Cellular release of IL-1β involves pyroptotic mechanisms that contribute to the release and accumulation of DAMPs in the injury site (Lopez-Castejon and Brough, 2011). IL-1β binds to interleukin-1 receptors (IL-1R) on the cell surface and intracellular signalling cascades lead to the formation of the inhibitor of nuclear factor B kinase (IKK) complex. Active IKK phosphorylates the inhibitor of nuclear factor B (IκB), targeting it for degradation by the proteasome which allows for p50 and p65 NF-κB subunits to be translocated out of the nucleus and activated. P65 is also called RelA. NF-κB transcription factor binds conserved DNA motifs to increase the transcription of IL-1β responsive pro-inflammatory genes (Weber et al., 2010). In zebrafish, *il-1β* gene expression in macrophages is increased following tissue injury, and blockade of signalling decreases recruitment of leukocytes to the injury site, perhaps preventing the detrimental consequences of cell migration (Ogryzko et al., 2014a). In ischemic stroke studies, directly inhibiting the action of the master pro-inflammatory cytokine IL-1β using an IL-1 receptor antagonist (IL-1Ra, Anakinra) is neuroprotective (Sobowale et al., 2016) and has since moved into phase II clinical trials with significant reduction of downstream IL-6 levels in patients (Smith et al., 2018). IL-1Ra for ICH is in clinical trials with the primary outcome measure being the oedema expansion at 72 hours post injury onset (Parry-Jones, 2018). These studies suggest that the neuroinflammatory secondary injury response that exacerbates BBB breakdown and oedema is a considerable contributor to neurological damage that can be inhibited by IL-1Ra with neuroprotective outcomes. Zebrafish Il-1β is structurally conserved in humans and therefore IL-1Ra can be applied in the zebrafish larval model to investigate therapeutic benefit (Ogryzko et al., 2014a).

In addition to the early innate immune response, other toxic blood compounds released in the hematoma contribute to brain damage and offer more targets for medical intervention. Literature suggests that iron influx from RBC lysis and heme breakdown following an ICH may offer a mechanistic explanation for brain swelling, by increasing aquaporin expression, a water channel protein (Qing et al., 2009). Metal chelating drugs bind toxic metal ions and enable excretion from the body. There are many iron chelating drugs that are safe for medical use, to reduce iron overload from a blood transfusion, and show potential to be approved for alternative therapeutic purposes. Deferoxamine (DFO), a bacterial siderophore, binds free iron in the

bloodstream enabling excretion in the urine (Summers et al., 1979). Clinical trials inhibiting iron accumulation after ICH using deferoxamine had progressed to phase II at the time of experimentation, though recently published trial data show it to be ineffective with further investigation deemed futile (Selim et al., 2019). DFO treatment is associated with unpredictable adverse effects such as hypotension, visual and auditory changes and acute respiratory distress, all of which could worsen the haemorrhage outcomes (Kontoghiorghes, 1995). The Hi-DEF trial (high-dose deferoxamine in ICH) initially treated patients for 5 consecutive days and was suspended due to pulmonary toxicity (NCT01662895). The modified i-DEF protocol lowered the dose for 3 days of treatment and proved ineffective, powered based on a previous Factor VII trial (NCT02175225). There was no difference between treatment and placebo groups in terms of mortality, long term modified Rankin Scale (mRS) scores or safety.

Our zebrafish larval model is amenable to drug studies and so using the outcomes characterised in chapter 3 (Crilly et al., 2018; Crilly et al., 2019) we progressed to testing for significant improvements with likely therapeutic candidates, IL-1Ra and DFO. To date, ICH drug studies in zebrafish have focussed on preventing blood vessel rupture and developmental deformity rather than rescuing the pathology after a bleed (Huang et al., 2017; S. Li et al., 2017; Yang et al., 2017). We believe that this strategy lacks translational relevance for human ICH as it is difficult to identify at risk populations for pre-treatment, to prevent a haemorrhage from occurring. Our approach to drug screening was to treat larvae after a haemorrhagic event had already occurred, and monitor outputs at 3 dpf, when we see the most striking pathology. If we can identify compounds that reduce the severity of pathology after ICH in the larval model, there may be potential for clinical translation.

5.2 Investigation of interleukin-1β expression and inhibition as a therapeutic for ICH

Initially, we focussed on interleukin-1β expression and action as the primary target for reducing brain cell death and oedema after ICH. If *il-1β* mRNA expression displayed a similar temporal pattern in the zebrafish model to the cell death (figure 3.3.3) then we could assume that the two may be linked and that by blocking Il-1β receptors, we would inhibit pro-inflammatory action and subsequent pathology. IL-1Ra is a potent, competitive, reversible inhibitor of IL-1β (and α) which acts by binding to the receptor in the active site. It is produced endogenously by immune cells, epithelial cells and adipocytes as an immune modulator (Arend, 1990). Anakinra, a modified recombinant human IL-1Ra protein, is used to treat auto-immune inflammatory diseases like rheumatoid arthritis and is currently in phase II and III clinical trials for ICH and subarachnoid haemorrhage respectively (Galea et al., 2017; Parry-Jones, 2018). The zebrafish gene *il1fma* encodes a similar functioning protein on chromosome 11, however structurally is not orthologous to human IL-1Ra (Zou and Secombes, 2016).

Interleukin-1 expression in zebrafish is increased following haemorrhage

It has been previously shown that IL-1β release in response to brain tissue injury is vital for the inflammatory response cascade (Murray et al., 2015). To determine whether the same was true in our model of ICH, we sought to detect *il-1β* mRNA expression differences in ICH+ larvae compared to ICH- siblings. Using quantitative PCR (qPCR) analysis in both ATV and *bbh* models we saw a significant increase in the relative quantification of mRNA expression levels (RQ) of *il-1β* 24 hours post injury (hpi) at 3 dpf when compared to ICH- sibling *hprt1* housekeeper gene expression (figure 5.2.1). Identifying this increase in expression was inconsistent and varied between clutch and time of sampling. To investigate the optimum time point samples were obtained from very early time points after haemorrhage up until 14 dpf and although detection was irregular, levels were most consistently elevated at 3 dpf. A trend for increased expression of other innate immune marker genes was also observed in whole *bbh* ICH+ larvae although these alterations were not significant (figure 5.2.1). This time point corresponds to the greatest brain cell death, macrophage recruitment and activation (figure 3.3.3, 3.3.7).

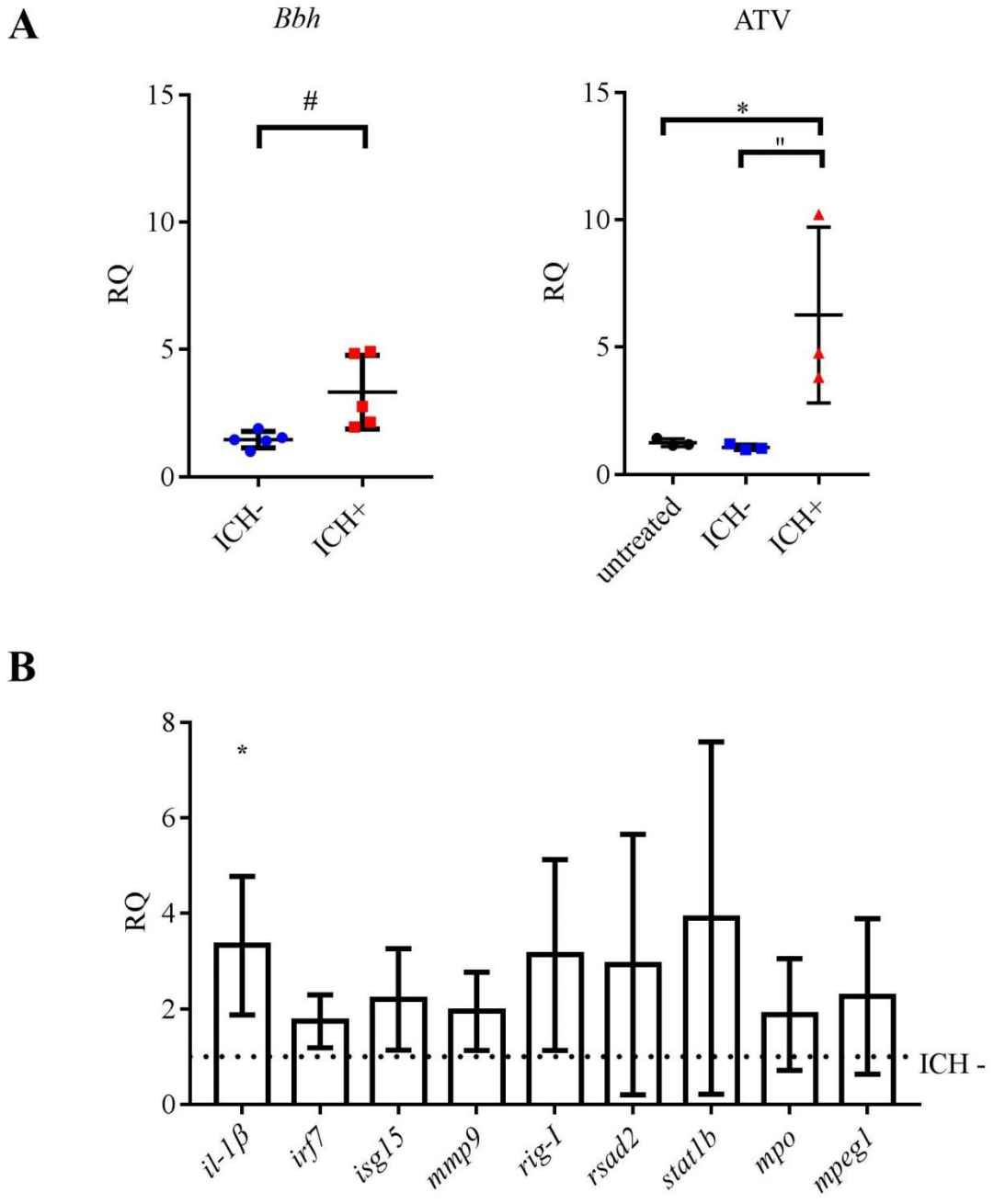

Figure 5.2.1 Expression of innate immune markers following ICH
(A) Expression levels of *il-1b* mRNA in ICH+ larvae, in comparison to ICH- siblings at 72hpf in both *bbh* (left panel) and ATV (right panel) models. RQ = relative quantification. Data from 3-5 independent replicates of RNA pooled from n=30 larvae (#p=0.022, *p=0.049, “p=0.043). (B) Expression levels of innate immune marker genes following haemorrhage. Data analysed using a two-tailed Student’s T Test comparing ICH+ to ICH- data. Large standard deviation from the mean as CT levels were at the limit of detection (5 independent replicates; *p=0.022).

Statins are most commonly recognised for their role in cholesterol inhibition, though they possess several other functions including anti-inflammatory properties (Abeles and Pillinger, 2006; Bu et al., 2011). ATV is a competitive antagonist of HMG-CoA reductase, the enzyme that converts HMG-CoA to mevalonate for isoprenoid and cholesterol synthesis (figure 1.8.1) (Eisa-Beygi et al., 2013). Statins are widely prescribed to patients with cardiovascular disease (CVD) to prevent secondary events like ischemia or ICH by reducing cholesterol levels (Westover et al., 2011). It has been debated whether this reduction in cholesterol increases the risk of ICH in ischemic stroke patients or increases recurrence of ICH, however this is usually overshadowed by the overall benefits of statins in CVD (Van Matre et al., 2016; Ziff et al., 2019). ATV is also known to reduce expression levels of several pro-inflammatory cytokines including IL-1β (Zhang et al., 2013). We treated *bbh* ICH+ larvae with 1.5μM ATV to determine if ATV-mediated anti-inflammatory action was protective in our model. There was no significant difference seen in brain cell death when compared to untreated *bbh* ICH+ however there was more individual variability in this group (figure 5.2.2A). ATV did show anti-inflammatory properties, by decreasing the level of *il-1β* (figure 5.2.2B). However, we also observed a reduction in expression of the anti-inflammatory cytokine *il-10* in contrast to the increase in expression reported to occur in human responses (figure 5.2.2B) (Jameel et al., 2013). A reduction in *il-10* may be related to the cholesterol inhibitive properties of ATV and the modulation of immune metabolism (Han et al., 2009). Therefore in order to avoid these potentially confounding effects of ATV as an ICH induction method, assessment of drug treatment was continued using the *bbh* model only.

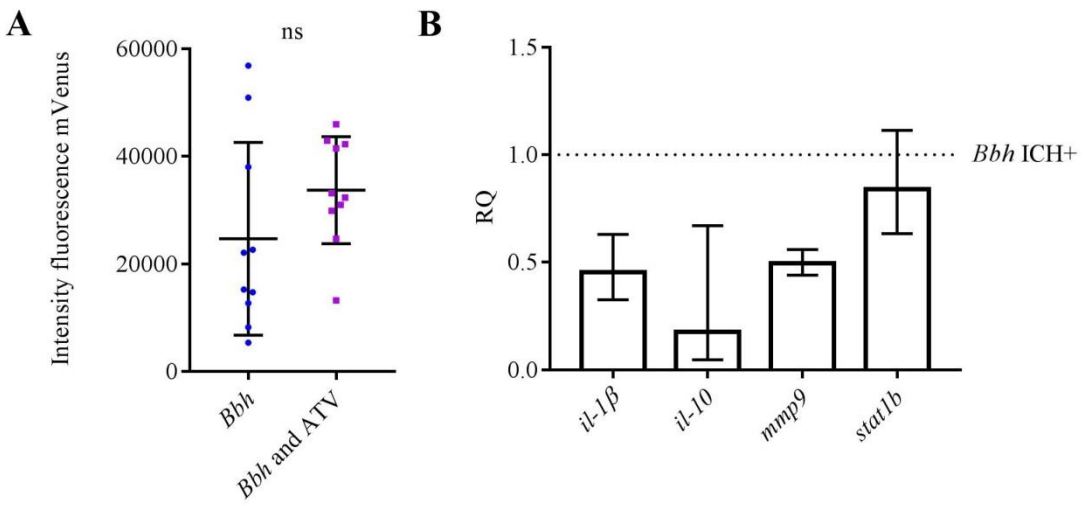

Figure 5.2.2 Effect of ATV treatment post ICH on cell death analysis and immune gene expression

(A) Cell death analysis of *bbh ubiq*:secAnnexinV-mVenus ICH+ larvae with and without treatment with 1.5µM ATV after haemorrhage shows no significant difference between groups. Data from n=10 larvae. (B) Gene transcript expression analysis shows a decrease in inflammatory genes *il-1β, il-10, mmp9* when compared to *bbh* ICH+ larvae without ATV treatment. Data acquired from one independent replicate with three technical replicates and bars show minimum and maximum RQ values.

To determine whether increased mRNA expression accurately correlated with an increase in Il-1β protein we used immunofluorescent staining on 3 dpf ICH- and ICH+ larvae to detect Il-1β (figure 5.2.3). Representative images were collected from stained larvae (n=50) and showed that Il-1β was detectable in the head following ICH, however not in all larvae. We hypothesise that this is because of the variability of the ICH time line and immune response observed in individuals. Il-1β was not detectable using western blot or WISH techniques, perhaps because total concentration was too low and these assays lack sensitivity. In a model of traumatic brain injury (TBI), known to upregulate Il-1β expression, we detected *il-1β* using WISH analysis and saw that expression is highest at 1 and 2 hours post injury (hpi) and undetectable at 5 hpi (figure 5.2.4). This suggests that *il-1β* expression is transient and perhaps why in the ICH model our detection results are variable. With larvae developing so quickly and heterogeneity within a clutch, *il-1β* in the ICH+ larvae was not always consistently increased at the sampling time.

Hematoma fluid acquired from human patients enrolled in the MISTIE III trial for minimally invasive hematoma evacuation was analysed for pro-inflammatory immune markers as part of the INFLAME-ICH trial. Data were collected to identify a time point where IL-1β was targetable by IL-1Ra treatment. Data show that IL-1β is increased in n=47 surgical patients until 4-5 days post randomisation (medical or surgical interventions) before returning close to baseline (Parry-Jones et al, unpublished, IRAS 163606). These data indicate that a comparable time line in zebrafish may draw parallels with human patients.

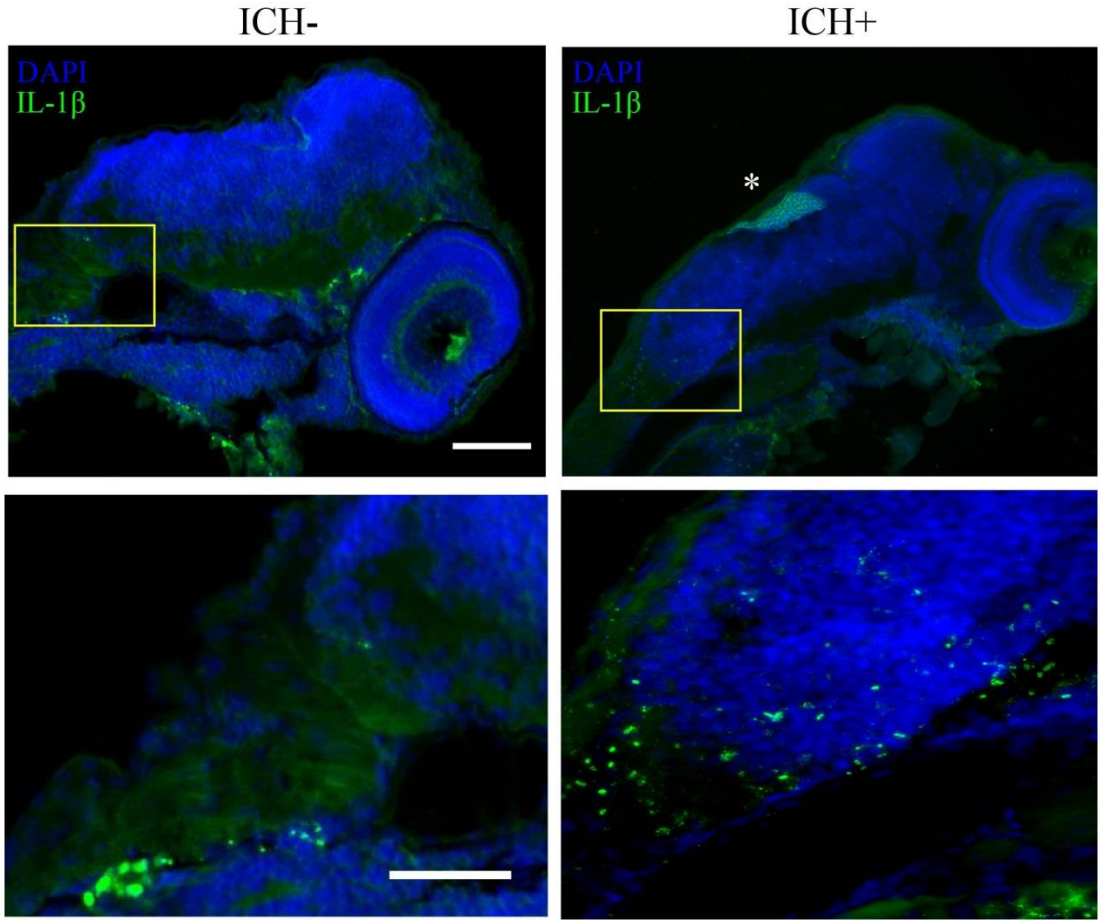

Figure 5.2.3 Detection of Il-1β in ICH+ larvae

At 3 dpf, ICH- and ICH+ *bbh* larvae were fixed and paraffin embedded before sectioning into 5µm sections. Tissue was stained using an antibody specific for zebrafish Il-1β and a blue DAPI counter stain for cell nuclei. Fluorescent images were acquired at 20X magnification (top panels, scale bar = 100µm). ICH- larvae show a high background for the secondary antibody as there was no specific binding or detection of Il-1β. Images from ICH+ larvae show cell populations in the hindbrain expressing Il-1β (green) in response to haemorrhage (*). Yellow boxes indicate regions imaged in bottom panels at 40x magnification, scale bar = 50µm.

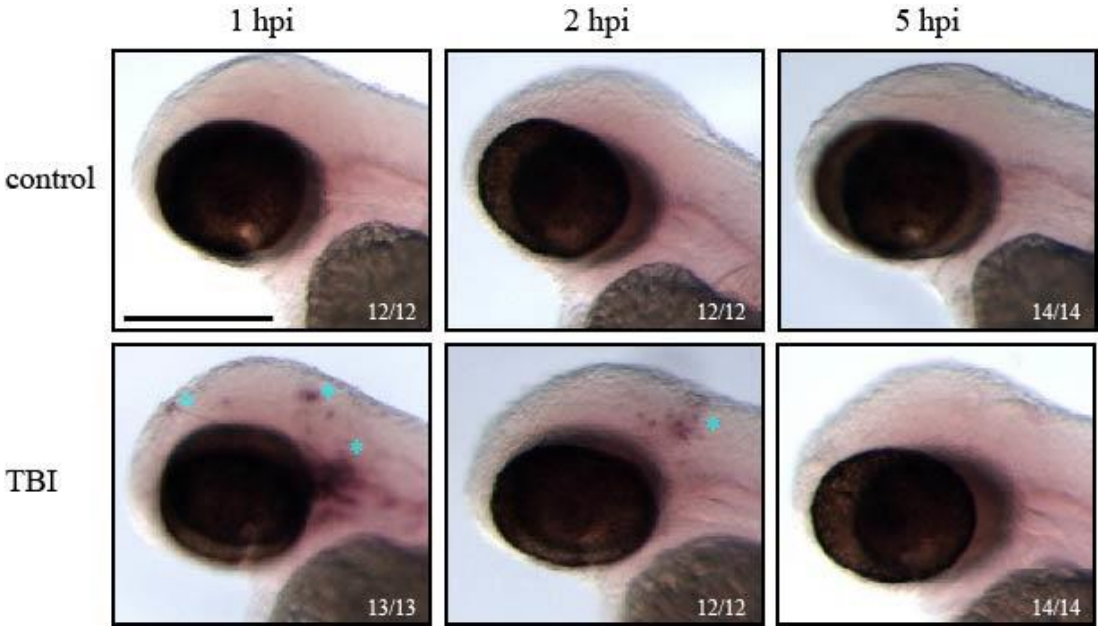

Figure 5.2.4 *il-1β* expression in a model of traumatic brain injury
At 2 dpf larvae were anesthetised and injured using a glass needle and a stab injury to the brain. Sibling controls were anesthetised without injury. Larvae were fixed and *il-1β* expression analysed using WISH staining. *Il-1β* mRNA expression is detectable in the head in distinct cells at 1 hpi (*). Images are representative of n=12-14, scale bar represents 250µm. TBI – traumatic brain injury, hpi – hours post injury.

In an attempt to worsen brain cell damage and confirm that Il-1β is detrimental to zebrafish post ICH, we injected human recombinant IL-1β (hrIL-1β) into the hindbrain ventricle of ICH+ larvae at 2 dpf (figure 5.2.5). Larvae were injected with 1nl of a low (100ng/ml) or a high (10µg/ml) dose of hrIL-1β or a water control. Larvae were then assayed for cell death by measuring annexinV expression at 3 dpf. We saw no difference in the total fluorescence of dying cells in the brain at this time point compared to uninjected and water controls. This suggests that either the cell death response is an 'all-or-nothing' measurement and cannot be worsened further than the damage already present, or that Il-1β is not driving the cell death response in the fish.

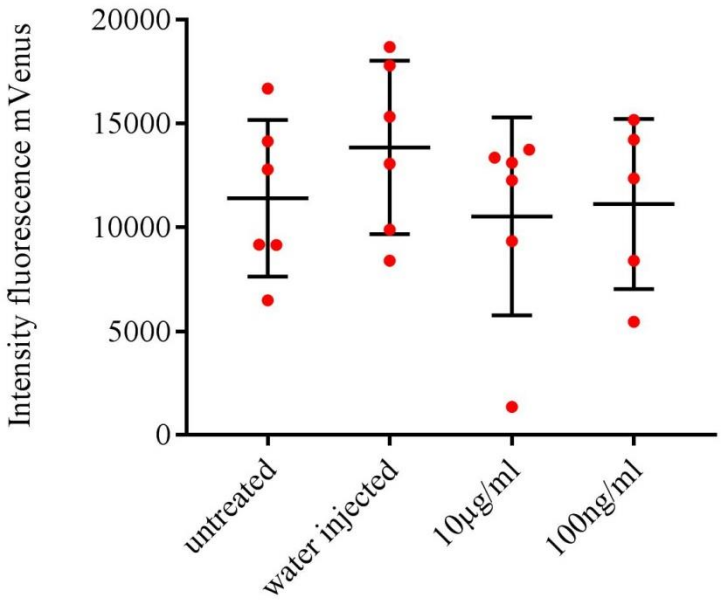

Figure 5.2.5 Effect of hrIL-1β on cell death following ICH
HrIL-1β was injected into the hindbrain ventricle of *ubiq*:secAnnexinV-mVenus ICH+ larvae at 2 dpf at a high (10µg/ml) and a low (100ng/ml) dose. Water was injected as a control. Larvae were then assayed at 3 dpf for cell death (n=6) and images analysed for intensity fluorescence.

Inhibition of Il-1β with Anakinra has no effect on pathological outcomes of ICH

IL-1Ra was administered to *bbh* larvae before a spontaneous haemorrhage occurred (24 hpf) in order to replicate the protection seen in rodent studies, however this was not a successful approach as we observed an increase in mortality. Administration of the drug post haemorrhage recreates a more realistic translational treatment window. IL-1Ra (100mg/ml) was therefore injected into the hindbrain ventricle of *bbh* homozygous and WT control animals early 2 dpf (~52 hpf) after all the homozygous animals had haemorrhaged. Cell death was analysed in *bbh ubiq*:secAnnexinV-mVenus animals at 3 dpf and motility assayed at 5 dpf (figure 5.2.6). Although there was a significant haemorrhage effect in both vehicle and treated groups as observed previously (figure 3.3.4) there was no effect of IL-1Ra treatment on cell death or motility (figure 5.2.6). IL-1Ra treatment appears to increase the locomotor deficit between ICH- and ICH+ siblings and worsen outcomes but this was not significantly different to vehicle treated ICH+ groups. The loss of significant haemorrhage effect seen on locomotion at 5 dpf in untreated larvae when data from 3 independent replicates is pooled may be due to variation in individual recovery time, as this has been seen to differ between clutches and experimental replicates (figure 3.3.6). Using R to carry out further statistical analysis considering independent repeats ('clutch') as a random variable, there was a significant overall haemorrhage effect, but a non-significant effect of treatment (appendix viii).

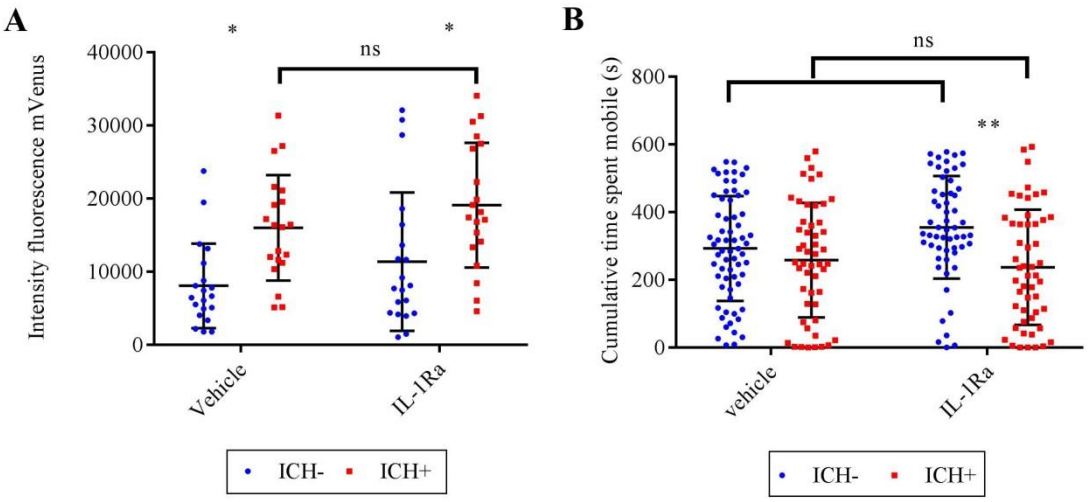

Figure 5.2.6 IL-1Ra treatment outcomes on cell death and motility

(A) ICH+ larvae showed an increase in brain cell death compared to ICH- siblings however treatment with IL-1Ra at 2 dpf showed no reduction in intensity fluorescence analysis. Data acquired from 3 independent replicates of n=6-7 larvae and analysed using a two-way ANOVA (*p=0.01) (B) IL-1Ra treatment showed no longer term beneficial response in motility assayed at 5 dpf. Data from 4 independent replicates of n=24 and analysed using a multi linear model analysis in R (**p=0.001).

Treatment with Anakinra modulates the innate immune response to ICH

We sought to investigate the cellular innate immune response to IL-1Ra treatment to determine whether it was having an inhibitory effect on cell migration and activation. Double transgenic *mpo*:GFP;*mpeg1*:mCherry *bbh* larvae were treated with IL-1Ra and live imaged using the light sheet microscope to analyse the number of immune cells in the head. Neutrophils (*mpo*:GFP) are the most numerous innate immune cell in developing zebrafish larvae (Ellett et al., 2011). When characterising the model, it was noted that there was a significant increase in the number of macrophages (*mpeg1*:mCherry), not neutrophils, as a result of ICH (figure 3.3.7). IL-1Ra treatment increased the number of neutrophils in the head in ICH+ larvae when compared to treated ICH- siblings (figure 5.2.7A). This increase was not significantly different from the haemorrhage effect in vehicle treated ICH+ controls (figure 5.2.7A). There was no increase in the number of macrophages following IL-1Ra treatment, in contrast to the increase seen in vehicle treated animals, suggesting that blocking Il-1β modifies cell migration (figure 5.2.7B). We analysed the morphology of the macrophages in the head in response to ICH after IL-1Ra treatment and found there were less activated cells with amoeboid morphology than in vehicle controls (figure 5.2.7C). These results taken together suggest that inhibiting the Il-1 response in the zebrafish with IL-1Ra modulates the immune response but does not rescue the neuropathological consequences of ICH.

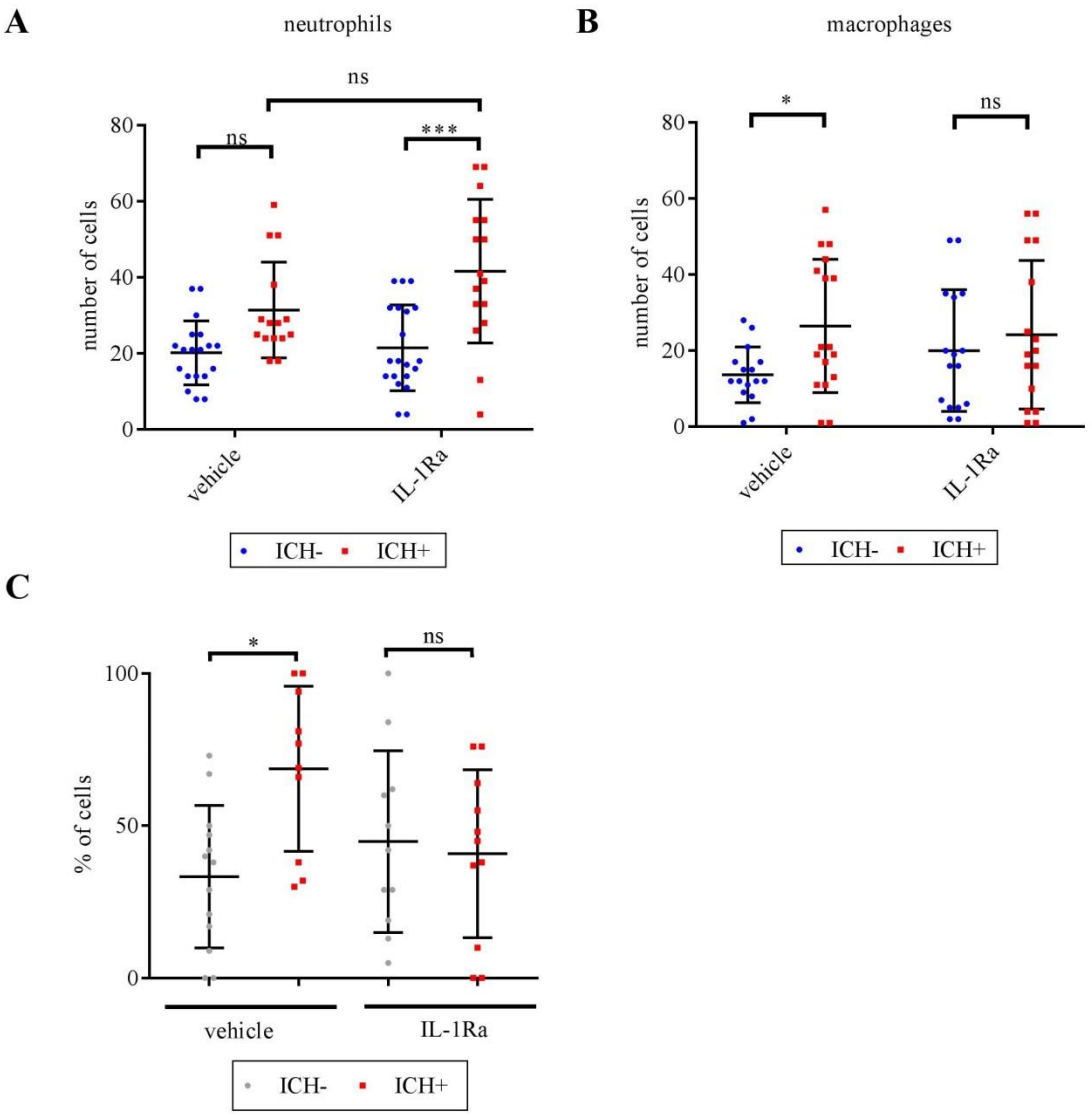

Figure 5.2.7 IL-1Ra treatment effect on the neuroinflammatory response
The number of *mpo*:GFP positive neutrophils and *mpeg1*:mCherry positive macrophage cells were counted in head from images taken of ICH- and ICH+ double transgenic larvae. (A) With IL-1Ra treatment, the number of *mpo* positive neutrophils was significantly increased compared to ICH- larvae however not significantly different from vehicle treated ICH+ larvae. Data analysed using a two-way ANOVA (3 independent replicates of n=5, ***p=0.0001). (B) The number of *mpeg1* positive cells was not significantly increased in ICH+ larvae with IL-1Ra as seen in vehicle treated larvae however we observed a large variability in response within the assayed group. (3 independent replicates of n=5, *p=0.049) (C) Macrophage morphology % analysis in larvae treated with IL-1Ra shows less activated 'amoeboid' cells than in vehicle treated groups. Data from 2 independent replicates n=8-11, analysed with one-way ANOVA (*p=0.016).

Anakinra treatment increases both* il-1β *and* relA *transcript expression

We analysed *relA* expression (the p65 subunit of NFκB) in conjunction to *il-1β* expression using qPCR in IL-1Ra treated larvae to estimate whether there was any activation of the Il-1 receptor. We observed a significant increase in both *il-1β* and *relA* mRNA expression in IL-1Ra treated ICH- and ICH+ groups (figure 5.2.8). However, we also did not observe a haemorrhage-associated increase in *il-1β* expression despite observing previously, and so control levels of *relA* activation may be not be accurate and this should be investigated further (figure 5.2.1). Increased transcription of *il-1β* implies that blocking the receptors may cause a compensatory over-expression (figure 5.2.8A). Downstream *relA* signalling increases with IL-1Ra treatment suggesting that there is incomplete inhibition of the receptors by the human recombinant protein (figure 5.2.8B). From this data it appears that IL-1Ra is effecting transcript levels however it is not known whether this translates to proteins translation and effective inhibition of the receptor.

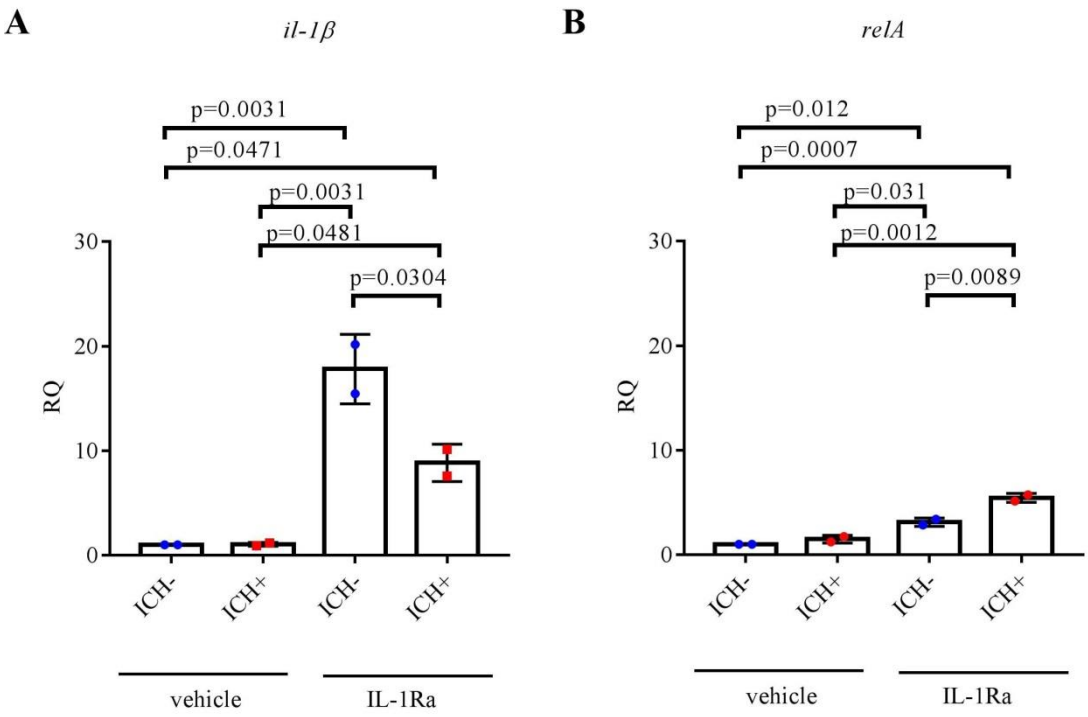

Figure 5.2.8 qPCR analysis of *relA* and *il-1β* expression with IL-1Ra treatment
(A) Expression of *il-1β* was analysed using qPCR with vehicle and IL-1Ra treatment. (B) Expression of *relA* with vehicle and IL-1Ra treatment to show downstream receptor activation. RNA pooled from larvae (n=30) and data collected from 2 independent replicates. Data analysed using a one-way ANOVA.

Here we have observed that IL-1Ra can modulate the innate immune response to ICH, as reported previously (Mazon-Moya et al., 2017). However, these data also suggest that targeting Il-1β is not adequate to rescue cell death caused by ICH. It may suggest that IL-1Ra is not the best way to inhibit zebrafish Il-1 receptors and these experiments could be verified by using a caspase inhibitor. Physiologically, the cascade of neuropathic events, mass effect, cerebral oedema, cellular debris build up and toxic compounds causes widespread cell death in the brain that is too severe to rescue by modulating the immune response alone. We hypothesised that by targeting iron accumulation to reduce cerebral oedema could lead to improved outcomes.

5.3 Investigation of iron accumulation and inhibition following ICH

With a view to modulating the pathological outcomes associated with brain haemorrhage in zebrafish larvae in conjunction with IL-1Ra treatment we sought to investigate iron accumulation as a therapeutic target. Reducing iron accumulation following ICH may prevent the severe oedema associated with worse outcomes in patients.

Iron is present and sustained in the head following ICH

Following an ICH, free ferric iron in tissue is invariably detectable as haemosiderin. Ferric iron in the zebrafish larval head was detected using a potassium ferrocyanide reaction to develop a Prussian blue complex (Lumsden et al., 2007). Further enhancement of the stain requires Prussian blue catalysis of H_2O_2-dependent oxidation of 3'-diaminobenzidine (DAB) leaving a brown stain. Tissue bound ferric iron was detectable in *bbh* homozygotes at 72, 96 and 120 hpf following a haemorrhage (figure 5.3.1). Areas of dark reddish brown were seen around the common bleed areas in the fore and hindbrain, and at later time points when the haematoma clears, in the hindbrain ventricle. Staining in the otolith bone in ICH- larvae acted as a procedural control.

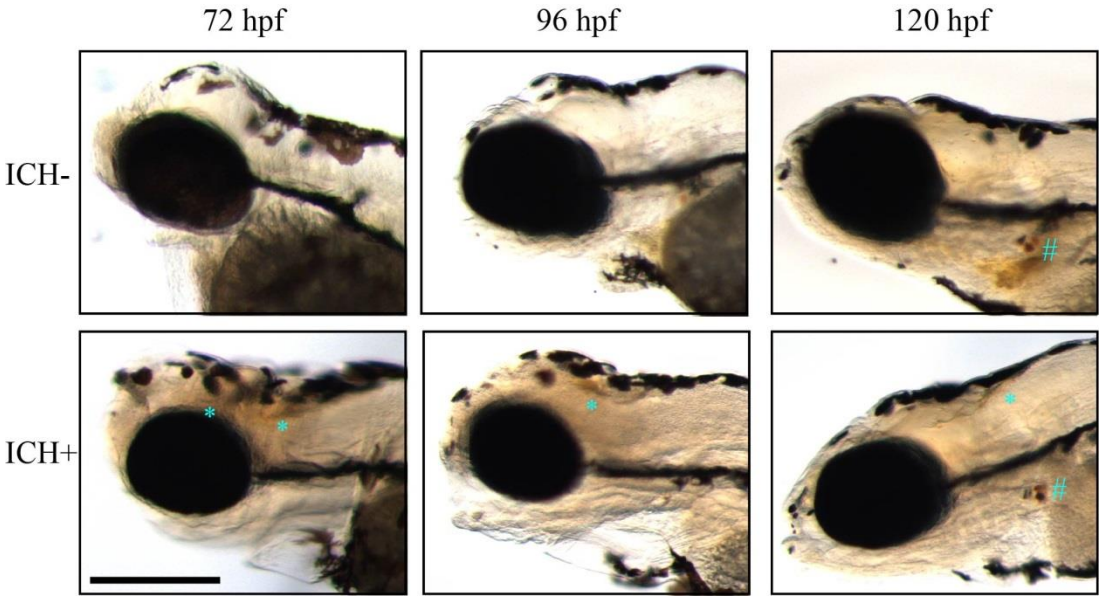

Figure 5.3.1 Detection of free iron in the head following ICH
Catalysis of DAB substrate shows presence of iron by increased reddish/brown stain (*) at 24, 48 and 72 hpf. Staining correlates to the common bleed areas in the midbrain and hindbrain ventricle. At 120 hpf iron is seen concentrated in the otoliths (#) in both ICH- and ICH+ larvae. Representative images from n=12 are shown, scale bars = 250µm.

Inhibition of iron accumulation alone has no effect on pathological outcomes of ICH

Deferoxamine (DFO) is soluble in water and therefore amenable to studies with zebrafish larvae (Nasrallah et al., 2018). It has been reported in rodent models of ICH to have efficacious outcomes on neurobehaviour, ICP and brain water content (Cui et al., 2015). We treated ICH- and ICH+ *bbh* larvae after haemorrhage event on 2 dpf (~52 hpf) with 100µM DFO and analysed cell death and motility as before. We observed a significant haemorrhage effect on total brain cell death between ICH- and ICH+ larvae in the DFO treated group (figure 5.3.2). However there was no significant decrease in cell death observed from untreated ICH+ groups compared to DFO treated ICH+ larvae showing that the drug had no effect. We aimed to investigate whether the variability between clutch repeats was affecting our independent replicates and therefore statistical analysis was performed using R taking clutch number as a random variable and fitting a multi linear model (appendix ix). This confirmed lack of significance in treated groups and therefore determined that DFO was ineffective.

Motility was assayed in treated larvae at 5 dpf. ICH- controls were *ubiq*:secAnnexinV-mVenus nacre larvae on a wildtype background instead of *bbh* WT siblings. Data showed that untreated ICH+ larvae moved more than ICH- controls, perhaps due to the different genetic background between fish groups (figure 5.3.3). In DFO treatment groups overall motility in ICH+ larvae was decreased compared to ICH-. There was no significant difference between DFO treated ICH- and ICH+ larvae however because of the inconsistency seen between groups, from using two different strains, data was analysed comparing ICH+ groups to identify a drug effect. DFO treated larvae still moved significantly less than untreated ICH+ larvae implying no benefit of drug treatment and implies that there is a deleterious effect of the drug.

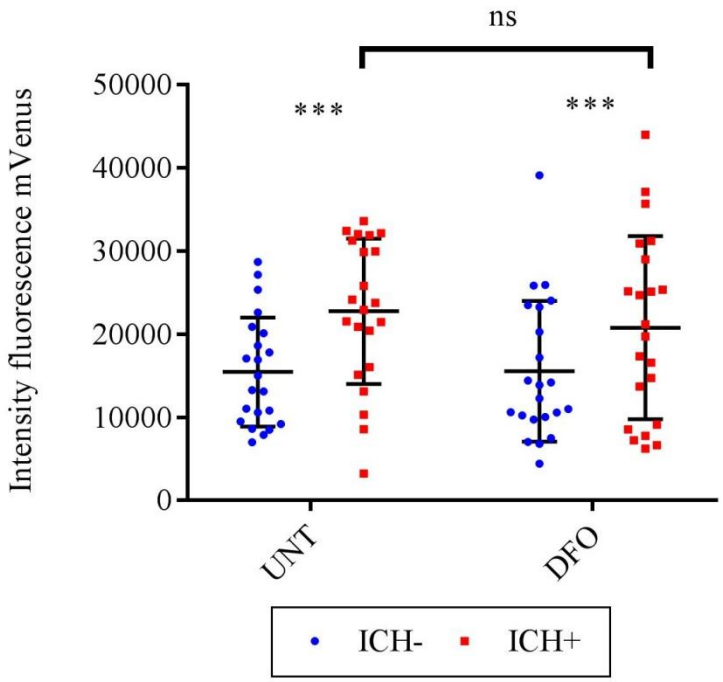

Figure 5.3.2 DFO treatment effect on cell death following ICH

Macro analysis of cell death in *bbh* homozygous *ubiq*:secAnnexinV-mVenus larvae at 3 dpf. No significant reduction in the level of cell death was associated with ICH, however haemorrhage did not significantly increase the intensity fluorescence compared to ICH- siblings in treated groups. Data acquired from n=6-8 from 3 independent replicates and analysed using a multi linear model in R (***$p<0.0001$).

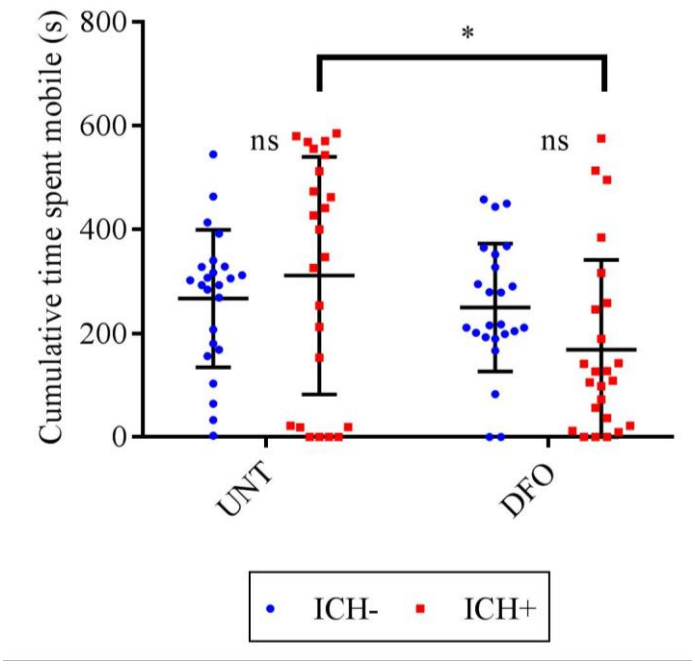

Figure 5.3.3 Effect of DFO treatment on locomotor function
Untreated and DFO treated larvae were analysed for locomotor function at 5 dpf. Data shows no significant differences between ICH- and ICH+ larvae in untreated or DFO treated groups. Comparing ICH+ groups, there is a significant decrease in motility in DFO treated groups compared to untreated, implying there is no benefit of treatment. Data collected from one replicate, analysed using a two-way ANOVA, n=24 (*p=0.025).

5.4 Development of a medium-throughput drug screen to identify novel therapeutics

One of the key advantages of the zebrafish model is the small size of larvae and speed of experiments, making it amenable to high-throughput drug screening (Margiotta-Casaluci et al., 2019). A large scale *in vivo* drug screen for targeted ICH therapies has never been possible before using the current surgical and spontaneous models in large mammals. This approach may identify targets that have not yet been tried in human ICH and may open an entirely new avenue of investigation. We devised an assay protocol to screen *bbh* ICH+ larvae for a reduction in annexinV positive cell death clusters using the Spectrum Collection library of drugs (MicroSource Discovery systems). The Spectrum collection contains 2000 drugs comprising 50% approved compounds from the US and international drug collections, 30% natural compounds and 20% novel bioactive compounds. We acquired 25 drug plates from the zebrafish facility at The Bateson Centre within The University of Sheffield to screen using our model. Haemorrhage was confirmed in *bbh* homozygotes and larvae were plated n=3 into 200µl embryo water in each well containing 10µM of drug in 1% DMSO at 2 dpf. We then assayed cell death at 3 dpf after 24 hours of incubation at 28°C, screening manually under a fluorescent microscope (figure 5.4.1). This presents a translatable treatment timeline, as human therapies are more likely to be administered after a haemorrhage has occurred, rather than as a preventative strategy. Drugs that showed a reduction in clusters of annexinV positive cells, cerebral oedema and good overall health of the larvae were repeated using n=5 larvae at the same concentration and outcomes recorded (appendix x). Functionalities of positive drug hits with beneficial outcomes in both repeats are outlined below in table 5.4.1. Currently we have identified 32 compounds from the 480 screened in 6 plates, resulting in a 6.7% success rate. Compounds target a range of pathways and the mechanism of action by which programmed cell death is prevented is unclear. These drugs selected from initial screening need further investigation to validate the positive outcome on cell death. We will treat larger sample numbers of larvae and assay the functional motility and the inflammatory response to see if there is a true beneficial effect on all pathological outcomes. Once validated in the animal, *in vitro* studies in neuronal cell lines or co-cultures with endothelial cells may help to deduce the mechanism of action by examining cell death responses. RNAseq analysis can be used from larval tissue to

identify targeted genetic pathways and we can identify whether these patterns in gene expression is the same in human post-mortem tissue acquired from the Edinburgh Brain Bank. Funding from the Stroke Association has recently been secured to continue this study.

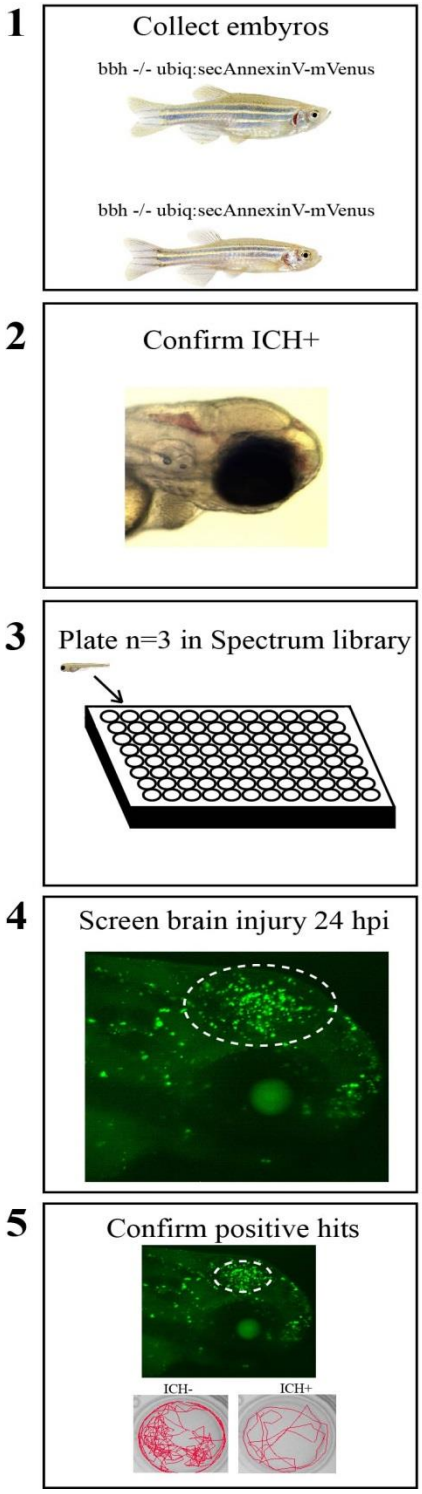

Figure 5.4.1 The drug screen protocol

Larvae from *bbh* -/- *ubiq*:secAnnexinV-mVenus transgenic adults were confirmed for ICH+ at 2 dpf before being plated (n=3) into a 96 well plate containing 10µM drug concentration in 1% DMSO. ICH+ and ICH- larvae were also plated in 1% DMSO alone as controls. At 3 dpf larvae were screened for cell death annexinV expression, oedema and overall health. Positive hits were screened again with n=5 larvae. Drugs with positive outcomes in both repeats were selected for further investigation.

Table 5.4.1 Drugs identified from the Spectrum Collection Library which were associated with positive outcomes on brain cell death in the zebrafish larval ICH model. Data acquired from plates 1-6. Full list of positive hits in appendix x.

Drug Name	**Formula**	**MolWT (g/mol)**	**Bioactivity**	**Source**
Naphazoline hydrochloride	$C_{14}H_{15}ClN_2$	246.74	adrenergic agonist, nasal decongestant	synthetic
Norepinephrine	$C_8H_{11}NO_3$	169.18	adrenergic agonist, antihypotensive	synthetic
Orphenadrine citrate	$C_{24}H_{31}NO_8$	461.52	muscle relaxant (skeletal), antihistaminic	synthetic
Phthalylsulfathiazole	$C_{17}H_{13}N_3O_5S_2$	403.44	antibacterial	synthetic
Oxolinic acid	$C_{13}H_{11}NO_5$	261.24	antibacterial	synthetic
Clomipramine hydrochloride	$C_{19}H_{24}Cl_2N_2$	351.32	antidepressant	synthetic
Gluconolactone	$C_6H_{10}O_6$	178.14	chelating agent	synthetic
Levalbuterol hydrochloride	$C_{13}H_{22}ClNO_3$	275.78	bronchodilator, tocolytic	synthetic
Sparteine sulfate	$C_{15}H_{28}N_2O_4S$	332.47	oxytocic	Leguminosae plant family
Sanguinarine sulfate	$C_{20}H_{15}NO_8S$	429.41	antineoplastic, antiplaque agent	Sanguinaria canadensis plant
Mitomycin C	$C_{15}H_{18}N_4O_5$	334.33	antineoplastic	Streptomyces verticillatus bacteria
Temefos	$C_{16}H_{20}O_6P_2S_3$	466.47	insecticide	synthetic
Clidinium bromide	$C_{22}H_{26}BrNO_3$	432.36	anticholinergic	synthetic
Clonidine hydrochloride	$C_9H_{10}Cl_3N_3$	266.56	antihypertensive	synthetic
Daunorubicin	$C_{27}H_{29}NO_{10}$	527.53	antineoplastic	Streptomyces peucetius bacteria
Deferoxamine mesylate	$C_{26}H_{52}N_6O_{11}S$	656.80	chelating agent (Fe & Al)	Streptomyces pilosus bacteria
Digoxin	$C_{41}H_{64}O_{14}$	780.96	cardiac stimulant	Digitalis and Lamiaceae

				plant families
Disopyramide phosphate	$C_{21}H_{32}N_3O_5P$	437.48	antiarrhythmic	synthetic
Adrenaline bitartrate	$C_{13}H_{19}NO_9$	333.30	adrenergic agonist, bronchodilator,	Portulaca grandiflora plant
Gentamicin sulfate	$C_{21}H_{45}N_5O_{11}S$	575.68	antibacterial	Micromonospora bacteria family
Halazone	$C_7H_5Cl_2NO_4S$	270.09	Anti-infectant	synthetic
Lincomycin hydrochloride	$C_{18}H_{35}ClN_2O_6S$	443.01	antibacterial	Streptomyces bacteria family
Nitrofurazone	$C_6H_6N_4O_4$	198.14	Anti-infectant (topical)	synthetic
Oxidopamine hydrochloride	$C_8H_{12}ClNO_3$	205.64	adrenergic agonist (opthalmic)	synthetic

5.5 Discussion

The aim of these studies was to determine whether the zebrafish model and assays for measuring the pathological outcomes could be utilised for drug screening to identify a specific therapeutic for ICH. Initially, we selected drugs based on clinical trials for ischemic stroke and early phases for ICH. We showed that IL-1Ra-mediated Il-1β inhibition modulated the immune response to blood in the brain however this did not show any efficacy when assayed for cell death and locomotion. Iron chelation treatment with DFO did not lead to better outcomes for ICH+ larvae. Applying the model to a large scale drug screen will identify new potentially therapeutic compounds that have not been investigated in ICH before. The novelty of this study is that the small size of zebrafish larvae allows for assaying in 96 well plates, screening large numbers of drugs for relatively simple outcome analysis, an approach which is impossible using the current rodent models. We hope that from this study, there can be further investigation into the mechanisms of the drug candidates identified and that with more rigorous testing some hold the potential for clinical trial.

In our study we found that ATV treatment in the *bbh* ICH+ larvae decreased *il-10* transcript expression rather than increasing expression as previously reported in a rat model of myocardial ischemia and human T cell studies (Jameel et al., 2013; Li and Fang, 2005). qPCR analysis only shows the temporal mRNA transcript levels and is not always indicative of protein levels. *Il-10* expression may appear lower in ATV treated larvae because transcription spiked at treatment time (2 dpf) and when samples were measured (3 dpf), subsequent high protein levels negatively regulated further transcription of *il-10* expression detected by qPCR. For a more robust analysis, protein could be detected temporally using western blot to ascertain the effects of ATV on inflammation.

We tried exacerbating damage by increasing the levels of hrIL-1β in the brain following ICH however we did not observe an increase in response severity. This could be due to cell death being an 'all or nothing' response to blood in the brain, but further investigation is necessary. It may be that zebrafish Il-1β is not driving the cell death response after haemorrhage, as we have seen that by antagonising the receptors there is no beneficial response. In order to test this hypothesis we could inject ICH-siblings with hrIL-1β to increase the baseline cell death response, or into the TBI

model larvae. However from IL-1Ra experiments we can now conclude that Il-1β mediated neuroinflammation is not the driving cause of the brain cell death and loss of locomotor function in this model.

Throughout this study we used motility at 5 dpf as a pathological outcome of ICH based on the study in chapter 3, however drug intervention assays with IL-1Ra and DFO show that there was no significant loss of motility in vehicle treated groups. When first characterising the *bbh* response in chapter 3, we found that although variable between clutches, 5 dpf gave the most consistent quantifiable response, as larvae exhibit little spontaneous swimming at 3 and 4 dpf. Practically, at these early time points it is difficult to detect the larvae using the DanioVision software. Once we pooled the data from three independent clutch repeats, significance was lost. When considering 'clutch' as a random variable, statistical analysis showed a significant overall effect of haemorrhage and a non-significant difference between treatment (appendices vii and viii). Retrospectively, in order to clarify the functional outcomes of DFO and IL-1Ra treatment on *bbh* larvae and strengthen this study, motility should have been recorded at 4 dpf as well. Without confirming a true haemorrhage effect in vehicle treated groups, we cannot be certain whether locomotor function was restored or worsened by the drug treatment.

The drug interventions tested here that were anticipated to be neuroprotective failed to show efficacy in our zebrafish model. There are many reasons why IL-1Ra treatment did not result in the neuroprotection seen in other stroke models. Firstly, the protein is human recombinant, which differs structurally from zebrafish protein and therefore may not bind as completely to receptors preventing full inhibition of Il-1β signalling as we observed through increased *relA* expression. Practically, treatment was difficult; IL-1Ra protein is prone to precipitation out of suspension and accumulates in the microneedle upon injection, and so dosage is not always consistent which may have contributed to the varied individual response. A dose response may have helped to optimise IL-1Ra treatment however no benefit at the high dose of 100mg/ml implied that this would be futile. IL-1Ra treatment was seen to modulate immune cell responses in larvae, increasing neutrophils at the site of injury in contrast to the macrophages in vehicle treated. We hypothesise that this could be due to neutrophils responding the CXCL2 recruitment marker released by endothelial cells and migrating to the brain (Wu et al., 2015). Macrophages are inhibited by IL-1Ra and

cannot activate in response to subsequent injury-mediated Il-1β release and therefore there might be a neutrophil compensation occurring at this time.

Inhibition of Il-1β in this model may not be beneficial because IL-1β has a plethora of biological roles within the organism (Sobowale et al., 2016). IL-1β-mediated activation of microglia is beneficial for recovery and repair following brain injury (Liu and Quan, 2018; Spulber et al., 2009). Il-1β is also a potent vasodilator which may imply that release following an ICH has an important role in restoring blood flow to the brain, and inhibition could be detrimental (Essayan et al., 1998). On the contrary, reduction of blood pressure in patients after an ICH is beneficial and reduces the precipitation of ischemia in the peri-haematomal region (Butcher et al., 2013). Inflammation is a necessary part of regular zebrafish developmental processes (Rangasamy et al., 2018). Il-1β is expressed at low levels in the zebrafish without any inflammatory stimuli during early development (Thisse, 2005). Early studies using an Il-1β mutant knockout fish from collaborators at the University of Sheffield showed delayed development and decreased larval survival, suggesting that this model might not be suitable to investigate Il-1 inhibition therapeutically. However, IL-1β inhibition has also been indicated as detrimental to the overall function in rodents following ICH (Barrington et al. *in preparation*) and so clinical trial results will determine the efficacy of IL-1Ra in ICH.

As discussed in the introduction to this chapter, TNF-α release and TLR4 signalling also play a role in ICH pathology however have not been investigated in this study. The TLR signalling pathway in fish differs vastly from mammalian cascades for example, zebrafish TLR4 is non-responsive to LPS stimulation and signalling does not require accessory proteins CD14 and Myd88, suggesting unique roles in PAMP responses from TLR4 stimulation exist in zebrafish (Y. Li et al., 2017). Zebrafish possess a number of fish specific TLRs that may also be active during DAMP recognition and due to these reasons we decided not to pursue TLR4 inhibition as a therapeutic strategy in our model. TNF-α expression has been attenuated in mouse models of ICH with no benefit to outcomes (Matsushita et al., 2014).

The results from the initial drug screening of the Spectrum collection have indicated some interesting compounds with beneficial outcomes on ICH larvae. Broadly, drugs can be grouped together by therapeutic action into adrenergic agonists, sodium

channel blockers, metal chelators and anti-bacterial compounds. It is not immediately clear how these mechanisms prevent cell death after haemorrhage, and further investigation is required to determine whether they result in positive outcomes with the other pathological assays. Five compounds were identified as adrenergic receptors agonists; norepinephrine, levabuterol, adrenaline bitartrate, naphazoline hydrochloride and clonidine hydrochloride. Sympathomimetic actions are complex as different subtypes of adrenoreceptors have opposing action. At low doses, activation of α adrenoreceptors is sympatholytic however at higher doses hypertensive action is the dominant response, causing contraction and vasoconstriction of smooth muscle surrounding blood vessels (Kamibayashi and Maze, 2000). The dominant action on heart tissue is to decrease heart rate resulting in hypotension (Kamibayashi and Maze, 2000). In the heart, β_1 adrenoreceptors activation increases intracellular cyclic adenosine monophosphate (cAMP) and raises the heart rate (Stiles et al., 1984). Depending on the specificity of the drug, a combination of these actions causes a raise in blood pressure. Furthermore, seven drugs were identified as muscarinic acetylcholine receptor antagonists and sodium channel blockers; sparteine sulfate, disopyramide phosphate, clomipramine, clidinium bromide, digoxin, sanguinarine sulfate and orphenadrine citrate. Muscarinic acetylcholine receptor antagonists reduce parasympathetic nervous activity. Sodium channel blockers are commonly used as anti-arrhythmic drugs to decrease cAMP and decrease cardiac activity. Overall these drugs have antihypertensive effects reducing cardiac output and blood pressure. The beneficial outcomes on cell death after ICH may be due to the reduction of HE and oedema, hypothesised by Butcher et al (2013) who showed that lowering blood pressure in human patients modestly reduced disability.

One consideration of the drug screen is the use of DMSO as a drug vehicle. All of the drugs in the Spectrum Library are solubilised in DMSO and it is a widely used solvent frequently used in zebrafish studies. Despite this, a range of studies have shown that DMSO can have unwanted effects on zebrafish larvae and is not an inert drug vehicle. We performed a dose response to determine DMSO effect on pro-inflammatory factors and found it to be proinflammatory at 1%, however cell death control experiments in the drug screen show this has no effect on cell death. *In vivo* studies that use DMSO as a solvent do not always report using a vehicle control. Although there is no related lethality or teratogenicity at low doses (Maes et al., 2012) DMSO

has been shown to modify the permeability of the egg chorion, increase hyperactivity, modulate gene expression, supress inflammatory responses, increase cell death in the CNS and induce developmental abnormalities at increasing concentrations in zebrafish (Chen et al., 2011; Elisia et al., 2016; Hallare et al., 2006; Hanslick et al., 2009; Kais et al., 2013). Alternatives to DMSO are not much better for zebrafish studies as solvents like ethanol, acetonitrile and dimethyl formamide are not well tolerated through developmental stages (Maes et al., 2012).

Interestingly, gluconolactone and DFO both metal chelating agents, resulted in a positive decrease in the cell death response to ICH, despite earlier experiments implying that deferoxamine treatment was ineffective. This may be due to DMSO used as a solvent in the drug screen plates, which ensures the drug is fully dissolved and increases absorption and bioavailability. Further analysis of the i-DEF clinical trial data shows that DFO treatment results in better outcomes for populations of women, younger patients and particularly for African Americans. These populations also have higher heme oxygenase 1 (HO-1) expression, the enzyme required for heme breakdown, and thus higher iron release in the haematoma (unpublished data from i-DEF trial). However there requires further investigation into how safe and efficacious DFO treatment would be in these ICH patients and if genomic testing for HO-1 would be feasible in a clinical setting. One could speculate that the dose of DFO needed to counteract endogenous mechanisms of free iron in the remaining population is too high and thus result in the adverse effects associated with the Hi-DEF trial. Targeting the removal of heme itself before degradation and release of iron and biliverdin may have potential to reduce damage in ICH, or prevent action of HO-1 by reducing free radicals which promote upregulation.

Additionally, drugs known to have completely unrelated functions also had a positive reduction on brain cell death after ICH. Toxic compounds like nitrofurazone, oxidopamine hydrochloride, daunorubicin and mitomycin C all had a positive effect however without any translational potential will not be taken for further investigation. Oxolinic acid, gentamicin, phthalylsulfathiazole and lincomycin hydrochloride are both reported to have prokaryotic targets, likewise temefos and halazone which are used for water purification. Future experiments will investigate whether these drugs

have a beneficial outcome on the functional deficit associated with ICH in the larval model.

This study has shown that the zebrafish larval model is amenable to drug intervention studies in pre-clinical ICH investigation and therefore offers a complementary tool to identify novel therapeutics from a high-throughput screen.

Chapter 6: Investigating cholesterol biosynthesis and metabolism in ICH using a zebrafish larval model

6.1 Introduction

Literature suggests that low serum cholesterol increases the risk of an ICH (Y.-W. Chen et al., 2017; Phuah et al., 2016; Rist et al., 2019; Valappil et al., 2012; X. Wang et al., 2013). Conversely, high cholesterol levels upon hospital admission with ICH decreases HE and stroke-associated mortality (Chang et al., 2018). There is also a correlation between low cholesterol and an increased risk of fatal stroke (Prospective Studies Collaboration, 2007). Low cholesterol is one of the many conditions that have been linked with ICH risk including age, gene-associated pathological morphology and chronic hypertension (An et al., 2017). The complex interactions between these factors make pre-clinical modelling of human co-morbidities difficult, and experimental models often over simplify the disease. Due to the lack of spontaneity in the current ICH rodent models, investigation into causative mechanisms is currently impossible. Here we utilise the spontaneous ICH in zebrafish larvae to investigate the link between cholesterol and ICH pathology.

Cholesterol is an essential component in brain cells from development to adulthood. The brain contains 25% of the total cholesterol in the body and biosynthesis occurs independently of peripheral tissues due to the BBB. Cholesterol from dietary sources is carried in the blood by low-density lipoprotein (LDL) and this is the main source of cholesterol synthesised in peripheral tissues. Some brain cholesterol can be made from LDL transport across the BBB by LDL receptors expressed on brain endothelial cells but to a much lesser degree (Dehouck et al., 1997; Méresse et al., 1989). Within brain tissue, cholesterol is found in myelin sheaths that surround the axons of nerve cells, and provides protein anchoring points and fluidity to the bilipid layer of the cell membrane. Cholesterol made in the brain is maintained for a long period of time in myelin and cell membranes and is then recycled within the organ (Morell and Jurevics, 1996). In patients cholesterol levels are measured from peripheral blood. High cholesterol is usually a result of poor diet and has been linked with increased risk of CVD and ischemic stroke (NCEP, 2001). Low cholesterol has been linked with cancer risk, psychological disorders and gestational problems in addition to ICH (Edison et al., 2007; Tedders et al., 2011; Törnberg et al., 1989).

Primarily, cholesterol is made *de novo* from acetyl CoA (figure 6.1.1). HMG-CoA reductase (HMGCR) catabolises the rate limiting step to generate mevalonate and subsequently cholesterol through a series of enzymatic steps. HMGCR is the main target in regulating cholesterol levels in the brain and transcription is modulated by the sterol response element binding protein (SREBP) (DeBose-Boyd and Ye, 2018). SREBP is normally inactive and anchored to intracellular membranes however when cholesterol levels are low, SREBP undergoes proteolytic activation where it drives the transcription of many of the cholesterol biosynthesis pathway enzymes (figure 6.1.1) (Berg et al., 2002).

About 1% of cholesterol made in neuronal cells is stored as esterified lipid droplets, or excreted as oxysterols (Zhang and Liu, 2015). Oxysterols can cross the BBB to be carried to the liver for catabolism into bile acids and hormones and are involved peripherally in a wide range of physiological processes (Kulig et al., 2016). One such oxysterol, 25-hydroxycholesterol (25-HC) is implicated in controlling cholesterol biosynthesis and the immune system. 25-HC inhibits SREBP from driving further synthesis of cholesterol in a negative feedback loop. SREBP is expressed abundantly in macrophages and acts as a transcription factor for the NLRP proteins that make up the inflammasome (Chen et al., 2014). The inflammasome is essential for the cleavage of pro-IL-1β to the mature form IL-1β that initiates a pro-inflammatory response (Im et al., 2011). Thus it has been shown that 25-HC can inhibit the activation and release of IL-1β through SREBP in response to viral infection (Reboldi et al., 2014) (figure 6.1.1). Additionally, 25-HC increases the expression of IL-10 in T cells, an immune regulatory cytokine (Perucha et al., 2019). On the other hand studies have shown that in autoimmune conditions, 25-HC can exacerbate the immune system (Jang et al., 2016) by increasing the intracellular signalling cascades of TLRs (Gold et al., 2014). This supports previous literature that shows hypercholesterolemia promotes an inflammatory phenotype (Tall and Yvan-Charvet, 2015).

25-HC is synthesised through cholesterol hydrolysis by cholesterol 25-hydroxylase (CH25H) enzyme. Although homeostatic expression is usually very low, CH25H is an interferon stimulated gene and transcription is activated in dendritic cells and macrophages in response to viral infection (Blanc et al., 2013; Park and Scott, 2010). CH25H has been shown to inhibit viral entry and replication (Xiang et al., 2015; Zhang et al., 2019) and knockout mutations increase infection susceptibility (Liu et al., 2013).

It has also been implicated in other neurological conditions such as multiple sclerosis diagnosis, and is over-expressed in Alzheimer's disease brain tissue (Bertram and Tanzi, 2008; Crick et al., 2017; Papassotiropoulos et al., 2005). In other parts of the body, studies have shown that CH25H is important for increasing insulin sensitivity (Noebauer et al., 2017), and so may link cholesterol and glucose dysmetabolism. Glucose metabolism is essential for brain function and both cholesterol and glucose metabolism influence the immune response (Jung et al., 2019; Reboldi and Dang, 2018). The links between CH25H, 25-HC and the pathological outcomes of ICH have not yet been studied experimentally, however understanding the mechanisms further could shed more light on how and why a haemorrhage occurs and the pathological outcomes.

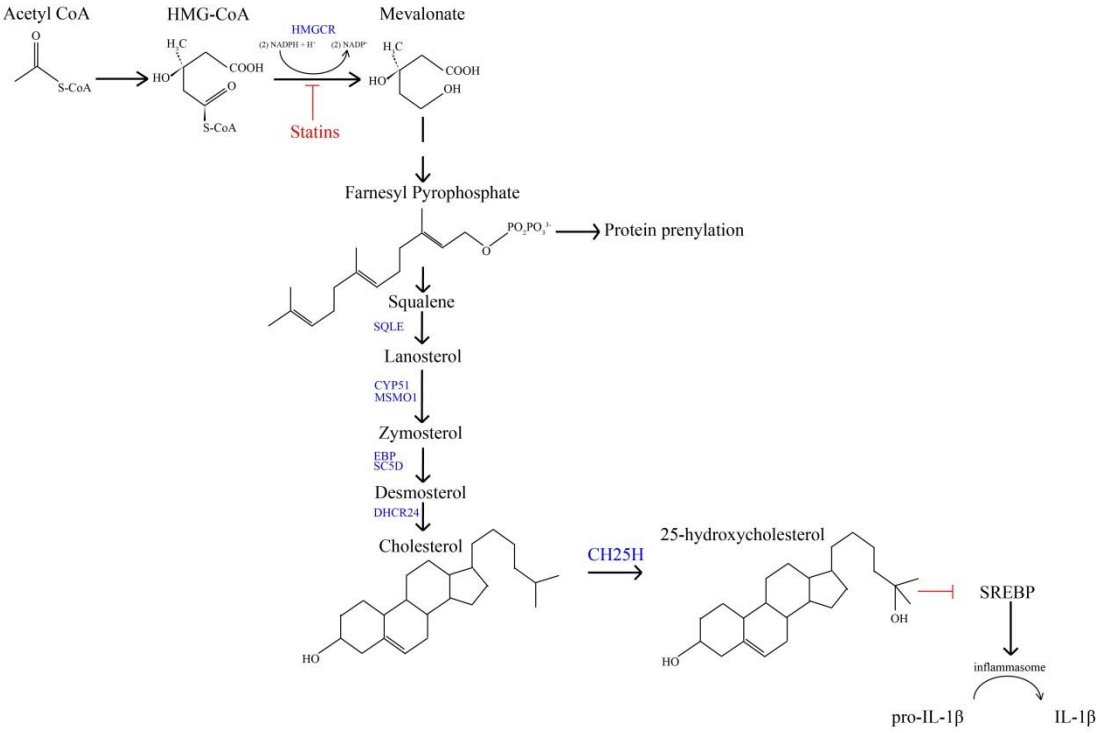

Figure 6.1.1 Cholesterol biosynthesis and downstream 25-hydroxycholesterol action in the brain

A simplified diagrammatic representation of the cholesterol biosynthesis pathway in brain endothelial cells from acetyl CoA. HMGCR is the enzyme that catalyses the rate-limiting and non-reversible step to cholesterol by making mevalonate. Cholesterol can be made from subsequent pre-cursors squalene and lanosterol from different entry points. Enzymes of interest in biosynthetic pathway in blue. CH25H hydrolyses cholesterol to oxysterol 25-hydroxycholesterol which has negative feedback on cholesterol synthesis and IL-1β activation. SQLE – squalene epoxidase, CYP51 - lanosterol 14α-Demethylase Cytochrome P450, MSMO1 - Methylsterol Monooxygenase 1, DHCR24 – 24-dehydrocholesterol reductase, EBP - 3β-hydroxysteroid-Δ8,Δ7-isomerase, SC5D - Sterol-C5-Desaturase.

Interestingly, we have shown that exposure of zebrafish larvae to ATV, a known inhibitor of cholesterol synthesis, causes an ICH which is associated with an increase in Il-1β expression. Despite the clinical link between low cholesterol and ICH risk, there has been no experimental work thus far to elucidate the mechanisms involved. Here we investigate the link between cholesterol biosynthesis, brain haemorrhage and neuroinflammation to determine whether our zebrafish model can offer mechanistic insight into the complex relationship in humans.

6.2 Investigating cholesterol biosynthesis and regulation in a zebrafish model of ICH

The ATV model of ICH in zebrafish larvae works mechanistically by inhibiting HMGCR catalysis of acetyl CoA. This inhibits the rate limiting production of mevalonate and reduces the total production of cholesterol, an essential part of cell membrane rafts that allow for protein anchoring. It also prevents the farnesyl pyrophosphate production necessary for the prenylation of Rac1 that allows for an anchoring point for actin remodelling. Without cytoskeleton remodelling and anchoring points in cholesterol rafts, there is a lack of tight adherens junctions between neuroendothelial cells thus leading to 'leaky vasculature' that is prone to rupture (Eisa-Beygi et al., 2013). Considering that ATV affects the cholesterol biosynthesis pathway directly, we sought to investigate cholesterol levels in *bbh* larvae and characterise any changes associated with brain haemorrhage and if there was any correlation to human disease.

Cholesterol biosynthesis gene expression is dysregulated following an ICH

To determine the expression of cholesterol biosynthesis genes we collected RNA from *bbh* homozygous mutants pre (1 dpf) and post (2 and 3 dpf) haemorrhage for qPCR analysis. Gene expression levels from *bbh* heterozygous ICH- samples were normalised to *hprt1* expression. Relative quantification of transcript levels in ICH+ samples were compared to ICH- samples from *bbh* heterozygous siblings (figure 6.2.1). Before a haemorrhage (1 dpf) ICH+ homozygous mutants have regular expression of cholesterol synthesis genes however post-haemorrhage (2 and 3 dpf), gene expression appears dysregulated and there is a significant (~70%) reduction in *ch25h* transcript (figure 6.2.1C). *Srebf1* levels remain constant implying that it is not a negative feedback mechanism.

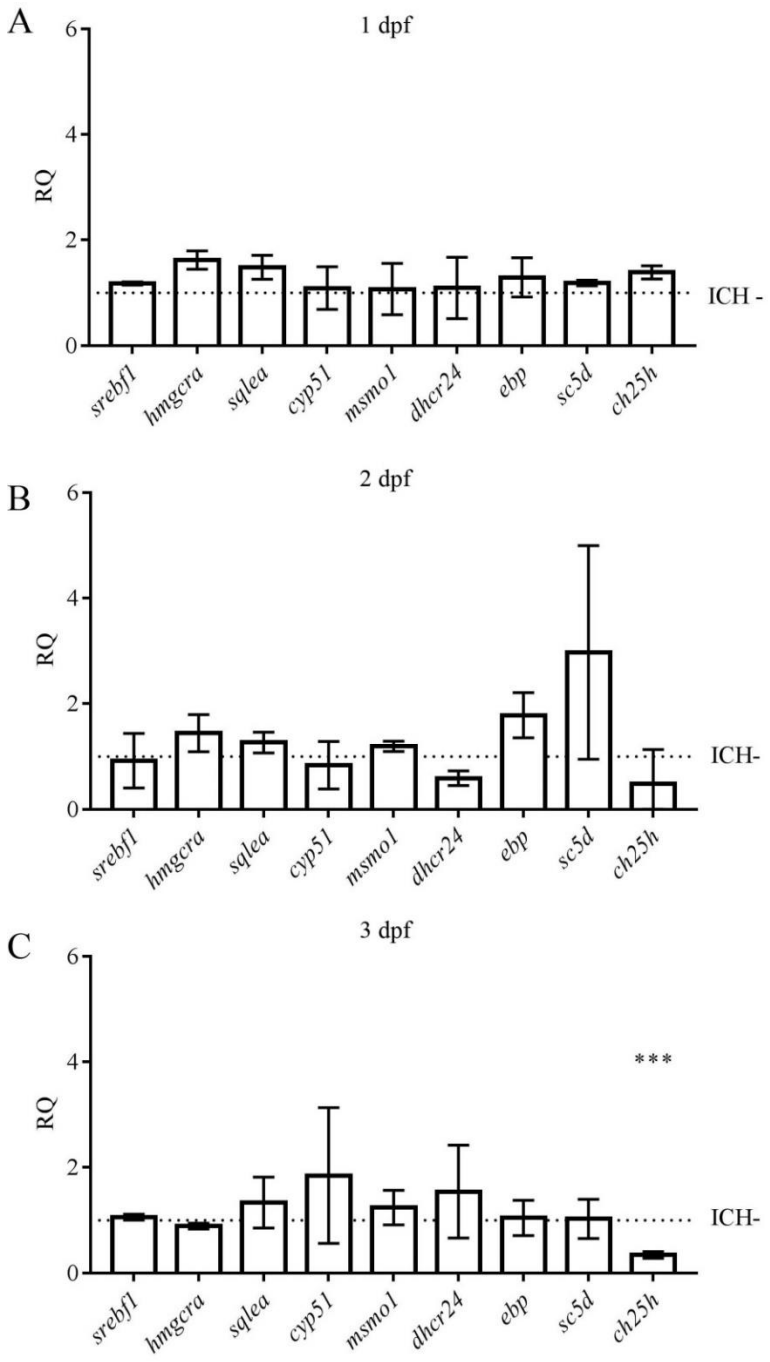

Figure 6.2.1 Cholesterol biosynthesis gene expression pre and post haemorrhage (A) Relative quantification (RQ) of enzymatic genes involved in cholesterol biosynthesis pathway in sequential order. At 1 dpf, pre-haemorrhage, *bbh* homozygous mutants show no difference in expression compared to *bbh* heterozygous ICH- mutant siblings. (B) At 2 dpf immediately post haemorrhage there is a trend towards dysregulation in cholesterol gene expression in ICH+ larvae although no significant differences were found. CT values are close to limit of detection. (C) At 3 dpf, 24 hours post haemorrhage there is a significant decrease in *ch25h* gene expression. RNA collected from n=30 larvae from 3 independent biological replicates and analysed using a two-tailed Student's T Test to compare ICH+ levels to ICH- (***$p<0.0001$).

Unesterified cholesterol is decreased in haemorrhaged larvae

In order to determine whether dysregulation of the biosynthesis genes translates to a loss of cholesterol, we investigated free cholesterol levels using a filipin stain at pre (1 dpf) and post (2 and 3 dpf) haemorrhage time points. Filipin is a naturally fluorescent molecule that binds free cholesterol and not esterified sterols (Maxfield and Wüstner, 2012). Intensity fluorescence was analysed using a macro (appendix iii) and comparisons made to *bbh* wild-type (WT) ICH- siblings. At 1 dpf no difference in filipin intensity between homozygotes and WTs was observed however at 2 and 3 dpf there was a significant decrease in total staining in the ICH+ mutants (figure 6.2.2). Between 1 and 3 dpf, larvae showed a ~30% reduction in unesterified cholesterol. Cholesterol was also analysed using a colourimetric assay however this was not sensitive enough to produce an accurate reading.

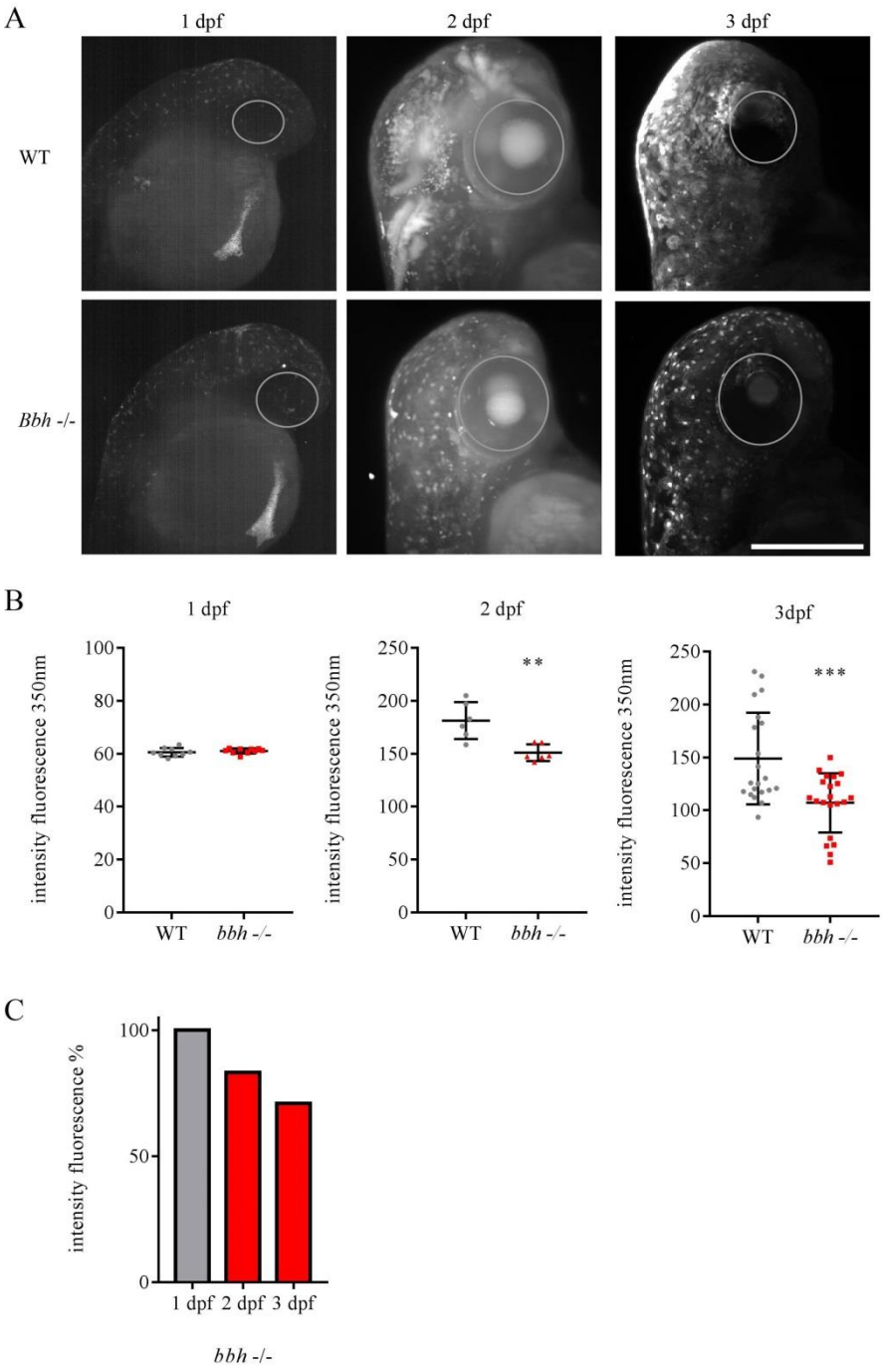

Figure 6.2.2 Quantification of unesterified cholesterol after ICH in the *bbh* larvae
(A) Unesterified cholesterol was stained using a filipin stain and images take from n=12 larvae per group on the lightsheet microscope. WT and homozygous mutant show comparable levels of staining at 1 dpf. At 2 and 3 dpf there is a reduction in the staining in ICH+ homozygous siblings compared to ICH- WT. Scale bar = 250µm (B) Comparison of intensity fluorescence between ICH+ *bbh -/-* and ICH- WTs at 1, 2 and 3 dpf and data analysed using a two-tailed Student's T Test (**p=0.0031, ***p=0.0006). (C) Percentage of total filipin fluorescence shows a 20% reduction immediately after haemorrhage (2dpf) and 30% reduction in homozygous mutants 24 hours after an ICH (3dpf) when compared to WT ICH- controls.

Injecting cholesterol into the yolk sac has no effect on preventing ICH

Considering the studies that show an association between low cholesterol and increased ICH risk and severity (Chang et al., 2018; Phuah et al., 2016), we decided to investigate increasing cholesterol in the larvae as a preventative measure. It has been shown that zebrafish larvae are a good model of fatty acid absorption from the yolk sac due to the hydrophilic/phobic structure (Miyares et al., 2014). Sterol lipids also have a hydrophobic and a hydrophilic end. We continued this investigation using the ATV model of ICH as a proof of principle; if our experimental method of increasing cholesterol worked, then the ATV treated larvae would exhibit less haemorrhages, as a direct counteraction of cholesterol lowering.

Initially, water soluble cholesterol at 1mg/ml or a water control was injected into the yolk sac at 1 cell stage. At this early injection time point all the treated larvae died before 2 dpf so we decided to treat at a later time. To investigate the ATV inducible model of ICH, cholesterol at 1mg/ml or a water control was injected at 1 dpf, into the yolk sac of WT nacre larvae. Nacre larvae treated and untreated groups were then incubated with 1.0µM ATV to induce a haemorrhage. Cholesterol injections were then carried out using *bbh* homozygous and WT groups to investigate the effect on a genetic model. All cholesterol injected larvae in both ATV treated and *bbh* homozygous groups exhibited ICH at 2 dpf, implying that the cholesterol into the yolk sac was not effective at improving vascular stability (figure 6.2.3).

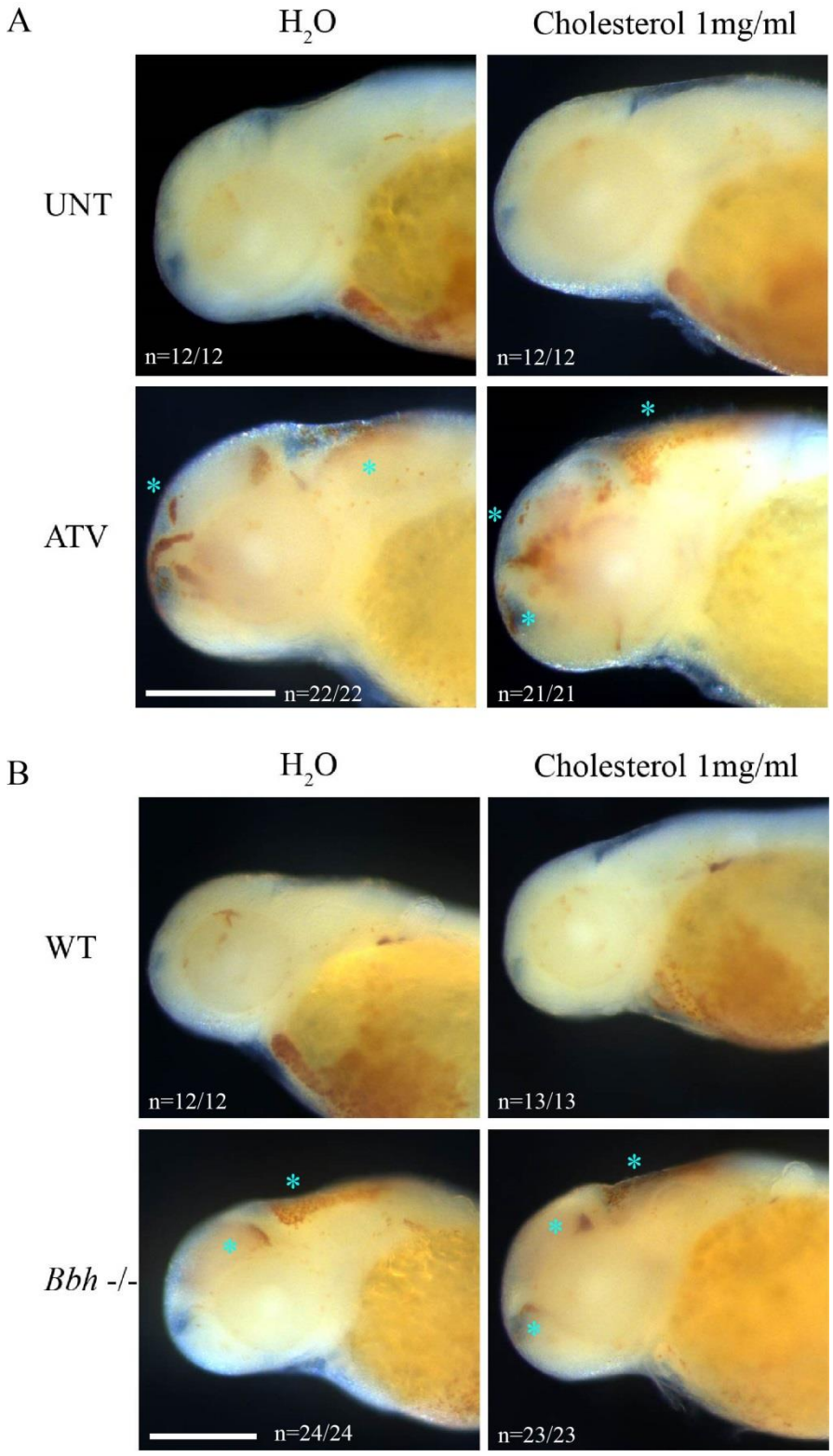

Figure 6.2.3 Cholesterol injections and the frequency of haemorrhages in ATV and *bbh* models

O-dianisidine staining at 2 dpf shows the presence of brown haemoglobin (*) in the heads of all cholesterol treated. (A) ATV ICH+ larvae and (B) *bbh* ICH+ larvae. Representative images shown (n ratio) from 3 independent replicates of n=4-15. Scale bar = 250µm.

High doses of miconazole can reduce haemorrhage size in ATV but not **bbh** *ICH and has no effect on pathological outcomes*

In humans, brain cholesterol is made *de novo* and acetyl Co-A synthetases have been shown to be expressed in the CNS from early development (Quinlivan and Farber, 2017). This led us to hypothesise that stimulating the intracellular biosynthesis of cholesterol might be more effective for regulating brain cholesterol levels rather than injecting the lipid. Previous studies have shown that miconazole, an antifungal compound, reduces haemorrhage rates in a different *βpix* allele mutation (*bbh*^{fn40a}) by increasing vascular stability (Yang et al., 2017). Miconazole increases the transcription of genes in the cholesterol biosynthesis pathway through activation of SREBF (Ashikawa et al., 2016). We sought to replicate this in our ICH model, to increase cholesterol biosynthesis and prevent haemorrhages in the *bbh* -/- larvae. The ATV model was also used to confirm that treatment was effective at increasing cholesterol.

Larvae were incubated with miconazole in 1% DMSO and stained using o-dianisidine to show presence of bleeds. We analysed the treated larvae for haemorrhage numbers and size. There was no difference in haemorrhage prevalence in either of the models; however there was a considerable reduction in the size of haemorrhages seen in ATV treated ICH+ larvae (figure 6.2.4). Haemorrhages in 100% of the ATV treated larvae were restricted to one hemisphere, smaller and only located in the forebrain. This proved that the miconazole treatment was effective in the ATV model, perhaps by an adequate increase in cholesterol; however increasing cholesterol did not prevent haemorrhages in the *bbh* model.

ICH+ larvae were then analysed for cell death (figure 6.2.5) and locomotion (figure 6.2.6). We observed no significant increase in cell death in miconazole treated ICH+ groups compared to ICH- however; there was also no difference seen in DMSO vehicle control animals. The locomotion assay also showed that motility was not significantly different from ICH- groups in either miconazole treated or DMSO control groups. This data suggests that miconazole is not effective in alleviating ICH associated pathology and functional deficit, but that the DMSO vehicle may be affecting outcomes.

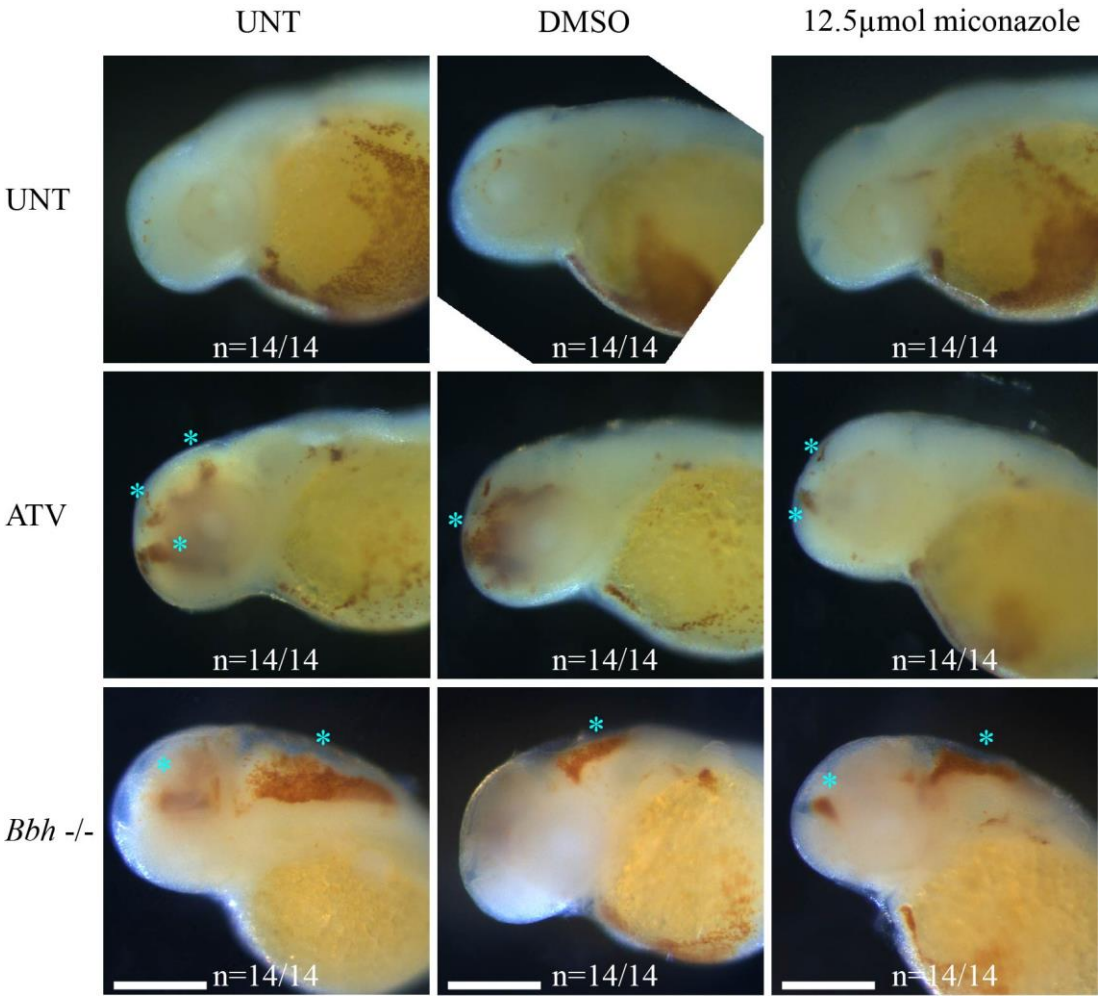

Figure 6.2.4 Miconazole treatment and the frequency of haemorrhages in the ATV and *bbh* ICH models

Haemoglobin stains in larvae that have been treated with 12.5µmol miconazole, or a DMSO control in both ATV and *bbh* models of ICH. Haemorrhages denoted by (*). Miconazole treatment prevented the large, midbrain haemorrhages in 100% of ATV treated larvae, which were observed in DMSO and untreated controls. Miconazole treatment showed no effect on *bbh* -/- mutants haemorrhage size or prevalence. Images are representative (n ratio) of n=14 per group, scale bar = 250µm.

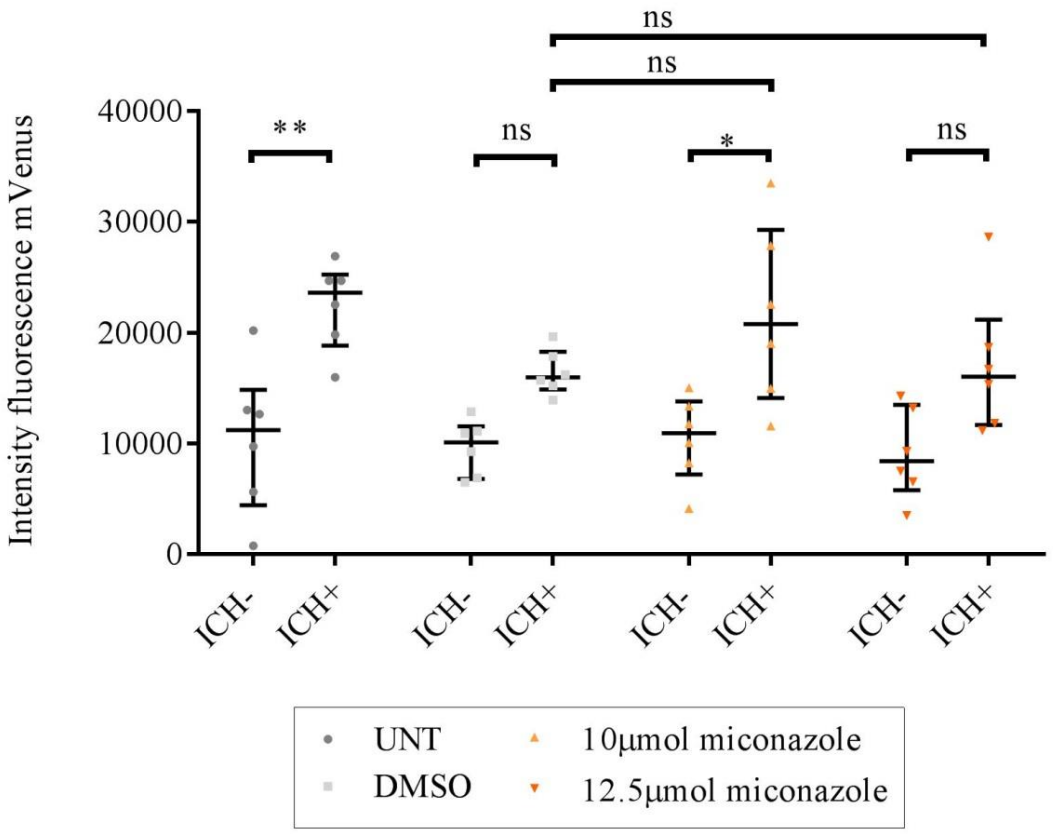

Figure 6.2.5 Effect of miconazole treatment on cell death in *bbh* ICH+ larvae
Cell death analysis data from *bbh* homozygous *ubiq:*secAnnexinV-mVenus miconazole treated groups. Intensity fluorescence data (n=6) was analysed using a two-way ANOVA. No significant increase was seen in DMSO controls (p=0.315) or the highest dose of miconazole (p=0.333). No significant differences were seen between miconazole and DMSO groups (**p=0.0046 *p=0.01).

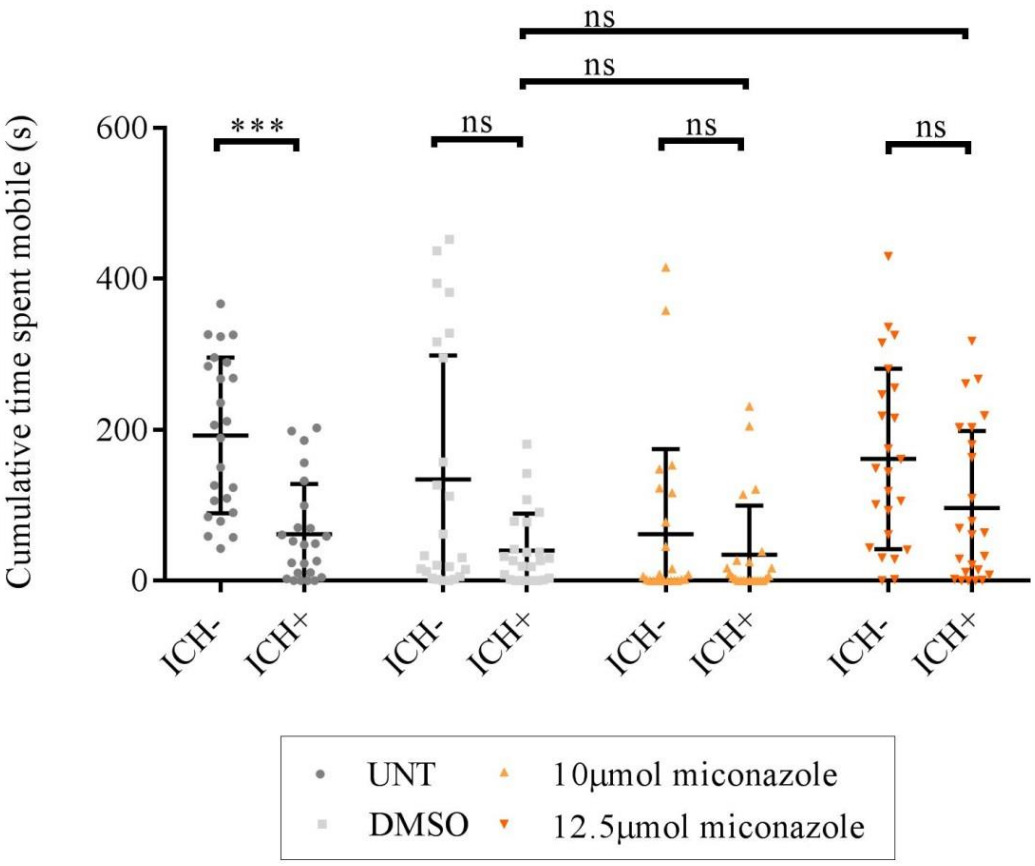

Figure 6.2.6 Effect of miconazole treatment on locomotor function of *bbh* ICH+ larvae

Motility analysis from *bbh* homozygous miconazole treated groups. Data from ICH- and ICH+ groups (n=24 per group) was analysed using a two-way ANOVA and a significant decrease in motility seen in untreated groups. Haemorrhage effect deficit was non-significant in treated (10µmol p=>0.9, 12µmol p=0.59) and DMSO control groups (p=0.052). There was no difference found between ICH+ miconazole treated and ICH+ DMSO control groups (***p=0.0006).

Treating larvae with 25-hydroxycholesterol does not improve brain cell atrophy and does not inhibit il-1β *expression*

Increasing cholesterol biosynthesis with miconazole showed no definitive positive outcomes on ICH pathology in zebrafish. We decided to treat the *bbh* -/- larvae with 25-HC, an oxysterol that is produced by Ch25h mediated hydrolysis of cholesterol. Ch25h expression is decreased in ICH+ larvae (figure 6.2.1) and therefore we hypothesise that this translates to a lack of 25-HC. We anticipated that by increasing 25-HC levels we could perhaps mediate the loss of cholesterol reported earlier (figure 6.2.2) by substituting the downstream product, and modulate the neuroinflammatory response (Gold et al., 2014; Reboldi et al., 2014).

We included a pre ICH treatment (1 dpf) to investigate whether intervention with 25-HC before a haemorrhage event was protective. A post treatment (2 dpf) was intended to see if there were any benefits of modulating the neuroinflammatory response after a haemorrhage. 25-HC has been shown to increase expression of IL-10, an immune regulatory cytokine (Perucha et al., 2019). Cell death analysis in *bbh ubiq:*secAnnexinV-mVenus larvae treated with 25-HC at 50µg/ml in 1% ethanol (Pereiro et al., 2017) showed a slight increase of the response compared to ICH+ untreated controls however this was not significantly different (figure 6.2.7). Time of treatment did not have an effect on the brain cell atrophy, implying that 25-HC treatment was ineffective and neither protective nor recovery promoting. Ethanol is reported to cause developmental defects in zebrafish larvae at high doses however 1% is generally considered to be low, and is widely used as a drug vehicle. In this study we found that 1% ethanol vehicle control and 25-HC treated larvae presented with a high rate of microcephaly and subsequent lower frequency of haemorrhage that we attributed to malformed heads and immature brain vasculature.

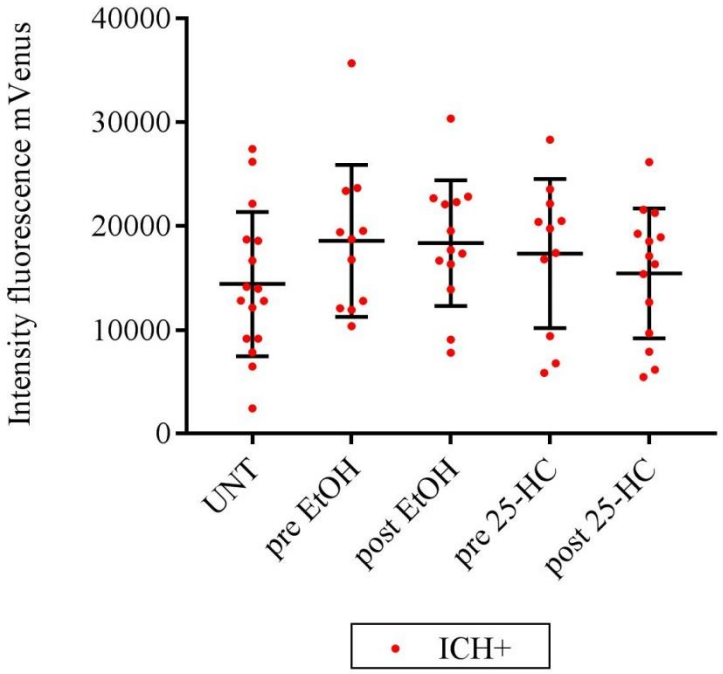

Figure 6.2.7 Cell death analysis with 25-HC treatment

Cell death analysis at 3 dpf following pre- or post- treatment with 25-HC or ethanol vehicle control. Data collected from two independent replicates of ICH+ larvae groups and analysed using a one-way ANOVA. No significant differences between groups.

To determine whether 25-HC treatment had an effect on immune gene expression and early cholesterol biosynthesis, gene expression levels were analysed using qPCR (figure 6.2.8). In comparison to ICH- groups, untreated ICH+ *bbh* larvae show a variable increase in *il-1β* expression and no detectable expression of *il-10*. We hypothesised whether 25-HC might have a stimulating effect on *il-10* as has been shown in human T cells (Perucha et al., 2019). Ethanol vehicle appears to increase the inflammatory stimulation of *il-1β* expression and also shows an increase in *il-10* levels; however without repeating the results no firm conclusions can be drawn. Treatment with 25-HC proved to increase *il-1β* transcription slightly, and also showed il-10 expression. No differences were seen between treatment and vehicle groups implying that the treatment was ineffective in the water. We hypothesise that a genetic approach to increasing 25-HC levels may show more benefit, due to the teratogenic effects of ethanol we observed. Alternatively, to investigate this intervention in an ATV-induced model of ICH, which we know has a direct impact on cholesterol levels.

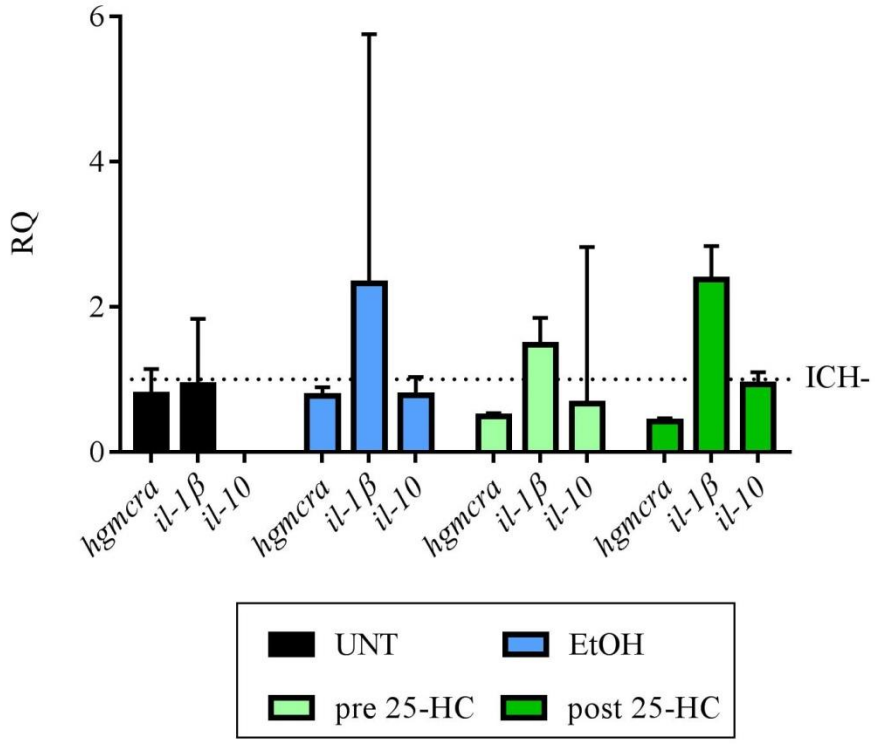

Figure 6.2.8 Immune gene expression qPCR data from 25-HC treated ICH- and ICH+ larvae

Data shows that there is no change in *il-1β* expression between treatment or vehicle groups implying that 25-HC is not blocking transcription. *Il-1β* is up-regulated in ICH+ larvae due to the effect of haemorrhage seen previously and is exacerbated by treatment. *Il-10* expression is unchanged between treatment groups implying that 25-HC treatment is ineffective at regulating the immune response following ICH. Data was collected from one experimental repeat and bars show minimum and maximum RQ values.

6.3 Investigating the expression of *ch25h* in ICH

Protein expression for CH25H in humans is most highly expressed in cerebral cortex, lungs, oesophagus and adipose tissue ((Uhlén et al., 2015) Human Protein Atlas available from www.proteinatlas.org). We have seen that in response to ICH, *ch25h* gene expression is down regulated, and it is unclear whether this is in response to a low level of cholesterol (figure 6.2.2) or due to the increased Il-1β expression that negatively regulates the block on transcription (Reboldi et al., 2014). Understanding the reason why *ch25h* expression is reduced, and how this links to cholesterol may elucidate the importance of cholesterol in either causation of ICH, or roles in recovery following haemorrhage.

Ch25h *expression in the zebrafish and the relationship with* il-1β

Data in this study alludes to a potential relationship between the expression of *ch25h* and *il-1β* in zebrafish following ICH. We have seen in both haemorrhage models that *il-1β* expression is highest at 3 dpf, 24 hours after injury (figure 5.2.1) and this correlates to a decrease in *ch25h* expression at 1 and 2 days post ICH (figure 6.2.1).

To determine a time line of expression of the two genes, we collected ICH- and ICH+ larvae from both ATV and *bbh* models at 1-5 dpf in order to represent pre-haemorrhage (1 dpf), hyper acute (2-3 dpf) and subacute (4-5 dpf) injury phases (figure 6.3.1). Expression of *ch25h* in both models is lower than ICH- larvae before a haemorrhage. There appears to be a slight increase in *ch25h* expression at 4 dpf in ATV treated ICH+ larvae however the large spread of data implies that this may not be a reliable conclusion and does not reach significance (figure 6.3.1A). ATV directly decreases the cholesterol levels in the zebrafish by inhibiting hmgcr and so *ch25h* expression changes may be a consequence of ATV treatment rather than of ICH. Data shows that haemorrhage causes an increase in *il-1β* expression in the ATV model and trends in *bbh* larvae, which decreases over 4 and 5 dpf (figure 6.3.1B).

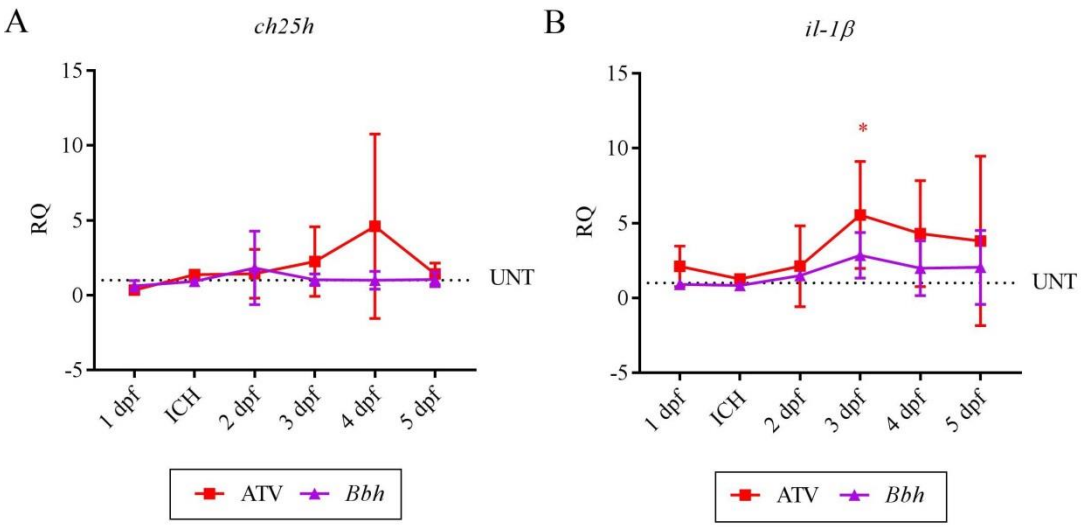

Figure 6.3.1 The temporal expression of *ch25h* and *il-1β* in both ATV and *bbh* models

(A) Relative quantification of expression levels of *ch25h* determined by qPCR in both ATV and *Bbh* models compared to ATV untreated ICH- controls. (B) Expression levels of *il-1β* determined by qPCR in both ATV and *Bbh* models compared to ATV untreated ICH- controls show increase in inflammation in response to ICH at ~2 dpf. Data collected by Miss Annabel Chadwick, from 3-5 independent replicates of each time point and data from each time point analysed using a two-tailed Student's T Test (*p=0.04).

We next investigated the spatial expression of *ch25h* using WISH in larvae collected at 1-5 dpf (figure 6.3.2). Untreated (UNT) ICH- controls show that the *ch25h* expression is high in the brain, and at later time points is visibly expressed in cranial vessels. There appears to be an overall decline in the expression between 2-5 dpf however this is not quantifiable. Larvae with ATV induced haemorrhages also show similar expression to the untreated groups, which is comparable to the qPCR data (figure 6.3.1). Expression pattern is seen in the primordial hindbrain channel and is visible from 2-5 dpf. Bbh ICH+ larvae show less staining at 2-5 dpf than ICH- controls, implying that there is reduced expression of *ch25h*, as observed previously from qPCR data (figures 6.2.1 and 6.3.1).

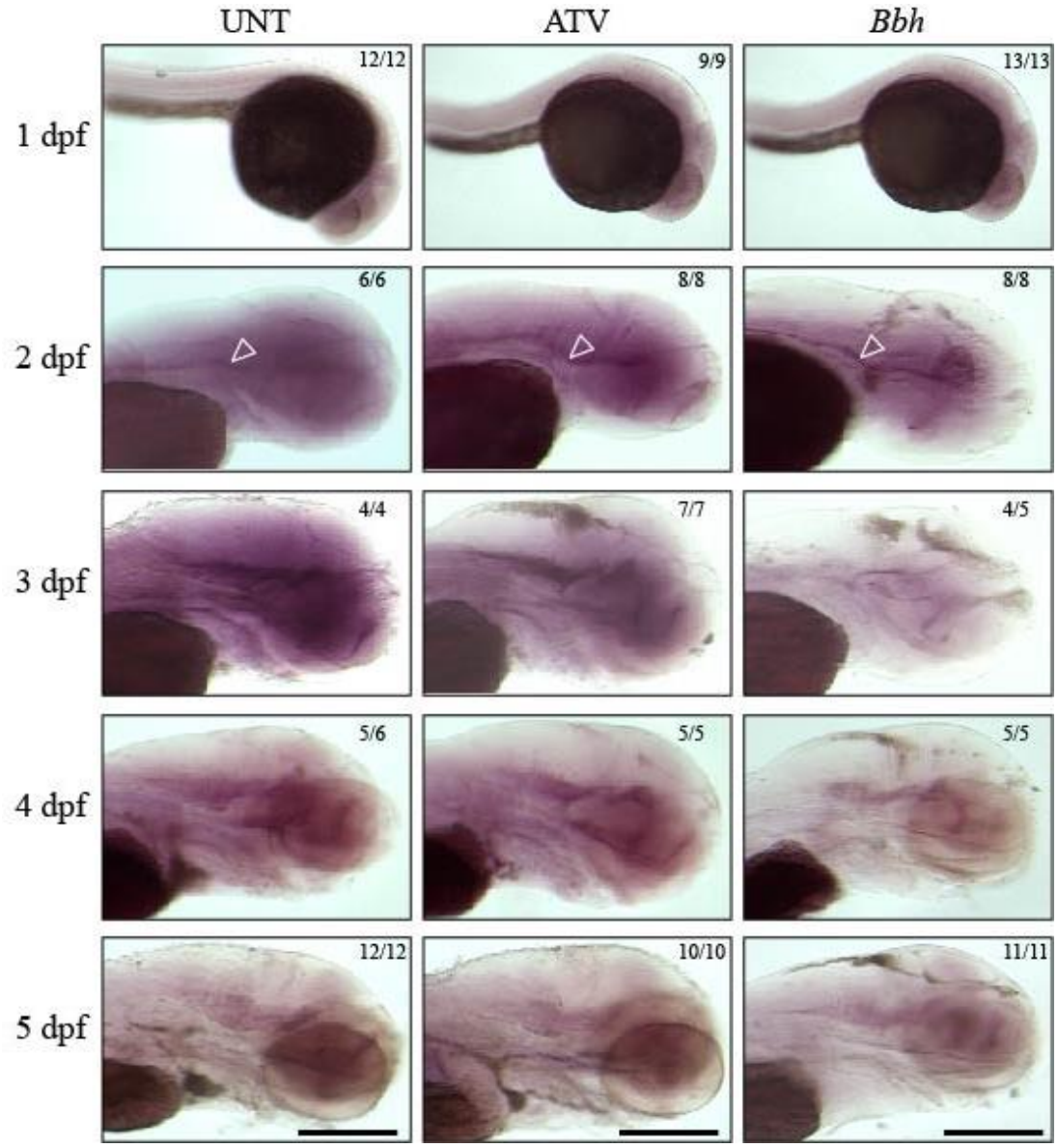

Figure 6.3.2 Spatial analysis of *ch25h* expression in 1-5 dpf ICH- and ICH+ larvae by WISH analysis

Spatial expression of *ch25h* measured by WISH analysis in UNT, ATV ICH+ and *bbh* ICH+ larvae at 1-5 dpf. UNT ICH- (left column), ATV ICH+ (middle column) and Bbh ICH+ (right column) larvae show expression of *ch25h* in the primordial hindbrain channel (PHBC) denoted by arrow. Images are representative acquired from 3 independent replicates of n=4-13 larvae from all days. Practical work was performed and images were acquired by Miss Annabel Chadwick. Scale bar represents 250µm.

At acute time points* CH25H *is reduced after stroke in mouse and human brain tissue

In order to investigate the translatability of the CH25H expression pattern in zebrafish we acquired mouse collagenase-induced ICH and human ICH brain tissue for immunofluorescent analysis of protein expression. Mouse brain tissue was acquired 24 hours after collagenase-induced ICH and was stained for CH25H expression. In sham and naive conditions (n=2) CH25H expression was seen in blood vessels (figure 6.3.3A). In ICH (n=2) there is no observed CH25H expression in either immune cells or vessels corresponding to what is observed in the zebrafish model (figure 6.3.3B). RBCs show high auto fluorescence in the 555nm channel and appear purple. IBA1 positive macrophage cells are seen to be activated with amoeboid morphology, closer to the haematomal regions. There were no neutrophils present in the brain detected by a Ly6G marker.

We acquired human brain tissue from ICH patients (n=3) at acute (48 hours - 3 days post haemorrhage) time points and age/region matched control tissue from the Edinburgh Brain Bank. CH25H was detected in control tissue at very low levels similar to the mouse tissue (figure 6.3.4A) however was not detectable in the ICH+ slices (figure 6.3.4B). At this acute time point, we see the highest expression of IL-1β in the peri-hematomal tissue (Barrington et al. *in preparation*). In zebrafish, mouse and human tissue we have shown that CH25H expression is impaired after a haemorrhage. This correlates to a time where IL-1β expression is high, potentially implying they are inversely expressed.

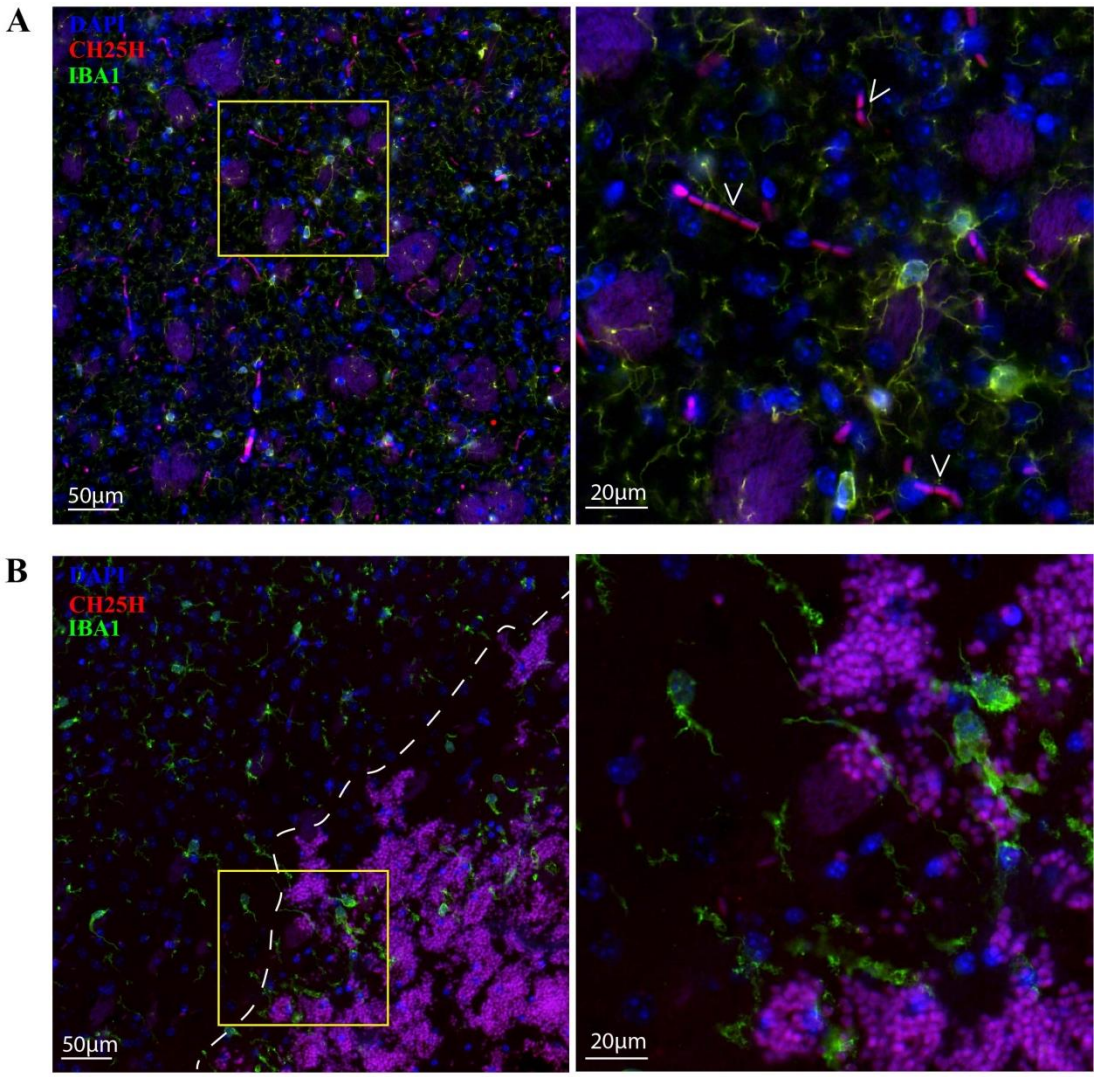

Figure 6.3.3 Immunofluorescent staining of CH25H and IBA1 macrophages in mouse ICH and sham brains at 24 hpi

(A) In control sham tissue CH25H (red) is expressed in blood vessels (arrows) and IBA1 positive cells (green) have a resting ramified morphology. Image in right panel is 60X magnification of yellow box (B) In ICH+ tissue CH25H expression is lost and IBA1 positive cells adopt a rounded activated morphology closer to the haematoma (white line). RBCs auto fluorescence appears purple. Image in right panel is 60X magnification of yellow box.

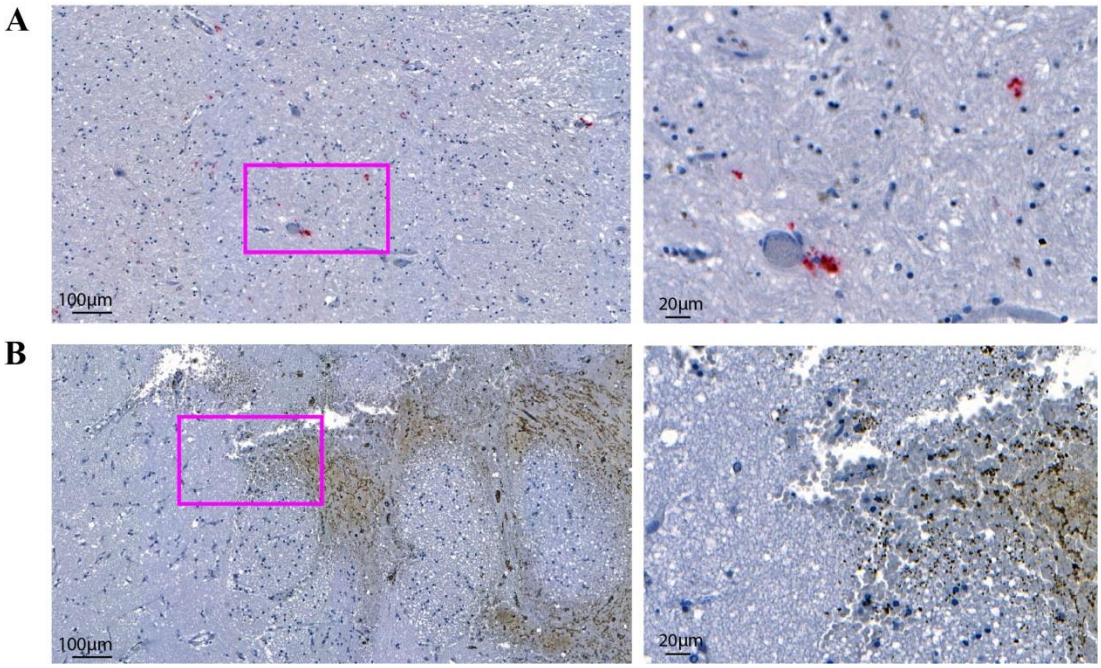

Figure 6.3.4 Histological stain for CH25H in acute human ICH tissue
Tissue acquired from ICH patient and age/region-matched control tissue was stained with HRP for CH25H (A) Control brain tissue shows basal levels of detection throughout the slice (B) ICH+ tissue shows a loss of CH25H expression. RBCs are brown, Haematoxylin was used as a counterstain. Images are representative of tissue sections and acquired at both 10X (left panels) and 40X magnification (right panels)

CH25H expression is detectable at subacute time points in human tissue

As was observed in the zebrafish, we confirmed that CH25H expression is reduced after haemorrhage in both mouse and human at acute injury time points. We acquired subacute (>10 days post haemorrhage) human tissue samples (n=3) from 10, 43 and 60 days post haemorrhage from the Edinburgh Brain Bank. At 60 days post ICH, but not at 10 or 43, strong CH25H signal was observed in human tissue in the haematoma, expressed by cells identified morphologically as macrophages (figure 6.3.5). Tissue stained for IL-1β was negative at this time point (not shown). Close observations show that the cells expressing CH25H are also positive for hemosiderin, orange/brown in the haematoxylin counter stain.

Comparing the expression across zebrafish, mouse and human tissue with data thus far we can hypothesise that there may be a similar pattern in all three species (figure 6.3.6). We still require evidence in order to support our predictions however we hypothesise that ch25h expression might be linked to recovery due to loss of expression at ICH event and a high expression in subacute human tissue.

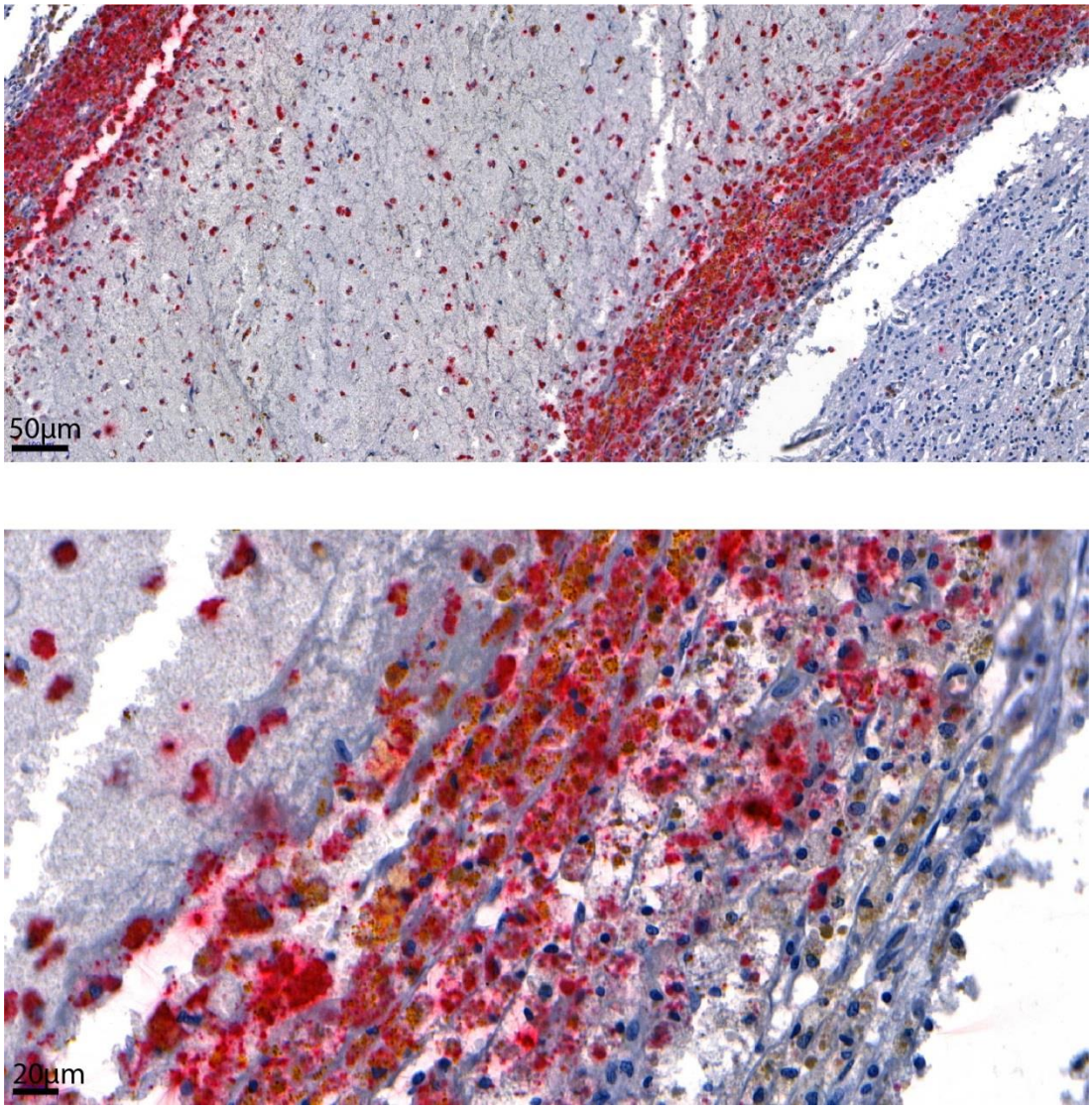

Figure 6.3.5 Histological staining for CH25H in human peri-haematomal brain regions

Tissue acquired from basal ganglia of an ICH patient in the subacute time frame (60 days post stroke) was stained using HRP for CH25H expression in the peri-haematomal tissue. Strong expression (red) seen in cells morphologically identified as macrophages also containing hemosiderin (orange). Haematoxylin was used as a counter stain. Images are representative of tissue section and acquired at 10X (top panel) and 40X magnification (bottom panel).

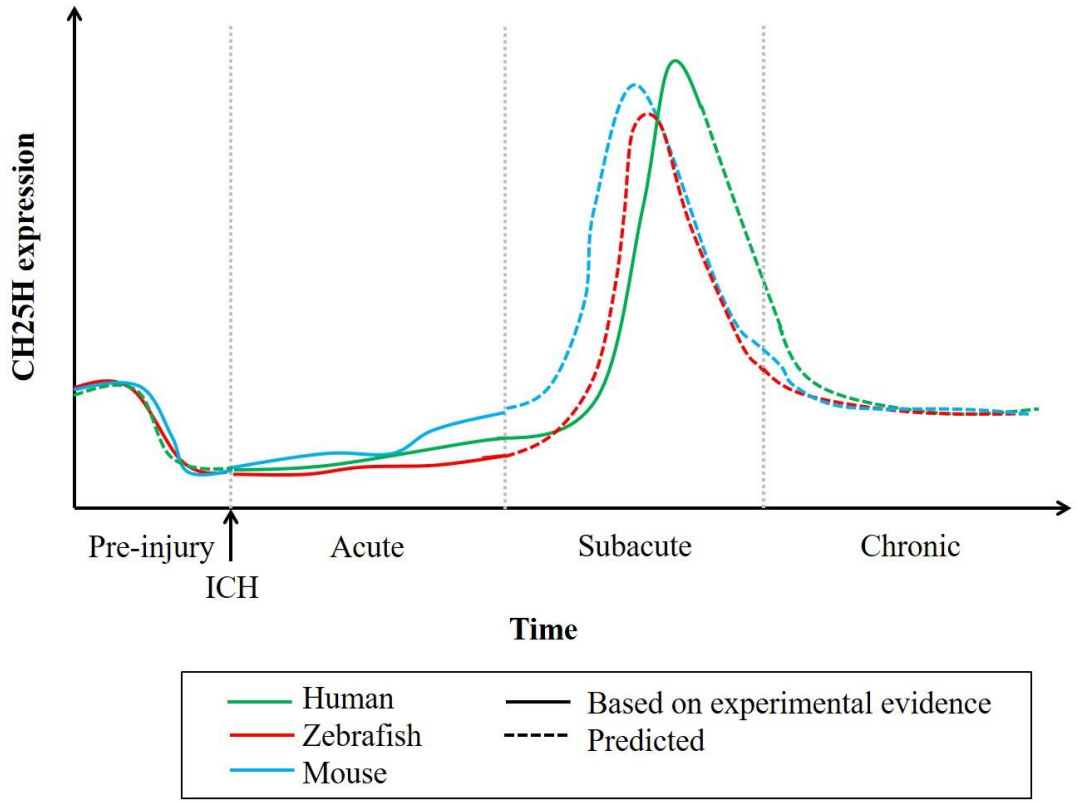

Figure 6.3.6 Timeline of CH25H expression in zebrafish larvae, mouse and human tissue.

Hypothesised time line of CH25H expression after an ICH event. Zebrafish data from pre-injury and acute periods are based on mRNA expression detected by qPCR and WISH. Human and mouse data are based on protein detection from histological staining evidence in brain tissue.

6.4 Discussion

Here we show that cholesterol metabolism is dysregulated in the zebrafish larval haemorrhage models and try to elucidate the relationship between zebrafish, mouse and human tissue. The advantage of spontaneous haemorrhage models is that we can investigate some of the co-morbidities that cause blood vessel rupture, with a view to exploiting preventative measures. Low total cholesterol levels are a risk factor for ICH (Y.-W. Chen et al., 2017; Phuah et al., 2016; Rist et al., 2019; Valappil et al., 2012; X. Wang et al., 2013). If we can understand more about how low cholesterol levels contribute to the loss of vascular stability, and whether this can be reversed, we may understand more about at-risk populations and how to prevent haemorrhage.

Our data shows that cholesterol gene synthesis is dysregulated in the 24 hours after haemorrhage, resulting in overall decrease of cholesterol in the *bbh* mutants. We sought to rescue this phenotype by increasing cholesterol levels; however this had no preventative or beneficial effect on haemorrhage outcomes. This may be due to the injected cholesterol not being taken up into the larvae, as previous studies have shown that lipids are metabolised in the yolk sac prior to absorption (Fraher et al., 2016). It may also be that there is not a large enough demand for absorption into the blood, or that brain cholesterol made *de novo* in the developing organism that is important in tight junction formation, cannot be influenced by injecting cholesterol in this way (Quinlivan and Farber, 2017). We might be targeting the wrong time point, cholesterol is important for nerve cell regeneration and therefore increasing levels in the zebrafish larvae immediately after ICH rather than before, may speed up the recovery process (Heacock et al., 1984). By treating larvae with miconazole we targeted cholesterol biosynthesis, upregulating the genetic pathway that we know to be dysregulated in ICH. Miconazole treatment was successful in reducing the size of the haemorrhages seen in the ATV model. We hypothesise that this was due to treatment counteracting the effect of ATV of reducing cholesterol however this has not been confirmed. Future studies may be carried out in transgenic animals to measure the volume of the bleeds and determine the reduction in size when treated with miconazole. Contrary, miconazole has also been widely reported to inhibit cholesterol biosynthesis, as part of the antifungal mechanism (Gupta et al., 1990). This implies we do not fully understand the mechanism in the zebrafish. We saw no effect of miconazole treatment in the *bbh* larvae, inconsistent with the Yang et al (2017) study who observed a

reduction in haemorrhage rates in the *bbh*^{fn40a} homozygotes. Yang et al did not study the *bbh*^{m292} mutant because they found the homozygotes to be embryonic lethal. Miconazole did change the gene expression pathway however did not restore ch25h levels to normal in ICH+ larvae (not shown). Despite modulating cholesterol levels, miconazole did not result in any functional or pathological benefit in the zebrafish larvae. This may have been due to a sustained loss of ch25h.

In order to further investigate CH25H expression and role in haemorrhage we took a translatable approach to investigate expression in mouse and human ICH tissue. This is the first time that CH25H has been investigated in terms of human ICH pathology. In the zebrafish we have shown that the transcript levels are low after a haemorrhage compared to ICH- controls. We confirmed this in mouse tissue that normal expression in the cerebrovasculature was absent 24 hours after a haemorrhage, and in human tissue which at the equivalent acute time point CH25H was not detectable. At a much later time point CH25H expression was increased dramatically in the human tissue however we do not have data from an equivalent time point in mice or zebrafish. Our data suggests that ch25h and il-1β are expressed at different time points and the increased expression of il-1β at the early time point may cause a reduction of ch25h as a negative feedback mechanism (Simon, 2014). Future experiments may investigate modulating ch25h expression in the zebrafish through genetic manipulation, a MO knockout or over-expression of mRNA. We may also investigate how effective ch25h over-expression is when cholesterol is also increased by either injection or simultaneously over-expressing hmgcr.

We aimed to decrease inflammation with 25-HC treatment. 25-HC has been reported to both activate and suppress IL-1β expression, and increase anti-inflammatory IL-10 (Gold et al., 2014; Perucha et al., 2019; Reboldi et al., 2014). We aimed to determine the relationship in zebrafish in the context of ICH. It was surprising to see that 25-HC treatment had no effect on the levels of *il-1β* and *il-10* gene expression however we did not continue with these experiments because the larvae were affected by the ethanol vehicle. This may suggest that our method of administering treatment was ineffective and that we did not observed the true effect of 25-HC treatment. 25-HC also drives the expression of *ch25h* and inhibits the expression of *hmgcr* reducing overall cholesterol levels, which may not be a beneficial strategy of reducing neuroinflammation (Liu et al., 2018).

The links between cholesterol and inflammation are numerous and complex. Cholesterol has been implicated in regulating immune cell proliferation, migration and intracellular signalling (Reboldi and Dang, 2018). It has been long known that cellular glucose metabolism and glycolysis effects cholesterol biosynthesis (Siperstein and Fagan, 1957) and recent studies are revealing the links to immune responses (Ganeshan and Chawla, 2014). In normal conditions glucose is converted to pyruvate by the process of glycolysis which is then used to drive the Krebs cycle for succinate and oxidative phosphorylation. In anaerobic conditions pyruvate is converted to lactate and removed from the cell. Without the oxidative decarboxylation of pyruvate, there is no production of acetyl CoA and a loss of cholesterol and fatty acid biosynthesis. Glycolysis is blocked in conditions such as hypoxia, cancer and viral infection (Buck et al., 2015). Viruses drive aerobic glycolysis to make pyruvate and increase lactate production as this rapidly produces ATP for synthesis of materials (Sanchez and Lagunoff, 2015). This may explain why viral infection has also been associated with increased risk of ICH as there is a subsequential inhibition of cholesterol (Tseng et al., 2015). Interferonopathies have also been linked to high ICH incidence rates (Meuwissen et al., 2016; Ramesh et al., 2010) as the cellular response and activation of the immune system mimics viral infection. Increased interferon stimulation drives CH25H expression as a defensive mechanism to prevent viral entry by depletion of cholesterol (Liu et al., 2013; Raniga and Liang, 2018). Loss of glycolysis in haemorrhage due to the hypoxic environment surrounding the haematoma may cause the sudden loss of cholesterol we observed after a haemorrhage.

This data has shown some interesting novel findings, that ch25h loss in the zebrafish model is also identified in the mouse and human brains, however more work is needed to conclude our hypothesis of how cholesterol is involved in ICH. Practical issues with using zebrafish limit this study. Measuring total cholesterol by filipin stain means that the quantification is not brain specific and also includes the cholesterol in the skin covering the head. We attempted to quantify cholesterol using a colourmetric assay however this was not sensitive enough to detect the small changes we observed by filipin measurement. In order to get a more robust quantification, cholesterol could be measured by gas chromatography or mass spectrometry however it is very difficult to isolate the brain tissue at this time point in large enough quantities for analysis. Additionally, when making comparisons between zebrafish and mouse and human

tissue, we could not perform the same experiments in all three tissues, and therefore are estimating the conclusions between them for example comparing genetic analysis and protein expression in histological stains. Despite confirming the loss of ch25h at acute time points across species, we have not yet obtained zebrafish and mouse data from a time point that reiterates the large increase of CH25H expression we observe in the human tissue which may allude to an important recovery process.

Future experiments may investigate making haemorrhage worse, by decreasing cholesterol levels further and see if this causes repetitive, or sustained haemorrhaging in the larvae. We could do this by knocking out or inhibiting proprotein convertase subtilisin/kexin type 9 (pcsk9) enzyme, responsible for the degradation of LDL receptors and thus inhibition increases cholesterol uptake into the liver. Additionally, in order to prove the translatability of the cholesterol mechanism of haemorrhage, we could test our hypothesis in rodents, to see if a low cholesterol diet and/or a genetic mutation in pcsk9 decreases cholesterol sufficiently to cause spontaneous cerebral haemorrhages. Alternatively we could test the protective outcomes of increasing cholesterol through raising zebrafish on a high-cholesterol diet, to determine whether this prevents haemorrhage or the associated pathologies as our current methods are not robust (Progatzky et al., 2014).

High cholesterol is a risk factor for ischemia, however it may be apparent now that too low cholesterol causes haemorrhage and therefore there is an optimal level of cholesterol to maintain (Krel et al., 2019). Further investigation into the causative mechanisms of ICH and how cholesterol biosynthesis pathway is involved in needed, as understanding these processes may allow for better ICH prevention in at risk populations.

Chapter 7: General discussion

7.1 Key findings

The work presented in this thesis has addressed the primary aims to 1. validate a zebrafish larval model for pre-clinical ICH investigation, 2. to characterise the associated disease pathology, 3. to employ the model in drug intervention studies and 4. to investigate the role of cholesterol in contributing to spontaneous ICH. In this work we have shown that both genetic and chemically-inducible models of blood vessel rupture in zebrafish larvae offer valuable platforms for pre-clinical ICH investigation. Both models exhibit comparable haemorrhage size and location, brain cell death, loss of cerebral circulation and a subsequent loss of mobility that is recovered 3 days post injury. This study has demonstrated that zebrafish larval models exhibit pathological outcomes that mimic human disease, which can be quantified to measure severity. Adult genetic mutants are viable breeders and exhibit no histological evidence of brain injury due to haemorrhage. There is an increase in neuroinflammation in the *bbh* model, and we have observed, for the first time to our knowledge, active macrophages responding to the dying cells and phagocytosing the ICH debris from the site of injury in whole, live, intact organisms. We have investigated specific drug interventions in the zebrafish model, to modulate the neuroinflammatory response and to ameliorate the iron load following an ICH. We verified the model can be used in a medium throughput screen for targeted ICH medications with potential for translation to clinical application. Utilising the spontaneous nature of ICH we have shown that cholesterol biosynthesis is dysregulated in the zebrafish larvae, which can be further interrogated to understand the link between hypocholesteraemia and ICH in patients.

These findings demonstrate that zebrafish larvae offer a novel, valid pre-clinical model of ICH that will hopefully be accepted by the stroke research community as an alternative approach to complement rodent studies. Incorporating the zebrafish model into the drug development pipeline will provide increased reliability to experiments, and speed up initial screening processes. The model can also be used to elucidate the specific mechanisms that trigger blood vessel rupture due to the spontaneous nature of disease. Rodent ICH studies typically use 6-8 animals per experimental group totalling around 50 per publication (Lim et al., 2019), and when longitudinal

experiments include multiple sample times and endpoints, a study can easily exceed 100 animals (Zhao et al., 2019). With ~120 and ~150 studies published annually reporting the use of mouse and rat models of ICH respectively (Pubmed search, 2019), a shift to using unprotected zebrafish larvae has potential to reduce this number of animals significantly. Publications sometimes fail to report the true number of animals used, as some die before data can be acquired (Dagistan et al., 2019). The zebrafish model offers a crucial new perspective on a vitally important field of medical research. Overall, the use of zebrafish models will allow for the future investigation of other risk factors for ICH, lend further insights into disease mechanisms and help understand the target outcomes from drug screening (Eisa-Beygi and Rezaei, 2016).

7.2 Targeting secondary injury in ICH

The secondary injury processes following an ICH present many therapeutic targets, to inhibit the activation of immune cells, reduce the release of toxic ROS and to upregulate the reparative properties of microglia. Clinically, IL-1Ra has been successful in reducing inflammatory markers in phase II trials for ischemic stroke (Smith et al., 2018) and subsequently has advanced in clinical trials for SAH and ICH patients (Galea et al., 2017; Parry-Jones, 2018). In this study, IL-1Ra showed no positive outcomes in the zebrafish model and may even worsen the condition. This correlates with pre-clinical data seen using the mouse collagenase model, which show ICH mice have a worse neurological deficit measured using the rotarod post IL-1Ra treatment (Barrington et al. *in preparation*). It should be noted that in this study IL-1Ra was administered both prior to and after ICH surgery and such a treatment regime lacks clinical relevance. The failure of IL-1Ra in the zebrafish and mouse collagenase models may be due to ICH being vastly different from other subtypes of stroke, and the success from ischemic stroke trials has yet to be demonstrated in clinical ICH (Parry-Jones, 2018).

Investigation into DFO therapy in this study also showed no overall benefit to the ICH+ larvae. Interestingly, DFO with DMSO did show positive reduction of cell death in initial drug screen assays and so ideally would warrant further investigation. Despite recently stopping the clinical trial there could be a link with HO-1 expression and response to DFO, previously identified in IVH that could be elucidated pre-clinically (LeBlanc et al., 2016). Other metal chelating agents that were identified by the drug

screen include gluconalactone, sparteine sulfate and aminolevulinic acid (appendix x). Aminolevulinic acid is presently used for cancer diagnosis and photosensitising therapy, and so may present an alternative strategy of breaking down the haematoma without the use of surgery (Jichlinski et al., 2003; Tetard et al., 2014; Yew et al., 2016). Sparteine is not currently approved for medical use however has function as an antiarrhythmic agent, such as digoxin and disopyramide also identified in the screen (Campbell and Williams, 1998). Drugs like sparteine, that offer potential translational leads, may be eliminated from the pipeline due to lack of mechanistic understanding or Medicines and Healthcare products Regulatory Agency (MHRA) approval. Screening in zebrafish larvae, on pre-regulated animals, means that these drugs can be tested further for clinical effect with minimal impact on animal welfare.

7.3 The role of cholesterol in ICH

In order to elucidate the real impact of low cholesterol on ICH risk and whether it can be targeted therapeutically more research is required. Currently, despite the clinical association studies, there is a lack of pre-clinical research into the causative mechanisms of hypocholesterolaemia and ICH. Future experiments will hopefully clarify the temporal expression of CH25H across species and determine why it is so highly expressed at late subacute time points in humans. Our preliminary RNASeq data from isolated zebrafish leukocytes at early time points after ICH, show reduced expression of *ch25h* in macrophages 24 hours after haemorrhage (unpublished). We have yet to understand the links between cholesterol pathways and the potent immunostimulator IL-1β in these specific cell types. Literature suggests that there is an inverse relationship between expression of IL-1β and CH25H within the macrophage (Simon, 2014). Previous studies have shown that when CH25H expression is knocked out, there is an increase in neutrophil recruitment to the injury site in a model of intestinal fibrosis, perhaps because the block on IL-1β transcription is removed (Raselli et al., 2018).

The link between type 1 interferon and ch25h has also not yet been investigated in the *bbh* model and the literature is conflicting (Raniga and Liang, 2018). It is still uncertain as to how the bleed event and the loss of cholesterol metabolism are linked. Low cholesterol may be due to overall cell loss and damage caused by the haematoma; however it may also be part of a recovery mechanism that can be exploited

therapeutically (Soriano et al., 2019). If cholesterol biosynthesis can be up-regulated clinically, immediately after haemorrhage, an overall increase in cholesterol levels may protect against neuronal damage or speed up regeneration (Hussain et al., 2019). There may be a link to viral infection, loss of cholesterol and interferon signalling which may contribute to the triggering point of a haemorrhage (Tseng et al., 2015). The interferon signalling pathway defends against viral infection has been shown to decrease cholesterol to prevent viral replication and budding, perhaps contributing to vessel weakening and rupture (Xiang et al., 2015; Zhang et al., 2019). It would be interesting to investigate whether ICH patients reported having a viral infection, or if viral load is detectable prior to ICH onset.

With regards to cholesterol as a risk factor for ICH, it is unlikely that this can be controlled in the wider population. Dietary cholesterol intake is variable amongst a human sample population and public health information for patients is currently to reduce cholesterol intake to reduce risk of CVD and ischemic strokes. The risk associated with hypocholesterolaemia needs to be clarified, particularly for vulnerable populations such as the aged, malnourished and those from low-middle income countries (Lewis and Tikkanen, 1994). Aggressive statin treatment to lower cholesterol has shown to increase the likelihood of haemorrhagic transformation after an ischemic attack, and increase ICH occurrence (SPARCL, 2006). One side effect of statin treatment is easy bruising, implying vulnerable vasculature is not only observed in the brain.

Despite a correlative relationship with ICH risk and serum cholesterol levels (Phuah et al., 2016; Rist et al., 2019) brain cholesterol is synthesised locally (Björkhem and Meaney, 2004) and peripheral samples do not directly indicate levels of brain cholesterol. This relationship has not been investigated in pre-clinical models due to lack of spontaneous ICH. Is low serum cholesterol the cause of ICH or a product of dysregulated biosynthesis? Thus far in experimental animal models, reducing cholesterol levels has not been investigated in terms of ICH risk, only to inhibit inflammation through 25-HC (Tall and Yvan-Charvet, 2015).

The zebrafish models offer a unique insight into the relationship between cholesterol and ICH. The ATV model decreases cholesterol biosynthesis in order to cause a haemorrhage. The *bbh* model has revealed that a loss of cholesterol occurs after ICH.

Thus far there have been no studies or clinical investigation into the immediate loss of cholesterol after ICH; the only links have been from the perspective of risk. We have associated this decrease in cholesterol with a loss of CH25H across species implying a novel pathological mechanism. However, because cholesterol is vital for a range of other bodily functions, targeting production for therapeutic purposes may result in unwanted side effects, especially in young patients. There have been recent advances in delivery techniques for brain specific therapies such as using liposomes, viral vectors and nanoparticles as vehicles (Dong, 2018). If we can understand more about the temporal control over CH25H this might help determine a therapeutic window for targeting cholesterol.

7.4 Drug screening

We have highlighted the merit of the zebrafish larval model in a drug screen, as we have been able to identify effective compounds that may never have been selected for clinical investigation otherwise. Drugs that are not MHRA approved, have unknown mechanism of action, or are current treatments for other cardiovascular diseases like arrhythmia, have been identified as advantageous in the zebrafish model of ICH (appendix x). The advantage of screening so many compounds at once will provide the stroke field new avenues of investigation, though further confirmatory studies of efficacy are required in zebrafish before any compound can be moved along the translational pathway.

We believe our drug screen strategy to be clinically translatable as we have investigated a potential benefit to brain cell death after ICH. Thus far, experiments investigating protection in the zebrafish larval models of neurovascular instability have attempted to prevent blood vessel rupture (Huang et al., 2017; S. Li et al., 2017; Yang et al., 2017). However, mechanisms for preventing blood vessel rupture in a developing zebrafish larva at onset of circulation are not equivalent to protecting the mature cerebrovasculature in an adult human. In the context of developing a therapy to reduce the impact of ICH that has already occurred, then it is more relevant to investigate reducing the damage after ICH, rather than stopping the bleed. We hope to identify medical therapies that can be administered to patients as early as possible after the ICH to prevent escalating primary and secondary injury processes.

7.5 Limitations of the model

As previously highlighted, the zebrafish model offers practical, scientific and ethical benefits compared to the rodent models of ICH. The zebrafish is proving to be a valuable tool for modelling neurological diseases as the early transparency and ease of genetic manipulation allow for real time non-invasive imaging as we have utilised in our work to perform a longitudinal study. Working with zebrafish models however has certain common limitations. Compared to rodents, zebrafish as model organisms are relatively new and understanding of the unique biology is not as complete, and so there is not the same availability of species specific reagents and resources. As a less inbred species, there are genetic differences between fish strains and single nucleotide polymorphisms (SNPs) in the genome that have not yet been outbred or mapped (Stewart et al., 2014). This generates a more heterogeneous group that more closely simulates human populations but can also generate more variability in experimental data. Using a developing organism to model a disease typical of old age, often clinically accompanied by many co-morbidities, may not seem immediately relevant. A juvenile organism may more closely represent childhood stroke, and by using the zebrafish at this stage we can exploit the transparency and spontaneous ICH onset that is not possible in older animals. Expected experimental disease related phenotypes often present in larvae as common developmental defects, that can occur randomly even in a wildtype clutch. Pericardial and yolk sac oedema, bent body axis, small eyes and loss of pigmentation are often used to screen for mutant phenotypes however can occur randomly as a result of a large clutch. Lack of a developed skull in larval stages mean that ICP is not affected in the same way as mammals, as the head can swell with increasing oedema. These factors may inhibit the wider uptake of the models amongst stroke pre-clinical researchers. On the other hand the large numbers of animals collected for larval studies means that experimental n numbers provide more confidence in identifying true results. It has been acknowledged amongst rodent researchers that the small n numbers used for sample sizes, often results in underpowered experiments, contributed to by random deaths (Holman et al., 2016). The regenerative properties of zebrafish offer a unique opportunity to investigate recovery after injury (González-Rosa et al., 2017). Adopting the zebrafish model in the pre-clinical stroke community will hopefully increase the availability of species

specific tools, provide increased validity to drug studies and will reduce the use of protected species used in experimentation.

7.6 Future experiments

Despite the common limitations with zebrafish, we have shown that they present a suitable model for ICH, however to gain a more robust understanding of the zebrafish pathology, further interrogation of the model is needed. There are questions that have arisen from this study that have not yet been addressed. Why do the annexinV positive cell populations always appear in the same cluster patterns? Are the dying cells motor neurons, or visual sensory neurons, that could have a direct link to the loss of motility we observe associated with ICH? Understanding more about the recovery/developmental processes in the zebrafish larvae to recover from haemorrhage would also be interesting and potentially offer new therapeutic opportunities. Can we activate these developmental pathways in the adult human brain in order to initiate full recovery as is observed in the zebrafish? In adult *bbh* zebrafish although we do not observe any morphological evidence of brain damage, there is still a visible difference between adult homozygotes that haemorrhaged in larval stages and sibling controls, such as a smaller body frame. Further investigation could determine why this might be, perhaps due to a developmental defect previously unrecorded, which may offer a chronic model of ICH pathology.

The zebrafish larval model may be used to further investigate the role of innate immune factors in ICH injury. Another pro-inflammatory molecule of interest TNF-α, increases after ICH and has been associated with severity of oedema (Hua et al., 2006b). Physiological roles of TNF-α alongside immunostimulation include driving inflammation induced apoptosis (Beyaert and Fiers, 1994) and mediating cell cycle arrest (Ott et al., 2007). Inhibition of TNF-α signalling in the developing zebrafish impairs blood circulation (Espín et al., 2013). Clinically, TNF-α has been highlighted as a peripherally detectable marker for oedema formation (Rendevski et al., 2018) however mediating the response after ICH has not been investigated in humans. Despite a single study suggesting blockade in ICH is not beneficial to outcomes in mice (Matsushita et al., 2014) TNF-α has a similar functional role to IL-1β in exacerbating the immune response and offers a relevant target to further understand the role in ICH pathology and repair. Using the zebrafish larval model we could

investigate the effect of inhibiting TNF-α signalling on pathological outcomes to see if there is a reduction in apoptosis and neuroinflammatory activation. Further inhibition of Il-1β in the zebrafish could be explored using a caspase inhibitor, YVAD, to ensure complete inhibition of Il-1β activation without using human recombinant protein. A novelty of the *bbh* larval model is ease of testing combination therapies, as we could introduce compounds to the water and through direct injection. If inhibiting Il-1β in combination with DFO treatment, or TNF-α inhibition in the larval model were successful at modulating the secondary injury response in ICH then this strategy could hold translational promise that has not yet been clinically investigated.

The transgenic leukocyte larvae can be used to identify the live immune response to blood breakdown compounds and inflammatory signals. Live imaging could determine the response to thrombin or heme, and elucidate the specific impact of these blood products. Injecting the animals with thrombin exclusively, we could determine whether it is driving the neuroprotective phenotype in microglial cells in this model (Rohatgi et al., 2004; Striggow et al., 2000).

Future *in vivo* experiments in the zebrafish model may include genetic manipulation and over-expression of proteins ho-1 (*hmox1a*) and ch25h. Over-expression of *hmox1a* may increase the effect of DFO treatment at ameliorating iron load in the brain after ICH and result in better outcomes. If DFO shows a true effect in a genetically distinct sub-population then this holds promise for those specific patients. Controlling expression of *ch25h* in larvae using a macrophage specific promotor and inducible expression using tamoxifen will enable us to modulate cholesterol levels in a temporal manner and we could determine the effect of expression on Il-1β release (Hans et al., 2009). Observing late subacute expression in humans poses the question of whether the role of CH25H is to inhibit the immune response at this late point, or is a result of an increase in cholesterol biosynthesis in recovery. We hypothesise whether *ch25h* over-expression in the zebrafish at a specific, early time point can speed up recovery by inhibiting the immune mediated secondary injury. In tamoxifen treated animals, where ch25h expression is driven, is there less Il-1β release? Does increased ch25h expression in macrophages affect endothelial cells, where loss of cholesterol would impact tight junctions? We could also over-express *hmgcra* globally in the *bbh* zebrafish to effect downstream cholesterol production and subsequent *ch25h* expression. Experimentally, increasing ch25h either by drug treatment or genetic

manipulation could produce more 25-HC for immunosuppression after ICH but it is not clear whether feedback mechanisms would result in increased cholesterol synthesis. In a zebrafish model, cholesterol levels in the larvae can be increased by feeding the parent fish a high cholesterol diet (Progatzky et al., 2014). We could use this model to investigate how cholesterol affects haemorrhage outcomes and frequencies in our *bbh* model as high cholesterol has been shown to be clinically protective (Chang et al., 2018).

In order to determine a mechanistic link between the release of blood products and cholesterol biosynthesis, we could use *in vitro* cultures of human endothelial, leukocyte or neuronal cells. By addition of blood break down products to these cultures, we may be able to determine which contribute to the dysregulation of cholesterol biosynthesis. We could also investigate CH25H over-expression by transfecting these *in vitro* leukocyte cultures to determine the impact on release of pro-inflammatory factors.

Realistically, to bypass the rodent models and progress the outcomes of our drug screen straight into clinical trial, we will require more evidence beyond the zebrafish model. If we could identify drug target pathways in zebrafish and confirm that they are dysregulated in human ICH tissue samples it would provide translational validity to our study. Next steps include proving that initial target drugs of interest show beneficial outcomes on locomotion and neuroinflammation in the zebrafish larvae in addition to preventing brain cell death. These results then need to be replicated in much larger groups of animals. Efficacy in mammals may need to be confirmed in a single rodent study (Paul et al., 2008b). Following the pre-clinical work, we need to prove a translational lead from clinical data. Previously published RNASeq data from studies of patient blood samples offer pre-existing databases to draw comparisons with interesting targets (Sang et al., 2017). Likewise, using human post mortem tissue will further allow us to analyse the links between humans and zebrafish. Many drugs identified thus far in our screen have already been approved by the MHRA and therefore could bypass phase I trials (appendix x).

7.7 The future of pre-clinical ICH research

With regards to the wider research field, pre-clinical ICH research is, in comparison to ischemic stroke, understudied and underfunded (NINDS ICH Workshop

Participants, 2005). Haemorrhagic stroke subtypes are very different from each other in causation and pathology, however are often grouped together in pre-clinical research. The blanket term ‘stroke’ implies that ischemia and haemorrhage are more similar than reality (Gorelick, 2019). Ischemic strokes are more prevalent in Western, developed countries, where most of the money for research funding is directed, meaning that the true global burden of ICH is overlooked. All subtypes of stroke have common lifestyle risk factors however as more research into blood lipids develop it may become apparent that there are unique differences (Ma et al., 2016).

Medications and therapies that are trialled for ICH have often been previously trialled for ischemia as it is easier to model pre-clinically, for example blood pressure lowering (Ahmed et al., 2009), IL-1Ra administration, and tissue plasminogen activator (tPA) for thrombolysis of the haematoma. Clinical trials have suggested that prevention of HE (FAST) (Mayer et al., 2008), removing the haematoma (STITCH and MISTIE) (Hanley et al., 2019; Mendelow et al., 2013) and blood pressure lowing (ADAPT) (Butcher et al., 2013) are successful in improving patient recovery following ICH. None of these interventions have shown efficacy in large scale trials and so have not been approved for use. There has been no clinical investigation thus far into combination therapies; surgical strategies and medical therapies together. Following minimally invasive haematoma evacuation, can we fill the haematoma cavity? Should it be filled or should the tissue be allowed space to close the gap to rebuild connections? Some pre-clinical studies suggest injectable hydrogel scaffolds stimulate endogenous stem cell migration for CNS repair increase healing after ICH (Lim et al., 2019). Utilising the cavity left after surgical haematoma extraction may be a way to administer any anti-inflammatory, iron chelating drugs directly to the brain cells, bypassing the BBB obstruction. These therapeutic options are unique to ICH condition and offer exciting advances for future pre-clinical research.

Pre-clinical ICH work could benefit from distancing from ischemic stroke research groups, for unique funding opportunities and different perspectives (Selim et al., 2018). Therefore the zebrafish larval model of ICH offers a unique approach to understanding disease in a new organism. The development of this model has addressed the pre-clinical need for a spontaneous ICH with clinically relevant haemorrhage sizes and offers the potential to investigate genetic causes and comorbidities (Selim et al., 2018). We have been able to identify drug candidates,

separately from ischemic stroke research that hold potential for specific treatments for ICH patients.

7.8 Conclusion

In conclusion, a new pre-clinical model of ICH in zebrafish larvae offers many advantages over traditional rodent models, and can provide novel insight into an urgent field of medical research. We ultimately aim to encourage the wide spread use of our model for a powerful, more ethical alternative for pre-clinical ICH investigation.

Appendices

i. Macro for cell death analysis

```
outputFolder = getDirectory("image")
Imagetitle = getTitle;
run("Split Channels");
selectWindow(Imagetitle+" (blue)");
close();
selectWindow(Imagetitle+" (red)");
close();
selectWindow(Imagetitle+" (green)");
//run("Threshold...");
setAutoThreshold("Default dark");
setThreshold(0, 120);
run("Measure");
selectWindow("Results");
saveAs("Measurements", "" + outputFolder + Imagetitle
+"Background.xls");
selectWindow(Imagetitle+" (green)");
//run("Threshold...");
setAutoThreshold("Default");
setThreshold(120, 255);
run("Analyze Particles...", "size=30-10000 show=[Overlay Masks] display");
selectWindow ("Results");
saveAs("Measurements", "" + outputFolder + Imagetitle +".xls");
selectWindow(Imagetitle+" (green)");
close();
```

ii. *Ch25h* primer design

cDNA

AGCAGGCGGCGGTGTTTAGCTATCTAACTATTCCCCTATCATTTTCATAATTGTTGTTCT
AGAAACAGTACACCAACGGACGTGAACATGACACACAGGCACACACACACACAAAATACT
AAACCATATTTTACCAGATTAATTATTATTTTGCCATGTTTACAAAATATAAAAGTGTGA
AATATCAATAAAGTAGCATTTATGCAGGATTGACAGATCCAGCTCGCAGATAATCACTCG
CAGTGTCATCACTAACTTTAAGTTCGTTAACAAGTTCTGATTTTACATTACTCTTCTTTG
TCGTATGTTTTGTCACTATGTCCACGTGTTGATTCAATACCTCCATCTTCTTTGGGAGTT
GAATCTTAATAGACTAAACCATTTTCAGTCTTTTTCGATATTACGTTATTTTTATATTTA
ATATGATCTAAAGTTTATAATCACCTATCTGATTATTCTAACATCCTCTGTGAGGTCACG
CACGCACACTACGTCGAGATATCCTGGAAATTCCAACAGGAAGAGCCATTTAGGGCAAGG
CATCAAGAGTAAGAGGCGGGACTTATTGCTTTATAAGGGCTTGAGAAAGCACCATGTGCC
ATCATTCAGATTTAGAACTGAAAAGAAATAGAAATGTTTGGACTACAGCACATCTGGGAC
TGCATTCTGCAGTACGAAGCACAGCTAAGGTCTCCATTTTTCCCAGTCCTCTTCTCAATT
ACAGTCTACCTAAGCTTCTGCCTGCCTTTTGTCCTTCTGGATGCCCTGTCTCCAAAGGTA
GAACTGATAAGGAGATACAAGATCCAACAGAAAGCCAGCGTGTCTTGGACTATGATGTGG
AGCTGCCTCGCACTCTCCCTCTACAACCACGTGGTGTACATCTTCCCGCTGAGTGTCCTG
CACTGGTACTGGAGACCTGTCAGCTACCTAGCGGAGGCACCTGGGGTCTTGCGGGTCGTC
TGGGATCTTGCTGCCTGCCTGCTTCTGTTTGACTTCCAGTACTTTGTGTGGCATCTTCTA
CATCACAAAGTGCCTTGGCTTTACCGGACTTTCCATAAGGTGCACCACAAATACACATCC
ACCTTCGCTCTGGCCACTGAGTACTCTGGGGCTTGGGAGACCCTGTCTTTGGGGTTCTTC
GCTGCGGTGAATCCCATGTTGCTTGGGGTTCATCCTATGACAGAGATGCTCTTCCACATG
CTGAACATGTGGCTGTCAGTTGAGGACCATTGTGGCTATGACCTGCCATGGGCCACGCAC
AGACTGATGCCTTTTGGACTTTACGGAGGAGCTCCACACCATGATGTCCACCATCAGAAG
TTCAAGTCCAACTACGCTCCATACTTCACTCACTGGGACAAGCTCTTTGGGACACTGCAC
TTTGAATGAACAGAACATTTGAAACAGACTCTTTTTTTTGTAAAAAGTTCTTTCTCATTC

TGTGAATGAATACCTTTGACTCTAAAACTTTATAAAAGATTATTTATAATTCAGATCTGT
TTGACCAATTTGTCTATTTATTGAGTGTCTGTATTTAAGAGTGACTGTAAAAACTGAGAT
GTAAGAAATGTATTATGTTAATCATATTATATTTATTATTTATAAGATTGTTGTTTTGCA
TTTATAAGTTTGTGTTGTTGTTATTACTAAATGTATTAACGTGGACCATGAAGAAATTCA
ACAAGCTAATTGCAATAAATCTGTGAAGTAGATAATATAAATACAGTGTCTGTGGTTACT
TTCTTTTGCATAATATGATAATTAGAATTGAATAAAAATGCTAACTATTTAGAGCTAGAT
ATGTTTTATGAATTAAATTTCATGAATGAAGTGATTCAGAGGTCTTAGCTAAAATAACTG
AACTTTAAATAACCTATATTAATAAGTTGTAGTTTTAAGGCTTTTTTAAAAAAAATAAAA
TTGACTAATTTAATATGCAGTTGAAGTCAAAATTAATAGCCCTACTGTGATTTTTTTATA
TGTATATATATATATTTCCAATAGAGCAAGAAATTGTTCACTGTATGTCCAATAATTTTT
TTTCTTAAGAGGGAAAGTCTTAATTGTTTTGTTCTGGCTAGAATAAAAGCAGTTTCTTAT
TAATATAAGAAAATATATAATATAATATAAAAACTATTATATATATATATATATATATAT
ATATATATATATATATATATATATATATATATATATATATATATATATATATATATATAT
ATATATATATATATAATTTATTTATAATTTCTGTTTGACGGAGAGCTGATTTTTTTCAAC
ACATTTTTAAACATAATAGTTTTAATTACTCATTCCTAATA

Forward primer

GCATGGATCCATGTTTGGACTACAGCACATCT

1. No blast hits on any other genes (blast.ncbi.nlm.nih.gov)
2. GC content = 53.1% (www.idtdna.com/calc/analyzer)
3. Tm = 65.8 ºC (www.idtdna.com/calc/analyzer)
4. Hairpin melts at 45 DeltaG is -1.79 (likeliness of formation) (www.idtdna.com/calc/analyzer)
5. Restriction site added for BamH1 (http://www.labtools.us/nebcutter-v2-0/) (https://en.wikipedia.org/wiki/BamHI)

Reverse primer

GGCCGAATTCTCATTCAAAGTGCAGTGTCC

1. No blast hits on any other genes (blast.ncbi.nlm.nih.gov)
2. GC = 50% (www.idtdna.com/calc/analyzer)
3. Tm = 62.7 ºC (www.idtdna.com/calc/analyzer)
4. Restriction site added for EcoR1 (http://www.labtools.us/nebcutter-v2-0/) (en.wikipedia.org/wiki/EcoRI)

Probe size = 776bp

iii. Macro for filipin analysis

```
outputFolder = getDirectory("image")
Imagetitle = getTitle;
run("Split Channels");
selectWindow(Imagetitle+" (green)");
close();
selectWindow(Imagetitle+" (red)");
close();
selectWindow(Imagetitle+" (blue)");
//run("Threshold...");
setAutoThreshold("Default");
setThreshold(0, 53);
run("Measure");
```

```
selectWindow("Results");
saveAs("Measurements", ""+ outputFolder + Imagetitle
+"Background.xls");
selectWindow(Imagetitle+" (blue)");
//run("Threshold...");
setAutoThreshold("Default dark");
setThreshold(54, 255);
run("Measure");
saveAs("Measurements", ""+ outputFolder + Imagetitle
+".xls");
selectWindow(Imagetitle+" (blue)");
close();
```

iv. Supplementary video information for Crilly et al 2018 (digital)

v. IMARIS 3D rendering of haematoma (digital)

vi. IMARIS 3D rendering of cell death region of interest (digital)

vii. Additional images for comparison of adult zebrafish brains

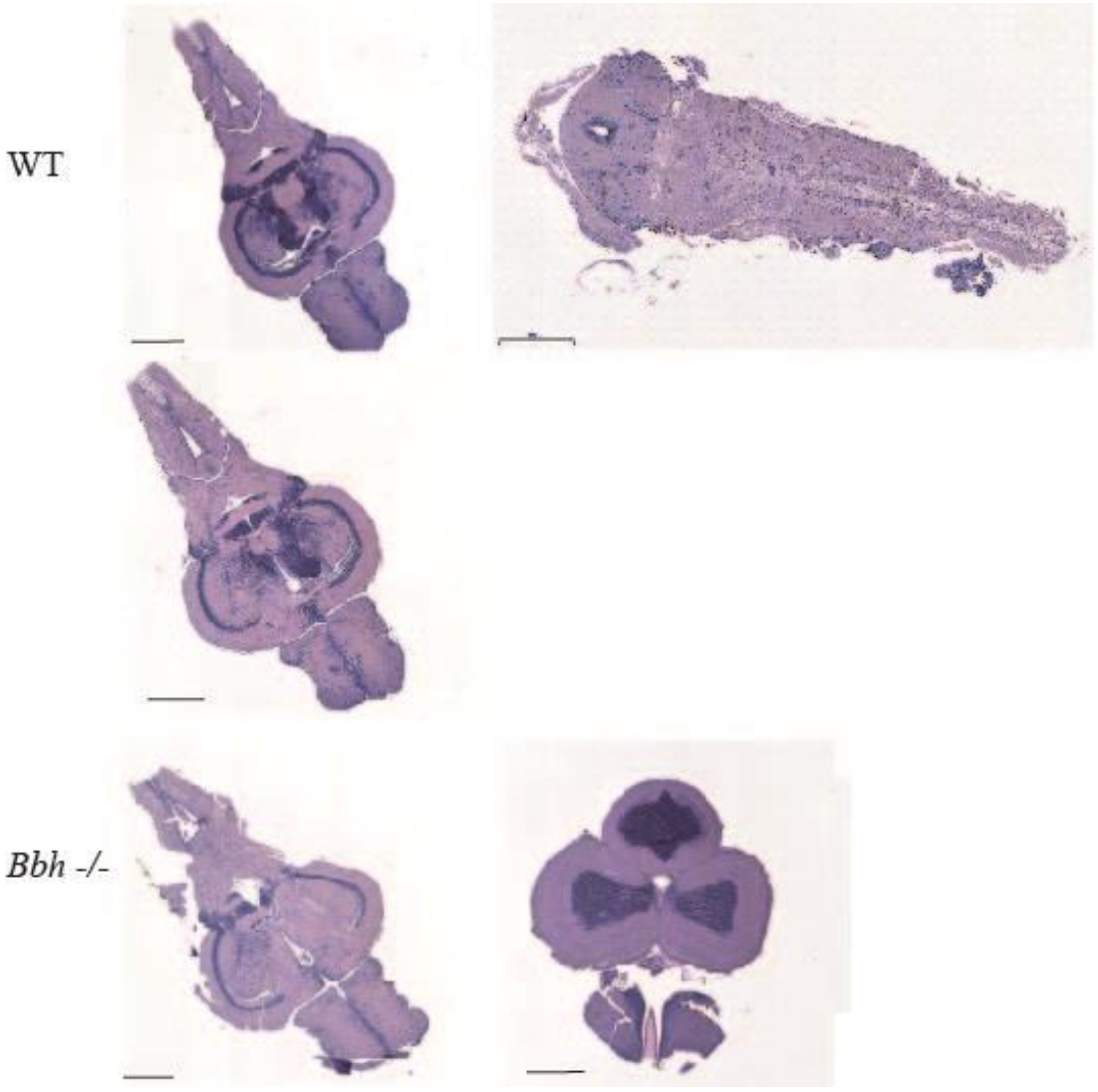

Further examples of the H and E staining from adult zebrafish brains, from WT and *bbh* ICH+ homozygotes. All images were analysed for morphological differences associated with ICH injury however, none were observed. Representative images presented in Chapter 4. Scale bar 500µm.

viii. Statistical analysis of IL-1Ra treatment motility assay

Motility data from IL-1Ra treatment and was analysed using a multi linear model on R as Graphpad Prism 7.0 fails to accommodate missing values from repeated measures or the random effect of clutch (Bates et al., 2015; R Core Team, 2018). There are two independent factor variables; Haemorrhage and Treatment, and one random variable Clutch (or experimental repeat), with motility being the dependent variable. Homoskedascity and normality of data was evaluated graphically using a residual vs fitted plot and a normal Q-Q plot showing that the parametric assumptions were met, the data fit the model, and no transformation was needed. Multi linear model analysis showed a significant main effect of

haemorrhage (ChiSq p=0.009) but no main effect of drug treatment (ChiSq p=0.961) or of treatment in haemorrhaged groups (ChiSq p=0.128).

```
#Models:
lme1: motility ~ 1 + (1 | clutch)
lme2: motility ~ (1 | clutch) + haemorrhage
lme3: motility ~ (1 | clutch) + haemorrhage + treatment
lme4: motility ~ (1 | clutch) + haemorrhage + treatment + haemorr
hage:treatment
     Df    AIC    BIC  logLik deviance  Chisq Chi Df Pr(>Chisq)
lme1  3 3945.0 3956.1 -1969.5   3939.0
lme2  4 3940.1 3955.0 -1966.0   3932.1 6.8729      1   0.008751 *
*
lme3  5 3942.1 3960.7 -1966.0   3932.1 0.0024      1   0.960937
lme4  6 3941.8 3964.1 -1964.9   3929.8 2.3183      1   0.127857
---
Signif. codes:  0 ‘***’ 0.001 ‘**’ 0.01 ‘*’ 0.05 ‘.’ 0.1 ‘ ’ 1


#Assumption check
plot(lme4)
```

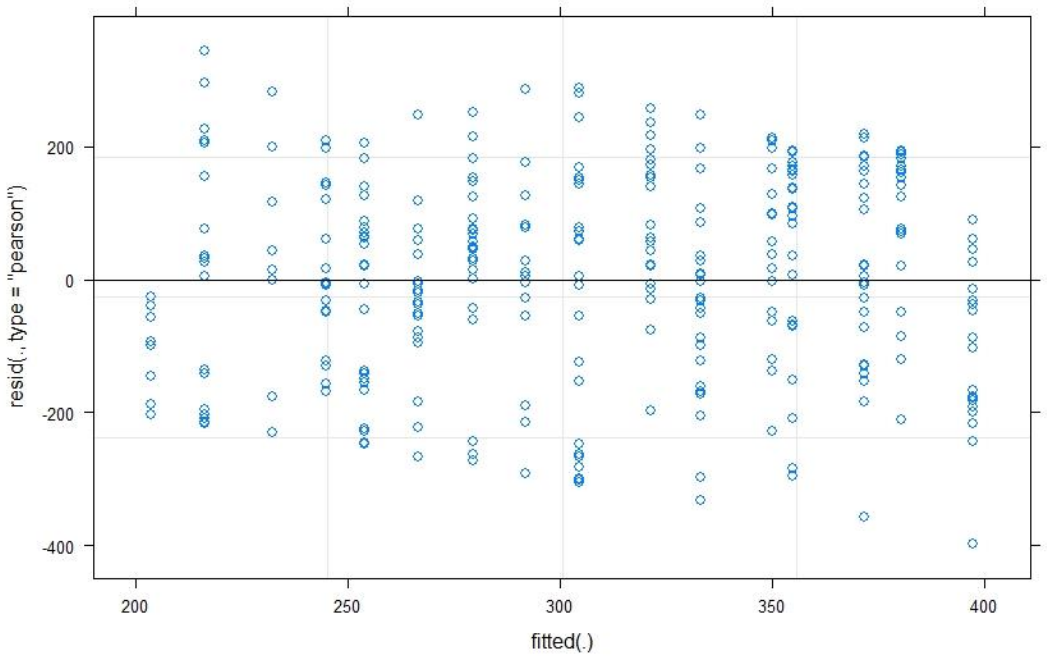


```
qqnorm(resid(lme4))
```

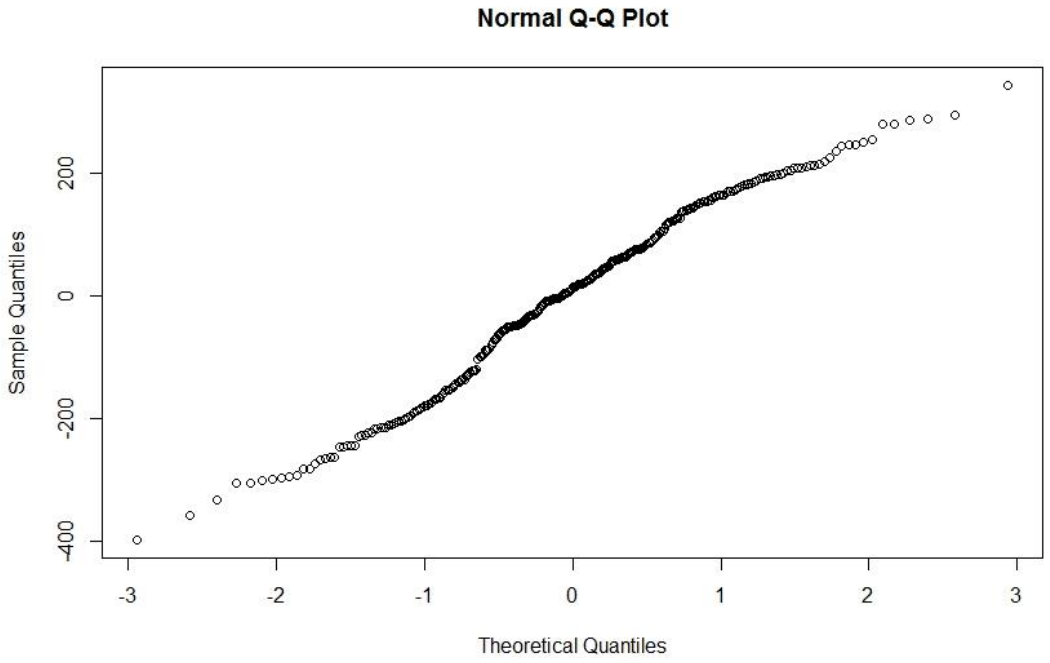

ix. Statistical analysis of DFO treatment cell death outcomes

Data from DFO IL-1Ra treatment was analysed using a multi linear model on R as Graphpad Prism 7.0 fails to accommodate missing values from repeated measures or the random effect of clutch (R Core Team, 2018) (Bates et al., 2015). There are two independent factor variables; Haemorrhage and Treatment, and one random variable Clutch (or experimental repeat), with fluorescence being the dependent variable. Homoskedascity and normality of data was evaluated graphically using a residual vs fitted plot and a normal Q-Q plot showing that the parametric assumptions were met, the data fit the model, and no transformation was needed. Multi linear model analysis showed a significant main effect of haemorrhage (ChiSq $p<0.0001$) but no main effect of drug treatment (ChiSq $p=0.8520$) or of treatment in haemorrhaged groups (ChiSq $p=0.6383$).

```
#Models:
lme1: fluor ~ 1 + (1 | clutch)
lme2: fluor ~ (1 | clutch) + treatment
lme3: fluor ~ (1 | clutch) + treatment + haemorrhage
lme4: fluor ~ (1 | clutch) + treatment + haemorrhage + treatment:
haemorrhage
     Df    AIC    BIC  logLik deviance   Chisq Chi Df Pr(>Chisq)
lme1  3 3752.1 3761.6 -1873.0   3746.1
lme2  6 3757.3 3776.3 -1872.6   3745.3  0.7893      3     0.8520
lme3  7 3730.4 3752.6 -1858.2   3716.4 28.9080      1   7.59e-08
***
lme4 10 3734.7 3766.4 -1857.3   3714.7  1.6938      3     0.6383
---
Signif. codes:  0 ‘***’ 0.001 ‘**’ 0.01 ‘*’ 0.05 ‘.’ 0.1 ‘ ’ 1

#Assumption check
plot(lme4)
```

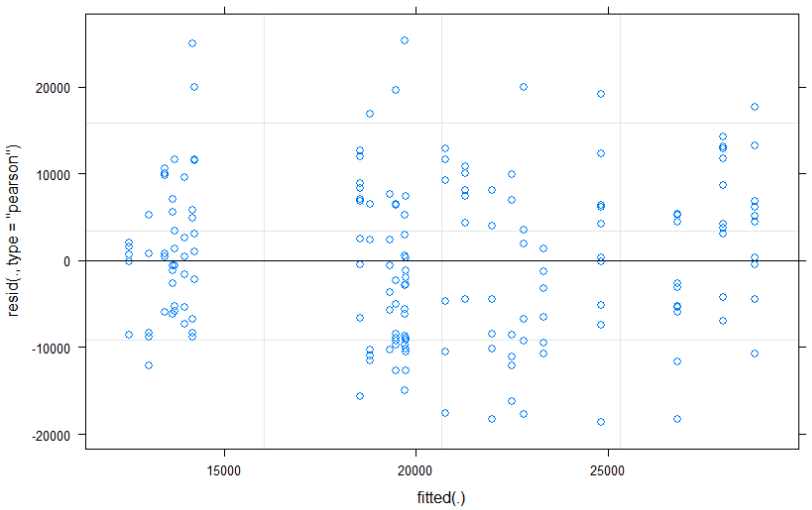


```
qqnorm(resid(lme4))
```

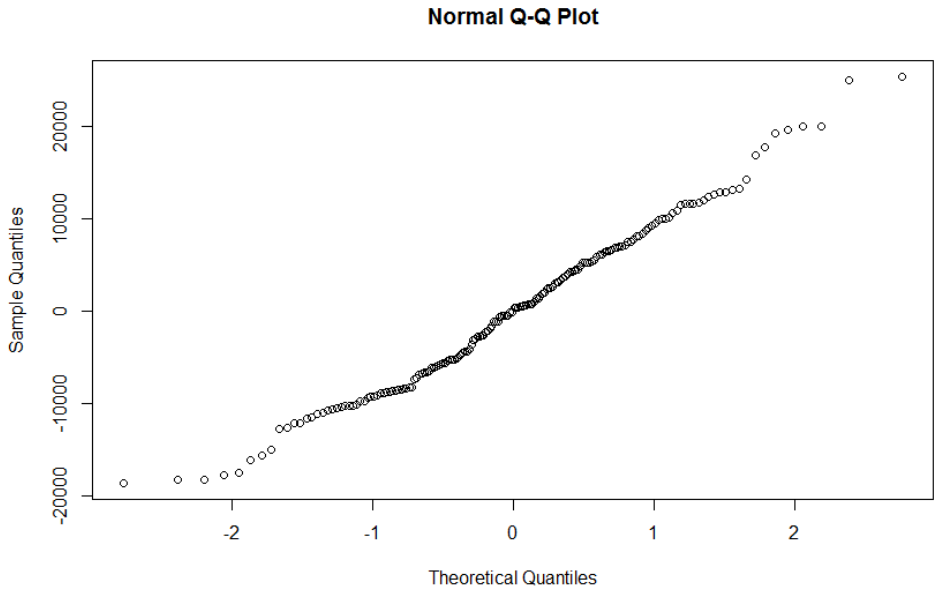

x. Outcomes for initial drug screen analysis

Drug Name	Formula	MolWt (g/mol)	Bioactivity	1st cell death assay	2nd cell death assay
Naphazoline hydrochloride	$C_{14}H_{15}ClN_2$	246.74	adrenergic agonist, nasal decongestant	VERY ACTIVE, OEDEMA	OEDEMA
Norepinephrine	$C_8H_{11}NO_3$	169.18	adrenergic agonist, antihypotensive	OEDEMA	OEDEMA
Orphenadrine citrate	$C_{24}H_{31}NO_8$	461.52	muscle relaxant (skeletal), antihistaminic	OEDEMA	OEDEMA
Phthalylsulfathiazole	$C_{17}H_{13}N_3O_5S_2$	403.44	antibacterial		
Oxolinic acid	$C_{13}H_{11}NO_5$	261.24	antibacterial		
Niacinamide	$C_6H_6N_2O$	122.13	Vitamin B3; enzyme cofactor; anti-pellagra		
Clomipramine hydrochloride	$C_{19}H_{24}Cl_2N_2$	351.32	antidepressant	1/3 CELL DEATH	

Trimethobenzamide hydrochloride	$C_{21}H_{29}ClN_2O_5$	424.93	antiemetic		
Gluconolactone	$C_6H_{10}O_6$	178.14	chelating agent	OEDEMA	
Aminolevulinic acid hydrochloride	$C_5H_{10}ClNO_3$	167.60	antineoplastic		
Levalbuterol hydrochloride	$C_{13}H_{22}ClNO_3$	275.78	bronchodilator, tocolytic	OEDEMA	
Sparteine sulfate	$C_{15}H_{28}N_2O_4S$	332.47	oxytocic		
Testosterone propionate	$C_{22}H_{32}O_3$	344.50	androgen, antineoplastic		
Testosterone	$C_{19}H_{28}O_2$	288.43	androgen, antineoplastic		
Sanguinarine sulfate	$C_{20}H_{15}NO_8S$	429.41	antineoplastic, antiplaque agent		
Mitomycin C	$C_{15}H_{18}N_4O_5$	334.33	antineoplastic	OEDEMA	
Temefos	$C_{16}H_{20}O_6P_2S_3$	466.47	insecticide	OEDEMA	
Chlorpromazine	$C_{17}H_{19}ClN_2S$	318.87	antiemetic, antipsychotic		1/5 CELL DEATH
Clidinium bromide	$C_{22}H_{26}BrNO_3$	432.36	anticholinergic	OEDEMA	OEDEMA
Clonidine hydrochloride	$C_9H_{10}Cl_3N_3$	266.56	antihypertensive		
Cortisone acetate	$C_{23}H_{30}O_6$	402.49	glucocorticoid	OEDEMA	
Daunorubicin	$C_{27}H_{29}NO_{10}$	527.53	antineoplastic	OEDEMA	OEDEMA
Deferoxamine mesylate	$C_{26}H_{52}N_6O_{11}S$	656.80	chelating agent (Fe & Al)		MILD HEART OEDEMA
Digoxin	$C_{41}H_{64}O_{14}$	780.96	cardiac stimulant	OEDEMA	
Disopyramide phosphate	$C_{21}H_{32}N_3O_5P$	437.48	antiarrhythmic	OEDEMA	
Adrenaline bitartrate	$C_{13}H_{19}NO_9$	333.30	adrenergic agonist, bronchodilator, antiglaucoma agent	OEDEMA	1/5 CELL DEATH
Gentamicin sulfate	$C_{21}H_{45}N_5O_{11}S$	575.68	antibacterial		
Halazone	$C_7H_5Cl_2NO_4S$	270.09	Anti-infectant	OEDEMA	
Homatropine bromide	$C_{16}H_{22}BrNO_3$	356.26	anticholinergic (opthalmic)		
Lincomycin hydrochloride	$C_{18}H_{35}ClN_2O_6S$	443.01	antibacterial	OEDEMA	
Nitrofurazone	$C_6H_6N_4O_4$	198.14	Anti-infectant (topical)	OEDEMA	1/5 CELL DEATH
Oxidopamine hydrochloride	$C_8H_{12}ClNO_3$	205.64	adrenergic agonist (opthalmic)	OEDEMA	1/5 CELL DEATH

xi. Author publications (digital)

References

Abbott, N. J. (2000). 'Inflammatory mediators and modulation of blood–brain barrier permeability', *Cellular and molecular neurobiology*, 20(2), pp. 131-147.

Abeles, A. M. & Pillinger, M. H. (2006). 'Statins as antiinflammatory and immunomodulatory agents: a future in rheumatologic therapy?', *Arthritis & Rheumatology*, 54(2), pp. 393-407.

Abid, K. A., Sobowale, O. A., Parkes, L. M., Naish, J., Parker, G. J., du Plessis, D., Brough, D., Barrington, J., Allan, S. M. & Hinz, R. (2018). 'Assessing Inflammation in Acute Intracerebral Hemorrhage with Pk11195 Pet and Dynamic Contrast-enhanced Mri', *Journal of Neuroimaging*, 28(2), pp. 158-161.

Abraham, M. K. & Chang, W.-T. W. (2016). 'Subarachnoid hemorrhage', *Journal of Emergency Medicine Clinics*, 34(4), pp. 901-916.

Ahmed, N., Wahlgren, N., Brainin, M., Castillo, J., Ford, G. A., Kaste, M., Lees, K. R. & Toni, D. (2009). 'Relationship of blood pressure, antihypertensive therapy, and outcome in ischemic stroke treated with intravenous thrombolysis: retrospective analysis from Safe Implementation of Thrombolysis in Stroke–International Stroke Thrombolysis Register (SITS-ISTR)', *Stroke*, 40(7), pp. 2442-2449.

Ahrens, M. B., Orger, M. B., Robson, D. N., Li, J. M. & Keller, P. J. (2013). 'Whole-brain functional imaging at cellular resolution using light-sheet microscopy', *Nature methods*, 10(5), pp. 413-420.

Alharbi, B. M., Tso, M. K. & Macdonald, R. L. (2016). 'Animal models of spontaneous intracerebral hemorrhage', *Journal of Neurological Research*, 38(5), pp. 448-455.

An, S. J., Kim, T. J. & Yoon, B.-W. (2017). 'Epidemiology, risk factors, and clinical features of intracerebral hemorrhage: an update', *Journal of stroke*, 19(1), p. 3.

Andaluz, N., Zuccarello, M. & Wagner, K. R. (2002). 'Experimental animal models of intracerebral hemorrhage', *Neurosurgery Clinics of North America*, 13(3), pp. 385-393.

Anderson, C. S., Heeley, E., Huang, Y., Wang, J., Stapf, C., Delcourt, C., Lindley, R., Robinson, T., Lavados, P. & Neal, B. (2013). 'Rapid blood-pressure lowering in patients with acute intracerebral hemorrhage', *New England Journal of Medicine*, 368(25), pp. 2355-2365.

Arend, W. P. (1990). 'Interleukin-1 receptor antagonist: discovery, structure and properties', *Progress in growth factor research*, 2(4), pp. 193-205.

Aronowski, J. & Zhao, X. (2011). 'Molecular pathophysiology of cerebral hemorrhage: secondary brain injury', *Stroke*, p. 110.596718.

Ashikawa, Y., Nishimura, Y., Okabe, S., Sasagawa, S., Murakami, S., Yuge, M., Kawaguchi, K., Kawase, R. & Tanaka, T. (2016). 'Activation of sterol regulatory element binding factors by fenofibrate and gemfibrozil stimulates myelination in zebrafish', *Frontiers in pharmacology*, 7, p. 206.

ASPA (1986 amendments 2012). *Animals (Scientific Procedures) Act 1986*. Available at: http://www.legislation.gov.uk/ukpga/1986/14/contents.

Ayerbe, L., Ayis, S. A., Crichton, S., Rudd, A. G. & Wolfe, C. D. (2015). 'Explanatory factors for the association between depression and long-term physical disability after stroke', *Age and ageing*, 44(6), pp. 1054-1058.

Badea, A., Ali-Sharief, A. & Johnson, G. A. (2007). 'Morphometric analysis of the C57BL/6J mouse brain', *Neuroimage*, 37(3), pp. 683-693.

Bakheit, A., Shaw, S., Barrett, L., Wood, J., Carrington, S., Griffiths, S., Searle, K. & Koutsi, F. (2007). 'A prospective, randomized, parallel group, controlled study of the effect of intensity of speech and language therapy on early recovery from poststroke aphasia', *Clinical Rehabilitation*, 21(10), pp. 885-894.

Bates, D., Mächler, M., Bolker, B. & Walker, S. (2015). Fitting Linear Mixed-Effects Models using lme4, 1–51. Computation.

Becker, T., Wullimann, M. F., Becker, C. G., Bernhardt, R. R. & Schachner, M. (1997). 'Axonal regrowth after spinal cord transection in adult zebrafish', *Journal of Comparative Neurology*, 377(4), pp. 577-595.

Belayev, L., Saul, I., Curbelo, K., Busto, R., Belayev, A., Zhang, Y., Riyamongkol, P., Zhao, W. & Ginsberg, M. D. (2003). 'Experimental intracerebral hemorrhage in the mouse: histological, behavioral, and hemodynamic characterization of a double-injection model', *Stroke,* 34(9), pp. 2221-2227.

Berg, J., Tymoczko, J. & Stryer, L. J. B. (2002). 'The complex regulation of cholesterol biosynthesis takes place at several levels', 5.

Bertram, L. & Tanzi, R. E. (2008). 'Thirty years of Alzheimer's disease genetics: the implications of systematic meta-analyses', *Nature Reviews Neuroscience,* 9(10), p. 768.

Best, J. & Alderton, W. K. (2008). 'Zebrafish: An in vivo model for the study of neurological diseases', *Neuropsychiatric disease and treatment,* 4(3), p. 567.

Beyaert, R. & Fiers, W. (1994). 'Molecular mechanisms of tumor necrosis factor-induced cytotoxicity: what we do understand and what we do not', *FEBS letters,* 340(1-2), pp. 9-16.

Björkhem, I. & Meaney, S. (2004). 'Brain cholesterol: long secret life behind a barrier', *Arteriosclerosis, thrombosis, vascular biology,* 24(5), pp. 806-815.

Blanc, M., Hsieh, W. Y., Robertson, K. A., Kropp, K. A., Forster, T., Shui, G., Lacaze, P., Watterson, S., Griffiths, S. J. & Spann, N. J. (2013). 'The transcription factor STAT-1 couples macrophage synthesis of 25-hydroxycholesterol to the interferon antiviral response', *Immunity,* 38(1), pp. 106-118.

Bray, N., Burrows, F. E., Jones, M., Berwick, J., Allan, S. M. & Schiessl, I. (2016). 'Decreased haemodynamic response and decoupling of cortical gamma-band activity and tissue oxygen perfusion after striatal interleukin-1 injection', *Journal of neuroinflammation,* 13(1), p. 195.

British Heart Foundation (2017). BHF CVD statistics compendium 2017. BHF London.

Broderick, J. P., Brott, T. G., Duldner, J. E., Tomsick, T. & Huster, G. (1993). 'Volume of intracerebral hemorrhage. A powerful and easy-to-use predictor of 30-day mortality', *Stroke,* 24(7), pp. 987-993.

Brouwers, H. B. & Greenberg, S. M. (2013). 'Hematoma expansion following acute intracerebral hemorrhage', *Cerebrovascular diseases,* 35(3), pp. 195-201.

Bu, D.-x., Griffin, G. & Lichtman, A. H. (2011). 'Mechanisms for the anti-inflammatory effects of statins', *Current opinion in lipidology,* 22(3), pp. 165-170.

Buchner, D. A., Su, F., Yamaoka, J. S., Kamei, M., Shavit, J. A., Barthel, L. K., McGee, B., Amigo, J. D., Kim, S. & Hanosh, A. W. (2007). 'pak2a mutations cause cerebral hemorrhage in redhead zebrafish', *Proceedings of the National Academy of Sciences,* 104(35), pp. 13996-14001.

Buck, M. D., O'sullivan, D. & Pearce, E. L. (2015). 'T cell metabolism drives immunity', *Journal of Experimental Medicine,* 212(9), pp. 1345-1360.

Butcher, K. S., Jeerakathil, T., Hill, M., Demchuk, A. M., Dowlatshahi, D., Coutts, S. B., Gould, B., McCourt, R., Asdaghi, N. & Findlay, J. M. (2013). 'The intracerebral hemorrhage acutely decreasing arterial pressure trial', *Stroke*, 44(3), pp. 620-626.

Button, K. S., Ioannidis, J. P., Mokrysz, C., Nosek, B. A., Flint, J., Robinson, E. S. & Munafò, M. R. (2013). 'Power failure: why small sample size undermines the reliability of neuroscience', *Nature Reviews Neuroscience*, 14(5), p. 365.

Caceres, J. A. & Goldstein, J. N. (2012). 'Intracranial hemorrhage', *Emergency medicine clinics of North America*, 30(3), p. 771.

Campbell, T. & Williams, K. (1998). 'Therapeutic drug monitoring: antiarrhythmic drugs', *British journal of clinical pharmacology*, 46(4), pp. 307-319.

Casals, J. B., Pieri, N. C., Feitosa, M. L., Ercolin, A., Roballo, K., Barreto, R. S., Bressan, F. F., Martins, D. S., Miglino, M. A. & Ambrósio, C. E. (2011). 'The use of animal models for stroke research: a review', *Comparative medicine*, 61(4), pp. 305-313.

Chang, J. J., Katsanos, A. H., Khorchid, Y., Dillard, K., Kerro, A., Burgess, L. G., Goyal, N., Alexandrov, A. W., Alexandrov, A. V. & Tsivgoulis, G. (2018). 'Higher low-density lipoprotein cholesterol levels are associated with decreased mortality in patients with intracerebral hemorrhage', *Atherosclerosis*, 269, pp. 14-20.

Chen, G. Y. & Nuñez, G. (2010). 'Sterile inflammation: sensing and reacting to damage', *Nature Reviews Immunology*, 10(12), p. 826.

Chen, S., Zhao, B., Wang, W., Shi, L., Reis, C. & Zhang, J. (2017). 'Predictors of hematoma expansion predictors after intracerebral hemorrhage', *Oncotarget*, 8(51), p. 89348.

Chen, T.-H., Wang, Y.-H. & Wu, Y.-H. (2011). 'Developmental exposures to ethanol or dimethylsulfoxide at low concentrations alter locomotor activity in larval zebrafish: implications for behavioral toxicity bioassays', *Aquatic toxicology*, 102(3-4), pp. 162-166.

Chen, Y.-W., Li, C.-H., Yang, C.-D., Liu, C.-H., Chen, C.-H., Sheu, J.-J., Lin, S.-K., Chen, A.-C., Chen, P.-K. & Chen, P.-L. (2017). 'Low cholesterol level associated with severity and outcome of spontaneous intracerebral hemorrhage: Results from Taiwan Stroke Registry', *PloS one*, 12(4), p. e0171379.

Chen, Z., Martin, M., Li, Z. & Shyy, J. Y. (2014). 'Endothelial dysfunction: the role of SREBP-induced NLRP3 inflammasome in atherosclerosis', *Current opinion in lipidology*, 25(5), p. 339.

Cherry, J. D., Olschowka, J. A. & O'Banion, M. K. (2014). 'Neuroinflammation and M2 microglia: the good, the bad, and the inflamed', *Journal of neuroinflammation*, 11(1), p. 98.

Clark, R. S., Kochanek, P. M., Schwarz, M. A., Schiding, J. K., Turner, D. S., Chen, M., Carlos, T. M. & Watkins, S. C. (1996). 'Inducible Nitric Oxide Synthase Expression in Cerebrovascular Smooth Muscle and Neutrophils after Traumatic Brain Injury in Immature Rats1', *Pediatric research*, 39(5), p. 784.

Crick, P. J., Griffiths, W. J., Zhang, J., Beibel, M., Abdel-Khalik, J., Kuhle, J., Sailer, A. W. & Wang, Y. (2017). 'Reduced plasma levels of 25-hydroxycholesterol and increased cerebrospinal fluid levels of bile acid precursors in multiple sclerosis patients', *Molecular neurobiology*, 54(10), pp. 8009-8020.

Crilly, S., Njegic, A., Laurie, S. E., Fotiou, E., Hudson, G., Barrington, J., Webb, K., Young, H. L., Badrock, A. P. & Hurlstone, A. (2018). 'Using zebrafish larval

models to study brain injury, locomotor and neuroinflammatory outcomes following intracerebral haemorrhage', *F1000Research*, 7.
Crilly, S., Njegic, A., Parry-Jones, A. R., Allan, S. M. & Kasher, P. R. (2019). 'Using Zebrafish Larvae to Study the Pathological Consequences of Hemorrhagic Stroke', *Jove*, (148), p. e59716.
Cui, H.-J., He, H.-y., Yang, A.-L., Zhou, H.-J., Wang, C., Luo, J.-K., Lin, Y. & Tang, T. (2015). 'Efficacy of deferoxamine in animal models of intracerebral hemorrhage: a systematic review and stratified meta-analysis', *PloS one*, 10(5), p. e0127256.
Cutler, C., Multani, P., Robbins, D., Kim, H. T., Le, T., Hoggatt, J., Pelus, L. M., Desponts, C., Chen, Y.-B. & Rezner, B. (2013). 'Prostaglandin-modulated umbilical cord blood hematopoietic stem cell transplantation', *Blood*, 122(17), pp. 3074-3081.
Dagistan, Y., Kilinc, E. & Nur, B. C. (2019). 'Cervical sympathectomy modulates the neurogenic inflammatory neuropeptides following experimental subarachnoid hemorrhage in rats', *Brain research*, p. 146366.
Dastur, C. K. & Yu, W. (2017). 'Current management of spontaneous intracerebral haemorrhage', *Stroke and v ascular neurology*, 2(1), pp. 21-29.
Davis, J. M. & Ramakrishnan, L. (2009). 'The role of the granuloma in expansion and dissemination of early tuberculous infection', *Cell*, 136(1), pp. 37-49.
DeBose-Boyd, R. A. & Ye, J. (2018). 'SREBPs in lipid metabolism, insulin signaling, and beyond', *Trends in biochemical sciences*, 43(5), pp. 358-368.
Dehouck, B., Fenart, L., Dehouck, M.-P., Pierce, A., Torpier, G. & Cecchelli, R. (1997). 'A new function for the LDL receptor: transcytosis of LDL across the blood–brain barrier', *The Journal of cell biology*, 138(4), pp. 877-889.
Diekmann, H. & Hill, A. (2013). 'ADMETox in zebrafish', *Drug Discovery Today: Disease Models*, 10(1), pp. e31-e35.
Dong, X. (2018). 'Current strategies for brain drug delivery', *Theranostics*, 8(6), p. 1481.
Donovan, F. M., Pike, C. J., Cotman, C. W. & Cunningham, D. D. (1997). 'Thrombin induces apoptosis in cultured neurons and astrocytes via a pathway requiring tyrosine kinase and RhoA activities', *Journal of Neuroscience*, 17(14), pp. 5316-5326.
Easter Jr, S. S. & Nicola, G. N. (1996). 'The development of vision in the zebrafish (Danio rerio)', *Developmental biology*, 180(2), pp. 646-663.
Edison, R. J., Berg, K., Remaley, A., Kelley, R., Rotimi, C., Stevenson, R. E. & Muenke, M. (2007). 'Adverse birth outcome among mothers with low serum cholesterol', *Pediatrics*, 120(4), pp. 723-733.
Eisa-Beygi, S., Hatch, G., Noble, S., Ekker, M. & Moon, T. W. (2013). 'The 3-hydroxy-3-methylglutaryl-CoA reductase (HMGCR) pathway regulates developmental cerebral-vascular stability via prenylation-dependent signalling pathway', *Developmental biology*, 373(2), pp. 258-266.
Eisa-Beygi, S. & Rezaei, M. (2016). 'Etiology of intracerebral hemorrhage (ICH): novel insights from Zebrafish embryos', *International Journal of Developmental Biology*, 60(4-5-6), pp. 119-126.
Elfenbein, H., Rosen, R., Stephens, S., Switzer, R., Smith, Y., Pare, J., Mehta, P., Warzok, R. & Walker, L. (2007). 'Cerebral alpha-amyloid angiopathy in aged squirrel monkeys', *Histol Histopathol*, 22, pp. 155-167.
Elisia, I., Nakamura, H., Lam, V., Hofs, E., Cederberg, R., Cait, J., Hughes, M. R., Lee, L., Jia, W. & Adomat, H. H. (2016). 'DMSO represses inflammatory

cytokine production from human blood cells and reduces autoimmune arthritis', *PLoS One*, 11(3), p. e0152538.

Ellenbroek, B. & Youn, J. (2016). 'Rodent models in neuroscience research: is it a rat race?', *Disease models & mechanisms*, 9(10), pp. 1079-1087.

Ellett, F., Pase, L., Hayman, J. W., Andrianopoulos, A. & Lieschke, G. J. (2011). 'mpeg1 promoter transgenes direct macrophage-lineage expression in zebrafish', *Blood*, 117(4), pp. e49-e56.

Espín, R., Roca, F. J., Candel, S., Sepulcre, M. P., González-Rosa, J. M., Alcaraz-Pérez, F., Meseguer, J., Cayuela, M. L., Mercader, N. & Mulero, V. (2013). 'TNF receptors regulate vascular homeostasis in zebrafish through a caspase-8, caspase-2 and P53 apoptotic program that bypasses caspase-3', *Disease models and mechanisms*, 6(2), pp. 383-396.

Essayan, D. M., Fox, C. C., Levi-Schaffer, F., Alam, R. & Rosenwasser, L. J. (1998). 'Biologic activities of IL-1 and its role in human disease', *Journal of allergy and clinical immunology*, 102(3), pp. 344-350.

Fang, H., Wang, P.-F., Zhou, Y., Wang, Y.-C. & Yang, Q.-W. (2013). 'Toll-like receptor 4 signaling in intracerebral hemorrhage-induced inflammation and injury', *Journal of neuroinflammation*, 10(1), p. 794.

Feigin, V. L., Forouzanfar, M. H., Krishnamurthi, R., Mensah, G. A., Connor, M., Bennett, D. A., Moran, A. E., Sacco, R. L., Anderson, L. & Truelsen, T. (2014). 'Global and regional burden of stroke during 1990–2010: findings from the Global Burden of Disease Study 2010', *The Lancet*, 383(9913), pp. 245-255.

Finnie, J. (2016). 'Forensic pathology of traumatic brain injury', *Veterinary pathology*, 53(5), pp. 962-978.

Fisher, M., Vasilevko, V., Passos, G. F., Ventura, C., Quiring, D. & Cribbs, D. H. (2011). 'Therapeutic modulation of cerebral microhemorrhage in a mouse model of cerebral amyloid angiopathy', *Stroke*, 42(11), pp. 3300-3303.

Fluri, F., Schuhmann, M. K. & Kleinschnitz, C. (2015). 'Animal models of ischemic stroke and their application in clinical research', *Drug design, development and therapy*, 9, p. 3445.

Fontana, B. D., Mezzomo, N. J., Kalueff, A. V. & Rosemberg, D. B. (2017). 'The developing utility of zebrafish models of neurological and neuropsychiatric disorders: A critical review', *Experimental neurology*.

Fournier, D. A., Skaug, H. J., Ancheta, J., Ianelli, J., Magnusson, A., Maunder, M. N., Nielsen, A. & Sibert, J. (2012). 'AD Model Builder: using automatic differentiation for statistical inference of highly parameterized complex nonlinear models', *Optimization Methods and Software*, 27(2), pp. 233-249.

Fraher, D., Sanigorski, A., Mellett, N. A., Meikle, P. J., Sinclair, A. J. & Gibert, Y. (2016). 'Zebrafish embryonic lipidomic analysis reveals that the yolk cell is metabolically active in processing lipid', *Cell reports*, 14(6), pp. 1317-1329.

Fuh, L., Sin, J. H., Goldstein, J. N. & Hayes, B. D. (2017). Reversal of oral anticoagulants for intracerebral hemorrhage patients: best strategies. *In:* Seminars in respiratory and critical care medicine, 2017. Thieme Medical Publishers. pp. 726-736.

Galea, J., Ogungbenro, K., Hulme, S., Patel, H., Scarth, S., Hoadley, M., Illingworth, K., McMahon, C. J., Tzerakis, N. & King, A. T. (2017). 'Reduction of inflammation after administration of interleukin-1 receptor antagonist following aneurysmal subarachnoid hemorrhage: results of the subcutaneous interleukin-1Ra in SAH (SCIL-SAH) study', *Journal of neurosurgery*, pp. 1-9.

Ganeshan, K. & Chawla, A. (2014). 'Metabolic regulation of immune responses', *Annual review of immunology*, 32, pp. 609-634.
Garg, R. K., Liebling, S. M., Maas, M. B., Nemeth, A. J., Russell, E. J. & Naidech, A. M. (2012). 'Blood pressure reduction, decreased diffusion on MRI, and outcomes after intracerebral hemorrhage', *Stroke*, 43(1), pp. 67-71.
Garton, T., Keep, R. F., Hua, Y. & Xi, G. (2016). 'Brain iron overload following intracranial haemorrhage', *Stroke and vascular neurology*, 1(4), pp. 172-184.
Ghosh, S. & Hui, S. P. (2018). 'Axonal regeneration in zebrafish spinal cord', *Regeneration*, 5(1), pp. 43-60.
Gold, E. S., Diercks, A. H., Podolsky, I., Podyminogin, R. L., Askovich, P. S., Treuting, P. M. & Aderem, A. (2014). '25-Hydroxycholesterol acts as an amplifier of inflammatory signaling', *Proceedings of the National Academy of Sciences*, 111(29), pp. 10666-10671.
González-Rosa, J. M., Burns, C. E. & Burns, C. G. (2017). 'Zebrafish heart regeneration: 15 years of discoveries', *Regeneration*, 4(3), pp. 105-123.
Gorelick, P. B. (2019). 'The global burden of stroke: Persistent and disabling', *The Lancet Neurology*, 18(5), pp. 417-418.
Gould, B., McCourt, R., Asdaghi, N., Dowlatshahi, D., Jeerakathil, T., Kate, M., Coutts, S. B., Hill, M. D., Demchuk, A. M. & Shuaib, A. (2013). 'Autoregulation of cerebral blood flow is preserved in primary intracerebral hemorrhage', *Stroke*, 44(6), pp. 1726-1728.
Gupta, A. K., Sexton, R. & Rudney, H. J. J. o. l. r. (1990). 'Differential regulation of low density lipoprotein suppression of HMG-CoA reductase activity in cultured cells by inhibitors of cholesterol biosynthesis', 31(2), pp. 203-215.
Haffter, P., Granato, M., Brand, M., Mullins, M. C., Hammerschmidt, M., Kane, D. A., Odenthal, J., Van Eeden, F., Jiang, Y.-J. & Heisenberg, C.-P. (1996). 'The identification of genes with unique and essential functions in the development of the zebrafish, Danio rerio', *Development*, 123(1), pp. 1-36.
Hallare, A., Nagel, K., Köhler, H.-R. & Triebskorn, R. (2006). 'Comparative embryotoxicity and proteotoxicity of three carrier solvents to zebrafish (Danio rerio) embryos', *Ecotoxicology and environmental safety*, 63(3), pp. 378-388.
Han, X., Kitamoto, S., Lian, Q. & Boisvert, W. A. (2009). 'Interleukin-10 facilitates both cholesterol uptake and efflux in macrophages', *Journal of Biological Chemistry*, 284(47), pp. 32950-32958.
Hanley, D. (2009). 'Intraventricular hemorrhage and intracerebral hemorrhage outcomes: severity factor and treatment target', *Stroke*, 40(4), pp. 1533-38.
Hanley, D. F., Thompson, R. E., Rosenblum, M., Yenokyan, G., Lane, K., McBee, N., Mayo, S. W., Bistran-Hall, A. J., Gandhi, D. & Mould, W. A. (2019). 'Efficacy and safety of minimally invasive surgery with thrombolysis in intracerebral haemorrhage evacuation (MISTIE III): a randomised, controlled, open-label, blinded endpoint phase 3 trial', *The Lancet*, 393(10175), pp. 1021-1032.
Hans, S., Kaslin, J., Freudenreich, D. & Brand, M. (2009). 'Temporally-controlled site-specific recombination in zebrafish', *PloS one*, 4(2), p. e4640.
Hanslick, J. L., Lau, K., Noguchi, K. K., Olney, J. W., Zorumski, C. F., Mennerick, S. & Farber, N. B. (2009). 'Dimethyl sulfoxide (DMSO) produces widespread apoptosis in the developing central nervous system', *Neurobiology of disease*, 34(1), pp. 1-10.
Heacock, A. M., Klinger, P. D., Seguin, E. B. & Agranoff, B. W. (1984). 'Cholesterol synthesis and nerve regeneration', *Journal of neurochemistry*, 42(4), pp. 987-993.

Holman, C., Piper, S. K., Grittner, U., Diamantaras, A. A., Kimmelman, J., Siegerink, B. & Dirnagl, U. (2016). 'Where have all the rodents gone? The effects of attrition in experimental research on cancer and stroke', *PLoS biology,* 14(1), p. e1002331.

Howe, K., Clark, M. D., Torroja, C. F., Torrance, J., Berthelot, C., Muffato, M., Collins, J. E., Humphray, S., McLaren, K. & Matthews, L. (2013). 'The zebrafish reference genome sequence and its relationship to the human genome', *Nature,* 496(7446), pp. 498-503.

Hua, Y., Keep, R. F., Hoff, J. T. & Xi, G. (2003). 'Thrombin preconditioning attenuates brain edema induced by erythrocytes and iron', *Journal of Cerebral Blood Flow & Metabolism,* 23(12), pp. 1448-1454.

Hua, Y., Nakamura, T., Keep, R. F., Wu, J., Schallert, T., Hoff, J. T. & Xi, G. (2006a). 'Long-term effects of experimental intracerebral hemorrhage: the role of iron', *Journal of neurosurgery,* 104(2), pp. 305-312.

Hua, Y., Wu, J., Keep, R. F., Nakamura, T., Hoff, J. T. & Xi, G. (2006b). 'Tumor necrosis factor-α increases in the brain after intracerebral hemorrhage and thrombin stimulation', *Neurosurgery,* 58(3), pp. 542-550.

Hua, Y., Xi, G., Keep, R. F. & Hoff, J. T. (2000). 'Complement activation in the brain after experimental intracerebral hemorrhage', *Journal of neurosurgery,* 92(6), pp. 1016-1022.

Huang, B., Zhou, Z.-Y., Li, S., Huang, X.-H., Tang, J.-Y., Hoi, M. P. M. & Lee, S. M. Y. (2017). 'Tanshinone I prevents atorvastatin-induced cerebral hemorrhage in zebrafish and stabilizes endothelial cell–cell adhesion by inhibiting VE-cadherin internalization and actin-myosin contractility', *Pharmacological research, 128,* pp. 389-398.

Huang, F.-P., Xi, G., Keep, R. F., Hua, Y., Nemoianu, A. & Hoff, J. T. (2002). 'Brain edema after experimental intracerebral hemorrhage: role of hemoglobin degradation products', *Journal of neurosurgery,* 96(2), pp. 287-293.

Hussain, G., Wang, J., Rasul, A., Anwar, H., Imran, A., Qasim, M., Zafar, S., Kamran, S. K. S., Razzaq, A. & Aziz, N. (2019). 'Role of cholesterol and sphingolipids in brain development and neurological diseases', *Lipids in health and disease,* 18(1), p. 26.

Iida, S., Baumbach, G. L., Lavoie, J. L., Faraci, F. M., Sigmund, C. D. & Heistad, D. D. (2005). 'Spontaneous stroke in a genetic model of hypertension in mice', *Stroke,* 36(6), pp. 1253-1258.

Im, S.-S., Yousef, L., Blaschitz, C., Liu, J. Z., Edwards, R. A., Young, S. G., Raffatellu, M. & Osborne, T. F. (2011). 'Linking lipid metabolism to the innate immune response in macrophages through sterol regulatory element binding protein-1a', *Cell metabolism,* 13(5), pp. 540-549.

Inagawa, S., Isoda, H., Kougo, H., Isogai, S. & Sakahara, H. (2003). 'In-vitro simulation of NBCA embolization for arteriovenous malformation', *Interventional Neuroradiology,* 9(4), pp. 351-358.

Institute for Health Metrics and Evaluation (2018). Findings from the Global Burden of Disease Study 2017. Seattle, WA: The Lancet.

Intercollegiate Stroke Working Party (2012). *National clinical guideline for stroke* (Vol. 20083): Citeseer.

Jaillon, O., Aury, J.-M., Brunet, F., Petit, J.-L., Stange-Thomann, N., Mauceli, E., Bouneau, L., Fischer, C., Ozouf-Costaz, C. & Bernot, A. (2004). 'Genome duplication in the teleost fish Tetraodon nigroviridis reveals the early vertebrate proto-karyotype', *Nature,* 431(7011), pp. 946-957.

Jameel, A., Ooi, K. G.-J., Jeffs, N. R., Galatowicz, G., Lightman, S. L. & Calder, V. L. (2013). 'Statin modulation of human T-cell proliferation, IL-1 and IL-17 production, and IFN-T cell expression: synergy with conventional immunosuppressive agents', *International journal of inflammation,* 2013.

Jang, J., Park, S., Hur, H. J., Cho, H.-J., Hwang, I., Kang, Y. P., Im, I., Lee, H., Lee, E. & Yang, W. (2016). '25-hydroxycholesterol contributes to cerebral inflammation of X-linked adrenoleukodystrophy through activation of the NLRP3 inflammasome', *Nature communications,* 7, p. 13129.

Jichlinski, P., Guillou, L., Karlsen, S. J., Malmstrom, P.-U., Jocham, D., Brennhovd, B., Johansson, E., Gartner, T., Lange, N. & van den Bergh, H. (2003). 'Hexyl aminolevulinate fluorescence cystoscopy: a new diagnostic tool for photodiagnosis of superficial bladder cancer—a multicenter study', *The Journal of urology,* 170(1), pp. 226-229.

Johnson, C. O., Nguyen, M., Roth, G. A., Nichols, E., Alam, T., Abate, D., Abd-Allah, F., Abdelalim, A., Abraha, H. N. & Abu-Rmeileh, N. M. (2019). 'Global, regional, and national burden of stroke, 1990–2016: a systematic analysis for the Global Burden of Disease Study 2016', *The Lancet Neurology*.

Johnson, W., Onuma, O., Owolabi, M. & Sachdev, S. (2016). 'Stroke: a global response is needed', *Bulletin of the World Health Organization,* 94(9), p. 634.

Jordan, L. C., Kleinman, J. T. & Hillis, A. E. (2009). 'Intracerebral hemorrhage volume predicts poor neurologic outcome in children', *Stroke,* 40(5), pp. 1666-1671.

Jung, J., Zeng, H. & Horng, T. (2019). 'Metabolism as a guiding force for immunity', *Nature cell biology,* 21(1), p. 85.

Kais, B., Schneider, K., Keiter, S., Henn, K., Ackermann, C. & Braunbeck, T. (2013). 'DMSO modifies the permeability of the zebrafish (Danio rerio) chorion-implications for the fish embryo test (FET)', *Aquatic toxicology,* 140, pp. 229-238.

Kamibayashi, T. & Maze, M. (2000). 'Clinical uses of α2-adrenergic agonists', *Anesthesiology: The Journal of the American Society of Anesthesiologists,* 93(5), pp. 1345-1349.

Kanungo, J., Cuevas, E., F Ali, S. & Paule, M. G. (2014). 'Zebrafish model in drug safety assessment', *Current pharmaceutical design,* 20(34), pp. 5416-5429.

Kasher, P. R., Jenkinson, E. M., Briolat, V., Gent, D., Morrissey, C., Zeef, L. A., Rice, G. I., Levraud, J.-P. & Crow, Y. J. (2015). 'Characterization of samhd1 morphant zebrafish recapitulates features of the human type I interferonopathy Aicardi-Goutieres syndrome', *The Journal of Immunology,* 194(6), pp. 2819-2825.

Kathirvelu, B. & Carmichael, S. T. J. M. b. d. (2015). 'Intracerebral hemorrhage in mouse models: therapeutic interventions and functional recovery', 30(2), pp. 449-459.

Keep, R. F., Hua, Y. & Xi, G. (2012). 'Intracerebral haemorrhage: mechanisms of injury and therapeutic targets', *The Lancet Neurology,* 11(8), pp. 720-731.

Kellner, C. P. & Connolly, E. S. (2010). 'Neuroprotective Strategies for Intracerebral Hemorrhage Trials and Translation', *Stroke,* 41(10 suppl 1), pp. S99-S102.

Kettleborough, R. N., Busch-Nentwich, E. M., Harvey, S. A., Dooley, C. M., de Bruijn, E., van Eeden, F., Sealy, I., White, R. J., Herd, C. & Nijman, I. J. (2013). 'A systematic genome-wide analysis of zebrafish protein-coding gene function', *Nature,* 496(7446), pp. 494-497.

Kimmel, C. B., Ballard, W. W., Kimmel, S. R., Ullmann, B. & Schilling, T. F. (1995). 'Stages of embryonic development of the zebrafish', *Developmental dynamics,* 203(3), pp. 253-310.

Kirkman, M. A., Allan, S. M. & Parry-Jones, A. R. (2011). 'Experimental intracerebral hemorrhage: avoiding pitfalls in translational research', *Journal of Cerebral Blood Flow and Metabolism,* 31(11), pp. 2135-2151.

Kishimoto, N., Shimizu, K. & Sawamoto, K. (2012). 'Neuronal regeneration in a zebrafish model of adult brain injury', *Disease models and mechanisms,* 5(2), pp. 200-209.

Kitago, T. & Ratan, R. R. (2017). 'Rehabilitation following hemorrhagic stroke: building the case for stroke-subtype specific recovery therapies', *F1000Research,* 6.

Klebe, D., McBride, D., Flores, J. J., Zhang, J. H. & Tang, J. (2015). 'Modulating the immune response towards a neuroregenerative peri-injury milieu after cerebral hemorrhage', *Journal of Neuroimmune Pharmacology,* 10(4), pp. 576-586.

Kleinman, J. T., Hillis, A. E. & Jordan, L. C. (2011). 'ABC/2: estimating intracerebral haemorrhage volume and total brain volume, and predicting outcome in children', *Developmental Medicine and Child Neurology,* 53(3), pp. 281-284.

Kloter, E., Wirz, M. & Dietz, V. (2011). 'Locomotion in stroke subjects: interactions between unaffected and affected sides', *Brain,* 134(3), pp. 721-731.

Kontoghiorghes, G. J. (1995). 'Comparative efficacy and toxicity of desferrioxamine, deferiprone and other iron and aluminium chelating drugs', *Toxicology letters,* 80(1-3), pp. 1-18.

Krel, M., Miulli, D. E., Jung, H., Wiginton IV, J. G., Brazdzionis, J., Wacker, M. R., Hoshek, S. & Menoni, R. (2019). 'Minimization of Intraparenchymal Hemorrhagic Stroke Size by Optimization of Serum Lipids', *Cureus,* 11(4).

Krishnamurthi, R. V., Moran, A. E., Forouzanfar, M. H., Bennett, D. A., Mensah, G. A., Lawes, C. M., Barker-Collo, S., Connor, M., Roth, G. A. & Sacco, R. (2014). 'The global burden of hemorrhagic stroke: a summary of findings from the GBD 2010 study', *Global heart,* 9(1), pp. 101-106.

Kulig, W., Cwiklik, L., Jurkiewicz, P., Rog, T. & Vattulainen, I. (2016). 'Cholesterol oxidation products and their biological importance', *Chemistry and physics of lipids,* 199, pp. 144-160.

Kyritsis, N., Kizil, C., Zocher, S., Kroehne, V., Kaslin, J., Freudenreich, D., Iltzsche, A. & Brand, M. (2012). 'Acute inflammation initiates the regenerative response in the adult zebrafish brain', *Science,* 338(6112), pp. 1353-1356.

Lan, X., Han, X., Li, Q., Yang, Q.-W. & Wang, J. (2017). 'Modulators of microglial activation and polarization after intracerebral haemorrhage', *Nature Reviews Neurology,* 13(7), p. 420.

Lawson, N. D. & Weinstein, B. M. (2002). 'In vivo imaging of embryonic vascular development using transgenic zebrafish', *Developmental biology,* 248(2), pp. 307-318.

LeBlanc, R. H., Chen, R., Selim, M. H. & Hanafy, K. A. (2016). 'Heme oxygenase-1-mediated neuroprotection in subarachnoid hemorrhage via intracerebroventricular deferoxamine', *Journal of neuroinflammation,* 13(1), p. 244.

Lee, K. R., Kawai, N., Kim, S., Sagher, O. & Hoff, J. T. (1997). 'Mechanisms of edema formation after intracerebral hemorrhage: effects of thrombin on cerebral blood flow, blood-brain barrier permeability, and cell survival in a rat model', *Journal of neurosurgery,* 86(2), pp. 272-278.

Lei, B., Dawson, H. N., Roulhac-Wilson, B., Wang, H., Laskowitz, D. T. & James, M. L. (2013). 'Tumor necrosis factor alpha antagonism improves neurological recovery in murine intracerebral hemorrhage', *Journal of neuroinflammation,* 10(1), p. 873.

Lenth, R. V. (2016). 'Least-squares means: the R package lsmeans', *Journal of statistical software,* 69(1), pp. 1-33.

LeVine, S. M., Connor, J. R. & Schipper, H. M. (2004). *Redox-active metals in neurological disorders*: New York Academy of Sciences.

Lewis, B. & Tikkanen, M. J. (1994). 'Low blood total cholesterol and mortality: causality, consequence and confounders', *American journal of cardiology,* 73(1), pp. 80-85.

Li, J.-J. & Fang, C.-H. (2005). 'Effects of 4 weeks of atorvastatin administration on the antiinflammatory cytokine interleukin-10 in patients with unstable angina', *Clinical chemistry,* 51(9), pp. 1735-1738.

Li, Q., Weiland, A., Chen, X., Lan, X., Han, X., Durham, F., Liu, X., Wan, J., Ziai, W. C. & Hanley, D. F. (2018). 'Ultrastructural characteristics of neuronal death and white matter injury in mouse brain tissues after intracerebral hemorrhage: coexistence of ferroptosis, autophagy, and necrosis', *Frontiers in neurology,* 9.

Li, S., Ai, N., Shen, M., Dang, Y., Chong, C.-M., Pan, P., Kwan, Y. W., Chan, S. W., Leung, G. P. H. & Hoi, M. P. M. (2017). 'Discovery of a ROCK inhibitor, FPND, which prevents cerebral hemorrhage through maintaining vascular integrity by interference with VE-cadherin', *Cell death discovery,* 3, p. 17051.

Li, Y., Li, Y., Cao, X., Jin, X. & Jin, T. (2017). 'Pattern recognition receptors in zebrafish provide functional and evolutionary insight into innate immune signaling pathways', *Cellular and molecular immunology,* 14(1), p. 80.

Lim, T. C., Mandeville, E., Weng, D., Wang, L.-S., Kurisawa, M., Leite-Morris, K., Selim, M. H., Lo, E. H. & Spector, M. (2019). 'Hydrogel-Based Therapy for Brain Repair After Intracerebral Hemorrhage', *Translational stroke research*, pp. 1-6.

Lin, S., Yin, Q., Zhong, Q., Lv, F.-L., Zhou, Y., Li, J.-Q., Wang, J.-Z., Su, B.-y. & Yang, Q.-W. (2012). 'Heme activates TLR4-mediated inflammatory injury via MyD88/TRIF signaling pathway in intracerebral hemorrhage', *Journal of neuroinflammation,* 9(1), p. 46.

Liu, C., Wu, C., Yang, Q., Gao, J., Li, L., Yang, D. & Luo, L. (2016). 'Macrophages mediate the repair of brain vascular rupture through direct physical adhesion and mechanical traction', *Immunity,* 44(5), pp. 1162-1176.

Liu, C., Xie, B., Li, M., Yang, G.-y. & Tong, S. (2011). Spatiotemporal changes of cerebral blood flow following hemorrhagic stroke by laser speckle imaging. *In:* 2011 Annual International Conference of the IEEE Engineering in Medicine and Biology Society, 2011. IEEE. pp. 6150-6153.

Liu, J., Fraser, S. D., Faloon, P. W., Rollins, E. L., Vom Berg, J., Starovic-Subota, O., Laliberte, A. L., Chen, J.-N., Serluca, F. C. & Childs, S. J. (2007). 'A βPix–Pak2a signaling pathway regulates cerebral vascular stability in zebrafish', *Proceedings of the National Academy of Sciences,* 104(35), pp. 13990-13995.

Liu, J., Zeng, L., Kennedy, R. M., Gruenig, N. M. & Childs, S. J. (2012). 'βPix plays a dual role in cerebral vascular stability and angiogenesis, and interacts with integrin αvβ8', *Developmental biology,* 363(1), pp. 95-105.

Liu, S.-Y., Aliyari, R., Chikere, K., Li, G., Marsden, M. D., Smith, J. K., Pernet, O., Guo, H., Nusbaum, R. & Zack, J. A. (2013). 'Interferon-inducible cholesterol-

25-hydroxylase broadly inhibits viral entry by production of 25-hydroxycholesterol', *Immunity,* 38(1), pp. 92-105.
Liu, X. & Quan, N. (2018). 'Microglia and CNS interleukin-1: beyond immunological concepts', *Frontiers in neurology,* 9, p. 8.
Liu, Y., Wei, Z., Ma, X., Yang, X., Chen, Y., Sun, L., Ma, C., Miao, Q. R., Hajjar, D. P. & Han, J. (2018). '25-Hydroxycholesterol activates the expression of cholesterol 25-hydroxylase in an LXR-dependent mechanism', *Journal of lipid research,* 59(3), pp. 439-451.
Livak, K. J. & Schmittgen, T. D. J. m. (2001). 'Analysis of relative gene expression data using real-time quantitative PCR and the 2− ΔΔCT method', 25(4), pp. 402-408.
Lively, S., Hutchings, S. & Schlichter, L. C. (2016). 'Molecular and cellular responses to interleukin-4 treatment in a rat model of transient ischemia', *Journal of Neuropathology and Experimental Neurology,* 75(11), pp. 1058-1071.
Lo, W. D. (2011). 'Childhood hemorrhagic stroke: an important but understudied problem', *Journal of child neurology,* 26(9), pp. 1174-1185.
Lok, J., Leung, W., Murphy, S., Butler, W., Noviski, N. & Lo, E. H. (2011). 'Intracranial hemorrhage: mechanisms of secondary brain injury', *Intracerebral Hemorrhage Research*: Springerpp. 63-69.
Lopez-Castejon, G. & Brough, D. (2011). 'Understanding the mechanism of IL-1β secretion', *Cytokine & growth factor reviews,* 22(4), pp. 189-195.
Lorenzo, A. V., Welch, K. & Conner, S. (1982). 'Spontaneous germinal matrix and intraventricular hemorrhage in prematurely born rabbits', *Journal of neurosurgery,* 56(3), pp. 404-410.
Louwette, S., Régal, L., Wittevrongel, C., Thys, C., Vandeweeghde, G., Decuyper, E., Leemans, P., De Vos, R., Van Geet, C. & Jaeken, J. (2012). 'NPC1 defect results in abnormal platelet formation and function: studies in Niemann–Pick disease type C1 patients and zebrafish', *Human molecular genetics,* 22(1), pp. 61-73.
Love, S. (2011). 'Autopsy approach to stroke', *Histopathology,* 58(3), pp. 333-351.
Lowell, H. M. & Bloor, B. M. (1971). 'The effect of increased intracranial pressure on cerebrovascular hemodynamics', *Journal of neurosurgery,* 34(6), pp. 760-769.
Luengo-Fernandez, R., Leal, J. & Gray, A. (2016). *Research spend in the UK*: Stroke Association. Available at: https://www.stroke.org.uk/sites/default/files/sa-research_spend_in_the_uk_july2016_web.pdf.
Lumsden, A. L., Henshall, T. L., Dayan, S., Lardelli, M. T. & Richards, R. I. (2007). 'Huntingtin-deficient zebrafish exhibit defects in iron utilization and development', *Human molecular genetics,* 16(16), pp. 1905-1920.
Lyden, P. D., Shuaib, A., Lees, K. R., Davalos, A., Davis, S. M., Diener, H.-C., Grotta, J. C., Ashwood, T. J., Hardemark, H.-G. & Svensson, H. H. (2007). 'Safety and tolerability of NXY-059 for acute intracerebral hemorrhage: the CHANT Trial', *Stroke,* 38(8), pp. 2262-2269.
Ma, Y., Li, Z., Chen, L. & Li, X. (2016). 'Blood lipid levels, statin therapy and the risk of intracerebral hemorrhage', *Lipids in health and disease,* 15(1), p. 43.
MacLellan, C. L., Silasi, G., Auriat, A. M. & Colbourne, F. (2010). 'Rodent models of intracerebral hemorrhage', *Stroke,* 41(10 suppl 1), pp. S95-S98.
MacLellan, C. L., Silasi, G., Poon, C. C., Edmundson, C. L., Buist, R., Peeling, J. & Colbourne, F. (2008). 'Intracerebral hemorrhage models in rat: comparing collagenase to blood infusion', *Journal of Cerebral Blood Flow & Metabolism,* 28(3), pp. 516-525.

MacRae, C. A. & Peterson, R. T. (2015). 'Zebrafish as tools for drug discovery', *Nature Reviews Drug Discovery,* 14(10), pp. 721-731.
Maes, J., Verlooy, L., Buenafe, O. E., De Witte, P. A., Esguerra, C. V. & Crawford, A. D. (2012). 'Evaluation of 14 organic solvents and carriers for screening applications in zebrafish embryos and larvae', *PloS one,* 7(10), p. e43850.
Manaenko, A., Chen, H., Zhang, J. H. & Tang, J. (2011). 'Comparison of different preclinical models of intracerebral hemorrhage', *Intracerebral Hemorrhage Research*: Springerpp. 9-14.
Margiotta-Casaluci, L., Owen, S. F., Rand-Weaver, M. & Winter, M. J. (2019). 'Testing the Translational Power of the Zebrafish: An Interspecies Analysis of Responses to Cardiovascular Drugs', *Frontiers in pharmacology,* 10.
Massey, J. B. (2001). 'Interaction of ceramides with phosphatidylcholine, sphingomyelin and sphingomyelin/cholesterol bilayers', *Biochimica et Biophysica Acta -Biomembranes,* 1510(1-2), pp. 167-184.
Matsushita, H., Hijioka, M., Ishibashi, H., Anan, J., Kurauchi, Y., Hisatsune, A., Seki, T., Shudo, K. & Katsuki, H. (2014). 'Suppression of CXCL2 upregulation underlies the therapeutic effect of the retinoid Am80 on intracerebral hemorrhage in mice', *Journal of neuroscience research,* 92(8), pp. 1024-1034.
Maxfield, F. R. & Wüstner, D. (2012). 'Analysis of cholesterol trafficking with fluorescent probes', *Methods in cell biology*: Elsevierpp. 367-393.
Mayer, S. A., Brun, N. C., Begtrup, K., Broderick, J., Davis, S., Diringer, M. N., Skolnick, B. E. & Steiner, T. (2008). 'Efficacy and safety of recombinant activated factor VII for acute intracerebral hemorrhage', *New England Journal of Medicine,* 358(20), pp. 2127-2137.
Mazon-Moya, M. J., Willis, A. R., Torraca, V., Boucontet, L., Shenoy, A. R., Colucci-Guyon, E. & Mostowy, S. (2017). 'Septins restrict inflammation and protect zebrafish larvae from Shigella infection', *PLoS pathogens,* 13(6), p. e1006467.
McKinney, W. T. & Bunney, W. E. (1969). 'Animal model of depression: I. Review of evidence: implications for research', *Archives of general psychiatry,* 21(2), pp. 240-248.
Mendelow, A. D., Gregson, B. A., Mitchell, P. M., Murray, G. D., Rowan, E. N. & Gholkar, A. R. (2011). 'Surgical trial in lobar intracerebral haemorrhage (STICH II) protocol', *Trials,* 12(1), p. 124.
Mendelow, A. D., Gregson, B. A., Rowan, E. N., Murray, G. D., Gholkar, A., Mitchell, P. M. & Investigators, S. I. (2013). 'Early surgery versus initial conservative treatment in patients with spontaneous supratentorial lobar intracerebral haematomas (STICH II): a randomised trial', *The Lancet,* 382(9890), pp. 397-408.
Meuwissen, M. E., Schot, R., Buta, S., Oudesluijs, G., Tinschert, S., Speer, S. D., Li, Z., Van Unen, L., Heijsman, D. & Goldmann, T. (2016). 'Human USP18 deficiency underlies type 1 interferonopathy leading to severe pseudo-TORCH syndrome', *Journal of Experimental Medicine,* 213(7), pp. 1163-1174.
Misra, U., Kalita, J., Vajpayee, A., Phadke, R., Hadique, A. & Savlani, V. (2007). 'Effect of single mannitol bolus in intracerebral hemorrhage', *European journal of neurology,* 14(10), pp. 1118-1123.
Miyares, R. L., de Rezende, V. B. & Farber, S. A. (2014). 'Zebrafish yolk lipid processing: a tractable tool for the study of vertebrate lipid transport and metabolism', *Disease models and mechanisms,* 7(7), pp. 915-927.
Morell, P. & Jurevics, H. (1996). 'Origin of cholesterol in myelin', *Neurochemical research,* 21(4), pp. 463-470.

Morgan, T., Zuccarello, M., Narayan, R., Keyl, P., Lane, K. & Hanley, D. (2008). 'Preliminary findings of the minimally-invasive surgery plus rtPA for intracerebral hemorrhage evacuation (MISTIE) clinical trial', *Cerebral Hemorrhage*: Springerpp. 147-151.

Morgenstern, L. B., Hemphill III, J. C., Anderson, C., Becker, K., Broderick, J. P., Connolly Jr, E. S., Greenberg, S. M., Huang, J. N., Macdonald, R. L. & Messe, S. R. (2010). 'Guidelines for the management of spontaneous intracerebral hemorrhage: a guideline for healthcare professionals from the American Heart Association/American Stroke Association', *Stroke,* 41(9), pp. 2108-2129.

Morsch, M., Radford, R., Lee, A., Don, E. K., Badrock, A. P., Hall, T. E., Cole, N. J. & Chung, R. (2015). 'In vivo characterization of microglial engulfment of dying neurons in the zebrafish spinal cord', *Frontiers in cellular neuroscience,* 9.

Mracsko, E. & Veltkamp, R. (2014). 'Neuroinflammation after intracerebral hemorrhage', *Frontiers in cellular neuroscience,* 8, p. 388.

Mueller, T. & Wullimann, M. (2015). *Atlas of early zebrafish brain development: a tool for molecular neurogenetics*: Academic Press.

Murray, K. N., Parry-Jones, A. R. & Allan, S. M. (2015). 'Interleukin-1 and acute brain injury', *Frontiers in cellular neuroscience,* 9, p. 18.

Méresse, S., Delbart, C., Fruchart, J. C. & Cecchelli, R. (1989). 'Low-density lipoprotein receptor on endothelium of brain capillaries', *Journal of neurochemistry,* 53(2), pp. 340-345.

Nasrallah, G. K., Younes, N. N., Baji, M. H., Shraim, A. M. & Mustafa, I. (2018). 'Zebrafish larvae as a model to demonstrate secondary iron overload', *European journal of haematology,* 100(6), pp. 536-543.

NCEP (2001). 'Executive summary of the third report of the National Cholesterol Education Program (NCEP) expert panel on detection, evaluation, and treatment of high blood cholesterol in adults (Adult Treatment Panel III)', *Jama,* 285(19), p. 2486.

NICE (2014). Head Injury: assessment and early management.

NINDS ICH Workshop Participants (2005). 'Priorities for clinical research in intracerebral hemorrhage: report from a National Institute of Neurological Disorders and Stroke workshop', *Stroke,* 36(3), pp. E23-E41.

Noebauer, B., Jais, A., Todoric, J., Gossens, K., Sutterlüty-Fall, H. & Einwallner, E. (2017). 'Hepatic Cholesterol-25-Hydroxylase Overexpression Improves Systemic Insulin Sensitivity in Mice', *Journal of diabetes research,* 2017.

North, T. E., Goessling, W., Walkley, C. R., Lengerke, C., Kopani, K. R., Lord, A. M., Weber, G. J., Bowman, T. V., Jang, I.-H. & Grosser, T. (2007). 'Prostaglandin E2 regulates vertebrate haematopoietic stem cell homeostasis', *Nature,* 447(7147), pp. 1007-1011.

Novoa, B. & Figueras, A. (2012). 'Zebrafish: model for the study of inflammation and the innate immune response to infectious diseases', *Current topics in innate immunity II*: Springerpp. 253-275.

Ogryzko, N. V., Hoggett, E. E., Solaymani-Kohal, S., Tazzyman, S., Chico, T. J., Renshaw, S. A. & Wilson, H. L. (2014a). 'Zebrafish tissue injury causes upregulation of interleukin-1 and caspase-dependent amplification of the inflammatory response', *Disease models & mechanisms,* 7(2), pp. 259-264.

Ogryzko, N. V., Renshaw, S. A. & Wilson, H. L. (2014b). 'The IL-1 family in fish: swimming through the muddy waters of inflammasome evolution', *Developmental & Comparative Immunology,* 46(1), pp. 53-62.

Osuka, K., Suzuki, Y., Watanabe, Y., Dogan, A., Takayasu, M., Shibuya, M. & Yoshida, J. (1997). 'Vasodilator effects on canine basilar artery induced by intracisternal interleukin-1β', *Journal of Cerebral Blood Flow & Metabolism,* 17(12), pp. 1337-1345.

Ott, L. W., Resing, K. A., Sizemore, A. W., Heyen, J. W., Cocklin, R. R., Pedrick, N. M., Woods, H. C., Chen, J. Y., Goebl, M. G. & Witzmann, F. A. (2007). 'Tumor necrosis factor-α-and interleukin-1-induced cellular responses: Coupling proteomic and genomic information', *Journal of proteome research,* 6(6), pp. 2176-2185.

Papassotiropoulos, A., Lambert, J.-C., Wavrant-De Vrièze, F., Wollmer, M. A., Von Der Kammer, H., Streffer, J. R., Maddalena, A., Huynh, K.-D., Wolleb, S. & Luetjohann, D. (2005). 'Cholesterol 25-hydroxylase on chromosome 10q is a susceptibility gene for sporadic Alzheimer's disease', *Neurodegenerative Diseases,* 2(5), pp. 233-241.

Park, K. & Scott, A. L. (2010). 'Cholesterol 25-hydroxylase production by dendritic cells and macrophages is regulated by type I interferons', *Journal of leukocyte biology,* 88(6), pp. 1081-1087.

Parry-Jones, A. (2018). 'BLOC-ICH: Interleukin-1 Receptor Antagonist in Intracerebral Haemorrhage (BLOC-ICH)'. Available at: https://clinicaltrials.gov/ct2/show/NCT03737344.

Parry-Jones, A. R., Sammut-Powell, C., Paroutoglou, K., Birleson, E., Rowland, J., Lee, S., Cecchini, L., Massyn, M., Emsley, R. & Bray, B. (2019). 'An Intracerebral Hemorrhage Care Bundle Is Associated with Lower Case Fatality', *Annals of neurology*.

Paul, B. Y., Deng, D. Y., Lai, C. S., Hong, C. C., Cuny, G. D., Bouxsein, M. L., Hong, D. W., McManus, P. M., Katagiri, T. & Sachidanandan, C. (2008a). 'BMP type I receptor inhibition reduces heterotopic ossification', *Nature medicine,* 14(12), pp. 1363-1369.

Paul, B. Y., Hong, C. C., Sachidanandan, C., Babitt, J. L., Deng, D. Y., Hoyng, S. A., Lin, H. Y., Bloch, K. D. & Peterson, R. T. (2008b). 'Dorsomorphin inhibits BMP signals required for embryogenesis and iron metabolism', *Nature chemical biology,* 4(1), pp. 33-41.

Pereiro, P., Forn-Cuní, G., Dios, S., Coll, J., Figueras, A. & Novoa, B. (2017). 'Interferon-independent antiviral activity of 25-hydroxycholesterol in a teleost fish', *Antiviral research,* 145, pp. 146-159.

Perry, A. & Brat, D. J. (2010). *Practical surgical neuropathology: a diagnostic approach*: Elsevier Health Sciences.

Perucha, E., Melchiotti, R., Bibby, J. A., Wu, W., Frederiksen, K. S., Roberts, C. A., Hall, Z., LeFriec, G., Robertson, K. A. & Lavender, P. (2019). 'The cholesterol biosynthesis pathway regulates IL-10 expression in human Th1 cells', *Nature communications,* 10(1), p. 498.

Phuah, C.-L., Raffeld, M. R., Ayres, A. M., Viswanathan, A., Greenberg, S. M., Biffi, A., Rosand, J. & Anderson, C. D. (2016). 'Subacute decline in serum lipids precedes the occurrence of primary intracerebral hemorrhage', *Neurology,* 86(22), pp. 2034-2041.

Plata-Salaman, C. R., Kelly, G., Agresta, C., Taylor, K. & Salzman, S. K. (1995). 'Interleukin-1 beta enhances spinal cord blood flow after intrathecal administration in the normal rat', *American Journal of Physiology-Regulatory, Integrative and Comparative Physiology,* 269(5), pp. R1032-R1037.

Poss, K. D., Wilson, L. G. & Keating, M. T. (2002). 'Heart regeneration in zebrafish', *Science*, 298(5601), pp. 2188-2190.

Poungvarin, N., Bhoopat, W., Viriyavejakul, A., Rodprasert, P., Buranasiri, P., Sukondhabhant, S., Hensley, M. J. & Strom, B. L. (1987). 'Effects of dexamethasone in primary supratentorial intracerebral hemorrhage', *New England journal of medicine*, 316(20), pp. 1229-1233.

Progatzky, F., Sangha, N. J., Yoshida, N., McBrien, M., Cheung, J., Shia, A., Scott, J., Marchesi, J. R., Lamb, J. R. & Bugeon, L. (2014). 'Dietary cholesterol directly induces acute inflammasome-dependent intestinal inflammation', *Nature communications*, 5, p. 5864.

Prospective Studies Collaboration (2007). 'Blood cholesterol and vascular mortality by age, sex, and blood pressure: a meta-analysis of individual data from 61 prospective studies with 55 000 vascular deaths', *The Lancet*, 370(9602), pp. 1829-1839.

Qing, W. G., Dong, Y. Q., Ping, T. Q., Lai, L. G., Fang, L. D., Min, H. W., Xia, L. & Heng, P. Y. (2009). 'Brain edema after intracerebral hemorrhage in rats: the role of iron overload and aquaporin 4', *Journal of neurosurgery*, 110(3), pp. 462-468.

Quinlivan, V. H. & Farber, S. A. (2017). 'Lipid uptake, metabolism, and transport in the larval zebrafish', *Frontiers in endocrinology*, 8, p. 319.

Quintana, C., Bellefqih, S., Laval, J., Guerquin-Kern, J., Wu, T., Avila, J., Ferrer, I., Arranz, R. & Patino, C. (2006). 'Study of the localization of iron, ferritin, and hemosiderin in Alzheimer's disease hippocampus by analytical microscopy at the subcellular level', *Journal of structural biology*, 153(1), pp. 42-54.

Qureshi, A. I., Mendelow, A. D. & Hanley, D. F. (2009). 'Intracerebral haemorrhage', *The Lancet*, 373(9675), pp. 1632-1644.

Qureshi, A. I., Palesch, Y. Y., Barsan, W. G., Hanley, D. F., Hsu, C. Y., Martin, R. L., Moy, C. S., Silbergleit, R., Steiner, T. & Suarez, J. I. (2016). 'Intensive blood-pressure lowering in patients with acute cerebral hemorrhage', *New England Journal of Medicine*, 375(11), pp. 1033-1043.

R Core Team (2018). 'R: A Language and Environment for Statistical Computing'.

Ramesh, V., Bernardi, B., Stafa, A., Garone, C., Franzoni, E., Abinun, M., Mitchell, P., Mitra, D., Friswell, M. & Nelson, J. (2010). 'Intracerebral large artery disease in Aicardi–Goutières syndrome implicates SAMHD1 in vascular homeostasis', *Developmental Medicine and Child Neurology*, 52(8), pp. 725-732.

Rangasamy, B., Hemalatha, D., Shobana, C., Nataraj, B. & Ramesh, M. (2018). 'Developmental toxicity and biological responses of zebrafish (Danio rerio) exposed to anti-inflammatory drug ketoprofen', *Chemosphere*, 213, pp. 423-433.

Raniga, K. & Liang, C. (2018). 'Interferons: reprogramming the metabolic network against viral infection', *Viruses*, 10(1), p. 36.

Raselli, T., Wyss, A., Alvarado, M. N. G., Weder, B., Mamie, C., Spalinger, M. R., van Haaften, W. T., Dijkstra, G., Sailer, A. W. & Silva, P. H. I. (2018). 'The oxysterol synthesizing enzyme CH25H contributes to the development of intestinal fibrosis', *Journal of Crohn's and Colitis*, p. 424820.

Reboldi, A. & Dang, E. (2018). 'Cholesterol metabolism in innate and adaptive response', *F1000Research*, 7.

Reboldi, A., Dang, E. V., McDonald, J. G., Liang, G., Russell, D. W. & Cyster, J. G. (2014). '25-Hydroxycholesterol suppresses interleukin-1–driven inflammation downstream of type I interferon', *Science,* 345(6197), pp. 679-684.

Rendevski, V., Aleksovski, B., Stojanov, D., Aleksovski, V., Rendevska, A. M., Kolevska, M., Stojanoski, K. & Gjorgoski, I. (2018). 'Peripheral glutamate and TNF-α levels in patients with intracerebral hemorrhage: Their prognostic values and interactions toward the formation of the edemal volume', *Neurologia i neurochirurgia polska,* 52(2), pp. 207-214.

Rennekamp, A. J. & Peterson, R. T. (2015). '15 years of zebrafish chemical screening', *Current opinion in chemical biology,* 24, pp. 58-70.

Renshaw, S. A., Loynes, C. A., Trushell, D. M., Elworthy, S., Ingham, P. W. & Whyte, M. K. (2006). 'A transgenic zebrafish model of neutrophilic inflammation', *Blood,* 108(13), pp. 3976-3978.

Renshaw, S. A. & Trede, N. S. (2012). 'A model 450 million years in the making: zebrafish and vertebrate immunity', *Disease models and mechanisms,* 5(1), pp. 38-47.

Rist, P. M., Buring, J. E., Ridker, P. M., Kase, C. S., Kurth, T. & Rexrode, K. M. (2019). 'Lipid levels and the risk of hemorrhagic stroke among women', *Neurology, 92* (19), pp. e2286-e2294.

Rodríguez-Yáñez, M., Brea, D., Arias, S., Blanco, M., Pumar, J. M., Castillo, J. & Sobrino, T. (2012). 'Increased expression of Toll-like receptors 2 and 4 is associated with poor outcome in intracerebral hemorrhage', *Journal of neuroimmunology,* 247(1-2), pp. 75-80.

Rohatgi, T., Sedehizade, F., Reymann, K. G. & Reiser, G. (2004). 'Protease-activated receptors in neuronal development, neurodegeneration, and neuroprotection: thrombin as signaling molecule in the brain', *The Neuroscientist,* 10(6), pp. 501-512.

Rosenberg, G. A., Mun-Bryce, S., Wesley, M. & Kornfeld, M. (1990). 'Collagenase-induced intracerebral hemorrhage in rats', *Stroke,* 21(5), pp. 801-807.

Sanchez, E. L. & Lagunoff, M. (2015). 'Viral activation of cellular metabolism', *Virology,* 479, pp. 609-618.

Sang, M., Wang, X., Zhang, H., Sun, X., Ding, X., Wang, P., Jiao, R., Cheng, H., Yang, S. & Zhang, G. (2017). 'Gene expression profile of peripheral blood mononuclear cells in response to intracerebral hemorrhage', *DNA cell biology,* 36(8), pp. 647-654.

Saulle, M. F. & Schambra, H. M. (2016). Recovery and rehabilitation after intracerebral hemorrhage. *In:* Seminars in neurology, 2016. NIH Public Access. p. 306.

Saver, J. L. (2006). 'Time is brain—quantified', *Stroke,* 37(1), pp. 263-266.

Schaar, K. L., Brenneman, M. M. & Savitz, S. I. (2010). 'Functional assessments in the rodent stroke model', *Experimental & translational stroke medicine,* 2(1), p. 13.

Schmidt, R., Beil, T., Strähle, U. & Rastegar, S. J. J. (2014). 'Stab wound injury of the zebrafish adult telencephalon: a method to investigate vertebrate brain neurogenesis and regeneration', (90), p. e51753.

Secombes, C. J., Wang, T. & Bird, S. (2011). 'The interleukins of fish', *Developmental C omparative Immunology,* 35(12), pp. 1336-1345.

Segal, A. Z., Chiu, R. I., Eggleston-Sexton, P. M., Beiser, A. & Greenberg, S. M. (1999). 'Low cholesterol as a risk factor for primary intracerebral hemorrhage: a case-control study', *Neuroepidemiology,* 18(4), pp. 185-193.

Selim, M., Foster, L. D., Moy, C. S., Xi, G., Hill, M. D., Morgenstern, L. B., Greenberg, S. M., James, M. L., Singh, V. & Clark, W. M. (2019). 'Deferoxamine mesylate in patients with intracerebral haemorrhage (i-DEF): a multicentre, randomised, placebo-controlled, double-blind phase 2 trial', *The Lancet Neurology,* 18, pp. 428-438.

Selim, M., Hanley, D., Broderick, J., Goldstein, J. N., Gregson, B. A., Falcione, G., Gonzales, N. R., Gurol, E., Kersten, J. & Lewkowicz, H. (2018). 'Basic and Translational Research in Intracerebral Hemorrhage: Limitations, Priorities, and Recommendations', *Stroke,* 49(5), pp. 1308-1314.

Semple, B. D., Blomgren, K., Gimlin, K., Ferriero, D. M. & Noble-Haeusslein, L. J. (2013). 'Brain development in rodents and humans: Identifying benchmarks of maturation and vulnerability to injury across species', *Progress in neurobiology,* 106, pp. 1-16.

Seshadri, S. & Wolf, P. A. (2007). 'Lifetime risk of stroke and dementia: current concepts, and estimates from the Framingham Study', *The Lancet Neurology,* 6(12), pp. 1106-1114.

Shaya, M., Dubey, A., Berk, C., Gonzalez-Toledo, E., Zhang, J., Caldito, G. & Nanda, A. (2005). 'Factors influencing outcome in intracerebral hematoma: a simple, reliable, and accurate method to grade intracerebral hemorrhage', *Surgical neurology,* 63(4), pp. 343-348.

Shen, M., Yu, H., Li, Y., Li, P., Pan, P., Zhou, S., Zhang, L., Li, S., Lee, S. M.-Y. & Hou, T. (2013). 'Discovery of Rho-kinase inhibitors by docking-based virtual screening', *Molecular BioSystems,* 9(6), pp. 1511-1521.

Shi, K., Wood, K., Shi, F.-D., Wang, X. & Liu, Q. (2018). 'Stroke-induced immunosuppression and poststroke infection', *Stroke and Vascular Neurology,* 3(1), pp. 34-41.

Shivane, A. & Chakrabarty, A. (2008). Pathology of intracerebral haemorrhage. ACNR.

Simon, A. (2014). 'Cholesterol metabolism and immunity', *New England Journal of Medicine,* 371(20), pp. 1933-1935.

Siperstein, M. D. & Fagan, V. M. (1957). 'Role of glycolysis in fatty acid and cholesterol synthesis in normal and diabetic rats', *Science,* 126(3281), pp. 1012-1013.

Skaug, H., Fournier, D., Nielsen, A., Magnusson, A. & Bolker, B. (2013). 'Generalized linear mixed models using AD model builder', *R package version 0.7,* 7.

Smith, C. J., Hulme, S., Vail, A., Heal, C., Parry-Jones, A. R., Scarth, S., Hopkins, K., Hoadley, M., Allan, S. M. & Rothwell, N. J. (2018). 'SCIL-STROKE (Subcutaneous Interleukin-1 Receptor Antagonist in Ischemic Stroke): A Randomized Controlled Phase 2 Trial', *Stroke,* 49, pp. 1210–1216.

Sobowale, O. A., Parry-Jones, A. R., Smith, C. J., Tyrrell, P. J., Rothwell, N. J. & Allan, S. M. (2016). 'Interleukin-1 in Stroke: From Bench to Bedside', *Stroke; a journal of cerebral circulation,* 47, pp. 2160-7.

Soriano, E., del Valle, J., Roselló Busquets, C., de la Oliva, N., Martínez Mármol, R., Hernaiz Llorens, M., Pascual, M., Navarro, X. & Muhaisen, A. (2019). 'Cholesterol depletion regulates axonal growth and enhances central and peripheral nerve regeneration', *Frontiers in cellular neuroscience,* 13, p. 40.

Spulber, S., Bartfai, T. & Schultzberg, M. (2009). 'IL-1/IL-1ra balance in the brain revisited–evidence from transgenic mouse models', *Brain, behavior, immunity,* 23(5), pp. 573-579.

Stainier, D., Fouquet, B., Chen, J.-N., Warren, K. S., Weinstein, B. M., Meiler, S. E., Mohideen, M., Neuhauss, S., Solnica-Krezel, L. & Schier, A. F. (1996). 'Mutations affecting the formation and function of the cardiovascular system in the zebrafish embryo', *Development*, 123(1), pp. 285-292.

Stewart, A. M., Braubach, O., Spitsbergen, J., Gerlai, R. & Kalueff, A. V. (2014). 'Zebrafish models for translational neuroscience research: from tank to bedside', *Trends in neurosciences*, 37(5), pp. 264-278.

Stichel, C. & Müller, H. W. (1998). 'The CNS lesion scar: new vistas on an old regeneration barrier', *Cell and tissue research*, 294(1), pp. 1-9.

Stiles, G. L., Caron, M. G. & Lefkowitz, R. J. (1984). 'Beta-adrenergic receptors: biochemical mechanisms of physiological regulation', *Physiological reviews*, 64(2), pp. 661-743.

Striggow, F., Riek, M., Breder, J., Henrich-Noack, P., Reymann, K. G. & Reiser, G. (2000). 'The protease thrombin is an endogenous mediator of hippocampal neuroprotection against ischemia at low concentrations but causes degeneration at high concentrations', *Proceedings of the National Academy of Sciences*, 97(5), pp. 2264-2269.

Stroke Prevention by Aggressive Reduction in Cholesterol Levels (SPARCL) Investigators (2006). 'High-dose atorvastatin after stroke or transient ischemic attack', *N engl J med*, 2006(355), pp. 549-559.

Summers, M., Jacobs, A., Tudway, D., Perera, P. & Ricketts, C. (1979). 'Studies in desferrioxamine and ferrioxamine metabolism in normal and iron-loaded subjects', *British journal of haematology*, 42(4), pp. 547-555.

Sun, L., Clarke, R., Bennett, D., Guo, Y., Walters, R. G., Hill, M., Parish, S., Millwood, I. Y., Bian, Z. & Chen, Y. (2019). 'Causal associations of blood lipids with risk of ischemic stroke and intracerebral hemorrhage in Chinese adults', *Nature medicine*, p. 1.

Takasugi, S., Ueda, S. & Matsumoto, K. (1985). 'Chronological changes in spontaneous intracerebral hematoma--an experimental and clinical study', *Stroke*, 16(4), pp. 651-658.

Tall, A. R. & Yvan-Charvet, L. (2015). 'Cholesterol, inflammation and innate immunity', *Nature Reviews Immunology*, 15(2), p. 104.

Taylor, R. A. & Sansing, L. H. (2013). 'Microglial responses after ischemic stroke and intracerebral hemorrhage', *Clinical and Developmental Immunology*, 2013.

Tedders, S. H., Fokong, K. D., McKenzie, L. E., Wesley, C., Yu, L. & Zhang, J. (2011). 'Low cholesterol is associated with depression among US household population', *Journal of affective disorders*, 135(1-3), pp. 115-121.

ten Klooster, J. P., Jaffer, Z. M., Chernoff, J. & Hordijk, P. L. (2006). 'Targeting and activation of Rac1 are mediated by the exchange factor β-Pix', *The Journal of cell biology*, 172(5), pp. 759-769.

Tetard, M.-C., Vermandel, M., Mordon, S., Lejeune, J.-P. & Reyns, N. (2014). 'Experimental use of photodynamic therapy in high grade gliomas: a review focused on 5-aminolevulinic acid', *Photodiagnosis and photodynamic therapy*, 11(3), pp. 319-330.

The Royal College of Physicians (2017). Sentinel Stroke National Audi Programme (SSNAP).

The Stroke Association (2016). 'A New Era for Stroke: Our campaign for a new national stroke strategy'.

The Stroke Association (2017). High blood pressure and stroke.

The Stroke Association (2018). *Stroke statistics 2018*. Available at: https://www.stroke.org.uk/system/files/sotn_2018.pdf (Accessed: 12/02/19).
The Wellcome Trust Sanger Institute (2001). *The Zebrafish Genome Project*. Available at: http://www.sanger.ac.uk/science/data/zebrafish-genome-project (Accessed: 11/10/16).
Thisse, C. (2005). 'High throughput expression analysis of ZF-models consortium clones. ZFIN Direct Data Submission'.
Thisse, C. & Thisse, B. (2008). 'High-resolution in situ hybridization to whole-mount zebrafish embryos', *Nature protocols*, 3(1), pp. 59-69.
Traver, D., Paw, B. H., Poss, K. D., Penberthy, W. T., Lin, S. & Zon, L. I. (2003). 'Transplantation and in vivo imaging of multilineage engraftment in zebrafish bloodless mutants', *Nature immunology*, 4(12), p. 1238.
Trede, N. S., Langenau, D. M., Traver, D., Look, A. T. & Zon, L. I. (2004). 'The use of zebrafish to understand immunity', *Immunity*, 20(4), pp. 367-379.
Treuting, P. M., Dintzis, S. M. & Montine, K. S. (2017). *Comparative anatomy and histology: a mouse, rat, and human atlas*: Academic Press.
Tseng, C.-H., Muo, C.-H., Hsu, C. Y. & Kao, C.-H. (2015). 'Increased risk of intracerebral hemorrhage among patients with hepatitis C virus infection', *Medicine*, 94(46).
Törnberg, S. A., Holm, L.-E., Carstensen, J. M. & Eklund, G. A. (1989). 'Cancer incidence and cancer mortality in relation to serum cholesterol', *JNCI: Journal of the National Cancer Institute*, 81(24), pp. 1917-1921.
Uhlén, M., Fagerberg, L., Hallström, B. M., Lindskog, C., Oksvold, P., Mardinoglu, A., Sivertsson, Å., Kampf, C., Sjöstedt, E. & Asplund, A. (2015). 'Tissue-based map of the human proteome', *Science*, 347(6220), p. 1260419.
Valappil, A. V., Chaudhary, N. V., Praveenkumar, R., Gopalakrishnan, B. & Girija, A. (2012). 'Low cholesterol as a risk factor for primary intracerebral hemorrhage: A case–control study', *Annals of Indian Academy of Neurology*, 15(1), p. 19.
Van Agtmael, T., Bailey, M. A., Schlötzer-Schrehardt, U., Craigie, E., Jackson, I. J., Brownstein, D. G., Megson, I. L. & Mullins, J. J. (2010). 'Col4a1 mutation in mice causes defects in vascular function and low blood pressure associated with reduced red blood cell volume', *Human molecular genetics*, 19(6), pp. 1119-1128.
van Ham, T. J., Brady, C. A., Kalicharan, R. D., Oosterhof, N., Kuipers, J., Veenstra-Algra, A., Sjollema, K. A., Peterson, R. T., Kampinga, H. H. & Giepmans, B. N. (2014). 'Intravital correlated microscopy reveals differential macrophage and microglial dynamics during resolution of neuroinflammation', *Disease models & mechanisms*, 7(7), pp. 857-869.
Van Matre, E. T., Sherman, D. S. & Kiser, T. H. (2016). 'Management of intracerebral hemorrhage–use of statins', *Vascular health and risk management*, 12, p. 153.
van Rossum, D. & Hanisch, U.-K. (2004). 'Microglia', *Metabolic brain disease*, 19(3-4), pp. 393-411.
Vaughan, P. J., Pike, C. J., Cotman, C. W. & Cunningham, D. D. (1995). 'Thrombin receptor activation protects neurons and astrocytes from cell death produced by environmental insults', *Journal of Neuroscience*, 15(7), pp. 5389-5401.
Vaz, R. L., Outeiro, T. F. & Ferreira, J. J. (2018). 'Zebrafish as an animal model for Drug Discovery in Parkinson's Disease and Other movement Disorders: a Systematic Review', *Frontiers in Neurology*, 9.

Veltkamp, R. & Gill, D. (2016). 'Clinical trials of immunomodulation in ischemic stroke', *Neurotherapeutics*, 13(4), pp. 791-800.
Veltkamp, R. & Purrucker, J. (2017). 'Management of spontaneous intracerebral hemorrhage', *Current Neurology and Neuroscience reports*, 17(10), p. 80.
Vojtech, L. N., Scharping, N., Woodson, J. C., Hansen, J. D. J. I. & immunity (2012). 'Roles of inflammatory caspases during processing of zebrafish interleukin-1β in Francisella noatunensis infection', 80(8), pp. 2878-2885.
Wakisaka, Y., Chu, Y., Miller, J. D., Rosenberg, G. A. & Heistad, D. D. (2010). 'Spontaneous intracerebral hemorrhage during acute and chronic hypertension in mice', *Journal of Cerebral Blood Flow & Metabolism*, 30(1), pp. 56-69.
Walcott, B. P. & Peterson, R. T. (2014). 'Zebrafish models of cerebrovascular disease', *Journal of Cerebral Blood Flow & Metabolism*, 34(4), pp. 571-577.
Wan, S., Cheng, Y., Jin, H., Guo, D., Hua, Y., Keep, R. F. & Xi, G. (2016). 'Microglia activation and polarization after intracerebral hemorrhage in mice: the role of protease-activated receptor-1', *Translational Stroke Research*, 7(6), pp. 478-487.
Wang, G., Rajpurohit, S. K., Delaspre, F., Walker, S. L., White, D. T., Ceasrine, A., Kuruvilla, R., Li, R.-j., Shim, J. S. & Liu, J. O. (2015). 'First quantitative high-throughput screen in zebrafish identifies novel pathways for increasing pancreatic β-cell mass', *ELife*, 4, p. e08261.
Wang, G., Wang, L., Sun, X. g. & Tang, J. (2018). 'Haematoma scavenging in intracerebral haemorrhage: from mechanisms to the clinic', *Journal of Cellular and Molecular Medicine*, 22(2), pp. 768-777.
Wang, J., Zhai, W., Yu, Z., Sun, L., Li, H., Shen, H., Li, X., Liu, C. & Chen, G. (2018). 'Neuroprotection Exerted by Netrin-1 and Kinesin Motor KIF1A in Secondary Brain Injury following Experimental Intracerebral Hemorrhage in Rats', *Frontiers in cellular neuroscience*, 11, p. 432.
Wang, X., Dong, Y., Qi, X., Huang, C. & Hou, L. (2013). 'Cholesterol levels and risk of hemorrhagic stroke: a systematic review and meta-analysis', *Stroke, 44* (7), pp. 1833-1839.
Wang, Y.-C., Wang, P.-F., Fang, H., Chen, J., Xiong, X.-Y. & Yang, Q.-W. (2013). 'Toll-like receptor 4 antagonist attenuates intracerebral hemorrhage–induced brain injury', *Stroke*, 44(9), pp. 2545-2552.
Weber, A., Wasiliew, P. & Kracht, M. (2010). 'Interleukin-1 (IL-1) pathway', *Sci. Signal.*, 3(105), pp. cm1-cm1.
Weinl, C., Vega, S. C., Riehle, H., Stritt, C., Calaminus, C., Wolburg, H., Mauel, S., Breithaupt, A., Gruber, A. D. & Wasylyk, B. (2015). 'Endothelial depletion of murine SRF/MRTF provokes intracerebral hemorrhagic stroke', *Proceedings of the National Academy of Sciences*, 112(32), pp. 9914-9919.
Westendorp, W. F., Nederkoorn, P. J., Vermeij, J.-D., Dijkgraaf, M. G. & van de Beek, D. (2011). 'Post-stroke infection: a systematic review and meta-analysis', *BMC neurology*, 11(1), p. 110.
Westerfield, M. (2000). 'The zebrafish book: a guide for the laboratory use of zebrafish', *http://zfin.org/zf_info/zfbook/zfbk.html*.
Westover, M. B., Bianchi, M. T., Eckman, M. H. & Greenberg, S. M. (2011). 'Should statins be avoided after intracerebral hemorrhage?', *Archives of neurology*, 68(5), p. 573.
White, R. M., Sessa, A., Burke, C., Bowman, T., LeBlanc, J., Ceol, C., Bourque, C., Dovey, M., Goessling, W. & Burns, C. E. (2008). 'Transparent adult zebrafish as a tool for in vivo transplantation analysis', *Cell stem cell*, 2(2), pp. 183-189.

WHO (2017). *The top 10 causes of death*. Available at: http://www.who.int/mediacentre/factsheets/fs310/en/ (Accessed: 18/09/19).

Willett, C. E., Cortes, A., Zuasti, A. & Zapata, A. G. (1999). 'Early hematopoiesis and developing lymphoid organs in the zebrafish', *Developmental dynamics: an official publication of the American Association of Anatomists*, 214(4), pp. 323-336.

Winkler, D. T., Bondolfi, L., Herzig, M. C., Jann, L., Calhoun, M. E., Wiederhold, K.-H., Tolnay, M., Staufenbiel, M. & Jucker, M. (2001). 'Spontaneous hemorrhagic stroke in a mouse model of cerebral amyloid angiopathy', *Journal of Neuroscience*, 21(5), pp. 1619-1627.

Wu, F., Zhao, Y., Jiao, T., Shi, D., Zhu, X., Zhang, M., Shi, M. & Zhou, H. (2015). 'CXCR2 is essential for cerebral endothelial activation and leukocyte recruitment during neuroinflammation', *Journal of neuroinflammation*, 12(1), p. 98.

Wu, G., Wu, J., Wang, L., Jiao, Y., Zhou, H. & Tang, Z. (2016). 'Minimally invasive surgery for ICH evacuation followed by rosiglitazone infusion therapy increased perihematomal PPARγ expression and improved neurological outcomes in rabbits', *Neurological research*, 38(3), pp. 261-268.

Wu, J., Yang, S., Xi, G., Song, S., Fu, G., Keep, R. & Hua, Y. (2008). 'Microglial activation and brain injury after intracerebral hemorrhage', *Cerebral Hemorrhage*: Springerpp. 59-65.

Xi, G., Keep, R. F. & Hoff, J. T. (2006). 'Mechanisms of brain injury after intracerebral haemorrhage', *The Lancet Neurology*, 5(1), pp. 53-63.

Xiang, Y., Tang, J.-J., Tao, W., Cao, X., Song, B.-L. & Zhong, J. (2015). 'Identification of cholesterol 25-hydroxylase as a novel host restriction factor and a part of the primary innate immune responses against hepatitis C virus infection', *Journal of virology*, 89(13), pp. 6805-6816.

Xue, M. & Del Bigio, M. R. (2000). 'Intracerebral injection of autologous whole blood in rats: time course of inflammation and cell death', *Neuroscience letters*, 283(3), pp. 230-232.

Xue, M. & Del Bigio, M. R. (2003). 'Comparison of brain cell death and inflammatory reaction in three models of intracerebral hemorrhage in adult rats', *Journal of Stroke and Cerebrovascular Diseases*, 12(3), pp. 152-159.

Yang, G.-Y., Betz, A. L., Chenevert, T. L., Brunberg, J. A. & Hoff, J. T. (1994). 'Experimental intracerebral hemorrhage: relationship between brain edema, blood flow, and blood-brain barrier permeability in rats', *Journal of neurosurgery*, 81(1), pp. 93-102.

Yang, J., Arima, H., Wu, G., Heeley, E., Delcourt, C., Zhou, J., Chen, G., Wang, X., Zhang, S. & Yu, S. (2015). 'Prognostic significance of perihematomal edema in acute intracerebral hemorrhage: pooled analysis from the intensive blood pressure reduction in acute cerebral hemorrhage trial studies', *Stroke*, p. STROKEAHA. 114.007154.

Yang, J., Ding, S., Huang, W., Hu, J., Huang, S., Zhang, Y. & Zhuge, Q. (2016). 'Interleukin-4 ameliorates the functional recovery of intracerebral hemorrhage through the alternative activation of microglia/macrophage', *Frontiers in Neuroscience*, 10, p. 61.

Yang, R., Zhang, Y., Huang, D., Luo, X., Zhang, L., Zhu, X., Zhang, X., Liu, Z., Han, J.-Y. & Xiong, J.-W. (2017). 'Miconazole protects blood vessels from MMP9-dependent rupture and hemorrhage', *Disease Models & Mechanisms*, 10(3), pp. 337-348.

Yang, S.-S., Lin, L., Liu, Y., Wang, J., Chu, J., Zhang, T., Ning, L.-N., Shi, Y., Fang, Y.-Y. & Zeng, P. (2016). 'High morphologic plasticity of microglia/macrophages following experimental intracerebral hemorrhage in rats', *International journal of molecular sciences,* 17(7), p. 1181.

Yeatts, S. D., Palesch, Y. Y., Moy, C. S. & Selim, M. (2013). 'High Dose Deferoxamine in Intracerebral Hemorrhage (H i-D ef) Trial: Rationale, Design, and Methods', *Neurocritical Care,* 19(2), pp. 257-266.

Yew, Y. W., Lai, Y. C., Lim, Y. L., Chong, W. & Theng, C. (2016). 'Photodynamic Therapy With Topical 5% 5-Aminolevulinic Acid for the Treatment of Truncal Acne in Asian Patients', *Journal of drugs in dermatology,* 15(6), pp. 727-732.

Yu, Y., Kumana, C., Lauder, I., Cheung, Y., Chan, F., Kou, M., Chang, C., Cheung, R. & Fong, K. (1992). 'Treatment of acute cerebral hemorrhage with intravenous glycerol. A double-blind, placebo-controlled, randomized trial', *Stroke,* 23(7), pp. 967-971.

Zafar, A. & Khan, F. S. (2008). 'Clinical and radiological features of intracerebral haemorrhage in hypertensive patients', *JPMA. The Journal of the Pakistan Medical Association,* 58(7), p. 356.

Zakrzewska, A., Cui, C., Stockhammer, O. W., Benard, E. L., Spaink, H. P. & Meijer, A. H. J. B. (2010). 'Macrophage-specific gene functions in Spi1-directed innate immunity', 116(3), pp. e1-e11.

Zaucker, A., Mercurio, S., Sternheim, N., Talbot, W. S. & Marlow, F. L. (2013). 'notch3 is essential for oligodendrocyte development and vascular integrity in zebrafish', *Disease models & mechanisms,* 6(5), pp. 1246-1259.

Zhang, J. & Liu, Q. (2015). 'Cholesterol metabolism and homeostasis in the brain', *Protein Cell,* 6(4), pp. 254-264.

Zhang, J., Shi, K., Li, Z., Li, M., Han, Y., Wang, L., Zhang, Z., Yu, C., Zhang, F. & Song, L. (2017). 'Organ-and cell-specific immune responses are associated with the outcomes of intracerebral hemorrhage', *The FASEB Journal,* 32(1), pp. 220-229.

Zhang, Y., Wang, L., Huang, X., Wang, S., Huang, Y. & Qin, Q. (2019). 'Fish Cholesterol 25-hydroxylase inhibits virus replication via regulating interferon immune response or affecting virus entry', *Frontiers in immunology,* 10.

Zhang, Y.-Y., Fan, Y.-C., Wang, M., Wang, D. & Li, X.-H. (2013). 'Atorvastatin attenuates the production of IL-1β, IL-6, and TNF-α in the hippocampus of an amyloid β1-42-induced rat model of Alzheimer's disease', *Clinical interventions in aging,* 8, p. 103.

Zhao, S., Liu, Z., Yu, Z., Wu, X., Li, R. & Tang, X. (2019). 'BIO alleviates inflammation through inhibition of GSK-3β in a rat model of intracerebral hemorrhage', *Journal of neurosurgery,* 1(aop), pp. 1-9.

Zhao, X., Sun, G., Zhang, J., Strong, R., Song, W., Gonzales, N., Grotta, J. C. & Aronowski, J. (2007). 'Hematoma resolution as a target for intracerebral hemorrhage treatment: Role for peroxisome proliferator-activated receptor γ in microglia/macrophages', *Annals of neurology,* 61(4), pp. 352-362.

Ziff, O. J., Banerjee, G., Ambler, G. & Werring, D. J. (2019). 'Statins and the risk of intracerebral haemorrhage in patients with stroke: systematic review and meta-analysis', *Journal of Neurology, Neurosurgery & Psychiatry,* 90(1), pp. 75-83.

Zille, M., Karuppagounder, S. S., Chen, Y., Gough, P. J., Bertin, J., Finger, J., Milner, T. A., Jonas, E. A. & Ratan, R. R. (2017). 'Neuronal death after hemorrhagic stroke in vitro and in vivo shares features of ferroptosis and necroptosis', *Stroke,* 48(4), pp. 1033-1043.

Zinnanti, W. J., Lazovic, J., Housman, C., Antonetti, D. A., Koeller, D. M., Connor, J. R. & Steinman, L. (2014). 'Mechanism of metabolic stroke and spontaneous cerebral hemorrhage in glutaric aciduria type I', *Acta neuropathologica communications*, 2(1), p. 13.
Zou, J. & Secombes, C. (2016). 'The function of fish cytokines', *Biology*, 5(2), p. 23.